Semiclassical spin dynamics and feedback control in quantum transport

vorgelegt von
Diplom-Physiker
Klemens Mosshammer
geb. in Dresden

von der Fakultät II – Mathematik und Naturwissenschaften
der Technischen Universität Berlin
zur Erlangung des akademischen Grades

Doktor der Naturwissenschaften
– Dr.rer.nat. –

genehmigte Dissertation

Promotionsausschuss

Vorsitzender: Prof. Dr. rer. nat. Otto Dopfer, TU Berlin
Gutachter: Prof. Dr. rer. nat. Tobias Brandes, TU Berlin
Gutachterin: Prof. PhD. Gloria Platero Coello, CSIC Madrid

Tag der wissenschaftlichen Aussprache: 17.04.2015

Berlin 2015

Contents

1. Preface

Not only in physical systems but also in chemical and biological systems transport processes, where matter and energy is exchanged between distinct and yet connected subsystems, occur widely. Wherever such processes have been discovered both theoretical and experimental researchers showed keen interest, as the study of transport processes often provided insights into basic laws of nature and also gave rise to promising applications. Over the last decades substantial progress has been made to improve the experimental capabilities and to gain deeper understanding of the underlying physical mechanisms. In particular the fact that one is able to develop smaller and ever smaller systems plays a key role. These days, the length scales on which one can reliably fabricate structures and manipulate their dynamics are of the order of a few nanometers. This corresponds to the wavelength of visible light as well as to the size of a few atoms or molecules and not least to the wavelength of the enveloping wave functions of electrons in semiconductors [1]. An immediate consequence of the scale reduction is that we can no longer neglect the quantum properties of transport processes through such tiny structures and devices. On these scales, in contrast to classical transport, quantum properties and effects, such as nonlocality and uncertainty, as well as superposition and interference of states and not least entanglement occur. Due to the growing interest that came with the cognition of the fundamentally different nature of quantum systems, an entirely new field of physics has emerged, the study of mesoscopic transport [2].

Widely studied examples for experimental systems where quantum transport can be observed are mesoscopic solid-state systems: self-assembling nanocrystals [3], quantum dots (QD) [4, 5, 6] nanowires [7] or carbon-nanotubes [8].
Of particular relevance are two-dimensional electron-gases (2DEG) generated in doped semiconductors. Usually additional metallic surface gates are applied on top of the semiconductor substrate, where the 2DEG is formed. When one applies a voltage to the metallic gates the 2DEG is locally depleted. This process enables experimentalists to define almost arbitrary nanostructures within the 2DEG. Beyond single QDs one can build devices in various geometries, such as quantum-point contacts (QPC) [9, 10], serially coupled QDs [11, 12, 13, 14] [compare. fig. 1.1], triple QDs [15, 16].
Another widely used method for the fabrication of quantum dot structures are lithographic methods [17, 18].
Especially transport spectroscopy of electrons in mesoscopic structures is a powerful tool, to get deeper insight into electronic structures. It not only enables researchers to study the level structures but also fundamental interactions springing from the quantum nature of matter. Also the investigation of the interplay of electronic structures with phonons, photons or nuclear spins of the surrounding material is possible. In recent years research on single-electron transport through single molecules [19], QDs [4], or quantum wires [20, 21] has developed rapidly. Quantum transport is also a tool for studying spin states [22] or coherent dynamics [23] on a microscopic level. Recent research – theoretically and experimentally – provides some insight into level structures [24, 25, 22], Coulomb- and spin blockade effects [26], phonon-emission [27] and also full counting statistics of electron-tunneling processes [28, 29, 30].
Electronic quantum coherence in a few-orbital conductor [such as coupled semiconductor or

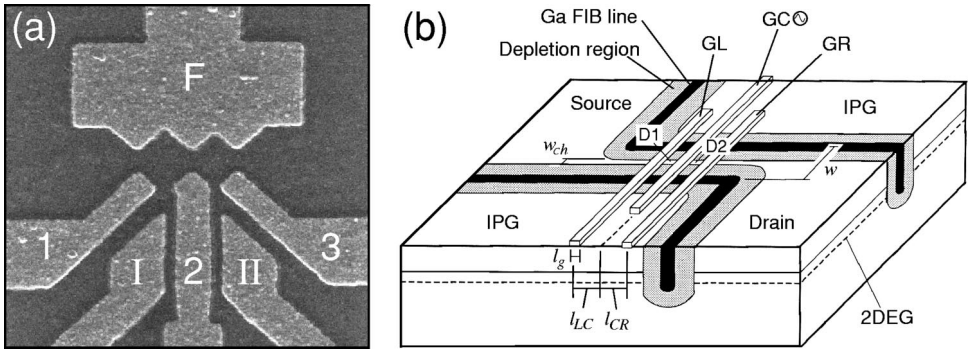

Figure 1.1.: Double quantum dot devices. (a) Scanning electron micrograph of a double dot defined by metallic gates (light gray areas). The dimensions of the dots defined by the gate pattern are 320×320 nm^2 (dot 1, left) and 280×280 nm^2 (dot 2, right). (b) Schematic diagram of a double dot defined by a combination of dry etching and metallic gates. A double quantum dot (dot 1, D1; dot 2, D2) can be formed by applying negative gate voltages to gates GL, GC, and GR. A microwave field can be applied to the center gate GC. – Images taken from Ref. [11]

molecular QDs] which is subject to single-electron transfer, can cause intriguing measurable effects such as transient current oscillations [31], complete current suppression [32], and enhanced current fluctuations [33, 34]. Such types of effects have been studied theoretically and experimentally in various QD geometries: in serially coupled dots [11, 13], in parallel QDs [35, 36, 37, 38], in triangular setups [39], and in coupled orbitals in single molecules [19].

In chapter 2 the theory of open quantum systems is reviewed. This theory relies on the idea of dividing a thermodynamical system into a part that contains the dynamics one is interested in and its environment with which matter and energy is exchanged. If the coupling between system and environment is weak a perturbation theory in their interaction can be exploited [40]. Together with further approximation, such as the Markovian approximations, we derive master equations that describe transport processes the validity of which has been proven in various experiments. Of special interest will be the theory of coarse grained Markovian dynamics [41], that makes it possible to reduce transport models when significantly different time scales occur. Moreover, the thermodynamical implications of the theory are reviewed.

We investigate models where electrons transported through QD structures are interacting with large external spins. Of particular relevance is the coupling of electrons in QD structures to the large number of nuclear spins in the host material. Therefore, in chapter 3, we, briefly, introduce the hyperfine interactions and corresponding effective magnetic fields [cf. fig. 1.2] originating from the ensemble of nuclei. In our transport models we are especially interested in the rich dynamics coming from anisotropic spin couplings and we also take into account the relations of quantum descriptions and semiclassical approaches for isotropic and anisotropic interactions.

Consequently, our transport models studied in chapters 4 and 6 consider the single electron transport through single QD (SQD) and double QD (DQD) devices where the electron spins are exchange coupled to large external spins. We develop a Markovian master equation for exchange-coupling assisted transport, where the transport theory is combined with semiclassical spin dynamics and we are left with a set of equations of motion, that can be solved numerically.

The last aspect of this thesis is the introduction of a closed-loop feedback model that is incorporated phenomenologically into the master equations. It is idealized as a mechanism

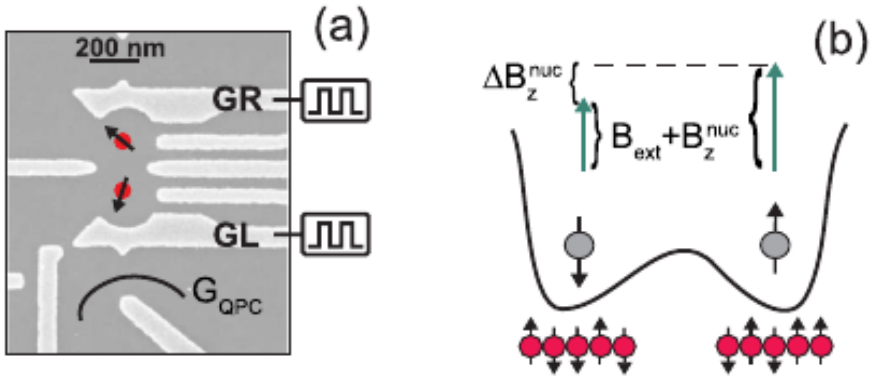

Figure 1.2.: (a) Scanning electron micrograph of a sample consisting of electrostatic gates on the surface of a 2DEG. Voltages on gates GR and GL control the number of electrons in the left and right dots. The state of the DQD is read out by the quantum point contact (QPC). (b) The electrons dwelling the device experience an additional effective field from the nuclear spins, B_z^{nuc}. Images taken from Ref. [42]

that is capable of modifying the entropy balance of the device without changing the energy balance, i.e. as a Maxwell demon. The simplest implementation of such a closed feedback loop for transport through a single electron transistor (SET) was shown by Schaller *et al.* where the demon gets its information from a nearby QPC [43] and conditioned on the measurement modifies the tunneling rates. A microscopic implementation of an actual demon feedback acting on the SET was given by Strasberg *et al.*, where the detection was realized by an capacitively coupled additional QD [44]. Via stochastic thermodynamics a regime could be identified that ensures that the SET's energetics are not affected.
Based on the ideas of Strasberg and coworkers we show a generic feedback model in chapter 5 that provides a microscopic interpretation of the feedback introduced phenomenologically in chapter 4.

2. Open quantum systems

2.1. Introduction

In this chapter we review the system-bath theory. It provides the basic framework to derive the dynamics of the transport setups considered in this thesis. The main idea is to divide a given thermodynamic system into two parts; One part describes the system of interest, with typically only few degrees of freedom. The second part is referred to as bath or environment, usually. It has many degrees of freedom the dynamics of which are not of particular interest. To simplify the treatment of the environment we often assume it to be in the thermodynamic limit, i.e. environments consist of an infinite number of particles in an infinitely large volume, where the particle density is kept constant.
The environment is weakly coupled to the system by matter- and energy- exchange processes, which is why it is often termed reservoir for heat and particles. Given these exchange processes the environment is clearly influencing the system significantly, which complicates the extraction of the dynamics of the interesting degrees of freedom. This influence can be analyzed by applying a perturbation theory in the system-bath-interaction. If the coupling between system and bath is sufficiently weak, the perturbation series can be truncated. This fundamental approach is called weak-coupling approximation. It is well studied and its theoretical results obtained by it have been proven in many experiments.
Furthermore, it is always possible to include higher order corrections of the perturbative approach, in order to add corrections to the weak coupling limit. However, the perturbation theory in low orders is in general still very complicated. In order to obtain numerical or even analytical results further approximations are needed.
In the following sections quantum master equations in the weak coupling limit are derived which describe the dynamics of few-level quantum systems weakly coupled to multiple baths. The major approximations performed are the Born (section 2.4), the Markov (2.5) and the secular approximation (2.6). We set $\hbar = 1$ throughout this thesis.
In the development of the open-quantum system theories and the resulting master equations we greatly benefit from the preeminent discussions by Breuer and Petruccione [40] and the just as well composed lecture notes by Gernot Schaller [45] and respective chapters in the PhD thesis of Christian Nietner [46]. To a large extent we follow their reasoning. Admitting this, we will refrain from giving multiple references to their work throughout this chapter.
An outstanding review of open quantum systems with respect to the mathematical structure, i.e. the quantum dynamical semigroups, is provided by Rivas and Huelga [47]. The book by Alicki and Lendi [48] does also give a deep insight into the mathematical structure.

2.2. System bath theory

We start from Hamiltonians of the form

$$\hat{H} = \hat{H}_{\mathrm{S}} \otimes \mathbb{1}_{\mathrm{B}} + \mathbb{1}_{\mathrm{S}} \otimes \hat{H}_{\mathrm{B}} + \hat{H}_{\mathrm{I}} \,, \tag{2.1}$$

where the system and bath Hamiltonian $\hat{H}_\mathrm{S}$ and $\hat{H}_\mathrm{B}$ act only on the system and bath Hilbert spaces, respectively. We assume that the environment is in a grand-canonical thermal equilibrium state, i.e.

$$\hat{\rho}_\mathrm{B}^\mathrm{eq} = \frac{\mathrm{e}^{-\beta(\hat{H}_\mathrm{B}-\mu\hat{N}_\mathrm{B})}}{\mathrm{Tr}\left\{\mathrm{e}^{-\beta(\hat{H}_\mathrm{B}-\mu\hat{N}_\mathrm{B})}\right\}}\,, \tag{2.2}$$

which is characterized by its chemical potential μ and its (inverse) temperature $\beta = 1/T$, with $k_B \equiv 1$ throughout. If the total number operator for the particles in the bath, $\hat{N}_\mathrm{B}$, commutes with the bath, $\left[\hat{H}_\mathrm{B}\,,\hat{N}_\mathrm{B}\right] = 0$, obviously, $\left[\hat{H}_\mathrm{B}\,,\hat{\rho}_\mathrm{B}^\mathrm{eq}\right] = 0$, follows directly.
The density operator for the entire system, including both system and bath degrees of freedom is denoted by $\hat{\rho} = \sum_i c_i \left|\psi_i\right\rangle\left\langle\psi_i\right|$. Although it is in general possible to calculate the evolution for the states $\left|\psi_i\right\rangle$ and extract expectation values, it is very complicated to find those states in the first place, which is why one has to revert to approximations.
The interaction Hamiltonian, however, acts on both Hilbert spaces

$$\hat{H}_\mathrm{I} = \sum_\alpha \hat{A}_\alpha \otimes \hat{B}_\alpha\,. \tag{2.3}$$

where system and bath operators $\hat{A}_\alpha$ and $\hat{B}_\alpha$ act on their Hilbert spaces only. As we consider physical observables here, all Hamiltonians are required to be self-adjoint, in particular $\hat{H}_\mathrm{I} = \hat{H}_\mathrm{I}^\dagger$. This puts some restrictions on our choice of the system and bath operators. However, we can always split them into hermitian and anti-hermitian parts

$$\hat{A}_\alpha = \hat{A}_\alpha^\mathrm{H} + \hat{A}_\alpha^\mathrm{A}\,, \quad \hat{B}_\alpha = \hat{B}_\alpha^\mathrm{H} + \hat{B}_\alpha^\mathrm{A}\,. \tag{2.4}$$

With

$$\hat{A}_\alpha^\mathrm{H} = \frac{1}{2}\left(\hat{A}_\alpha + \hat{A}_\alpha^\dagger\right), \quad \hat{A}_\alpha^\mathrm{A} = \frac{1}{2}\left(\hat{A}_\alpha - \hat{A}_\alpha^\dagger\right), \tag{2.5}$$

$$\hat{B}_\alpha^\mathrm{H} = \frac{1}{2}\left(\hat{B}_\alpha + \hat{B}_\alpha^\dagger\right), \quad \hat{B}_\alpha^\mathrm{A} = \frac{1}{2}\left(\hat{B}_\alpha - \hat{B}_\alpha^\dagger\right), \tag{2.6}$$

we can rewrite the interaction Hamiltonian as

$$\hat{H}_\mathrm{I} = \frac{1}{2}\left(\hat{H}_\mathrm{I} + \hat{H}_\mathrm{I}^\dagger\right) = \sum_\alpha \left(\hat{A}_\alpha^\mathrm{H} \otimes \hat{B}_\alpha^\mathrm{H} + \hat{A}_\alpha^\mathrm{A} \otimes \hat{B}_\alpha^\mathrm{A}\right) = \sum_\alpha \left(\hat{A}_\alpha^\mathrm{H} \otimes \hat{B}_\alpha^\mathrm{H} - \mathbf{i}\,\hat{A}_\alpha^\mathrm{A} \otimes \mathbf{i}\,\hat{B}_\alpha^\mathrm{A}\right). \tag{2.7}$$

Note that for any anti-hermitian operator $\hat{O}^\mathrm{A}$ it holds that $(\mathbf{i}\,\hat{O}^\mathrm{A})^\dagger = \mathbf{i}\,\hat{O}^\mathrm{A}$ is hermitian. Therefore, all parts of (2.7) are hermitian and we can always define the system and bath operators in terms of hermitian operators

$$\tilde{A}_\alpha = \tilde{A}_\alpha^\dagger\,, \quad \tilde{B}_\alpha = \tilde{B}_\alpha^\dagger\,. \tag{2.8}$$

It is, therefore, valid to assume that the interaction Hamiltonian (2.3) consists of hermitian system and bath operators.

2.3. Weak coupling limit

When the interaction $\hat{H}_\mathrm{I}$ is small, perturbation theory is justified.

We start our considerations from the von-Neumann equation that describes the full evolution of the combined density matrix,

$$\frac{\partial}{\partial t}\hat{\rho} = -\mathbf{i}\left[\hat{H}_\mathrm{S}\otimes\mathbb{1} + \mathbb{1}\otimes\hat{H}_\mathrm{B} + \hat{H}_\mathrm{I}, \hat{\rho}\right] . \tag{2.9}$$

We obtain a formal solution by the unitary evolution

$$\hat{\rho}(t) = \mathrm{e}^{-\mathbf{i}\hat{H}t}\,\hat{\rho}(0)\,\mathrm{e}^{+\mathbf{i}\hat{H}t} . \tag{2.10}$$

This is impractical, since the full Hamiltonian $\hat{H}$ involves too many degrees of freedom.
We transform the latter to the interaction picture (interaction picture operators are denoted by bold symbols)

$$\hat{\boldsymbol{\rho}}(t) = \mathrm{e}^{-\mathbf{i}(\hat{H}_\mathrm{S}+\hat{H}_\mathrm{B})t}\,\hat{\rho}(0)\,\mathrm{e}^{+\mathbf{i}(\hat{H}_\mathrm{S}+\hat{H}_\mathrm{B})t} . \tag{2.11}$$

Thus, the von-Neumann-equation now reads

$$\frac{\partial}{\partial t}\hat{\boldsymbol{\rho}}(t) = -\mathbf{i}\left[\hat{\boldsymbol{H}}_\mathrm{I}(t), \hat{\boldsymbol{\rho}}(t)\right] , \tag{2.12}$$

where we introduced the time-dependent interaction Hamiltonian

$$\begin{aligned}\hat{\boldsymbol{H}}_\mathrm{I}(t) &= \mathrm{e}^{+\mathbf{i}(\hat{H}_\mathrm{S}+\hat{H}_\mathrm{B})t}\,\hat{H}_\mathrm{I}\,\mathrm{e}^{-\mathbf{i}(\hat{H}_\mathrm{S}+\hat{H}_\mathrm{B})t} = \sum_\alpha \mathrm{e}^{+\mathbf{i}\hat{H}_\mathrm{S}t}\,\hat{A}_\alpha\,\mathrm{e}^{-\mathbf{i}\hat{H}_\mathrm{S}t}\otimes\mathrm{e}^{+\mathbf{i}\hat{H}_\mathrm{B}t}\,\hat{B}_\alpha\,\mathrm{e}^{-\mathbf{i}\hat{H}_\mathrm{B}t} \\ &= \sum_\alpha \hat{\boldsymbol{A}}_{\boldsymbol{\alpha}}(t)\otimes\hat{\boldsymbol{B}}_{\boldsymbol{\alpha}}(t) .\end{aligned} \tag{2.13}$$

This prerequisites allow for perturbation theory.
We formally integrate (2.12) and reinsert it self-consistently into the right-hand side. Then we get the time-derivative of the system density matrix by tracing out the bath, i.e. we apply the partial trace and obtain with $\hat{\rho}_\mathrm{S} = \mathrm{Tr}_\mathrm{B}\{\hat{\rho}\}$

$$\frac{\partial}{\partial t}\hat{\boldsymbol{\rho}}_\mathrm{S} = -\mathbf{i}\mathrm{Tr}_\mathrm{B}\left\{\left[\hat{\boldsymbol{H}}_\mathrm{I}(t), \hat{\rho}(0)\right]\right\} - \int_0^t \mathrm{Tr}_\mathrm{B}\left\{\left[\hat{\boldsymbol{H}}_\mathrm{I}(t), \left[\hat{\boldsymbol{H}}_\mathrm{I}(t'), \hat{\boldsymbol{\rho}}(t')\right]\right]dt'\right\} . \tag{2.14}$$

The latter equation is a still exact integro-differential equation, but not closed as the right-hand side does depend on the complete density matrix at all previous times. In order to close the equation we will apply some approximations as carried out in the next sections.

2.4. Factorization of the initial density matrix (Born)

The idea behind this approximation is the assumption that if system and environment initially were well separated, such that they could not interact, the initial state of the whole system could be written as direct product state

$$\hat{\rho}(0) = \hat{\rho}_\mathrm{S}^0\otimes\hat{\rho}_\mathrm{B}^0 . \tag{2.15}$$

Here $\hat{\rho}_\mathrm{S}^0$ is the initial state of the system and $\hat{\rho}_\mathrm{B}^0 = \hat{\rho}_\mathrm{B}^\mathrm{eq}$ is the initial equilibrium density matrix of the environment, (2.2). Additionally, we assume that $\hat{\boldsymbol{H}}_\mathrm{I}(t) = \mathcal{O}\{\lambda\}$, where λ is a small dimensionless perturbation parameter. Moreover we note, that the environment is large enough to assume that it is hardly affected by the system.

We can thus write the full density matrix in the interaction picture as follows

$$\hat{\boldsymbol{\rho}}(t) = \hat{\boldsymbol{\rho}}_{\mathrm{S}}(t) \otimes \hat{\rho}_{\mathrm{B}}^{\mathrm{eq}} + \mathcal{O}\{\lambda\}\,. \tag{2.16}$$

We neglect all orders higher than two, which is usually referred to as Born-approximation. In conclusion we see, that it is equivalent to a perturbation theory in the interaction Hamiltonian, i.e.

$$\frac{\partial}{\partial t}\hat{\boldsymbol{\rho}}_{\mathrm{S}} = -\mathbf{i}\mathrm{Tr}_{\mathrm{B}}\left\{\left[\hat{\boldsymbol{H}}_{\mathrm{I}}(t), \hat{\rho}_{\mathrm{S}}^{0} \otimes \hat{\rho}_{\mathrm{B}}^{\mathrm{eq}}\right]\right\} - \int_{0}^{t} \mathrm{Tr}_{\mathrm{B}}\left\{\left[\hat{\boldsymbol{H}}_{\mathrm{I}}(t), \left[\hat{\boldsymbol{H}}_{\mathrm{I}}(t'), \hat{\boldsymbol{\rho}}_{\mathrm{S}}(t') \otimes \hat{\rho}_{\mathrm{B}}^{\mathrm{eq}}\right]\right] dt'\right\} + \mathcal{O}\{\lambda^{3}\}\,. \tag{2.17}$$

At this point a couple of further simplifications follow directly. First, we include the definition (2.13) into (2.17) and use the cyclic property of the trace

$$\begin{aligned}\frac{\partial}{\partial t}\hat{\boldsymbol{\rho}}_{\mathrm{S}} = &-\mathbf{i}\sum_{\alpha}\mathrm{Tr}_{\mathrm{B}}\left\{\hat{\boldsymbol{B}}_{\boldsymbol{\alpha}}(t)\,\hat{\rho}_{\mathrm{B}}^{\mathrm{eq}}\right\}\left[\hat{\boldsymbol{A}}_{\boldsymbol{\alpha}}(t), \hat{\rho}_{\mathrm{S}}^{0}\right] \\ &- \sum_{\alpha\beta}\int_{0}^{t} dt'\Big[\mathrm{Tr}_{\mathrm{B}}\left\{\hat{\boldsymbol{B}}_{\boldsymbol{\alpha}}(t)\hat{\boldsymbol{B}}_{\boldsymbol{\beta}}(t')\,\hat{\rho}_{\mathrm{B}}^{\mathrm{eq}}\right\}\left[\hat{\boldsymbol{A}}_{\boldsymbol{\alpha}}(t), \hat{\boldsymbol{A}}_{\boldsymbol{\beta}}(t')\hat{\boldsymbol{\rho}}_{\mathrm{S}}(t')\right] \\ &+ \mathrm{Tr}_{\mathrm{B}}\left\{\hat{\boldsymbol{B}}_{\boldsymbol{\beta}}(t')\hat{\boldsymbol{B}}_{\boldsymbol{\alpha}}(t)\,\hat{\rho}_{\mathrm{B}}^{\mathrm{eq}}\right\}\left[\hat{\boldsymbol{\rho}}_{\mathrm{S}}(t')\hat{\boldsymbol{A}}_{\boldsymbol{\beta}}(t'), \hat{\boldsymbol{A}}_{\boldsymbol{\alpha}}(t)\right]\Big]\,.\end{aligned} \tag{2.18}$$

Second, we assume that the single bath coupling operator expectation value vanishes

$$\langle \hat{B}_{\alpha}\rangle_{\mathrm{B}} = \langle \hat{\boldsymbol{B}}_{\boldsymbol{\alpha}}(t)\rangle_{\mathrm{B}} = \mathrm{Tr}_{\mathrm{B}}\left\{\hat{\boldsymbol{B}}_{\boldsymbol{\alpha}}(t)\,\hat{\rho}_{\mathrm{B}}^{\mathrm{eq}}\right\} = 0\,. \tag{2.19}$$

This assumption is convenient, as it simplifies the calculation, but not restrictive. However, it is always possible to shift the energy scale of the interaction Hamiltonian, such that

$$\hat{H}_{\mathrm{I}} \to \hat{H}_{\mathrm{I}}' = \sum_{\alpha}\hat{A}_{\alpha}\otimes\left(\hat{B}_{\alpha} - \langle\hat{B}_{\alpha}\rangle_{\mathrm{B}}\right) = \sum_{\alpha}\hat{A}_{\alpha}\otimes\hat{B}_{\alpha} - \sum_{\alpha}\langle\hat{B}_{\alpha}\rangle_{\mathrm{B}}\left(\hat{A}_{\alpha}\otimes\mathbb{1}_{\mathrm{B}}\right)\,, \tag{2.20}$$

where it does not matter whether numbers $\langle\hat{B}_{\alpha}\rangle_{\mathrm{B}}$ are zero or not. However, if we take the average of (2.20) with respect to the bath Hilbert space we obtain

$$\langle\hat{H}_{\mathrm{I}}'\rangle_{\mathrm{B}} = \sum_{\alpha}\hat{A}_{\alpha}\left(\langle\hat{B}_{\alpha}\rangle_{\mathrm{B}} - \langle\hat{B}_{\alpha}\rangle_{\mathrm{B}}\right) = 0\,. \tag{2.21}$$

Combining eqs. (2.1) and (2.20) we see that the total Hamiltonian is not changed if we also rescale the system operators $\hat{A}_{\alpha}$

$$\begin{aligned}\hat{H} &= \hat{H}_{\mathrm{S}}\otimes\mathbb{1}_{\mathrm{B}} + \mathbb{1}_{\mathrm{S}}\otimes\hat{H}_{\mathrm{B}} + \hat{H}_{\mathrm{I}} = \hat{H}_{\mathrm{S}}\otimes\mathbb{1}_{\mathrm{B}} + \mathbb{1}_{\mathrm{S}}\otimes\hat{H}_{\mathrm{B}} + \hat{H}_{\mathrm{I}}' + \sum_{\alpha}\langle\hat{B}_{\alpha}\rangle_{\mathrm{B}}\left(\hat{A}_{\alpha}\otimes\mathbb{1}_{\mathrm{B}}\right) \\ &= \left(\hat{H}_{\mathrm{S}} + \sum_{\alpha}\langle\hat{B}_{\alpha}\rangle_{\mathrm{B}}\,\hat{A}_{\alpha}\right)\otimes\mathbb{1}_{\mathrm{B}} + \mathbb{1}_{\mathrm{S}}\otimes\hat{H}_{\mathrm{B}} + \hat{H}_{\mathrm{I}}'\,.\end{aligned} \tag{2.22}$$

This shows that is valid to assume (2.19).
Finally, we define the so-called bath correlation functions

$$C_{\alpha\beta}(t_1, t_2) = \mathrm{Tr}\left\{\hat{\boldsymbol{B}}_{\boldsymbol{\alpha}}(t_1)\hat{\boldsymbol{B}}_{\boldsymbol{\beta}}(t_2)\,\hat{\rho}_{\mathrm{B}}^{\mathrm{eq}}\right\}\,. \tag{2.23}$$

We obtain

$$\frac{\partial}{\partial t}\hat{\boldsymbol{\rho}}_{\mathrm{S}} = -\sum_{\alpha\beta}\int_0^t dt'\Big[C_{\alpha\beta}(t,t')\left[\hat{\boldsymbol{A}}_{\boldsymbol{\alpha}}(t),\hat{\boldsymbol{A}}_{\boldsymbol{\beta}}(t')\hat{\boldsymbol{\rho}}_{\mathrm{S}}(t')\right] + C_{\beta\alpha}(t',t)\left[\hat{\boldsymbol{\rho}}_{\mathrm{S}}(t')\hat{\boldsymbol{A}}_{\boldsymbol{\beta}}(t'),\hat{\boldsymbol{A}}_{\boldsymbol{\alpha}}(t)\right]\Big]. \tag{2.24}$$

Let us analyze this equation, briefly. The integro-differential equation (2.24) is a nonmarkovian master equation as its right-hand side still depends on the density matrix at all previous times. The bath correlation functions act as weights. While trace and hermiticity of the density matrix are preserved by this equation, this does not necessarily hold for the positivity. This type of equations have a solution only in special cases. As a consequence we have to use additional approximations. The key to further processing of this equation is the analysis of the properties of the bath-correlation functions.

As mentioned above, the bath Hamiltonian commutes with the bath equilibrium density operator, $\left[\hat{H}_{\mathrm{B}}\,,\hat{\rho}_{\mathrm{B}}^{\mathrm{eq}}\right]=0$. Together with the cyclic property of the trace it is straightforward to show, that the bath correlation functions are homogeneous in time, i.e. just depend on the difference of their time arguments

$$C_{\alpha\beta}(t_1,t_2) = C_{\alpha\beta}(t_1-t_2) = \mathrm{Tr}\left\{\mathrm{e}^{+\mathbf{i}\hat{H}_{\mathrm{B}}(t_1-t_2)}\,\hat{B}_\alpha\,\mathrm{e}^{-\mathbf{i}\hat{H}_{\mathrm{B}}(t_1-t_2)}\,\hat{B}_\beta\,\hat{\rho}_{\mathrm{B}}^{\mathrm{eq}}\right\}. \tag{2.25}$$

Given that the bath coupling operators $\hat{B}_\alpha$ are chosen to be self-adjoint, we further can state

$$C_{\alpha\beta}(\tau) = C^*_{\beta\alpha}(-\tau)\,. \tag{2.26}$$

Moreover, if the bath has a dense spectrum the bath correlation functions are typically strongly peaked around zero.

2.5. Markov approximation

The assumption that the bath correlation functions are peaked around zero has an immediate consequence, namely that the density matrices far in the past are weighted much less than the one an instant ago. In the most extreme case we could express the bath correlation functions as delta distributions $C_{\alpha\beta}(t_1,t_2)\approx\Gamma_{\alpha\beta}\delta(t_1-t_2)$. Nonetheless, at this point we only need to assume that the variation of the system density matrix is slower than the decay of the bath correlation functions [49].

2.5.1. First Markov approximation

This is reflected in the first Markov approximation. We replace $\hat{\boldsymbol{\rho}}_{\mathrm{S}}(t')\to\hat{\boldsymbol{\rho}}_{\mathrm{S}}(t)$ in (2.24) and obtain with the above properties of the bath correlation functions

$$\frac{\partial}{\partial t}\hat{\boldsymbol{\rho}}_{\mathrm{S}} = -\int_0^t \mathrm{Tr}_{\mathrm{B}}\left\{\left[\hat{\boldsymbol{H}}_{\mathrm{I}}(t),\left[\hat{\boldsymbol{H}}_{\mathrm{I}}(t'),\hat{\boldsymbol{\rho}}_{\mathrm{S}}(t)\otimes\hat{\rho}_{\mathrm{B}}^{\mathrm{eq}}\right]\right]\right\}dt'\,, \tag{2.27}$$

which is known as Born-Redfield equation. It is local in time, preserves trace and hermiticity but has still time-dependent coefficients. For convenience we also substitute $\tau = t - t'$

$$\frac{\partial}{\partial t}\hat{\boldsymbol{\rho}}_{\mathrm{S}} = -\int_0^t \mathrm{Tr}_{\mathrm{B}}\left\{\left[\hat{\boldsymbol{H}}_{\mathrm{I}}(t),\left[\hat{\boldsymbol{H}}_{\mathrm{I}}(t-\tau),\hat{\boldsymbol{\rho}}_{\mathrm{S}}(t)\otimes\hat{\rho}_{\mathrm{B}}^{\mathrm{eq}}\right]\right]\right\}d\tau \tag{2.28}$$

$$= -\sum_{\alpha\beta}\int_0^t d\tau\Big\{C_{\alpha\beta}(\tau)\left[\hat{\boldsymbol{A}}_{\boldsymbol{\alpha}}(t),\hat{\boldsymbol{A}}_{\boldsymbol{\beta}}(t-\tau)\hat{\boldsymbol{\rho}}_{\mathrm{S}}(t)\right] + C_{\beta\alpha}(-\tau)\left[\hat{\boldsymbol{\rho}}_{\mathrm{S}}(t)\hat{\boldsymbol{A}}_{\boldsymbol{\beta}}(t-\tau),\hat{\boldsymbol{A}}_{\boldsymbol{\alpha}}(t)\right]\Big\}.$$

2.5.2. Second Markov approximation

The right-hand side of eq. (2.28) still depends on t, which can be overcome by extending the integration boundaries to "∞". That yields

$$\frac{\partial}{\partial t}\hat{\boldsymbol{\rho}}_{\mathrm{S}} = -\sum_{\alpha\beta}\int_0^\infty d\tau\Big\{C_{\alpha\beta}(\tau)\left[\hat{\boldsymbol{A}}_{\boldsymbol{\alpha}}(t),\hat{\boldsymbol{A}}_{\boldsymbol{\beta}}(t-\tau)\hat{\boldsymbol{\rho}}_{\mathrm{S}}(t)\right] + C_{\beta\alpha}(-\tau)\left[\hat{\boldsymbol{\rho}}_{\mathrm{S}}(t)\hat{\boldsymbol{A}}_{\boldsymbol{\beta}}(t-\tau),\hat{\boldsymbol{A}}_{\boldsymbol{\alpha}}(t)\right]\Big\}. \tag{2.29}$$

This is justified as the two point correlation function evaluates to significant values only when $t \approx \tau$, and thus extension of the upper limit is valid.
To put it in other words: the 2nd Markov approximation is justified if the integrand disappears sufficiently fast for $\tau \gg \tau_{\mathrm{B}}$, where τ_{B} is the time scale over which the bath correlation functions decay. Moreover, the time scale τ_{S} over which the system state varies appreciably is large compared to τ_{B}.
Going back to the Schrödinger picture (2.29) reads

$$\frac{\partial}{\partial t}\hat{\rho}_{\mathrm{S}} = -\mathbf{i}\left[\hat{H}_{\mathrm{S}},\hat{\rho}_{\mathrm{S}}(t)\right] - \sum_{\alpha\beta}\int_0^\infty d\tau\Big\{C_{\alpha\beta}(\tau)\left[\hat{A}_\alpha,\mathrm{e}^{-\mathbf{i}\hat{H}_{\mathrm{S}}\tau}\,\hat{A}_\beta\,\mathrm{e}^{+\mathbf{i}\hat{H}_{\mathrm{S}}\tau}\,\hat{\rho}_{\mathrm{S}}(t)\right]$$
$$+ C_{\beta\alpha}(-\tau)\left[\hat{\rho}_{\mathrm{S}}(t)\,\mathrm{e}^{-\mathbf{i}\hat{H}_{\mathrm{S}}\tau}\,\hat{A}_\beta\,\mathrm{e}^{+\mathbf{i}\hat{H}_{\mathrm{S}}\tau},\hat{A}_\alpha\right]\Big\}. \tag{2.30}$$

The system density matrix does not depend on system states at former times. Equation (2.30) has constant coefficients, it preserves the trace and the hermiticity, but does not necessarily preserve the positivity of the reduced density matrix.
The most general form of the master equation that assures the positivity of $\hat{\rho}_{\mathrm{S}}$ is the so-called Lindblad form, as we will show in the next sections.
Note that the dynamical behavior over times of the order of magnitude of τ_{B} is not resolved in this description!

2.6. Secular approximation

In order to make sure that the positivity of the density matrix is preserved we need another approximation: the secular approximation. It is also termed rotating wave approximation, due to its frequent use in quantum optics. Its essence is to neglect the fast oscillating terms in the master equations. The identification of the fast oscillating terms requires at least formal calculation of the interaction picture dynamics of the system coupling operators. We write the Markovian master equation again in the interaction picture.

We, therefore, evaluate (2.29) by using the system energy eigenbasis $\hat{H}_\mathrm{S}\,|a\rangle = E_a\,|a\rangle$ and by using the hermiticity of the coupling operators. Inserting the completeness relation of the system eigenstates yields

$$\begin{aligned}\frac{\partial}{\partial t}\hat{\boldsymbol{\rho}}_\mathrm{S} = -\sum_{\alpha\beta}\sum_{abcd}\int_0^\infty d\tau\Big\{&C_{\alpha\beta}(\tau)\left[|a\rangle\langle a|\,\hat{\boldsymbol{A}}_{\boldsymbol{\alpha}}(t)\,|b\rangle\langle b|\,,|c\rangle\langle c|\,\hat{\boldsymbol{A}}_{\boldsymbol{\beta}}(t-\tau)\,|d\rangle\langle d|\,\hat{\boldsymbol{\rho}}_\mathrm{S}(t)\right]\\ &+C_{\beta\alpha}(-\tau)\left[\hat{\boldsymbol{\rho}}_\mathrm{S}(t)\,|c\rangle\langle c|\,\hat{\boldsymbol{A}}_{\boldsymbol{\beta}}(t-\tau)\,|d\rangle\langle d|\,,|a\rangle\langle a|\,\hat{\boldsymbol{A}}_{\boldsymbol{\alpha}}(t)\,|b\rangle\langle b|\right]\Big\}\,. \end{aligned} \tag{2.31}$$

With the definition of the system- and bath-operators in the interaction picture (2.13) this reads

$$\begin{aligned}\frac{\partial}{\partial t}\hat{\boldsymbol{\rho}}_\mathrm{S} = -\sum_{\alpha\beta}\sum_{abcd}\int_0^\infty d\tau\,&\langle a|\,\hat{A}_\alpha\,|b\rangle\langle c|\,\hat{A}_\beta\,|d\rangle\,\mathrm{e}^{\mathbf{i}(E_a-E_b)t}\,\mathrm{e}^{\mathbf{i}(E_c-E_d)(t-\tau)}\\ &\times\Big\{C_{\alpha\beta}(\tau)\left[|a\rangle\langle b|\,,|c\rangle\langle d|\,\hat{\boldsymbol{\rho}}_\mathrm{S}(t)\right]+C_{\beta\alpha}(-\tau)\left[\hat{\boldsymbol{\rho}}_\mathrm{S}(t)\,|c\rangle\langle d|\,,|a\rangle\langle b|\right]\Big\}\,. \end{aligned} \tag{2.32}$$

For large times t the terms proportional to $\mathrm{e}^{\mathbf{i}\omega t}$ average out. We replace $\mathrm{e}^{\mathbf{i}\omega t}\to\delta_{\omega,0}$, introduce $\omega_{a,b}=E_a-E_b$ and the Lindblad operators $\hat{L}_{ab}=|a\rangle\langle b|$. Thus, we obtain

$$\begin{aligned}\frac{\partial}{\partial t}\hat{\boldsymbol{\rho}}_\mathrm{S} &= -\sum_{\alpha\beta}\sum_{abcd}\langle a|\,\hat{A}_\alpha\,|b\rangle\langle c|\,\hat{A}_\beta\,|d\rangle\Big\{\int_0^\infty d\tau C_{\alpha\beta}(\tau)\,\mathrm{e}^{\mathbf{i}\omega_{d,c}\tau}\left[\hat{L}_{ab}\,,\hat{L}_{cd}\,\hat{\boldsymbol{\rho}}_\mathrm{S}(t)\right]\\ &\quad+\int_0^\infty d\tau C_{\beta\alpha}(-\tau)\,\mathrm{e}^{\mathbf{i}\omega_{d,c}\tau}\left[\hat{\boldsymbol{\rho}}_\mathrm{S}(t)\,\hat{L}_{cd}\,,\hat{L}_{ab}\right]\Big\}\delta_{\omega_{a,b},\omega_{d,c}}\\ &= -\sum_{\alpha\beta}\sum_{abcd}\langle a|\,\hat{A}_\alpha\,|b\rangle\langle c|\,\hat{A}_\beta\,|d\rangle\Big\{\Gamma^+_{\alpha\beta}(\omega_{d,c})\left[\hat{L}_{ab}\,,\hat{L}_{cd}\,\hat{\boldsymbol{\rho}}_\mathrm{S}(t)\right]\\ &\quad+\Gamma^-_{\beta\alpha}(-\omega_{d,c})\left[\hat{\boldsymbol{\rho}}_\mathrm{S}(t)\,\hat{L}_{cd}\,,\hat{L}_{ab}\right]\Big\}\delta_{\omega_{a,b},\omega_{d,c}}\,. \end{aligned} \tag{2.33}$$

In the last step we introduced the half-sided Fourier transformations of the bath correlation functions, which are defined as

$$\Gamma^\pm_{\alpha\beta}(\omega)=\int_{-\infty}^\infty d\tau\Theta(\pm\tau)C_{\alpha\beta}(\tau)\,\mathrm{e}^{\mathbf{i}\omega\tau}\,, \tag{2.34}$$

where $\Theta(t)$ is the Heaviside step function, defined in terms of the sign-function

$$\Theta(x)=\frac{1}{2}\left(\mathrm{sgn}(x)+1\right)\,,\text{with }\mathrm{sgn}(x)=\begin{cases}+1\,, & x>0\\ -1\,, & x<0\end{cases}\,. \tag{2.35}$$

Equation (2.33) is already preserving trace, hermiticity and positivity of the reduced density matrix $\hat{\rho}_\mathrm{S}$, as it is of Lindblad form. We will introduce and substantiate the Lindblad form in section 2.7.

At this point a little remark should be made: In eq. (2.33) we have to be sure that the Fourier transforms $\Gamma^\pm_{\alpha\beta}$ converge. Thus, the bath correlation functions have to decrease as τ increases. We can decompose the bath operators $\hat{B}_\alpha$ into eigenoperators of the bath Hamiltonian (which is similarly possible for the system operators $\hat{A}_\alpha$). We have

$$\hat{B}_\alpha(\omega)=\sum_{\varepsilon-\varepsilon'=\omega}\hat{\Pi}(\varepsilon)\,\hat{B}_\alpha\,\hat{\Pi}(\varepsilon')\,, \tag{2.36}$$

where we used the projection $\hat{\Pi}(\varepsilon)$ on the eigenspace of $\hat{H}_\mathrm{B}$ with the corresponding eigenenergy ε. Equivalently we get

$$\hat{B}_\alpha = \sum_\omega \hat{B}_\alpha(\omega)\,, \tag{2.37}$$

Therefore, the bath operator in the interaction picture can be decomposed into

$$\hat{\boldsymbol{B}}_{\boldsymbol{\alpha}}(\tau) = \sum_\omega \mathrm{e}^{-\mathbf{i}\omega\tau}\,\hat{B}_\alpha(\omega)\,, \tag{2.38}$$

and we find for the bath correlation functions

$$C_{\alpha\beta}(\tau) = \mathrm{Tr}\left\{\hat{\boldsymbol{B}}_{\boldsymbol{\alpha}}(\tau)\,\hat{B}_\beta\,\hat{\rho}_\mathrm{B}^\mathrm{eq}\right\} = \sum_\omega \mathrm{e}^{-\mathbf{i}\omega\tau}\,\mathrm{Tr}\left\{\hat{B}_\alpha(\omega)\,\hat{B}_\beta\,\hat{\rho}_\mathrm{B}^\mathrm{eq}\right\}\,. \tag{2.39}$$

This shows, that the bath correlation functions are periodic in τ and, thus, the integral to infinity would diverge. We can prevent the integral from diverging by assuming that the environment has infinite degrees of freedom (thermodynamic limit) and a continuous spectrum. Then eq. (2.37) is rewritten as

$$\hat{B}_\alpha = \int_{-\Omega}^{\Omega} d\omega\,\hat{B}_\alpha(\omega)\,, \tag{2.40}$$

where Ω is the maximum eigenfrequency. Correspondingly, (2.39) becomes

$$C_{\alpha\beta}(\tau) = \int_{-\Omega}^{\Omega} d\omega\,\mathrm{e}^{-\mathbf{i}\omega\tau}\,\mathrm{Tr}\left\{\hat{B}_\alpha(\omega)\,\hat{B}_\beta\,\hat{\rho}_\mathrm{B}^\mathrm{eq}\right\}\,. \tag{2.41}$$

Now, the bath correlation functions are not periodic any more as according to the Lemma of Riemann-Lebesgue, that states

$$\lim_{\tau\to\infty}\int_a^b d\omega\,\mathrm{e}^{-\mathbf{i}\omega\tau}\,f(\omega) = 0\,, \tag{2.42}$$

if $f(\omega)$ is integrable in $[a,b]$. In terms of the bath correlation function we, therefore, obtain

$$\lim_{\tau\to\infty}\int_{-\Omega}^{\Omega} d\omega\,\mathrm{e}^{-\mathbf{i}\omega\tau}\,\mathrm{Tr}\left\{\hat{B}_\alpha(\omega)\,\hat{B}_\beta\,\hat{\rho}_\mathrm{B}^\mathrm{eq}\right\} = 0\,. \tag{2.43}$$

Recall, that in the weak coupling regime we could rewrite $\hat{H}_\mathrm{I} \to \lambda\hat{H}_\mathrm{I}$, where λ accounts for the strength of the system-bath-interaction. For small λ the variation of $\hat{\rho}_\mathrm{S}$ is slow (with the corresponding time scale τ_S). The weak-coupling regime is, thus, characterized by $\tau_\mathrm{S} \gg \tau_\mathrm{B}$. In the limit $\lambda \to 0$ we would get $\tau_\mathrm{S}/\tau_\mathrm{B} \to \infty$ for a fixed τ_B. However, as $\lambda \to 0$ means that there is no interaction a rescaling of the time parameter is needed. The limiting procedure was studied carefully by Davies [50]. Our reasoning above shows, that it is a necessary condition for the weak coupling limit to exist that the bath has a continuous spectrum. Davies formulated a sufficient and more rigorous condition for the decreasing behavior of the bath correlation functions (compare Theorem 3.5 in [50]).

Now, we will discuss and reshape eq. (2.33). As a beginning, we will split the half-sided Fourier transforms in their hermitian $\gamma_{\alpha\beta}$ and anti-hermitian $\sigma_{\alpha\beta}$ parts, which yield

$$\Gamma^{\pm}_{\alpha\beta}(\omega) = \frac{1}{2}\gamma_{\alpha\beta}(\omega) \pm \frac{1}{2}\sigma_{\alpha\beta}(\omega)\,. \tag{2.44}$$

Accordingly, the full even and odd Fourier transforms of the bath correlation functions read

$$\gamma_{\alpha\beta}(\omega) = \Gamma^{+}_{\alpha\beta}(\omega) + \Gamma^{-}_{\alpha\beta}(\omega) = \int_{-\infty}^{\infty} d\tau C_{\alpha\beta}(\tau)\, \mathrm{e}^{\mathbf{i}\omega\tau}\,, \tag{2.45}$$

$$\sigma_{\alpha\beta}(\omega) = \Gamma^{+}_{\alpha\beta}(\omega) - \Gamma^{-}_{\alpha\beta}(\omega) = \int_{-\infty}^{\infty} d\tau C_{\alpha\beta}(\tau)\, \mathrm{sgn}(\tau)\, \mathrm{e}^{\mathbf{i}\omega\tau}\,. \tag{2.46}$$

The latter, (2.46), can be rewritten in terms of Cauchy's principal value, i.e.

$$\sigma_{\alpha\beta}(\omega) = \frac{1}{2\pi}\int_{-\infty}^{\infty} d\Omega \left[\int_{-\infty}^{\infty} d\tau\, \mathrm{e}^{-\mathbf{i}(\omega-\Omega)\tau}\, \mathrm{sgn}(\tau)\right]\gamma_{\alpha\beta}(\Omega) = \frac{\mathbf{i}}{\pi}\mathrm{P.V.}\int_{-\infty}^{\infty}\frac{\gamma_{\alpha\beta}(\Omega)}{\omega-\Omega}d\Omega\,, \tag{2.47}$$

where we used that the Fourier transform of the sign function evaluates to $2/\mathbf{i}\omega$ and where 'P.V.' denotes the principal value.
The master equation (2.33), thus, can be rewritten as

$$\begin{aligned}\frac{\partial}{\partial t}\hat{\boldsymbol{\rho}}_{\mathrm{S}} = -\frac{1}{2}\sum_{\alpha\beta}\sum_{abcd}\langle a|\,\hat{A}_\alpha\,|b\rangle\,\langle c|\,\hat{A}_\beta\,|d\rangle\Big[\,\big(\gamma_{\alpha\beta}(\omega_{d,c}) + \sigma_{\alpha\beta}(\omega_{d,c})\big)\big[\hat{L}_{ab}\,,\hat{L}_{cd}\,\hat{\boldsymbol{\rho}}_{\mathrm{S}}(t)\big] \\ + \big(\gamma_{\beta\alpha}(-\omega_{d,c}) - \sigma_{\beta\alpha}(-\omega_{d,c})\big)\big[\hat{\boldsymbol{\rho}}_{\mathrm{S}}(t)\,\hat{L}_{cd}\,,\hat{L}_{ab}\big]\,\Big]\delta_{\omega_{a,b},\omega_{d,c}}\,.\end{aligned} \tag{2.48}$$

We now transform the indices $\alpha \leftrightarrow \beta$, $a \leftrightarrow c$ and $b \leftrightarrow d$ in the second line and collect the terms proportional to the even and odd Fourier transforms, to obtain

$$\frac{\partial}{\partial t}\hat{\boldsymbol{\rho}}_{\mathrm{S}} = -\mathbf{i}\big[\hat{H}_{\mathrm{LS}}\,,\hat{\boldsymbol{\rho}}_{\mathrm{S}}\big] + \sum_{abcd}\gamma_{ab,cd}\Big[\,\hat{L}_{cd}\,\hat{\boldsymbol{\rho}}_{\mathrm{S}}\,\hat{L}^{\dagger}_{ba} - \frac{1}{2}\Big\{\hat{L}^{\dagger}_{ba}\,\hat{L}_{cd}\,,\hat{\boldsymbol{\rho}}_{\mathrm{S}}\Big\}\,\Big]\,, \tag{2.49}$$

with the so-called Lamb-shift Hamiltonian

$$\hat{H}_{\mathrm{LS}} = \frac{1}{2\mathbf{i}}\sum_{\alpha\beta}\sum_{abcd}\sigma_{\alpha\beta}(\omega_{d,c})\,\langle a|\,\hat{A}_\alpha\,|b\rangle\,\langle c|\,\hat{A}_\beta\,|d\rangle\,\hat{L}^{\dagger}_{ba}\,\hat{L}_{cd}\,\delta_{\omega_{a,b},\omega_{d,c}}\,, \tag{2.50}$$

and the transition rates

$$\gamma_{ab,cd} = \sum_{\alpha,\beta}\gamma_{\alpha\beta}(\omega_{d,c})\,\langle a|\,\hat{A}_\beta\,|b\rangle\,\langle c|\,\hat{A}_\alpha\,|d\rangle\,\delta_{\omega_{a,b},\omega_{d,c}}\,. \tag{2.51}$$

The Lamb-shift Hamiltonian renormalizes the system Hamiltonian due to the interaction with the baths. It is self-adjoint, $\hat{H}_{\mathrm{LS}} = \hat{H}^{\dagger}_{\mathrm{LS}}$, and commutes with the system hamiltonian, $\big[\hat{H}_{\mathrm{S}}\,,\hat{H}_{\mathrm{LS}}\big] = 0$, which implies the existence of a basis that diagonalizes both operators.
Let's assume that the system has orthogonal eigenstates, i.e. $\langle a|b\rangle = \delta_{ab}$, which simplifies the Lamb-shift Hamiltonian to

$$\hat{H}_{\mathrm{LS}} = \frac{1}{2\mathbf{i}}\sum_{\alpha\beta}\sum_{abd}\sigma_{\alpha\beta}(\omega_{d,b})\,\langle a|\,\hat{A}_\alpha\,|b\rangle\,\langle b|\,\hat{A}_\beta\,|d\rangle\,\hat{L}_{ad}\,\delta_{E_a,E_d}\,. \tag{2.52}$$

If, additionally, the system's eigenvalues are nondegenerate, $\delta_{E_a,E_d} = \delta_{a,d}$, the basis that diagonalizes $\hat{H}_\mathrm{S}$ is unique and also diagonalizes the Lamb-shift Hamiltonian

$$\hat{H}_\mathrm{LS} = \frac{1}{2\mathbf{i}} \sum_{\alpha\beta} \sum_{ab} \sigma_{\alpha\beta}(\omega_{a,b}) \langle a| \hat{A}_\alpha |b\rangle \langle b| \hat{A}_\beta |a\rangle \hat{L}_{aa} \ . \tag{2.53}$$

Hence, for systems where the density matrix $\hat{\rho}_\mathrm{S}$ is diagonal in the eigenbasis, the commutator in (2.49) vanishes.
For systems with nondegenerate eigenvalues an effective rate equation description for the system density matrix can be written. It follows from that description, that $\hat{\rho}_\mathrm{S}$ is also diagonal in the system eigenbasis. Consequently, if we go back to the Schrödinger picture the dynamics of systems with nondegenerate eigenvalues are described by

$$\frac{\partial}{\partial t} \hat{\rho}_\mathrm{S} = \sum_{abcd} \gamma_{ab,cd} \Big[\hat{L}_{cd} \hat{\rho}_\mathrm{S} \hat{L}^\dagger_{ba} - \frac{1}{2} \left\{ \hat{L}^\dagger_{ba} \hat{L}_{cd}, \hat{\rho}_\mathrm{S} \right\} \Big], \tag{2.54}$$

where we use that $\hat{H}_\mathrm{S}$ and $\hat{\rho}_\mathrm{S}$ have a common eigenbasis and that $\left[\hat{H}_\mathrm{S}, \hat{\rho}_\mathrm{S}\right]$ vanishes.

2.6.1. Preservation of positivity

Now, we are left to show that the matrix $\gamma_{ab,cd}$ is positive definite and, therefore, (2.49) preserves positivity of the system density matrix. It suffices to show that the matrix $\boldsymbol{\gamma} = \left(\gamma_{\alpha,\beta}\right)$ is positive semidefinite for all ω. The reasoning is as follows, compare [47]:
For any vector $\vec{v}$ we have

$$\begin{aligned}
(\vec{v}, \boldsymbol{\gamma}\vec{v}) &= \sum_{\alpha\beta} v_\alpha \gamma_{\alpha\beta}(\omega) v_\beta = \int_{-\infty}^{\infty} d\tau \, \mathrm{e}^{\mathbf{i}\omega\tau} \sum_{\alpha\beta} v^*_\alpha \mathrm{Tr}\left\{ \hat{\boldsymbol{B}}_\alpha(\tau) \hat{B}_\beta \hat{\rho}^\mathrm{eq}_\mathrm{B} \right\} v_\beta \\
&= \int_{-\infty}^{\infty} d\tau \, \mathrm{e}^{\mathbf{i}\omega\tau} \sum_{\alpha\beta} v^*_\alpha \mathrm{Tr}\left\{ \mathrm{e}^{\mathbf{i}\hat{H}_\mathrm{B}\tau} \hat{B}_\alpha \mathrm{e}^{-\mathbf{i}\hat{H}_\mathrm{B}\tau} \hat{B}_\beta \hat{\rho}^\mathrm{eq}_\mathrm{B} \right\} v_\beta \\
&= \int_{-\infty}^{\infty} d\tau \, \mathrm{e}^{\mathbf{i}\omega\tau} \, \mathrm{Tr}\left\{ \mathrm{e}^{\mathbf{i}\hat{H}_\mathrm{B}\tau} \hat{C}^\dagger \mathrm{e}^{-\mathbf{i}\hat{H}_\mathrm{B}\tau} \hat{C} \hat{\rho}^\mathrm{eq}_\mathrm{B} \right\},
\end{aligned} \tag{2.55}$$

where $\hat{C} = \sum_\alpha \hat{B}_\alpha v_\alpha$. Now, we can use the so-called Bochner-theorem [51], that states that the Fourier transform of a "positive type" function is a positive quantity.
A function $f(t)$ is of "positive type" if it is complex-valued, bounded and continuous on $\mathbb{R}^n$ with the property that a matrix $\mathbf{f} = (f_{ij})$ with $f_{ij} = f(t_i - t_j)$ is positive semidefinite on $\mathbb{C}^N$, where $t_1 \ldots t_N \in \mathbb{R}^n$.
According to this definition we can show, that $f(t) = \mathrm{Tr}\left\{ \mathrm{e}^{\mathbf{i}\hat{H}_\mathrm{B}t} \hat{C}^\dagger \mathrm{e}^{-\mathbf{i}\hat{H}_\mathrm{B}t} \hat{C} \hat{\rho}^\mathrm{eq}_\mathrm{B} \right\}$ is a function of "positive type". If we take the trace in the eigenbasis of $\hat{H}_\mathrm{B}$ (with the assumption of a continuous spectrum), we obtain

$$\begin{aligned}
f(t) &= \mathrm{Tr}\left\{ \mathrm{e}^{\mathbf{i}\hat{H}_\mathrm{B}t} \hat{C}^\dagger \mathrm{e}^{-\mathbf{i}\hat{H}_\mathrm{B}t} \hat{C} \hat{\rho}^\mathrm{eq}_\mathrm{B} \right\} = \int d\varepsilon \, \langle \psi_\varepsilon | \, \mathrm{e}^{\mathbf{i}\hat{H}_\mathrm{B}t} \hat{C}^\dagger \mathrm{e}^{-\mathbf{i}\hat{H}_\mathrm{B}t} \hat{C} \hat{\rho}^\mathrm{eq}_\mathrm{B} | \psi_\varepsilon \rangle \\
&= \int d\varepsilon \, \mathrm{e}^{\mathbf{i}\varepsilon t} \, p_\varepsilon \langle \psi_\varepsilon | \hat{C}^\dagger \mathrm{e}^{-\mathbf{i}\hat{H}_\mathrm{B}t} | \psi_\varepsilon \rangle \ ,
\end{aligned} \tag{2.56}$$

with

$$\hat{\rho}^\mathrm{eq}_\mathrm{B} |\psi_\varepsilon\rangle \equiv p_\varepsilon |\psi_\varepsilon\rangle \ . \tag{2.57}$$

Since $\hat{\rho}_{\mathrm{B}}^{\mathrm{eq}}$ is a positive operator we have $p_\varepsilon \geq 0$. By using the completeness relation $\mathbb{1} = \int d\varepsilon' \, |\psi_{\varepsilon'}\rangle \langle\psi_{\varepsilon'}|$ we can show the positivity of $f(t)$

$$\begin{aligned} f(t) &= \int d\varepsilon d\varepsilon' e^{\mathbf{i}\varepsilon t} p_\varepsilon \langle\psi_\varepsilon| \hat{C}^\dagger \, \mathrm{e}^{-\mathbf{i}\hat{H}_{\mathrm{B}} t} |\psi_{\varepsilon'}\rangle \langle\psi_{\varepsilon'}| \hat{C} |\psi_\varepsilon\rangle \\ &= \int d\varepsilon d\varepsilon' e^{\mathbf{i}(\varepsilon-\varepsilon')t} p_\varepsilon \left| \langle\psi'_\varepsilon| \hat{C} |\psi_\varepsilon\rangle \right|^2 \geq 0 \,. \end{aligned} \tag{2.58}$$

With this result we can construct the positive semidefinite matrix that proves that $f(t)$ is of positive type. We take another arbitrary vector $\vec{w}$ and evaluate the inner product

$$\begin{aligned} (\vec{w}, \mathbf{f}\vec{w}) &= \sum_{ij} w_i^* f(t_i - t_j) w_j = \int d\varepsilon d\varepsilon' \sum_{ij} w_i^* e^{\mathbf{i}(\varepsilon-\varepsilon')(t_i - t_j)} w_j p_\varepsilon \left| \langle\psi'_\varepsilon| \hat{C} |\psi_\varepsilon\rangle \right|^2 \\ &= \int d\varepsilon d\varepsilon' \left| \sum_i w_i^* e^{\mathbf{i}(\varepsilon-\varepsilon')t_i} \right|^2 p_\varepsilon \left| \langle\psi'_\varepsilon| \hat{C} |\psi_\varepsilon\rangle \right|^2 \geq 0 \,, \end{aligned} \tag{2.59}$$

as the integrand is positive on the whole domain of integration.
According to Bochner's theorem the matrix $\gamma_{\alpha\beta}$ is positive semidefinite$(\vec{v}, \boldsymbol{\gamma}\vec{v}) \geq 0$.

2.7. Excursus: Quantum dynamical semigroups

In this section we want to introduce briefly the mathematical background of the Markovian evolution in the field of open quantum systems, in particular the general properties of the underlying dynamical maps. The reader may skip this section, but note that at the very end the most general form of a master equation that describes the Markovian dynamics of the reduced density matrix is presented. We recommend the books of Alicki and Lendi [48], Breuer and Petruccione [40] as well as the very recent review by Rivas and Huelga [47] for further reading.

A Banach space is a complete vector space with a norm $\|\cdot\|$. A space is complete if every Cauchy sequence converges in it. Let's consider the Banach space $\mathfrak{B}$ of the trace-class operators on a Hilbert space $\mathcal{H}$ that has a trace-norm $\|\cdot\|_1$, such that,

$$\| \hat{A} \|_1 = \mathrm{Tr}\left\{ \sqrt{\hat{A}^\dagger \hat{A}} \right\} = \mathrm{Tr}\left\{ \sqrt{\hat{A}^2} \right\}, \hat{A} \in \mathfrak{B} \,. \tag{2.60}$$

In the following we denote an operator $\hat{\rho} \in \mathfrak{B}$ as quantum state if it is positive-semidefinite, i.e.

$$\langle\psi| \hat{\rho} |\psi\rangle \geq 0 \,, \quad |\psi\rangle \in \mathcal{H} \,, \tag{2.61}$$

and it has trace one, which is - due to the positivity of its spectrum - equal to the trace norm. Briefly,

$$\hat{\rho} \in \mathfrak{B} \text{ is a quantum state } \iff \hat{\rho} \geq 0 \text{ and } \| \hat{\rho} \|_1 = 1 \,. \tag{2.62}$$

The set of quantum states is now denoted by $\bar{\mathfrak{B}}^+ \subset \mathfrak{B}$. where $\mathfrak{B}$ is actually the smallest linear space that contains $\bar{\mathfrak{B}}^+$.
Let's recall that we can extract the evolution of our subsystem of interest, labeled S, from the evolution of the entire system by taking the partial trace, namely

$$\hat{\rho}_{\mathrm{S}}(t_1) = \mathrm{Tr}_{\mathrm{B}} \left\{ \hat{U}(t_1, t_0) \, \hat{\rho}(t_0) \, \hat{U}^\dagger(t_1, t_0) \right\} . \tag{2.63}$$

We want to define dynamical maps. We introduce the map acting on $\mathcal{H}_\mathrm{S}$ that connects states of S at times t_0 and t_1

$$\mathcal{E}_{(t_1,t_0)} : \hat{\rho}_\mathrm{S}(t_0) \mapsto \hat{\rho}_\mathrm{S}(t_1) . \tag{2.64}$$

In general this dynamical maps depend not only on the global evolution $\hat{U}(t_1,t_0)$ and the properties of system B (the bath) but on the system S itself. We can resolve this problem by assuming initially uncorrelated product states $\hat{\rho}(t_0) = \hat{\rho}_\mathrm{S}(t_0) \otimes \hat{\rho}_\mathrm{B}(t_0)$ (Born assumption). Each dynamical map that is induced from an initial condition like this is called universal dynamical map (UDM). The UDM is given by

$$\hat{\rho}_\mathrm{S}(t_1) = \mathcal{E}_{(t_1,t_0)}[\hat{\rho}_\mathrm{S}(t_0)] = \sum_\alpha \hat{K}_\alpha(t_1,t_0)\,\hat{\rho}_\mathrm{S}\,\hat{K}_\alpha^\dagger(t_1,t_0) , \tag{2.65}$$

with $\sum_\alpha \hat{K}_\alpha^\dagger(t_1,t_0)\,\hat{K}_\alpha(t_1,t_0) = \mathbb{1}_\mathrm{S}$, which is fulfilled because the dynamical map is trace preserving $\mathrm{Tr}\left\{\mathcal{E}_{(t_1,t_0)}[\hat{\rho}_\mathrm{S}(t_0)]\right\} = \mathrm{Tr}\{\hat{\rho}_\mathrm{S}(t_1)\} = 1$ for any intial state $\hat{\rho}_\mathrm{S}(t_0)$. The dynamical maps are positive, i.e. $\mathcal{E}[\hat{A}]$ is positive for any positive $\hat{A}$ acting on the Hilbert space $\mathcal{H}_\mathrm{S}$. However, we require an even stronger property. Consider a second Hilbert space $\tilde{\mathcal{H}}$ of arbitrary dimensions. Then, if the combined operation $\mathcal{E}\otimes\mathbb{1}$ maps positive operators on the combined Hilbert space $\mathcal{H}_\mathrm{S}\otimes\tilde{\mathcal{H}}$ to positive operators then $\mathcal{E}$ is called completely positive. This is a reasonable condition as we can regard the dynamical map $\mathcal{E}\otimes\mathbb{1}$ as an operation that acts on the first of two separated systems while it does not influence the second one. Note that eq. (2.65) is often referred to as Kraus decomposition of a completely positive map [52]. Figure 2.1 shows the diagramatic representation of the UDM.

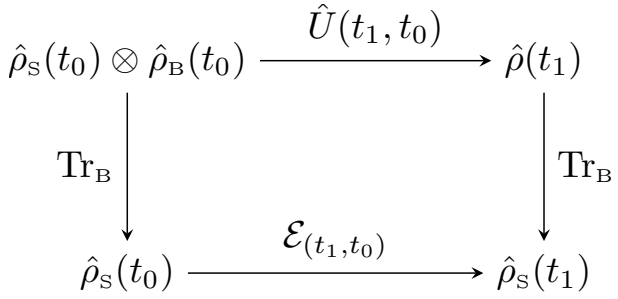

Figure 2.1.: Commutative diagram of the universal dynamical map (UDM).

Our focus is now on possible linear transitions on the Banach space $\mathfrak{B}$, namely $\mathcal{E}(\mathfrak{B}) : \mathfrak{B} \to \mathfrak{B}$. On the other hand, the set of this maps forms the dual space $\mathfrak{B}^*$ with the induced norm

$$\|\mathcal{E}\|_1 = \sup_{\hat{\rho}\in\mathfrak{B},\hat{\rho}\neq 0} \left\{ \frac{\|\mathcal{E}(\hat{\rho})\|_1}{\|\hat{\rho}\|_1} \right\} . \tag{2.66}$$

Of particular interest are of course the maps $\mathcal{E} \in \mathfrak{B}^*$ that leave the subset $\bar{\mathfrak{B}}^+$ invariant, i.e. that connects a quantum state with another quantum state. In fact Kossakowski [53] showed that this is fulfilled if and only if $\mathcal{E}$ preserves the trace and is a contraction on $\mathfrak{B}$, that is defined as a map whose norm is $\|\mathcal{E}\|_1 \leq 1$.
One last requirement is to be met in order describe Markovian dynamics, which as already known from classical Markovian processes described by the Chapman-Kolmogorov equation (compare [40]). This requirement states that in a Markov process a random variable X which depends on a parameter t (identified with time) and takes a value x_n at any arbitrary time t_n is

conditioned only by the value x_{n-1} that it took at time t_{n-1} but does not depend on the values at earlier times.
In the quantum version this can be expressed such that maps $\mathcal{E}$ that act as propagators for an evolution of $\hat{\rho}$ form a quantum dynamical semigroup.
The dynamical maps $\{\mathcal{E}_\tau | \tau \geq 0\}$ constitute a one-parameter family, where $\tau = t_2 - t_1$ and where the identity map is $\mathcal{E}_0 = \mathbb{1}$ and that has the property

$$\mathcal{E}_{(t_2,t_0)} = \mathcal{E}_{(t_2,t_1)} \mathcal{E}_{(t_1,t_0)} \,. \tag{2.67}$$

The latter can be written in terms of time differences, which yields

$$\mathcal{E}_{\tau_1+\tau_2} = \mathcal{E}_{\tau_2} \mathcal{E}_{\tau_1} \,. \tag{2.68}$$

Note that this defines only a semigroup, as in general the inverse elements are not UDMs. That is due to the fact that a general $\mathcal{E}_{(t_1,t_0)}$ can be inverted only a by unitary map, which is not always the case.
In conclusion a quantum system undergoes a Markovian evolution if it is described by a contractive evolution family on $\mathfrak{B}$ where eq. (2.67) holds.
Now we can show that there exists a linear map, called a generator of a semigroup, compare [48], such that

$$\frac{\partial}{\partial t} \hat{\rho}_\mathrm{S}(t) = \lim_{\epsilon \to 0} \frac{\hat{\rho}_\mathrm{S}(t+\epsilon) - \hat{\rho}_\mathrm{S}(t)}{\epsilon} = \lim_{\epsilon \to 0} \frac{\left(\mathcal{E}_{(t+\epsilon,t)} - \mathbb{1}\right)[\hat{\rho}_\mathrm{S}(t)]}{\epsilon} = \hat{\mathcal{L}}_t [\hat{\rho}_\mathrm{S}(t)] \,. \tag{2.69}$$

We now define the most general form of $\hat{\mathcal{L}}_t$ along the lines of [40, 47, 48]. If $\mathcal{E}_{(t_2,t_1)}$ is a UDM for any $t_2 \geq t_1$ it can be decomposed as in eq. (2.65). Let $\{\hat{F}_j, j = 1, \ldots, N^2\}$ be a complete orthonormal basis with respect to the Hilber-Schmidt inner product $(\hat{F}_j, \hat{F}_k) = \delta_{jk}$ where we choose $\hat{F}_{N^2} = \mathbb{1}_\mathrm{S}/\sqrt{N}$, which implies that the rest of the operators is traceless. Therefore, the Kraus operators can be rewritten in this basis

$$\mathcal{E}_{(t_2,t_1)}[\hat{\rho}_\mathrm{S}(t_0)] = \sum_{j,k} c_{jk}(t_2,t_1)\, \hat{F}_j\, \hat{\rho}_\mathrm{S}\, \hat{F}_k^\dagger \,, \tag{2.70}$$

with the coefficients

$$c_{jk}(t_2,t_1) = \sum_\alpha (\hat{F}_j, \hat{K}_\alpha(t_2,t_1))(\hat{F}_k, \hat{K}_\alpha(t_2,t_1))^* \,. \tag{2.71}$$

These coefficients form a positive semidefinite matrix $\mathbf{c}(t_2,t_1)$, which is easy to prove by taking a N^2 vector $\vec{v}$ and evaluating the inner product

$$(\vec{v}, \mathbf{c}(t_2,t_1)\vec{v}) = \sum_{j,k} v_j^* c_{jk}(t_2,t_1) v_k = \sum_\alpha \left| \left(\sum_k v_k (\hat{F}_k, \hat{K}_\alpha(t_2,t_1)) \right) \right|^2 \geq 0 \,. \tag{2.72}$$

This is valid for all $t_2 \geq t_1$. When we substitute $t_1 \to t$ and $t_2 \to t + \epsilon$ the generator reads

$$\begin{aligned}
\hat{\mathcal{L}}_t[\hat{\rho}_\mathrm{S}] &= \lim_{\epsilon \to 0} \sum_{j,k} \frac{c_{jk}(t+\epsilon,t)\, \hat{F}_j\, \hat{\rho}_\mathrm{S}\, \hat{F}_k^\dagger + \mathbb{1}_\mathrm{S}}{\epsilon} \\
&= \lim_{\epsilon \to 0} \Bigg[\frac{1}{N} \frac{c_{N^2N^2}(t+\epsilon,t) - N}{\epsilon} \hat{\rho}_\mathrm{S} + \sum_{j,k=1}^{N^2-1} \frac{c_{jk}(t+\epsilon,t)}{\epsilon} \hat{F}_j\, \hat{\rho}_\mathrm{S}\, \hat{F}_k^\dagger \\
&\qquad + \frac{1}{\sqrt{N}} \sum_{j=1}^{N^2-1} \left(\frac{c_{jN^2}(t+\epsilon,t) - N}{\epsilon} \hat{F}_j\, \hat{\rho}_\mathrm{S} + \frac{c_{N^2j}(t+\epsilon,t) - N}{\epsilon} \hat{\rho}_\mathrm{S}\, \hat{F}_j^\dagger \right) \Bigg] .
\end{aligned} \tag{2.73}$$

We now identify the new coefficients $a_{jk}(t)$ by

$$\begin{aligned} a_{N^2N^2}(t) &= \lim_{\epsilon\to 0}\frac{c_{N^2N^2}(t+\epsilon,t)-N}{\epsilon}\,,\\ a_{jN^2}(t) &= \lim_{\epsilon\to 0}\frac{c_{jN^2}(t+\epsilon,t)}{\epsilon}\,, j=1,\ldots,N^2-1\,,\\ a_{jk}(t) &= \lim_{\epsilon\to 0}\frac{c_{jk}(t+\epsilon,t)}{\epsilon}\,, j,k=1,\ldots,N^2-1\,, \end{aligned} \tag{2.74}$$

and introduce the operators

$$\begin{aligned} \hat{F}(t) &= \frac{1}{\sqrt{N}}\sum_{j=1}^{N^2-1} a_{jN^2}(t)\,\hat{F}_j\,,\\ \hat{G}(t) &= \frac{a_{N^2N^2}}{2N}\mathbb{1}_{\mathrm{S}} + \frac{1}{2}\left(\hat{F}^\dagger(t)+\hat{F}(t)\right),\\ \hat{H}(t) &= \frac{1}{2\mathbf{i}}\left(\hat{F}^\dagger(t)-\hat{F}(t)\right). \end{aligned} \tag{2.75}$$

In terms of these operators the generator yields

$$\hat{\mathcal{L}}_t[\hat{\rho}_{\mathrm{S}}] = -\mathbf{i}\left[\hat{H}(t),\hat{\rho}_{\mathrm{S}}\right] + \left\{\hat{G}(t),\hat{\rho}_{\mathrm{S}}\right\} + \sum_{j,k=1}^{N^2-1} a_{jk}(t)\,\hat{F}_j\,\hat{\rho}_{\mathrm{S}}\,\hat{F}_k^\dagger\,. \tag{2.76}$$

This equation can be even more compactly rephrased by taking into account that the generator preserves the trace, $\mathrm{Tr}\left\{\hat{\mathcal{L}}_t[\hat{\rho}_{\mathrm{S}}]\right\}=0$,

$$\hat{\mathcal{L}}_t[\hat{\rho}_{\mathrm{S}}] = -\mathbf{i}\left[\hat{H}(t),\hat{\rho}_{\mathrm{S}}\right] + \sum_{j,k=1}^{N^2-1} a_{jk}(t)\left(\hat{F}_j\,\hat{\rho}_{\mathrm{S}}\,\hat{F}_k^\dagger - \frac{1}{2}\left\{\hat{F}_k^\dagger\,\hat{F}_j\,,\hat{\rho}_{\mathrm{S}}\right\}\right). \tag{2.77}$$

The matrix $(a_{jk})(t)$ is, like $(c_{jk})(t+\epsilon,t)$, positive semidefinite. Therefore, we can diagonalize it for any time t by using a unitary matrix $\mathbf{u}(t)$,

$$\sum_{j,k} u_{mj}(t)a_{jk}(t)u^*_{nk}(t) = \gamma_m(t)\delta_{mn}\,. \tag{2.78}$$

Each eigenvalue of the diagonal matrix is positive at all times $\gamma_m(t)\geq 0$. With the operators $\hat{L}_k(t)$

$$\hat{L}_k(t) = \sum_{j=1}^{N^2-1} u^*_{kj}\,\hat{F}_j(t)\,,\quad \hat{F}_j = \sum_{j=1}^{N^2-1} u_{kj}\,\hat{L}_k(t)\,. \tag{2.79}$$

we can eventually write the diagonal form of the generator

$$\hat{\mathcal{L}}_t[\hat{\rho}_{\mathrm{S}}] = -\mathbf{i}\left[\hat{H}(t),\hat{\rho}_{\mathrm{S}}\right] + \sum_{k=1}^{N^2-1}\gamma_k(t)\left(\hat{L}_k(t)\,\hat{\rho}_{\mathrm{S}}\,\hat{L}_k^\dagger(t) - \frac{1}{2}\left\{\hat{L}_k^\dagger(t)\,\hat{L}_k(t),\hat{\rho}_{\mathrm{S}}\right\}\right). \tag{2.80}$$

with $\gamma_k(t)\geq 0, \forall k,t$ and $\hat{H}(t)$ is self-adjoint.
When the problem is time-homogeneous, i.e. the dynamical maps depend merely on time-differences τ than the generator becomes time-independent, with $\mathcal{E}_\tau = \exp[\hat{\mathcal{L}}\,\tau]$. That was proven

by Kossakowski [53] for finite dimensional semigroups and by Lindblad for inifinite dimensional semigroups [54], which is why the most general generator of the Markovian dynamics,

$$\hat{\mathcal{L}}\left[\hat{\rho}_{\mathrm{S}}\right] = -\mathbf{i}\left[\hat{H}\,,\hat{\rho}_{\mathrm{S}}\right] + \sum_{k=1}^{N^2-1}\gamma_k\left(\hat{L}_k\,\hat{\rho}_{\mathrm{S}}\,\hat{L}_k^{\dagger} - \frac{1}{2}\left\{\hat{L}_k^{\dagger}\,\hat{L}_k\,,\hat{\rho}_{\mathrm{S}}\right\}\right), \tag{2.81}$$

is called Lindblad master equation.
In section 2.6.1 we have shown, that the matrix $\gamma_{\alpha\beta}$ is positive semidefinite and, therefore, (2.49) has Lindblad form.

2.8. Effective rate equations

The shape of the Lindblad operators $\hat{L}_{ab}$ in (2.49) suggest evaluation in the eigenbasis. Let's assume an orthogonal eigenbasis and that the eigenvalues are nondegenerate. If we compute the matrix elements $\rho_{nm} = \langle n|\,\hat{\boldsymbol{\rho}}_{\mathrm{S}}\,|m\rangle$ the commutator in (2.49) vanishes.

$$\begin{aligned}\dot{\rho}_{nm} &= \sum_{abcd}\gamma_{ab,cd}\left[\delta_{n,c}\delta_{b,m}\rho_{da} - \frac{1}{2}\delta_{b,c}\left\{\delta_{n,a}\rho_{dm},\delta_{m,d}\rho_{na}\right\}\right]\\ &= \sum_{a,d}\gamma_{am,nd}\rho_{da} - \frac{1}{2}\sum_{a,b}\left[\gamma_{nb,ba}\rho_{am} + \gamma_{ab,bm}\rho_{na}\right].\end{aligned} \tag{2.82}$$

Taking into account the definition for the rates, eq. (2.51), further simplification follows straightforwardly

$$\dot{\rho}_{nm} = \sum_{ab}\gamma_{bm,na}\rho_{ab} - \frac{1}{2}\sum_{b}\left[\gamma_{nb,bn} + \gamma_{mb,bm}\right]\rho_{nm}\,. \tag{2.83}$$

We now consider only the populations, which decouple from the coherences. They read

$$\dot{\rho}_{nn} = \sum_{b}\left[\gamma_{bn,nb}\rho_{bb} - \gamma_{nb,bn}\rho_{nn}\right], \tag{2.84}$$

and the respective rates

$$\gamma_{nb,bn} = \sum_{\alpha\beta}\gamma_{\alpha\beta}(\omega_{nb})\,\langle n|\,\hat{A}_{\alpha}\,|b\rangle\,\langle b|\,\hat{A}_{\beta}\,|n\rangle\,, \tag{2.85}$$

are nonnegative. $\gamma_{nb,bn}$ are the diagonal elements of the rate matrix $\gamma_{ab,cd}$, therefore the effective rate equations (2.84) also preserve the positivity of the density matrix. As the equations for the populations are decoupled from those for the coherences, the steady-states are determined by the dynamics of the populations only, since the coherences decay in the limit of long times.

2.9. Liouville space

The Lindblad master equation (2.81) is often written in a form analogous to the Schrödinger equation, namely

$$\frac{\partial}{\partial t}\,\hat{\rho}_{\mathrm{S}} = \hat{\mathcal{L}}\left[\hat{\rho}_{\mathrm{S}}\right]. \tag{2.86}$$

The generator of the Markovian dynamics is a so called Liouville super-operator $\hat{\mathcal{L}}[\hat{\rho}_\mathrm{S}]$ acting on the system density operator. We can define it (compare (2.54)) as

$$\hat{\mathcal{L}}[\hat{\rho}_\mathrm{S}] = \sum_{abcd} \gamma_{ab,cd}\Big[\,\hat{L}_{cd}\,\hat{\rho}_\mathrm{S}\,\hat{L}_{ba}^\dagger - \frac{1}{2}\Big\{\hat{L}_{ba}^\dagger\,\hat{L}_{cd}\,,\hat{\rho}_\mathrm{S}\Big\}\Big]\,. \tag{2.87}$$

The Liouville super-operator is linear with respect to $\hat{\rho}_\mathrm{S}$. For convenience one can switch to the Liouville space representation, in which the system density matrix is rearranged as a vector, $\hat{\rho}_\mathrm{S} \to \vec{\rho}_\mathrm{S}$ and hence the Liouvillian super-operator can be represented by a matrix. If the considered system has dimension d the vector $\vec{\rho}_\mathrm{S}$ has d^2 entries and the Liouvillian super-operator is represented by the $(d^2 \times d^2)$-rate matrix $\mathcal{W}$, which can have complex eigenvalues and is in general not self-adjoint.
The elements of the density matrix are rearranged in a specific ordering in a vector, commonly populations followed by coherences.

$$\hat{\rho}_\mathrm{S} = \begin{pmatrix} \rho_{11} & \cdots & \rho_{1d} \\ \vdots & \ddots & \vdots \\ \rho_{d1} & \cdots & \rho_{dd} \end{pmatrix} \Rightarrow \vec{\rho}_\mathrm{S} = \begin{pmatrix} \rho_{11} \\ \vdots \\ \rho_{dd} \\ \rho_{12} \\ \vdots \\ \rho_{dd-1} \end{pmatrix}. \tag{2.88}$$

This ordering is not unique. However, with this choice the rate matrix, which corresponds to Eq. (2.83), assumes block form if the spectrum of the system is nondegenerate as the dynamics of occupations and coherences decouple.
For the sake of simplicity we omit the vector-notation from now on and simply write ρ_S. In this convenient representation the evolution of the reduced system density matrix reads

$$\frac{\partial}{\partial t}\rho_\mathrm{S} = \mathcal{W}\rho_\mathrm{S}\,, \tag{2.89}$$

which can formally be solved by the matrix exponential

$$\rho_\mathrm{S}(t) = \mathrm{e}^{\mathcal{W}t}\,\rho_\mathrm{S}(0)\,. \tag{2.90}$$

In general it is rather difficult to find analytic solutions to the matrix exponentials since the Liouvillian is nonhermitian and has no spectral decomposition. Nonetheless, for systems that can be described by effective rate equations (2.84) the Liouvillian assumes block form with at least two decoupled blocks; $\mathcal{W}^\mathrm{pop}$ that contains the transition rates for the occupations and $\mathcal{W}^\mathrm{coh}$ for the coherences. Than the matrix exponential for the occupations only can be calculated by $\exp[\mathcal{W}^\mathrm{pop}]$, which is in general much easier than calculating the full expression.
The matrix elements of the population block $\mathcal{W}^\mathrm{pop}$ are given by

$$\mathcal{W}_{nn}^\mathrm{pop} = \gamma_{nn,nn} - \sum_b \gamma_{nb,bn}\,, \qquad \mathcal{W}_{nm}^\mathrm{pop} = \gamma_{nm,mn}\,, \qquad (m \neq n)\,. \tag{2.91}$$

It is straightforward to show the following trace preserving property

$$\sum_n \mathcal{W}_{nm}^\mathrm{pop} = 0\,. \tag{2.92}$$

2.9.1. Multiple reservoirs

Formally, the master equation is not changed for multiple noninteracting reservoirs. The methods and quantities we introduced above can be generalized to multiple reservoir setups, i.e. each reservoir is equipped with an index ν and will be characterized by its corresponding thermal equilibrium state $\hat{\rho}_{\mathrm{B}}^{\mathrm{eq},(\nu)}$ with its respective chemical potential μ_ν and inverse temperature β_ν. The total Liouvillian (the total rate matrix) can be decomposed as a sum over the respective single reservoir Liouvillians

$$\mathcal{W} = \sum_{\nu} \mathcal{W}^{(\nu)} \,. \tag{2.93}$$

2.10. Conditional master equations

One point of particular interest in system-bath theories is the exchange of particle and/or energy between the system of interest and one or more reservoirs. Moreover, one often finds that the combined system obeys conservation laws, the most prominent of which are particle number and energy conservation, obviously. On the other hand, particle number and energy conservation imply that the loss of particles and/or quanta of energy in the system is accompanied by a gain in the respective reservoirs, except for generic pure dephasing models [55, 56]. As a consequence, counting or tracking of particles/energy quanta that leave or enter the respective reservoir is sufficient to characterize the flow of particles and energy, respectively.
As the contributions due to the coupling to different reservoirs are additive, it is possible to uniquely identify to which reservoir they belong. Therefore, it is sufficient to consider just one bath, as we can – without loss of generality – generalize the obtained results.

Our starting point to resolve the particle numbers and energy quanta exchanged between the considered system and a bath is to rewrite the rate equation (2.89), where we keep only track of the occupations, as a set of rate equation for the probabilities p_i to find the system in state $|i\rangle$, which reads

$$\dot{p}_i = \sum_j \mathcal{W}_{ij} p_j \,. \tag{2.94}$$

We find the change of the probability during the small time interval dt, accordingly,

$$dp_i = \sum_j \mathcal{W}_{ij} p_j dt \,, \tag{2.95}$$

where $\mathcal{W}_{ij} p_j dt$ expresses the probability to reach state $|i\rangle$ during dt from an initial state $|j\rangle$ invoked by the action of the (jump) operator $\mathcal{W}_{ij}$. Summing over this probabilities yields the total change of the probability p_i. Due to the conservation of energy and the number of particles, the transitions between states $|j\rangle$ and $|i\rangle$ are accompanied by the exchange of $\Delta n_{ij} = n_i - n_j; n_i \in \mathbb{Z}$ particles and a certain amount of energy $\Delta E_{ij} = E_i - E_j$ between system and the reservoir. In the following we denote the probability to find the system in state $|i\rangle$ – given that n particles and the energy E have been transported to the reservoir – by $p_i^{(n,E)}$. The probability without any information about the prior transfers is then, obviously

$$p_i = \sum_{n=-\infty}^{\infty} \sum\!\!\!\!\!\!\int_{E=-\infty}^{\infty} p_i^{(n,E)} \,. \tag{2.96}$$

We can now relate the conditional probabilities $p_i^{(n,E)}$ to eq. (2.95) and deduce the rate equation

$$dp_i^{(n,E)} = \sum_j \mathcal{W}_{ij}^{(\Delta n_{ij},\Delta E_{ij})} p_j^{(n+\Delta n_{ij},E+\Delta E_{ij})} dt\,. \tag{2.97}$$

This equation is to be interpreted in the following way: the system is in an initial state $|j\rangle$ with n_j particles and an energy E_j while the reservoir has $n+\Delta n_{ij}$ excess particles and an energy of $E+\Delta E_{ij}$. When a jump to state $|i\rangle$ takes place Δn_{ij} particles and the transition energy ΔE_{ij} are exchanged with the bath.
In the following we want to take into account only the transitions where no particles or one particle is transferred, i.e. we explicitly neglect co- and pair tunneling processes, which holds for the transport setups considered throughout this work. The transition energy for a single jump is in general not restricted, as long as the transition $|j\rangle \to |i\rangle$ is allowed.
In conclusion, when taking into account all system states we obtain the conditional master equation

$$\frac{d}{dt}\rho_{\mathrm{S}}^{(n,E)}(t) = \mathcal{W}_0\rho_{\mathrm{S}}^{(n,E)}(t) + \sum_{\Delta E}\left(\mathcal{J}_{\Delta E}^{+}\rho_{\mathrm{S}}^{(n-1,E-\Delta E)}(t) + \mathcal{J}_{\Delta E}^{-}\rho_{\mathrm{S}}^{(n+1,E+\Delta E)}(t)\right). \tag{2.98}$$

This master equation describes the evolution of the system density operator $\rho_{\mathrm{S}}^{(n,E)}$ provided that n particles and an amount of energy E has been exchanged with the reservoir. The operator $\mathcal{W}_0$ describes the dynamics of the system that don't involve any particle or energy exchange with the monitored bath, while the operators $\mathcal{J}_{\Delta E}^{\pm}$ cause the hopping of a single particle and the transfer of an energy ΔE between the reservoir and the system. The summation takes into account all possible energy transitions ΔE between system states.
As, in general, the amount of transferred particles and energy is not constrained Eq.(2.98) yields an infinite set of equations for the density matrix. Furthermore, we note that the evolution and jump operators $\mathcal{W}_0$ and $\mathcal{J}^{\pm}$ do neither depend on n nor E, which suggests to simplify the set of equations by suitable Fourier transformations with respect to n and E. For n we obviously have to choose a discrete Fourier transformation. For the transition energies we can choose both discrete or continuous Fourier transformation. The continuous Fourier transformation is justified where the possible transition energies lie dense if we consider a large number of jump processes. However, in this work we have systems where only few different jump processes happen and the transition energies are sharp. Therefore, we use

$$\rho_{\mathrm{S}}(\chi,\eta,t) = \sum_{n=-\infty}^{\infty}\int_{E=-\infty}^{\infty} dE\,\rho_{\mathrm{S}}^{(n,E)}(t)\,\mathrm{e}^{\mathbf{i}(n\chi+E\eta)}\,. \tag{2.99}$$

Its inverse Fourier transformation reads

$$\rho_{\mathrm{S}}^{(n,E)}(t) = \left(\frac{1}{2\pi}\right)^2\int_{-\pi}^{\pi} d\chi\int_{-\infty}^{\infty} d\eta\,\rho_{\mathrm{S}}(\chi,\eta,t)\,\mathrm{e}^{-\mathbf{i}(n\chi+E\eta)}\,. \tag{2.100}$$

The set of equations, (2.98), is transformed to a single equation by applying the Fourier transform (2.99), which yields

$$\begin{aligned}\frac{\partial}{\partial t}\rho_{\mathrm{S}}(\chi,\eta,t) &= \left\{\mathcal{W}_0 + \sum_{\Delta E}\left[\mathcal{J}_{\Delta E}^{+}\,\mathrm{e}^{+\mathbf{i}(\chi+\Delta E\eta)} + \mathcal{J}_{\Delta E}^{-}\,\mathrm{e}^{-\mathbf{i}(\chi+\Delta E\eta)}\right]\right\}\rho_{\mathrm{S}}(\chi,\eta,t)\\ &= \mathcal{W}(\chi,\eta)\rho_{\mathrm{S}}(\chi,\eta,t)\,.\end{aligned} \tag{2.101}$$

As additional terminals enter additively we can write the multiterminal differential equation

$$\frac{\partial}{\partial t}\rho_{\mathrm{S}}(\vec{\chi},\vec{\eta},t) = \mathcal{W}(\vec{\chi},\vec{\eta})\rho_{\mathrm{S}}(\vec{\chi},\vec{\eta},t)\,. \tag{2.102}$$

Here the vectors $\vec{\chi} = (\chi_1,\ldots,\chi_N)$ and $\vec{\eta} = (\eta_1,\ldots,\eta_N)$ contain the particle and energy counting fields for all reservoirs.
Equation (2.102) is formally solved by

$$\rho_{\mathrm{S}}(\vec{\chi},\vec{\eta},t) = \mathrm{e}^{\mathcal{W}(\vec{\chi},\vec{\eta})t}\,\rho_{\mathrm{S}}(\vec{\chi},\vec{\eta},0)\,. \tag{2.103}$$

In the following section we want to discuss the meaning of the counting fields in more detail.

2.11. Full counting statistics

Up to now we have derived the equations describing the dynamics of probabilities that are conditioned on the number of particles and the amount of energy quanta exchanged with the environment. The information that is contained in these probability distributions is closely related to measurable transfer events in nonequilibrium between a system and its environment. Recent experiments showed that it is possible to track the tunneling of single electrons through mesoscopic structures in real-time [28, 57, 58, 59].
These real-time techniques allow for precise measurements of the statistical distribution of the number of transferred charges, the so-called full counting statistics [60].
Typically, one is not interested in the internal state of the system but in the exchange processes, which gives rise to a probability distribution

$$p^{(\vec{n},\vec{E})}(t) = \sum_i p_i^{(\vec{n},\vec{E})}(t) = \mathrm{Tr}\left\{\rho^{(\vec{n},\vec{E})}(t)\right\}\,. \tag{2.104}$$

The inverse Fourier transformation, eq. (2.100), can be generalized for setups with M terminals, which relates the $p^{(\vec{n},\vec{E})}(t)$ to the particle and energy counting fields

$$p^{(\vec{n},\vec{E})}(t) = \left(\frac{1}{2\pi}\right)^{2M}\int_{-\pi}^{+\pi} d\chi_1\ldots d\chi_M \int_{-\infty}^{+\infty} d\eta_1\ldots\eta_M\,\mathrm{Tr}\left\{\mathrm{e}^{\mathcal{W}(\vec{\chi},\vec{\eta})t}\,\rho_{\mathrm{S}}(\vec{\chi},\vec{\eta},0)\right\}\mathrm{e}^{-\mathbf{i}(\vec{n}\vec{\chi}+\vec{E}\vec{\eta})}\,. \tag{2.105}$$

The moments of the probability distribution are given by derivatives with respect to the counting fields. We define the moment generating function (MGF) $\mathfrak{M}$

$$\mathfrak{M}(\vec{\chi},\vec{\eta},t) \equiv \mathrm{Tr}\left\{\rho_{\mathrm{S}}(\vec{\chi},\vec{\eta},t)\right\} = \mathrm{Tr}\left\{\mathrm{e}^{\mathcal{W}(\vec{\chi},\vec{\eta})t}\,\rho_{\mathrm{S}}(\vec{\chi},\vec{\eta},0)\right\}\,, \tag{2.106}$$

and calculate moments of particle and energy distributions

$$\left\langle\vec{n}^k(t)\right\rangle = \sum_{\vec{n}}\vec{n}^k p^{(\vec{n},\vec{E})}(t) = (-\mathbf{i}\partial_{\vec{\chi}})^k\,\mathfrak{M}(\vec{\chi},\vec{\eta},t)\Big|_{\vec{\chi}=\vec{\eta}=0}\,, \tag{2.107}$$

$$\left\langle\vec{E}^k(t)\right\rangle = \int d\vec{E}\vec{E}^k p^{(\vec{n},\vec{E})}(t) = (-\mathbf{i}\partial_{\vec{\eta}})^k\,\mathfrak{M}(\vec{\chi},\vec{\eta},t)\Big|_{\vec{\chi}=\vec{\eta}=0}\,. \tag{2.108}$$

On the other hand, one can recover the probability distributions by taking the Fourier transforms of the MGF.

Thus, the full particle and energy distributions for a single reservoir ν read

$$p_n^{(\nu)}(t) = \frac{1}{2\pi}\int_{-\pi}^{\pi} d\chi_\nu \mathfrak{M}(\vec{\chi},\vec{\eta},t)\,\mathrm{e}^{-\mathbf{i}n\chi_\nu}\Big|_{\vec{\chi}=\vec{\eta}=\vec{0}}, \tag{2.109}$$

$$p_E^{(\nu)}(t) = \frac{1}{2\pi}\int_{-\infty}^{\infty} d\eta_\nu \mathfrak{M}(\vec{\chi},\vec{\eta},t)\,\mathrm{e}^{-\mathbf{i}E\eta_\nu}\Big|_{\vec{\chi}=\vec{\eta}=\vec{0}}. \tag{2.110}$$

The most simple characterization of nonequilibrium processes is to investigate the particle (matter) and energy currents; i.e. to calculate the time derivatives of the first moments. Therefore, the particle (M) and energy (E) currents yield

$$I_{\mathrm{M}}^{(\nu)} = \langle \dot{n}\rangle_\nu = -\mathbf{i}\frac{d}{dt}\frac{\partial}{\partial\chi_\nu}\mathfrak{M}(\vec{\chi},\vec{\eta},t)\Big|_{\vec{\chi}=\vec{\eta}=\vec{0}} = -\mathbf{i}\mathrm{Tr}\left\{\frac{\partial}{\partial\chi_\nu}\dot{\rho}_{\mathrm{S}}(\vec{\chi},\vec{\eta},t)\right\}\Big|_{\vec{\chi}=\vec{\eta}=\vec{0}}, \tag{2.111}$$

$$I_{\mathrm{E}}^{(\nu)} = \langle \dot{E}\rangle_\nu = -\mathbf{i}\frac{d}{dt}\frac{\partial}{\partial\eta_\nu}\mathfrak{M}(\vec{\chi},\vec{\eta},t)\Big|_{\vec{\chi}=\vec{\eta}=\vec{0}} = -\mathbf{i}\mathrm{Tr}\left\{\frac{\partial}{\partial\eta_\nu}\dot{\rho}_{\mathrm{S}}(\vec{\chi},\vec{\eta},t)\right\}\Big|_{\vec{\chi}=\vec{\eta}=\vec{0}}. \tag{2.112}$$

It is now straightforward to obtain the higher moments of the distributions that disclose information about variance, skewness and kurtosis. For simple structures, e.g., the tunneling through single quantum dots, the higher moments are even accessible in experiments [58, 59], although in general this is more complicated.

2.11.1. Steady-state currents

We now want to investigate setups with more than one reservoir connected to the same system of interest, which can lead to the formation of nonvanishing steady-state currents. They arise from nonequilibrium steady-states, that the system runs into in the limit of long times. Its properties are useful to gain more information about the physical properties of the system or they might be used to perform work in terms of thermoelectric devices.
In the next sections we want to discuss in more detail the nonequilibrium properties.
To begin with, however, we just want to derive the simplest characterization of the steady-state: the steady-state currents.
The first step is to determine the steady-state density matrix $\bar{\rho}_{\mathrm{S}}$. With eq. (2.102) we can define

$$\frac{\partial}{\partial t}\bar{\rho}_{\mathrm{S}} = 0 = \mathcal{W}(\vec{0},\vec{0})\bar{\rho}_{\mathrm{S}} \tag{2.113}$$

where it is necessary to require normalization of the steady-state density matrix, i.e. $\mathrm{Tr}\{\bar{\rho}_{\mathrm{S}}\} = 1$. Thus, the steady-state of the system is uniquely defined, given the system under consideration is not bistable.
With the above definition, eq. (2.106), the MGF reads in the limit of long times

$$\lim_{t\to\infty}\mathfrak{M}(\vec{\chi},\vec{\eta},t) = \mathrm{Tr}\left\{\mathrm{e}^{\mathcal{W}(\vec{\chi},\vec{\eta})t}\,\bar{\rho}_{\mathrm{S}}\right\}. \tag{2.114}$$

Then, the steady-state currents with respect to the reservoir ν follow directly. We obtain

$$\begin{aligned}
\bar{I}_{\mathrm{M}}^{(\nu)} &= -\mathbf{i}\frac{\partial}{\partial\chi_\nu}\mathrm{Tr}\left\{\frac{d}{dt}\,\mathrm{e}^{\mathcal{W}(\vec{\chi},\vec{\eta})t}\,\bar{\rho}_{\mathrm{S}}\right\}\Big|_{\vec{\chi}=\vec{\eta}=\vec{0}} = -\mathbf{i}\frac{\partial}{\partial\chi_\nu}\mathrm{Tr}\left\{\mathcal{W}(\vec{\chi},\vec{\eta})\,\mathrm{e}^{\mathcal{W}(\vec{\chi},\vec{\eta})t}\,\bar{\rho}_{\mathrm{S}}\right\}\Big|_{\vec{\chi}=\vec{\eta}=\vec{0}} \\
&= -\mathbf{i}\mathrm{Tr}\left\{\left[\frac{\partial}{\partial\chi_\nu}\mathcal{W}(\vec{\chi},\vec{\eta})\Big|_{\vec{\chi}=\vec{\eta}=\vec{0}}\right]\mathrm{e}^{(\mathcal{W}\vec{0},\vec{0})t}\,\bar{\rho}_{\mathrm{S}}\right\} - \mathbf{i}\mathrm{Tr}\left\{\mathcal{W}(\vec{0},\vec{0})\left[\frac{\partial}{\partial\chi_\nu}\,\mathrm{e}^{\mathcal{W}(\vec{\chi},\vec{\eta})t}\,\bar{\rho}_{\mathrm{S}}\Big|_{\vec{\chi}=\vec{\eta}=\vec{0}}\right]\right\} \\
&= -\mathbf{i}\mathrm{Tr}\left\{\left(\frac{\partial}{\partial\chi_\nu}\mathcal{W}(\vec{\chi},\vec{\eta})\Big|_{\vec{\chi}=\vec{\eta}=\vec{0}}\right)\bar{\rho}_{\mathrm{S}}\right\} = -\mathbf{i}\mathrm{Tr}\left\{\frac{\partial}{\partial\chi_\nu}\mathcal{W}(\vec{\chi},\vec{\eta})\bar{\rho}_{\mathrm{S}}\right\}\Big|_{\vec{\chi}=\vec{\eta}=\vec{0}},
\end{aligned} \tag{2.115}$$

where we used the properties $\mathrm{Tr}\left\{\mathcal{W}(\vec{0},\vec{0})\,\hat{\sigma}\right\} = 0$ for all operators $\hat{\sigma}$ and $\mathrm{e}^{\mathcal{W}(\vec{0},\vec{0})t}\,\bar{\rho}_{\mathrm{S}} = \bar{\rho}_{\mathrm{S}}$.
The steady-state energy current can be calculated analogously and we obtain

$$\bar{I}_{\mathrm{E}}^{(\nu)} = -\mathbf{i}\mathrm{Tr}\left\{\frac{\partial}{\partial\eta_\nu}\mathcal{W}(\vec{\chi},\vec{\eta})\bar{\rho}_{\mathrm{S}}\right\}\Big|_{\vec{\chi}=\vec{\eta}=\vec{0}}. \tag{2.116}$$

The steady-state currents have to comply with the conservation of total particle number and the total energy in the full system, which implies

$$\sum_\nu \bar{I}_{\mathrm{M}}^{(\nu)} = \sum_\nu \bar{I}_{\mathrm{E}}^{(\nu)} = 0\,. \tag{2.117}$$

2.12. Entropy production

In this section we want to shed some light onto the concepts of stochastic thermodynamics. Classical thermodynamics deals with the general laws governing the transformations in a system, mainly the exchange of heat, work and matter with the respective environment. The microscopic justification for the thermodynamic characterization comes from equilibrium statistical mechanics. One central result is that in any process the entropy never decreases. Classical thermodynamics are concerned with time-dependent phenomena close to equilibrium, that relax towards a thermal equilibrium.
On the contrary, in stochastic thermodynamics one deals with small systems far from thermal equilibrium that do not thermalize, which means that their probability currents do not vanish even if the system reaches a steady-state, which is called nonequilibrium steady-state (NESS) [61, 62]. Such systems typically need external driving forces that prevent them from thermalizing. Of particular interest is driving with time-independent external forces, where NESS are reached. For this class of systems strong results exist: temperatures remain well-defined and if there is a clear time scale separation between the degrees of freedom in slow systems and the very fast ones in the reservoirs, such situations allow for a consistent thermodynamical description.
We consider systems in contact with a number of reservoirs ν, that are at fixed temperature T_ν, i.e. $(\beta_\nu = 1/T_\nu)$ and chemical potential μ_ν. The system has discrete and nondegenerate states i, with energy E_i and the number of particles n_i.
For simplicity we consider a single species of particles. Additionally, the system might also exchange work with external sources of work. The effect of those sources on the energies $E_i(\xi)$ and particle numbers $n_i(\xi)$ is parametrized by the control parameter $\xi = \xi(t)$. In the ensemble picture, the system state is described by the probability distribution p_i to be in state i, with the normalization $\sum_i p_i = 1$. These distributions do not need to be in equilibrated states and, therefore, thermodynamic concepts are not necessarily well defined for the system. The reservoirs, however, are assumed to be ideal and, therefore, T_ν and μ_ν are referring to them. Although the actual stochastic path of the system is unpredictable, the probabilities $p_i(t)$ evolve according to the Markovian master equation (2.94); compare [63, 64]. The transition rates satisfy the probability conservation condition

$$\sum_i \mathcal{W}_{ij} = 0\,, \tag{2.118}$$

and the rates describing transitions induced by different contacts add up

$$\mathcal{W}_{ij} = \sum_\nu \mathcal{W}_{ij}^{(\nu)}\,. \tag{2.119}$$

The basic thermodynamic state functions total energy, particle number and entropy in the system are given by

$$E_{\mathrm{S}} = \sum_i p_i E_i \,, \tag{2.120}$$

$$N_{\mathrm{S}} = \sum_i p_i n_i \,, \tag{2.121}$$

$$S = -\sum_i p_i \ln p_i \,. \tag{2.122}$$

There are two different mechanisms that contribute to their change, i.e. to the energy, matter and entropy balance: a) due to the change of E_i and n_i and b) a change in the occupation of the levels due to the Markovian dynamics. The energy and particle balances read

$$\dot{E}_{\mathrm{S}} = \sum_i \dot{E}_i p_i + \sum_i E_i \dot{p}_i = \dot{\xi}\frac{\partial}{\partial \xi} E_{\mathrm{S}} + \sum_\nu J_{\mathrm{E}}^{(\nu)} \,, \tag{2.123}$$

$$\dot{N}_{\mathrm{S}} = \sum_i \dot{n}_i p_i + \sum_i N_i \dot{p}_i = \dot{\xi}\frac{\partial}{\partial \xi} N_{\mathrm{S}} + \sum_\nu J_{\mathrm{M}}^{(\nu)} \,, \tag{2.124}$$

where the first parts on the right hand side accounts for changes induced by external sources of work. In the absence of external driving these parts vanish. The second contributions are the energy and matter currents *entering* the system from the reservoir ν

$$J_{\mathrm{M}}^{(\nu)} = \sum_{i,j} \mathcal{W}_{ij}^{(\nu)} p_j \Delta n_{ij} \,, \tag{2.125}$$

$$J_{\mathrm{E}}^{(\nu)} = \sum_{i,j} \mathcal{W}_{ij}^{(\nu)} p_j \Delta E_{ij} \,. \tag{2.126}$$

Note that, as in the derivation for the currents in section 2.11, we assume that at one time only one particle is tunneling, which implies $\Delta n_{ij} = \{-1, 0, +1\}$. Contrarily to our definition for the currents $I_{\mathrm{M}}^{(\nu)}, I_{\mathrm{E}}^{(\nu)}$, eqs. (2.111) and (2.112), where qua definition particles/energy *leaving* the system towards the reservoir constitute positive currents, we define the currents here to be positive when *entering* the system; compare [41, 65]. Aside from the opposite signs the two current expressions are equivalent, i.e.

$$I_{\mathrm{M}}^{(\nu)} = -J_{\mathrm{M}}^{(\nu)} \,, \qquad I_{\mathrm{B}}^{(\nu)} = -J_{\mathrm{B}}^{(\nu)} \,. \tag{2.127}$$

The energy balance leads to the formulation of a *first law* of thermodynamics, namely

$$\dot{E}_{\mathrm{S}} = \dot{W} + \sum_\nu \dot{Q}^{(\nu)} \,, \tag{2.128}$$

where we define the work flow, that is contributed to by the coupling to the baths and external work sources

$$\dot{W} = \sum_\nu \mu_\nu J_{\mathrm{M}}^{(\nu)} + \dot{\xi}\frac{\partial}{\partial \xi} E_{\mathrm{S}} \,. \tag{2.129}$$

The second contribution to the right-hand side of (2.128) defines the heat flow with respect to the reservoirs

$$\dot{Q}^{(\nu)} = J_{\mathrm{E}}^{(\nu)} - \mu_\nu J_{\mathrm{M}}^{(\nu)} \,. \tag{2.130}$$

Turning to the *second law*, we see that the definition (2.122) is a proper choice that reduces to the standard thermodynamic entropy at equilibrium. Additionally, it preserves in nonequilibrium situations the second law, namely the relation between heat and entropy exchange and the positivity of the entropy production, i.e.

$$\dot{S} = \dot{S}_{\mathrm{e}} + \dot{S}_{\mathrm{i}}\,, \tag{2.131}$$

$$\dot{S}_{\mathrm{e}} = \sum_{\nu} \frac{\dot{Q}^{(\nu)}}{T_\nu}\,, \tag{2.132}$$

$$\dot{S}_{\mathrm{i}} \geq 0\,. \tag{2.133}$$

These properties can be verified as follows

$$\begin{aligned}\dot{S} &= -\sum_i \dot{p}_i \ln p_i = -\sum_\nu \sum_{i,j} \mathcal{W}_{ij}^{(\nu)} p_j \ln p_i = -\sum_{i,j} \mathcal{W}_{ij}^{(\nu)} p_j \ln \frac{p_i}{p_j} \\ &= \sum_\nu \frac{1}{2} \sum_{i,j} \left(\mathcal{W}_{i,j}^{(\nu)} p_j - \mathcal{W}_{j,i}^{(\nu)} p_i \right) \ln \frac{p_j}{p_i} = \frac{1}{2} \sum_\nu \sum_{i,j} J_{i,j}^{(\nu)} \left[\ln \frac{\mathcal{W}_{ij}^{(\nu)} p_j}{\mathcal{W}_{ji}^{(\nu)} p_i} + \ln \frac{\mathcal{W}_{ji}^{(\nu)}}{\mathcal{W}_{ij}^{(\nu)}} \right],\end{aligned} \tag{2.134}$$

where we introduce using the trace-preservation of the rate matrix,

$$J_{ij}^{(\nu)} = \mathcal{W}_{i,j}^{(\nu)} p_j - \mathcal{W}_{j,i}^{(\nu)} p_i\,, \tag{2.135}$$

$$X_{ij}^{(\nu)} = \ln \frac{\mathcal{W}_{ij}^{(\nu)} p_j}{\mathcal{W}_{ji}^{(\nu)} p_i}\,, \tag{2.136}$$

$$q_{ij}^{(\nu)} = \Delta E_{ij} - \mu_\nu \Delta n_{ij}\,. \tag{2.137}$$

The probability current $J_{ij}^{(\nu)}$ is the net transition rate from state j to i, and $X_{ij}^{(\nu)}$ is the corresponding thermodynamical force. We can now identify the entropy flow to the environment $\dot{S}_{\mathrm{e}}$ and the internal entropy production $\dot{S}_{\mathrm{i}}$. They read

$$\dot{S}_{\mathrm{e}} \equiv \frac{1}{2} \sum_{\nu,i,j} J_{ij}^{(\nu)} \frac{q_{ij}^{(\nu)}}{T_\nu} = -\sum_{\nu,i,j} \mathcal{W}_{ij}^{(\nu)} p_j \ln \frac{\mathcal{W}_{ij}^{(\nu)}}{\mathcal{W}_{ji}^{(\nu)}}\,, \tag{2.138}$$

$$\dot{S}_{\mathrm{i}} \equiv \frac{1}{2} \sum_{\nu,i,j} J_{ij}^{(\nu)} X_{ij}^{(\nu)} = \sum_{\nu,i,j} \mathcal{W}_{ij}^{(\nu)} p_j \ln \frac{\mathcal{W}_{ij}^{(\nu)} p_j}{\mathcal{W}_{ji}^{(\nu)} p_i} \geq 0\,. \tag{2.139}$$

The entropy flow $\dot{S}_{\mathrm{e}}$ reads after some algebra

$$\begin{aligned}\dot{S}_{\mathrm{e}} &= \frac{1}{2} \sum_{\nu,i,j} J_{ij}^{(\nu)} \frac{q_{ij}^{(\nu)}}{T_\nu} = \sum_\nu \frac{1}{T_\nu} \sum_{ij} \left[\mathcal{W}_{ij}^{(\nu)} p_j \Delta E_{ij} - \mu_\nu \mathcal{W}_{ij}^{(\nu)} p_j \Delta n_{ij} \right] \\ &= \sum_\nu \frac{1}{T_\nu} \left[J_{\mathrm{E}}^{(\nu)} - \mu_\nu J_{\mathrm{M}}^{(\nu)} \right] = \sum_\nu \frac{\dot{Q}^{(\nu)}}{T_\nu}\,,\end{aligned} \tag{2.140}$$

as desired.
Also, it is obvious that $\dot{S}_{\mathrm{i}}$ is clearly nonnegative and it only vanishes when *detailed balance* is fullfilled, i.e. every process is equilibrated by its reverse process, such that

$$\mathcal{W}_{ij}^{(\nu)} p_j = \mathcal{W}_{ji}^{(\nu)} p_i\,. \tag{2.141}$$

This is a purely mathematical statement. To connect it with the physical setups we are interested in, we associate to each reservoir (i.e. decoherence mechanism) ν - that is responsible for transitions between system states - a set of variables at their own equilibrium. That means we assume idealized reservoirs with well-defined temperatures and chemical potentials. As a consequence the transition rates associated to a reservoir ν need to obey the *local detailed balance* property,

$$\ln \frac{\mathcal{W}_{ij}^{(\nu)}}{\mathcal{W}_{ji}^{(\nu)}} = -\beta_\nu \left[(E_i - E_j) - \mu_\nu \left(n_i - n_j \right) \right] . \tag{2.142}$$

This property makes sure that a system in contact with a single reservoir of temperature T and chemical potential μ and without being subject to external driving will reach the grand-canonical equilibrium with probabilities

$$p_i^{\mathrm{eq}} = \exp \left[-\beta \left(E_i - \mu n_i - \Omega^{\mathrm{eq}} \right) \right] . \tag{2.143}$$

The equilibrium grand potential Ω^{eq} is obtained by normalization of the probability distribution p^{eq}

$$\exp \left[-\beta \Omega^{\mathrm{eq}} \right] = \sum_i \exp \left[-\beta \left(E_i - \mu n_i \right) \right] . \tag{2.144}$$

If the system is coupled to multiple reservoirs each reservoir tries to impose its equilibrium on the system which would clearly violate detailed balance, (2.141), except if all reservoirs had the same thermodynamic properties (i.e. T and μ). This, on the other hand, would render the distinction between the reservoirs useless.
We are in particular interested in nonequilibrium steady-states, where one has $\dot{S} = 0$, i.e. the entropy production compensates the entropy flow to the environment

$$\dot{\bar{S}}_{\mathrm{i}} = -\dot{\bar{S}}_{\mathrm{e}} = -\sum_\nu \frac{\dot{Q}^{(\nu)}}{T_\nu} , \tag{2.145}$$

which introduces the extracted power

$$\mathcal{P} = -\dot{W} = \sum_\nu \dot{Q}^{(\nu)} . \tag{2.146}$$

2.13. Separation of time scales

In the following section we want to address the situation where the rate matrix has a structure that reveals significantly different time scales. We want to outline a description of the thermodynamical implications in terms of *mesostates*, a concept that was introduced in an excellent publication by Esposito [41], who developed therein a theory for the coarse grained Markovian dynamics of arbitrary open systems that exchange particles and energy with multiple reservoirs.
The mesostates, denoted by σ, are corresponding to the *microstates* i, such that that the microstate i leads to the unique mesostate $\sigma = \sigma(i)$. The microstates can be denoted $i_\sigma, j_{\sigma'}$ in the way, that system state i leads to mesostate σ while state j is associated with mesostate σ'. The probability to find the system in mesostate σ is

$$P_\sigma = \sum_{i_\sigma} p_{i_\sigma} . \tag{2.147}$$

We also introduce the conditional probability to be in a microstate i_σ being in the mesostate σ reads

$$\mathbb{P}_{i|\sigma} = \frac{p_{i_\sigma}}{P_\sigma}\,, \tag{2.148}$$

which of course satisfies probability conservation $\sum_{i_\sigma} \mathbb{P}_{i|\sigma} = 1$.
We now write the rate equations (2.94) in terms of the conditional probabilities (2.148) and obtain

$$\dot{P}_\sigma \mathbb{P}_{i|\sigma} + P_\sigma \dot{\mathbb{P}}_{i|\sigma} = \sum_{\sigma'} P_{\sigma'} \sum_{\nu, j_{\sigma'}} \mathcal{W}^{(\nu)}_{i_\sigma j_{\sigma'}} \mathbb{P}_{j|\sigma'}\,. \tag{2.149}$$

This enables us to write a master equation that rules the dynamics of the mesostates. We sum this equation over i_σ,

$$\dot{P}_\sigma = \sum_{\nu,\sigma'} \mathcal{V}^{(\nu)}_{\sigma\sigma'} P_{\sigma'}\,. \tag{2.150}$$

Note that the mesoscopic rate matrix

$$\mathcal{V}^{(\nu)}_{\sigma\sigma'} = \sum_{i_\sigma, j_{\sigma'}} \mathcal{W}^{(\nu)}_{i_\sigma j_{\sigma'}} \mathbb{P}_{j|\sigma'} \quad \text{with} \quad \sum_{\sigma} \mathcal{V}^{(\nu)}_{\sigma\sigma'} = 0\,, \tag{2.151}$$

depends on $\mathbb{P}_{j_{\sigma'}}$ and thus on the dynamics of the microstates. Therefore (2.150) do not close. Although we assume time-independent microstate rate matrices $\mathcal{W}^{(\nu)}$, $\mathcal{V}^{(\nu)}_{\sigma\sigma'}$ will be time-dependent. This is due to the fact that the conditional probabilities $\mathbb{P}_{i|\sigma}$ are time-dependent, as long as the distribution of the microlevels evolve.
The notion of mesostate dynamics is of particular usefulness if we consider systems that suggest a coarse graining procedure such that the dynamics between microstates belonging to the same mesostate evolve on a time scale much faster than the transitions between microstates that belong to different mesostates. This implies for the elements of the rate matrix

$$\mathcal{W}_{i_\sigma j_\sigma} \gg \mathcal{W}_{i_\sigma j_{\sigma'}}, (\sigma \neq \sigma')\,. \tag{2.152}$$

This is to be taken seriously; this condition makes sure that the mesostate approach is valid, which is formally proven in the appendix in [41].

Given that condition (2.152) is met, the probabilities $\mathbb{P}_{i|\sigma}$ will evolve much faster than the mesoscopic probabilities P_σ. Consider the characteristic short time scale τ_{mic}: $\mathbb{P}_{i|\sigma}$ will be governed by almost isolated dynamics within the mesostates σ and eventually relax to its stationary distribution $\bar{\mathbb{P}}_{i|\sigma}$ given by

$$\sum_{j_\sigma} \mathcal{W}_{i_\sigma j_\sigma} \bar{\mathbb{P}}_{j|\sigma} = 0\,. \tag{2.153}$$

On the same time scale τ_{mic} the mesostate probabilities P_σ will barely change.
If the transitions between different microstates belonging to the mesostate σ are due to just one reservoir the stationary conditional distribution will be given by the equilibrium distribution in close analogy to eq. (2.143),

$$\mathbb{P}^{\text{eq}}_{i|\sigma} = \exp\left[-\beta\left(E_{i_\sigma} - \mu n_{i_\sigma} - \Omega^{\text{eq}}(\sigma)\right)\right]\,, \tag{2.154}$$

which implies a detailed balance condition within mesostate dynamics. We obtain

$$\mathcal{W}_{i_\sigma j_\sigma} \mathbb{P}^{\mathrm{eq}}_{j_\sigma} = \mathcal{W}_{j_\sigma i_\sigma} \mathbb{P}^{\mathrm{eq}}_{i_\sigma} \,. \tag{2.155}$$

For multiterminal setups we will thus observe an evolution of the mesostate distributions P_σ on time scales $\tau \gg \tau_{\mathrm{mic}}$ according to the master equation (2.150)

$$\dot{P}_\sigma = \sum_{\nu,\sigma'} \bar{\mathcal{V}}^{(\nu)}_{\sigma\sigma'} P_{\sigma'} \quad \text{with} \quad \bar{\mathcal{V}}^{(\nu)}_{\sigma\sigma'} = \sum_{i_\sigma, j_{\sigma'}} \mathcal{W}^{(\nu)}_{i_\sigma j_{\sigma'}} \bar{\mathbb{P}}_{j|\sigma'} \,. \tag{2.156}$$

We immediately see the time scale τ_{mes} on which the mesostate distributions will reach their stationary state, obtained by

$$\sum_{\nu\sigma'} \bar{\mathcal{V}}^{(\nu)}_{\sigma\sigma'} \bar{P}_{\sigma'} = 0 \,. \tag{2.157}$$

In the last paragraphs of this sections we want to, very briefly, study which are the consequences of the coarse graining description in terms of the system's entropy production. In our reference [41] Esposito has not only introduced the coarse graining method in the first place, but also investigated in-depth what follows for the thermodynamical description. For the purposes of this work we only need to highlight some of the statements therein.
Let us start by noting that the evolution of the system entropy S can be separated into three parts,

$$\dot{S} = \dot{S}^{(1)} + \dot{S}^{(2)} + \dot{S}^{(3)} \,, \tag{2.158}$$

where the first part accounts for the Shannon-like entropy in terms of the mesoscopic probabilities, i.e. it describes a system made of mesostates without knowing the internal dynamics of the microstates constituting them. We have already seen above, that the mesostate description recovers the structure of microscopic dynamics, i.e. the evolution of the mesostate probabilities obeys a Markovian master equation, eq. (2.150). Accordingly, we find

$$\dot{S}^{(1)} = -\sum_{\sigma} \dot{P}_\sigma \ln P_\sigma \,. \tag{2.159}$$

The second contribution to eq. (2.158) averages the entropy changes occuring within each mesostate over the mesostates. Likewise, the third contribution averages the entropy change due to transitions between microstates pertaining to different mesostates. We will omit the discussion of these contributions here and refer to Esposito's work ([41]).
However, the entropy production and entropy flow of the total system can be split up into three contribution as well

$$\dot{S}_{\mathrm{i}} = \dot{S}^{(1)}_{\mathrm{i}} + \dot{S}^{(2)}_{\mathrm{i}} + \dot{S}^{(3)}_{\mathrm{i}} \geq 0 \,, \qquad \dot{S}_{\mathrm{e}} = \dot{S}^{(1)}_{\mathrm{e}} + \dot{S}^{(2)}_{\mathrm{e}} + \dot{S}^{(3)}_{\mathrm{e}} \,. \tag{2.160}$$

Again, the first contributions to entropy production and entropy flow are associated with the dynamics of the structureless mesostates, the second belong to the internal dynamics of the mesostates and the third to the different ways in which mesostate transitions can occur. Note that the separation of the entropy balance is consistent such that

$$\dot{S}^{(j)} = \dot{S}^{(j)}_{\mathrm{i}} + \dot{S}^{(j)}_{\mathrm{e}} \,, \qquad j \in \{1,2,3\} \,. \tag{2.161}$$

Here, we only mention the entropy production and flow pertaining to the structureless mesostate dynamics, which assume the following form

$$\dot{S}_{\mathrm{i}}^{(1)} = \sum_{\nu,\sigma,\sigma'} \mathcal{V}_{\sigma\sigma'}^{(\nu)} P'_{\sigma} \ln \frac{\mathcal{V}_{\sigma\sigma'}^{(\nu)} P'_{\sigma}}{\mathcal{V}_{\sigma'\sigma}^{(\nu)} P_{\sigma}} \geq 0\,, \tag{2.162}$$

and

$$\dot{S}_{\mathrm{e}}^{(1)} = -\sum_{\nu,\sigma,\sigma'} \mathcal{V}_{\sigma\sigma'}^{(\nu)} P'_{\sigma} \ln \frac{\mathcal{V}_{\sigma\sigma'}^{(\nu)}}{\mathcal{V}_{\sigma'\sigma}^{(\nu)}}\,. \tag{2.163}$$

These expressions provide further evidence that when microstates within mesostates are at equilibirum stochastic thermodynamics at mesostate level assumes the same form as on the microstate level, which can be seen by comparing the last expression to eqs. (2.138) and (2.139). One interesting consequence of the partition of the entropy balance should be noted: we recall that the entropy production $\dot{S}_{\mathrm{i}}$ is always a nonnegative quantity. This clearly holds also for $\dot{S}_{\mathrm{i}}^{(1)}$ and we can prove this property also for the remaining contributions, $\dot{S}_{\mathrm{i}}^{(2,3)}$ [41]. This, on the other hand, implies that $\dot{S}_{\mathrm{i}}^{(1)}$ underevaluates $\dot{S}_{\mathrm{i}}$

$$\dot{S}_{\mathrm{i}} - \dot{S}_{\mathrm{i}}^{(1)} = \dot{S}_{\mathrm{i}}^{(2)} + \dot{S}_{\mathrm{i}}^{(3)} \geq 0\,. \tag{2.164}$$

If the system runs into a steady-state, we find also analogously to the microstate dynamics, that entropy production $\dot{S}_{\mathrm{i}}^{(1)}$ and entropy flow $\dot{S}_{\mathrm{e}}^{(1)}$ cancel each other out, namely

$$\bar{\dot{S}}_{\mathrm{i}}^{(1)} = -\bar{\dot{S}}_{\mathrm{e}}^{(1)} = \sum_{\nu,\sigma,\sigma'} \mathcal{V}_{\sigma\sigma'}^{(\nu)} \bar{P}'_{\sigma} \ln \frac{\mathcal{V}_{\sigma\sigma'}^{(\nu)}}{\mathcal{V}_{\sigma'\sigma}^{(\nu)}}\,. \tag{2.165}$$

3. Spin interactions

3.1. Introduction

In this chapter we want to motivate the basic model of interacting spins studied in the course of this thesis.
On the one hand, we consider effective conservative systems to learn about the interesting nonlinear dynamics that result from the coupling between spins. We do this in the hope to understand more of the complicated dynamics that appear in spin systems that are subject to different mechanisms of dissipation and decoherence. In later chapters we study spin resolved single-electron transport through quantum dots (QD), which gives rise to modeling the electrons dwelling in the QD structures as electronic (pseudo)-spins. On the other hand, a semiconductor QD typically consists of a large number of atoms (typically 10^2 to 10^6). Electrons tunneling through QD devices experience, for instance, hyperfine and spin-orbit interactions with the nuclear spins of the host material.
The effect of these couplings on the transport characteristics has been subject to research for various kinds of transport systems, such as self assembled quantum dots [66] or molecular magnets [67, 68, 69]. Moreover, the decoherence and spin-relaxation due to coupling to ensembles of nuclear spins have been subject to many theoretical [70, 71, 72] and experimental work [73, 74]. In section 3.2 we want to derive the hyperfine interactions terms for electrons dwelling in quantum dots.
However, the huge number of nuclear spins can be described as one external spin with a large magnitude, which gives rise to effective spin-spin interactions, between a collective nuclear spin and the electronic spin. The general exchange interactions between spin centers can be described by

$$\hat{H}_{\text{exch}} = \sum_{i,j} \hat{\vec{S}}_i \cdot \mathcal{J}_{ij} \cdot \hat{\vec{S}}_j \,. \tag{3.1}$$

where $\mathcal{J}_{ij}$ is a second-rank tensor. To distinguish the nature of different interactions we decompose the tensor

$$\mathcal{J}_{ij} = \frac{1}{2} J_{ij} \mathbb{1} + \mathcal{J}_{ij}^{\text{S}} + \mathcal{J}_{ij}^{\text{A}} \,, \tag{3.2}$$

where the symmetric exchange interaction is divided into an isotropic part $J_{ij} = \frac{2}{3}\text{Tr}\{\mathcal{J}_{ij}\}$ and a traceless tensor for anisotropic exchange interactions $\mathcal{J}_{ij}^{\text{S}} = \frac{1}{2}\left(\mathcal{J}_{ij} + \mathcal{J}_{ij}^{\text{T}}\right) - \frac{1}{2} J_{ij}\mathbb{1}$. The antisymmetric exchange interactions are described by the likewise traceless tensor $\mathcal{J}_{ij}^{\text{A}} = \frac{1}{2}\left(\mathcal{J}_{ij} - \mathcal{J}_{ij}^{\text{T}}\right)$.
In most cases the interaction between spin centers is isotropic and the exchange interaction is modeled by the widely used Heisenberg Hamiltonian

$$\hat{H} = \sum_{i,j} J_{ij} \hat{\vec{S}}_i \cdot \hat{\vec{S}}_j \,, \tag{3.3}$$

which was derived in the theory of ferromagnetism as a result of the interplay between Coulomb repulsion and the Pauli principle [75]. The Heisenberg interaction describes the dominant

magnetic interaction in molecular nanomagnets [67, 68, 69], and it is also useful to describe super-exchange via shared ligands.

The anisotropic symmetric exchange interaction is often very weak. It contains contributions like dipolar interactions and it is often neglected. It is not negligible in cobalt(II) and rare earth (lanthanide) ions [76] as well as in quantum dots where the ground states are in p,d,f - orbitals, such as certain graphene or carbon nanotube QDs [77]. If we neglect the antisymmetric exchange we can perform a transformation to principal axes and rewrite the exchange tensor to obtain

$$\mathcal{J}_{ij} = \mathrm{Diag}\left(J_{ij,xx}, J_{ij,yy}, J_{ij,zz}\right) . \tag{3.4}$$

3.2. Hyperfine interaction in quantum dots

In the following we want to derive the hyperfine interaction terms for electrons which are confined in quantum dots. Naively, the coupling between the electron and nuclear spins leads to a hyperfine structure, which can be described, basically, by the dipole-dipole interaction between the electronic and nuclear magnetic moments. However, this classical form is an oversimplification and leads to ill-definitions.
A relativistic derivation of the interactions can be found, e.g., in References [78, 79, 80, 81]. We start from the Dirac Hamiltonian for a spin-1/2 particle in the presence of an EM-field in the potential of a nucleus

$$\hat{H}_{\mathrm{D}} = c\vec{\alpha}\cdot\vec{\pi} + \beta mc^2 - eV(\vec{r}) , \tag{3.5}$$

where m and $-e$ are the rest mass and the charge of the electron, respectively and $V(\vec{r})$ represents the electric potential due to the considered nucleus, c the speed of light. The 4×4-matrix $\vec{\pi} = \vec{p} + e/c\vec{A}$ is the canonical momentum, where $\vec{A}$ is the vector-potential due to the nuclear spin. $\vec{\alpha}$ is a vector of the Dirac matrices γ, with $\gamma_0\gamma_k = \alpha_k$ and $\beta = \gamma_0$

$$\vec{\alpha} = \begin{pmatrix} 0 & \vec{\sigma} \\ \vec{\sigma} & 0 \end{pmatrix}, \beta = \begin{pmatrix} \mathbb{1}_2 & 0 \\ 0 & -\mathbb{1}_2 \end{pmatrix} . \tag{3.6}$$

The Dirac equation for an electron with energy $E = \varepsilon + mc^2$ reads

$$\hat{H}_{\mathrm{D}}\,\Psi = E\Psi , \tag{3.7}$$

where the four-component spinor Ψ can be written as vector of two-component spinors, which leads to a pair of coupled linear equations

$$\begin{aligned} \left(\varepsilon + eV(\vec{r})\right)\psi_1 - \vec{\sigma}\cdot\vec{\pi}\psi_2 &= 0 , \\ -\vec{\sigma}\cdot\vec{\pi}\psi_1 + \left(\varepsilon + 2mc^2 + eV(\vec{r})\right)\psi_2 &= 0 . \end{aligned} \tag{3.8}$$

By expressing ψ_1 through ψ_2 these equations can be rearranged into the eigenvalue equation

$$\hat{H}_{\mathrm{D},2}\,\psi_2 = \varepsilon\psi_2 . \tag{3.9}$$

The electric field produced by the nucleus is $\vec{E} = -\vec{\nabla}V(\vec{r})$ and we find that three parts of $\hat{H}_{\mathrm{D},2}$

explicitly contribute to the hyperfine interaction, namely

$$\hat{H}_{\mathrm{ihf}} = \frac{e^2\hbar c}{\left(\varepsilon + 2mc^2 + eV(\vec{r})\right)^2}\left(\vec{E}\times\vec{A}\right)\cdot\vec{\hat{\sigma}}\,, \tag{3.10}$$

$$\hat{H}_{\mathrm{ahf}} = \frac{e\hbar c}{\varepsilon + 2mc^2 + eV(\vec{r})}\left(\vec{\nabla}\times\vec{A}\right)\cdot\vec{\hat{\sigma}}\,, \tag{3.11}$$

$$\hat{H}_{\mathrm{orb}} = \frac{e\hbar c^2}{\left(\varepsilon + 2mc^2 + eV(\vec{r})\right)^2}\vec{A}\cdot\vec{\hat{p}}\,. \tag{3.12}$$

The three parts describe the isotropic and anisotropic hyperfine coupling as well as the nuclear-orbital interaction. Note that $\vec{\hat{\sigma}}$ and $\vec{\hat{p}}$ are explicit notations for the electronic spin and momentum operators, respectively. Additionally, $\hat{H}_{\mathrm{D},2}$ contains a spin-orbit contribution that reads

$$\hat{H}_{\mathrm{SO}} = \frac{e\hbar c^2}{\left(\varepsilon + 2mc^2 + eV(\vec{r})\right)^2}\left(\vec{E}\times\vec{\hat{p}}\right)\cdot\vec{\hat{\sigma}}\,. \tag{3.13}$$

The electric potential reads (in SI-units)

$$V(\vec{r}) = -\frac{Ze}{4\pi\varepsilon_0 r}\,, \tag{3.14}$$

where Ze is the nuclear charge. The vector potential is expressed in terms of the nuclear magnetic moment operator $\vec{\hat{\mu}}$ and the electron position operator $\vec{\hat{r}}$

$$\vec{A} = \frac{\mu_0}{4\pi}\frac{\vec{\hat{\mu}}\times\vec{\hat{r}}}{r^3}\,. \tag{3.15}$$

3.2.1. Isotropic hyperfine interaction

Together with the vector identity $\vec{\hat{r}}\times(\vec{\hat{\mu}}\times\vec{\hat{r}}) = \vec{\hat{\mu}}(\vec{\hat{r}}\cdot\vec{\hat{r}}) - \vec{\hat{r}}(\vec{\hat{\mu}}\cdot\vec{\hat{r}})$ the isotropic interaction part (3.10) reads

$$\hat{H}_{\mathrm{ihf}} = \frac{\mu_0}{4\pi}\frac{\hbar c Z e^3}{\left(\varepsilon + 2mc^2 + eV(\vec{r})\right)^2}\frac{1}{4\pi\varepsilon_0 r^6}\left(r^2\vec{\hat{\sigma}}\cdot\vec{\hat{\mu}} - (\vec{\hat{\sigma}}\cdot\vec{\hat{r}})(\vec{\hat{\mu}}\cdot\vec{\hat{r}})\right)\,. \tag{3.16}$$

In the next step we define the nuclear length scale $d \equiv Ze^2/2mc^2 \sim 1.5\times10^{-5}Zm$ and neglect the relativistic corrections to the electron rest mass ($\varepsilon \ll mc^2$) and obtain with the insertion of the Bohr magneton $\mu_B = e\hbar/2m$

$$\hat{H}_{\mathrm{ihf}} = \frac{\mu_0\mu_B}{4\pi r^6}\frac{d}{(1+d/r)^2}\left(r^2\vec{\hat{\sigma}}\cdot\vec{\hat{\mu}} - (\vec{\hat{\sigma}}\cdot\vec{\hat{r}})(\vec{\hat{\mu}}\cdot\vec{\hat{r}})\right)\,. \tag{3.17}$$

We can now take matrix elements of $\hat{H}_{\mathrm{ihf}}$ in the basis of electron wave functions $\varphi_i(\vec{r})$

$$\langle\varphi_i|\,\hat{H}_{\mathrm{ihf}}\,|\varphi_j\rangle = \frac{\mu_0\mu_B}{4\pi}\int_0^\infty dr\frac{d}{(r+d)^2}f(\vec{r})\,, \tag{3.18}$$

with

$$f(\vec{r}) = \int d\Omega\varphi_i^*(\vec{r})\left[\vec{\hat{\sigma}}\cdot\vec{\hat{\mu}} - (\vec{\hat{\sigma}}\cdot\vec{\hat{r}})(\vec{\hat{\mu}}\cdot\vec{\hat{r}})\right]\varphi_j(\vec{r})\,. \tag{3.19}$$

The radial integral is dominated by small $r \lesssim d$ and, thus, the electron wave functions only need to be evaluated near the nucleus. Therefore, we approximate the $f(\vec{r})$ by $f(0)$ and obtain

$$\langle\varphi_i|\,\hat{H}_{\text{ihf}}\,|\varphi_j\rangle \approx \frac{\mu_0\mu_B}{4\pi}\int d\Omega \int_0^\infty dr \frac{d}{(r+d)^2} f(0) = \frac{2\mu_0\mu_B}{3}\vec{\hat{\sigma}}\cdot\vec{\hat{\mu}}\,. \tag{3.20}$$

Note that this approximation is only valid for s-type orbital electron wave functions, i.e. for conduction band states in quantum dots. By inserting $\vec{\hat{\mu}} = g_N\mu_N\vec{\hat{I}}$, where $\mu_N = e\hbar/2m_p = 5.05\times10^{-27}J/T$ is the nuclear magneton and g_N is the nuclear g-factor, and replacing $\vec{\hat{\sigma}} = 2\vec{\hat{S}}$ and introducing the projector $|\vec{r}=0\rangle\langle\vec{r}=0| = \delta(\vec{r})$ we finally obtain

$$\hat{H}_{\text{ihf}} = \frac{2\mu_0 g\mu_B g_N\mu_N}{3}\vec{\hat{S}}\cdot\vec{\hat{I}}\delta(\vec{r})\,, \tag{3.21}$$

which is often referred to as *Fermi contact interaction.*
In quantum dots electrons usually interact with a large number of nuclear spins sitting at lattice sites k, i.e. positions $\vec{r}_k$. We introduce the electron spin density operator $\vec{\hat{S}}(\vec{r}) = \frac{1}{2}\sum_{s,s'=\{\uparrow,\downarrow\}}\hat{\psi}_s^\dagger(\vec{r})\vec{\hat{\sigma}}_{ss'}\hat{\psi}_{s'}(\vec{r})$, $\sigma_{ss'} = \langle s|\,\vec{\hat{\sigma}}\,|s'\rangle$ and generalize (3.21)

$$\hat{H}_{\text{ihf}} = \frac{2\mu_0 g\mu_B}{3}\sum_k g_{N_{j_k}}\mu_{N_{j_k}}\vec{\hat{S}}(\vec{r}_k)\cdot\vec{\hat{I}}_k\,. \tag{3.22}$$

The general field operators are $\hat{\psi}_s(\vec{r}) = \sum_n \varphi_n(\vec{r})\,\hat{d}_{ns}$, where $\hat{d}_{ns}$ is the annihilation operator for an electron of spin s and with the single-particle orbital wave function $\varphi_n(\vec{r})$. The wave functions form a complete set; if the level spacing between single-particle orbitals is larger than the hyperfine energy scale, it is justified to project onto the subspace of the orbital ground state φ_0 to obtain an effective isotropic hyperfine Hamiltonian for the quantum dot, i.e.

$$\hat{H}^{\text{eff}}_{\text{QDihf}} = \langle\varphi_0|\,\hat{H}_{\text{ihf}}\,|\varphi_0\rangle = \sum_k A_k\vec{\hat{S}}\cdot\vec{\hat{I}}_k\,. \tag{3.23}$$

Here we also took into account that for low temperatures the wave function of the ground state is given by the product of the Bloch wave function at $\vec{k}=0$ and an enveloping part $F(\vec{r})$, i.e. $\varphi_0(\vec{r}_i) \approx u_0(\vec{r}_i)F(\vec{r}_i)$. The enveloping function is normalized: $\int d^3r|F(\vec{r})|^2 = 1$.
The coupling constant

$$A_k = A_{j_k}\nu_0|F(\vec{r}_k)|^2 \tag{3.24}$$

takes into account the inhomogeneous couplings of each lattice site (ν_0 is the volume of the primitive unit cell of the crystal)

$$A_{j_k} = \frac{2\mu_0 g\mu_B}{3}g_{N_{j_k}}\mu_{N_{j_k}}|u_0(\vec{r})|^2\,. \tag{3.25}$$

Note that the nuclear Landé factor $g_{N_{j_k}}$ depends on the nuclear species and can be both positive and negative and, thus, the coupling constant can take either sign.
The effective Hamiltonian (3.23) is a common description of the electron-nuclear spin-dynamics for electrons in the conduction band of III-V semiconductors. The effective magnetic field of all nuclei

$$\vec{\hat{h}} = \sum_k A_k\vec{\hat{I}}_k\,, \tag{3.26}$$

is often referred to as *Overhauser field*.
In conclusion the isotropic or contact hyperfine interaction plays an important role in materials where electrons occupy s-type orbitals. In a number of works it was shown that the isotropic hyperfine interaction as modeled by the Hamiltonian (3.23) is responsible for the loss of coherence of a conduction band electron-spin in GaAs quantum dots [70, 72, 82, 83], as well as for the lifting of Coulomb or spin blockades in quantum dots [84, 85].

3.2.2. Anisotropic hyperfine interaction

The same procedure as above can be applied to the anisotropic interaction, Eq. (3.11), and we get

$$\hat{H}_{\mathrm{ahf}} = \frac{\mu_0\mu_B}{4\pi r^5}\frac{1}{(1+d/r)}\left(3(\vec{\hat{\sigma}}\cdot\vec{\hat{r}})(\vec{\hat{\mu}}\cdot\vec{\hat{r}}) - r^2\vec{\hat{\sigma}}\cdot\vec{\hat{\mu}}\right), \tag{3.27}$$

which is the classical dipole-dipole interaction between the electron and nuclear moments if the electron and nucleus are spatially separated. In quantum dots this is typically not the case and the strength of this interaction depends strongly on the symmetry of the electron wave functions. Projecting onto an electronic orbital wave function φ_0 yields

$$\langle\varphi_0|\,\hat{H}_{\mathrm{ahf}}\,|\varphi_0\rangle = \frac{\mu_0\mu_B}{4\pi}\int dr\frac{1}{(r+d)}\int d\Omega\varphi_0^*(\vec{r})\left(3(\vec{\hat{\sigma}}\cdot\vec{\hat{r}})(\vec{\hat{\mu}}\cdot\vec{\hat{r}})/r^2 - \vec{\hat{\sigma}}\cdot\vec{\hat{\mu}}\right)\varphi_0(\vec{r})\,. \tag{3.28}$$

Here, the angular integral vanishes for s-type orbitals, for states of higher angular momentum (p,d,f ...-orbitals) it is nonzero. These states, on the other hand, vanish at the origin, and, therefore, we can set $d = 0$.
An effective Hamiltonian for the anisotropic hyperfine interaction in quantum dots with many nuclear spins then reads

$$\hat{H}^{\mathrm{eff}}_{\mathrm{ahf}} = \sum_k \frac{\mu_0 g\mu_B g_{N_{j_k}}\mu_{N_{j_k}}}{4\pi|\vec{r}-\vec{r}_{kI}|^3}\left(3(\vec{\hat{n}}_k\cdot\vec{\hat{S}})(\vec{\hat{n}}_k\cdot\vec{\hat{I}}_k) - \vec{\hat{S}}\cdot\vec{\hat{I}}_k\right), \tag{3.29}$$

where $\vec{\hat{n}}_k = (\vec{\hat{r}}-\vec{\hat{r}}_k)/|\vec{r}-\vec{r}_k|$. This can be rewritten by introducing

$$\hat{H}^{\mathrm{eff}}_{\mathrm{ahf}} = \sum_k \vec{\hat{S}}(\vec{r})\cdot\mathcal{T}_k(\vec{r})\cdot\vec{\hat{I}}(\vec{r})\,, \tag{3.30}$$

where the traceless tensor $\mathcal{T}_k$ [the symmetric anisotropy tensor introduced in (3.2)] is given by its components

$$T_k^{\alpha\beta}(\vec{r}) = \frac{\mu_0 g\mu_B g_{N_{j_k}}\mu_{N_{j_k}}}{4\pi}\frac{\delta_{\alpha\beta}-3n_k^\alpha n_k^\beta}{|\vec{r}-\vec{r}_k|^3}, \quad \alpha,\beta\in\{x,y,z\}\,. \tag{3.31}$$

For simplicity we rotate to the principal axes and obtain

$$\hat{H}^{\mathrm{eff}}_{\mathrm{ahf}} = \sum_k T_k^{xx}\,\hat{S}_x\,\hat{I}_{kx} + T_k^{yy}\,\hat{S}_y\,\hat{I}_{ky} + T_k^{zz}\,\hat{S}_z\,\hat{I}_{kz}\,, \tag{3.32}$$

which defines an anisotropic (XYZ-type) exchange between electron and nuclear spin.
Thus, the anisotropic hyperfine term (3.32), together with the nuclear-orbital hyperfine interaction (3.12), facilitates the major interaction between electron spins of p-orbital electrons and the nuclear spins of the host material [86]. They are also relevant for the physics of electrons occupying the π-orbital in carbon nanotubes as well as in graphene [77, 87].

3.2.3. Nuclear-orbital interaction

For the sake of completeness we also denote the third contribution to the hyperfine interaction, (3.12), which reads

$$\hat{H}_{\text{orb}}^{\text{eff}} = -\frac{\mu_0 g \mu_B}{4\pi} \sum_k \mu_N g_{N_{j_k}} \frac{\hat{\vec{L}}_k \times \hat{\vec{I}}_k}{|\vec{r} - \vec{r}_k|^3} \,. \tag{3.33}$$

Here, $\hat{\vec{L}}_k$ is the electron orbital angular momentum at the nuclear site $\vec{r}_k$ and $\hat{\vec{I}}_k$ is the spin operator of the k-th nucleus. This interaction is in particular important for dynamics where the electron has an nonzero angular momentum, which typically happens when the electron occupies p-type valence bands in III-V semiconductors [86, 88].
The nuclear spins are not only subject to an interaction with the electron spin but couple to each other as well as, i.e. nuclear dipolar terms and nuclear quadrupolar terms occur. We will not go into detail here, but refer to the Review by Coish and Baugh [89].

3.2.4. Quantum versus classical dynamics for isotropic coupling

In Ref. [90] Coish *et al.* analyze the dynamics of electrons trapped in semiconductor QDs due to the isotropic hyperfine interaction we just introduced. Particularly, they compare the classical mean-field evolution of the electron in the presence of a nuclear field and an additional external magnetic field with the exact quantum evolution. Consider the Hamiltonian

$$\hat{H} = \hat{\vec{S}} \cdot \left(\vec{B} + \hat{\vec{h}} \right) . \tag{3.34}$$

Again, $\hat{\vec{S}}$ is the vector of components of the electron spin, and the magnetic field $\vec{B}$ is directed along the z axis. For GaAs the coefficient A_{j_k}, (3.25), in the contact hyperfine coupling constants eq. (3.24) takes an approximate value of $A \approx 90\mu$eV, which is the weighted average over the coupling for the three naturally occurring isotopes ^{69}Ga,^{71}Ga and ^{75}As that all have a total nuclear spin of $I = 3/2$ [91]. In this kind of QD with $N \approx 10^4 - 10^6$ nuclear spins it seems to be justified to replace the Overhauser operator by a classical Overhauser field $\hat{\vec{h}} \to \vec{B}_N$, which has been done in a number of works, cf. References [70, 71, 83, 84, 92, 93].
However, according to Coish *et al.* this approximation is for many cases only accurate at times $t < \tau_c = N^\eta / A$ with $\eta > 0$ [94], as effects of the quantum fluctuations of $\hat{\vec{h}}$ set in for longer times and the nuclear spins – as they are quantum objects – can even be entangled [95]. Moreover, the classical description predicts no decay of the electron spin, when one not takes the ensemble average over the initial Overhauser fields, which contradicts analytical studies by Coish and Loss [82, 72] and numerical results [96], that show that the interaction with nuclear spins can lead to the complete decay of the transverse electron spin. This decay is due to the quantum nature of the nuclei and it can occur even in a static environment, i.e. fixed initial conditions. Schliemann *et al.* show that the time evolution of a system described by the Hamiltonian (3.34) with vanishing magnetic field and an inhomogeneous coupling depends significantly on the type of the initial state of the spin environment [96]. The time evolution of simple tensor product states can be quite individual. Randomly correlated, and thus entangled states, however, show a time evolution that is reproduced by the time average over the time traces of all possible tensor product states. In Ref. [96] this effect is termed as *quantum parallelism*: the time evolution of all classical-like (i.e. uncorrelated) nuclear states is "present" in the time evolution of a linear superposition of all uncorrelated states. To put it differently, the time evolutions of all simple

tensor product states are performed in parallel when computing the time evolution of a randomly correlated state.

Quantum description for uniform coupling

Let us assume uniform contact hyperfine coupling of the form $A_k = A/N = \lambda$. Then the Overhauser operator reads

$$\vec{\hat{h}} = \lambda \vec{\hat{J}}\,, \quad \vec{\hat{J}} = \sum_{k=1}^{N} \vec{\hat{I}}_k\,, \quad (N \gg 1)\,, \tag{3.35}$$

where we introduced the collective nuclear spin operator $\vec{\hat{J}}$. As initial state we take an arbitrary product state of electronic and nuclear system

$$|\psi(0)\rangle = |\psi_S(0)\rangle \otimes |\psi_J(0)\rangle = \sum_{m=-j}^{j} \left(\alpha_m^{\uparrow} |\uparrow; j, m\rangle + \alpha_m^{\downarrow} |\downarrow; j, m\rangle\right)\,, \tag{3.36}$$

which is a superposition of the simultaneous eigenkets $|\sigma; j, m\rangle$ of $\hat{S}_z$, $\hat{J}_z$ and $\hat{J}^2$ with eigenvalues $\sigma = \pm 1/2$, $m = -j, \ldots, j$ and $j(j+1)$. The wave function at later times t is then given by

$$|\psi(t)\rangle = \sum_{m=-j}^{j} \left(\alpha_m^{\uparrow}(t) |\uparrow; j, m\rangle + \alpha_m^{\downarrow}(t) |\downarrow; j, m\rangle\right)\,. \tag{3.37}$$

The solution then follows by using the time-dependent Schrödinger equation $\mathbf{i}\partial_t |\psi(t)\rangle = \hat{H} |\psi(t)\rangle$ (with $\hbar = 1$) to generate the set of coupled differential equations for the coefficients $\{\alpha_m^{\uparrow}(t), \alpha_m^{\downarrow}(t)\}$ with $m = -j, \ldots, j-1$

$$\begin{aligned} \dot{\alpha}_m^{\uparrow} &= -\frac{\mathbf{i}}{2}\left(B + \lambda m\right)\alpha_m^{\uparrow} - \mathbf{i}\frac{\lambda}{2} C_{jm+1}^{-} \alpha_{m+1}^{\downarrow}\,, \\ \dot{\alpha}_{m+1}^{\downarrow} &= \frac{\mathbf{i}}{2}\left(B + \lambda(m+1)\right)\alpha_{m+1}^{\downarrow} - \mathbf{i}\frac{\lambda}{2} C_{jm}^{+} \alpha_m^{\uparrow}\,, \end{aligned} \tag{3.38}$$

where the $C_{jm}^{\pm} = \langle jm \pm 1 | \hat{J}_{\pm} | jm \rangle = \sqrt{j(j+1) - m(m \pm 1)}$ are the matrix elements of the operator $\hat{J}_{\pm}$ that flips one nuclear spin, i.e. raises/lowers the z component of $\vec{\hat{J}}$ by one. Together with the time-dependent coefficients

$$\begin{aligned} \alpha_j^{\uparrow}(t) &= \mathrm{e}^{-\frac{\mathbf{i}}{2}(B+\lambda j)t}\, \alpha_j^{\uparrow}(0)\,, \\ \alpha_{-j}^{\downarrow}(t) &= \mathrm{e}^{\frac{\mathbf{i}}{2}(B-\lambda j)t}\, \alpha_{-j}^{\downarrow}(0)\,, \end{aligned} \tag{3.39}$$

which are the prefactors for the stationary states $|\uparrow, j, j\rangle$, $|\downarrow, j, -j\rangle$ where electron spin and collective nuclear spin are (anti-)aligned with the magnetic field. Coish *et al.* obtain the solution to eq. (3.38) by the means of a Laplace transform [90]. This solutions and eq. (3.39), i.e. the set $\{\alpha_m^{\uparrow}(t), \alpha_m^{\downarrow}(t) : m = -j, \ldots, j\}$, provide an exact solution for the dynamics of the wave function $|\psi(t)\rangle$ at any time $t > 0$. The exact dynamics of the expectation values to all spin components follow straightforwardly,

$$\langle \vec{\hat{S}} \rangle_t = \langle \psi(t) | \vec{\hat{S}} | \psi(t) \rangle\,, \quad \langle \vec{\hat{J}} \rangle_t = \langle \psi(t) | \vec{\hat{J}} | \psi(t) \rangle\,. \tag{3.40}$$

Mean-field dynamics

In order to evaluate the classical spin-dynamics we carry out a mean-field decomposition of the Hamiltonian (3.34), as done in [90, 94]. This is done by rewriting the spin operator $\vec{\hat{S}}$ in terms of its expectation value and its fluctuation, i.e. $\vec{\hat{S}} = \langle\vec{\hat{S}}\rangle + \delta\vec{\hat{S}}$ and $\vec{\hat{J}} = \langle\vec{\hat{J}}\rangle + \delta\vec{\hat{J}}$. In the next step the term that contains the product of spin fluctuations ($\delta\vec{\hat{S}} \cdot \delta\vec{\hat{J}}$) is neglected. Moreover, we approximate the dynamics of the spins' expectation values by their self-consistent mean-field dynamics, i.e. by classical vectors of conserved length,

$$\langle\vec{\hat{S}}\rangle_t \approx \vec{s}(t)\,, \qquad \langle\vec{\hat{J}}\rangle_t \approx \vec{j}(t)\,. \tag{3.41}$$

Thus, the contact hyperfine Hamiltonian (3.34) is replaced by the time-dependent mean-field Hamiltonian (up to a number shift)

$$\hat{H}^{\mathrm{MF}}(t) = \left(\vec{B} + \lambda\vec{j}(t)\right) \cdot \vec{\hat{S}} + \lambda\vec{s}(t) \cdot \vec{\hat{J}}\,. \tag{3.42}$$

Then, the mean-field dynamics are given by the Heisenberg equation of motion (EOM) for the angular momentum operators $\hat{S}_i$, $\hat{J}_i$ ($i \in \{x, y, z\}$),

$$\frac{d}{dt}\hat{S}_i = \frac{1}{\mathbf{i}}\left[\hat{S}_i\,, \hat{H}^{\mathrm{MF}}(t)\right], \qquad \frac{d}{dt}\hat{J}_i = \frac{1}{\mathbf{i}}\left[\hat{J}_i\,, \hat{H}^{\mathrm{MF}}(t)\right], \tag{3.43}$$

With the replacements (3.41) and using the angular momentum computation relations

$$\begin{aligned}
&\left[\hat{S}_i\,, \hat{S}_j\right] = \mathbf{i}\sum_k \varepsilon_{ijk}\,\hat{S}_k\,, \qquad \left[\hat{J}_i\,, \hat{J}_j\right] = \mathbf{i}\sum_k \varepsilon_{ijk}\,\hat{J}_k\,, \\
&\left[\hat{S}_i\,, \hat{J}_j\right] = \left[\hat{S}_i\,, \mathbb{1}\right] = \left[\hat{J}_i\,, \mathbb{1}\right] = 0\,,
\end{aligned} \tag{3.44}$$

where ε_{ijk} is the Levi-Civita symbol. We obtain

$$\begin{aligned}
\dot{\vec{s}}(t) &= \left[\vec{B} + \lambda\vec{j}(t)\right] \times \vec{s}(t)\,, \\
\dot{\vec{j}}(t) &= -\lambda\vec{j}(t) \times \vec{s}(t)\,.
\end{aligned} \tag{3.45}$$

Yuzbashyan *et al.* show that these equations are integrable and provide an analytic solution to this equations [94]. Integrability is discussed in terms of anisotropic two-spin models in section section 3.3.

Equation (3.45) can as well be solved via numerical integration. Coish *et al.* compared their numerical solutions to the exact quantum ones by considering the correlation between the solutions [90]. It turns out that the correlation function decays faster with increased magnetic fields B. At zero magnetic field the total spin $\vec{\hat{K}} \cdot \vec{\hat{K}}$, with ($\vec{\hat{K}} = \vec{\hat{J}} + \vec{\hat{S}}$) commutes with the Hamiltonian. When the system evolution is started in an eigenstate of $\vec{\hat{J}}^2$ then only one single frequency occurs in the quantum dynamics [corresponding to energy differences with $k = j \pm 1/2$ [97]] and the quantum dynamics correspond to simple periodic precession and coincides with the classical dynamics for $j \ll 1$ [90]. The states for fixed k are degenerate. If one adds a term – the electron Zeeman term, for instance, – that does not commute with $\vec{\hat{K}}^2$, additional frequencies are involved in the quantum dynamics, which may lead to decay in the quantum solution. At the same time the classical solution is still described by the electron spin precession [cf. solutions provided by Coish *et al.* [90]].

3.3. Anisotropic two-spin models

In a number of previous works the anisotropic interaction between two spins in a conservative system and under the presence of an external magnetic field was a subject of investigation [98, 99, 100, 101, 102]. We consider a system of two localized quantum spins $\hat{S}_1 = \hbar\,\hat{\sigma}_1$ and $\hat{S}_2 = \hbar\,\hat{\sigma}_2$ with an applied magnetic field B in z direction that are anisotropically exchange coupled with the coupling strength λ. The interaction induces nonlinear dynamics. The Hamiltonian

$$\hat{H} = \hbar^2\lambda\left(\hat{\sigma}_1^x\,\hat{\sigma}_2^x + \hat{\sigma}_1^z\,\hat{\sigma}_2^z\right) + \hbar B(\hat{\sigma}_1^z + \hat{\sigma}_2^z)\,, \tag{3.46}$$

is a constant of motion. The system has a second constant of motion for vanishing magnetic field $B = 0$, namely $\hat{\sigma}_{\mathrm{tot}}^y = \hat{\sigma}_1^y + \hat{\sigma}_2^y$, which is easily varified using

$$\left[\hat{\sigma}_m^i\,,\hat{\sigma}_l^j\right] = \mathbf{i}\hbar\delta_{l,m}\sum_k \varepsilon_{ijk}\,\hat{\sigma}_l^k \quad (i,j,k\in\{x,y,z\})\,. \tag{3.47}$$

3.3.1. Classical description

To begin with we treat the two spins classically. We rewrite the Hamiltonian in the semiclassical limit, i.e. $\hbar\to 0$, $\sigma_l\to\infty$ and $\hbar\sqrt{\sigma_l(\sigma_l+1)} = s_l$, where we associate the magnitudes of classical angular momenta with the magnitudes of quantum spins.
Thus, we obtain a system of two angular momenta $\vec{S}_1, \vec{S}_2$ interacting via the time-independent Hamiltonian function

$$H\left(\vec{S}_1,\vec{S}_2\right) = \lambda\left(S_1^xS_2^x + S_1^zS_2^z\right) + B\left(S_1^z + S_2^z\right)\,. \tag{3.48}$$

The system obeys the mean-field EOM ($l\neq m$)

$$\begin{aligned}\frac{d}{dt}\vec{S}_l &= -\vec{S}_l\times\frac{\partial H}{\partial\vec{S}_l} = \left\{H,\vec{S}_l\right\}\\ &= -\sum_i\sum_j\sum_k \varepsilon_{ijk}\vec{e}_i S_l^j\frac{\partial H}{\partial S_l^k}\\ &= -(S_l^x,S_l^y,S_l^z)^{\mathrm{T}}\times(\lambda S_m^x,0,B+\lambda S_m^z)^{\mathrm{T}}\,,\end{aligned} \tag{3.49}$$

where

$$\left\{S_l^i,S_m^j\right\} = -\delta_{l,m}\sum_k\varepsilon_{ijk}S_l^k\,, \tag{3.50}$$

are the Poisson brackets for classical spin variables.
The structure of (3.49) implies that the length $\left|\vec{S}_l\right| = s_l$ of each spin remains constant. In other words the number of independent EOM reduces to $2N$ instead of $3N$, where $N = 2$ is the number of spins. This gives rise to writing the components of the spins $\vec{S}_l$ in terms of spherical coordinates θ_l,ϕ_l, i.e.

$$\vec{S}_l = (S_l^x,S_l^y,S_l^z)^{\mathrm{T}} = \left|\vec{S}_l\right|(\sin\theta_l\cos\phi_l,\sin\theta_l\sin\phi_l,\cos\theta_l)^{\mathrm{T}}\,. \tag{3.51}$$

One can proof that any given system of N classical spins with a corresponding Hamilton function can be represented by a system of N degrees of freedom, with canonical variables $p_l = S_l^z = \left|\vec{S}_l\right|\cos\theta_l, q_l = \phi_l, l\in\{1,\ldots,N\}$.
According to the Liouville-Arnold-theorem [103], autonomous systems of N degrees of freedom or N classical spins, i.e. a system with a time-independent Hamilton function, are called *completely*

integrable if there exist N independent constants of motion $C_k(S_1, \ldots, S_N)$ which are mutually in an involution. That means that their Poisson-bracket vanishes [cf. [99]]

$$\{C_k, C_{k'}\} = \sum_l \frac{\partial C_k}{\partial p_l}\frac{\partial C_{k'}}{\partial q_l} - \frac{\partial C_k}{\partial q_l}\frac{\partial C_{k'}}{\partial p_l} = 0 \quad (l \in \{1, \ldots, N\}) \,. \tag{3.52}$$

The first constant of motion is the Hamiltonian function itself. With a vanishing external magnetic field ($B \to 0$) the system has a second constant of motion, as stated above: $C_2 = S_1^y + S_2^y$, which is easily verified by the equation

$$\frac{d}{dt}C_2 = \sum_l \frac{\partial C_2}{\partial \vec{S}_l} \cdot \frac{d}{dt}\vec{S}_l = \sum_l \frac{\partial C_2}{\partial \vec{S}_l} \cdot \left(-\vec{S}_l \times \frac{\partial H}{\partial \vec{S}_l}\right) = 0 \,. \tag{3.53}$$

Each phase-space trajectory $(p_l(t), q_l(t))$ is confined to one N-torus which is diffeomorphic to the intersection of the $(2N-1)$-dimensional hypersurfaces $C_k, k \in \{1, \ldots, N\}$. Thus, for given initial values and couplings λ only parts of the respective Bloch-spheres are accessible. For a completely integrable system of N spins the motion of the phase point has at most N characteristics frequencies, which is, clearly, the case for $B = 0$. Nevertheless, there might be further constants of motion that are not obvious, which is indicated by more complicated periodic orbits and a number of additional frequencies.
If there aren't N invariants in mutual involution the integrability condition is not met, and therefore, at least for parts of the phase-space new types of trajectories occur that are very sensitive to slight changes of the initial conditions. These trajectories are referred to as *chaotic* and they have a continuous Fourier spectrum.

Throughout this thesis our interest focuses on models where the spins are differing much in magnitude. Let us introduce the labels $\vec{S} = \vec{S}_1$ and $\vec{J} = \vec{S}_2$ and denote their respective magnitudes by $s = |\vec{S}|$ and $j = |\vec{J}|$. It is to expect that in the limit $r \equiv \frac{j}{s} \gg 1$ the larger spin $\vec{J}$ acts as external "driving" for the smaller spin $\vec{S}$, while the back action from $\vec{S}$ to $\vec{J}$ is rather small.
Poincaré surfaces of section (PSS) for the motion of the small spin suggest that there exist regions of the parameter space B, λ with a mixed phase-space for the small spin, i.e. regular or chaotic motion for different initial conditions. In fig. 3.1 we show the PSS where we plot ϕ_S versus θ_S for a fixed θ_J.

Fixed points. To describe the domain of regular motion it is of particular interest to investigate the system's fixed points. We denote the fixed points introducing the notation

$$\mathcal{P} = \left(S_x^*, S_y^*, S_z^*, J_x^*, J_y^*, J_z^*\right) \,. \tag{3.54}$$

Due to the nature of the spin interaction one can easily see that there exist trivial fixed points when both spins are aligned (anti-)parallel with the magnetic field since the spins decouple then. Thus, we obtain for the spin polarization

$$\begin{aligned} \mathcal{P}^+ &= (0, 0, +s, 0, 0, \pm j) \\ \mathcal{P}^- &= (0, 0, -s, 0, 0, \pm j) \,. \end{aligned} \tag{3.55}$$

These fixed points are independent of the parameters B and λ, and, therefore, exist in the whole parameter regime. The usual path one would want to go from here is to investigate the fixed points further via a linear stability analysis. In the limit $r \gg 1$ one could linearize the equations for the larger spin around the fixed points and compute the Jacobian. In contrast to

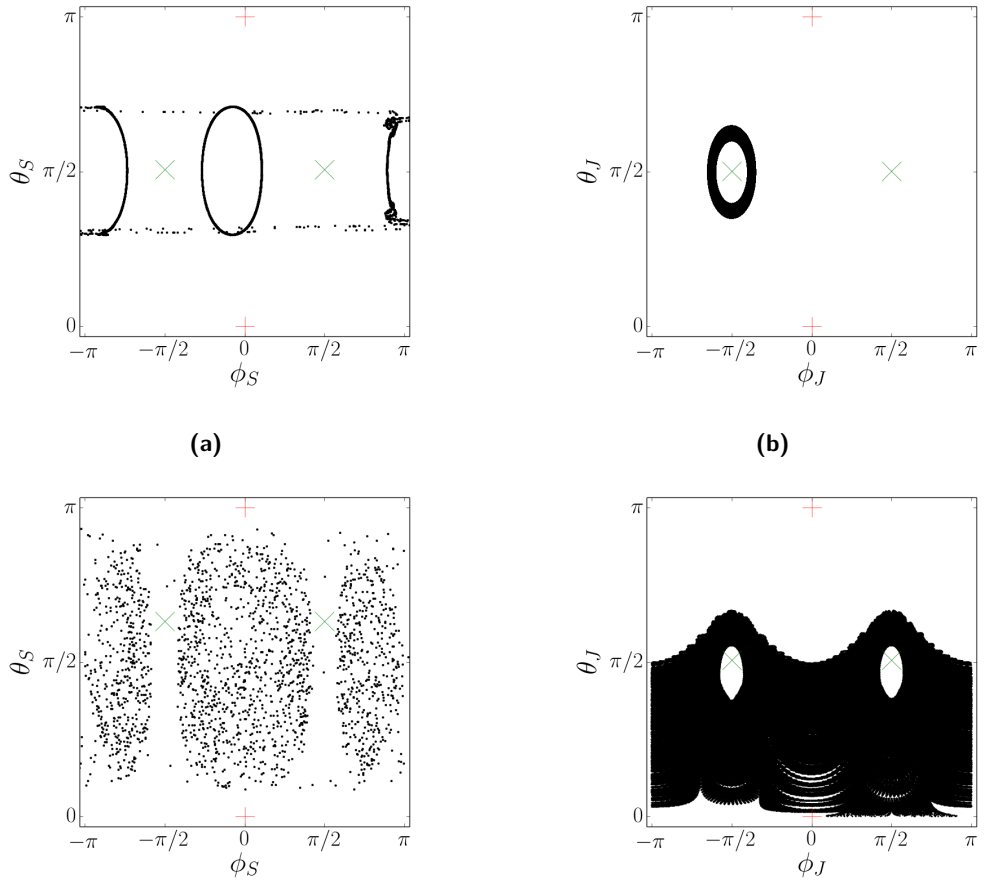

Figure 3.1.: PSS for spherical coordinates of the small spin $\vec{S}$,(a) and (c), and the corresponding dynamics of the spherical coordinates for $\vec{J}$, (b) and (d). The sections were taken with $\theta_J = \frac{\pi}{2}$. For small magnetic fields ($B/\lambda = 0.01$) the dynamics of $\vec{S}$ remain regular and are restricted to a torus as depicted in (a) and (b). When increasing the magnetic field ($B/\lambda = 0.2$) the dynamics become chaotic, cf. (c) and (d). $\vec{S}$ covers the whole phase-space, except for the area around the fixed points $\mathcal{P}^{\pm}$ (red '+') and $\mathcal{P}^{y}$ (green '×'). The ratio of the spins' magnitudes is $r = j/s = 20$. The initial conditions for both solutions are $\theta_S^{(0)} = \frac{8}{9}\pi, \phi_S^{(0)} = \frac{2}{9}\pi, \theta_J^{(0)} = 0.416\pi, \phi_J^{(0)} = 0.573\pi$.

two-dimensional systems knowing trace and determinant of the Jacobian are not sufficient and one needs the Jacobian's eigenvalues in order to characterize the fixed points as stable centers or saddle points by computing its eigenvalues [104, 105]. Such analysis, however, requires the knowledge of the partial derivatives of the small spin's components with respect to the large spin's components, which are in general not accessible, as there are no analytical solutions for eq. (3.49) with arbitrary nonvanishing magnetic field $B \neq 0$.

We observe, however, that systems with initial conditions close to $\mathcal{P}^{+}$ are stable centers with the spins performing periodic oscillations around it. Contrarily, we find the fixed point $\mathcal{P}^{-}$ to be a saddle point repelling approaching trajectories to induce a quasiperiodic switching between $+s$ and $-s$ when the system's dynamics is started in its vicinity, which resembles a strange attractor that is known, e.g., from the Rössler system [106], cf. the right hand side of fig. 3.2b.

A numerical Fourier analysis reveals the frequencies in the spins' motions for the periodic oscillations: we identify the frequencies ω_s and ω_j, which are appearing dominantly in the spins' motions. For $r \gg 1$ we find $\omega_s \gg \omega_j$. For the z components we find a frequency doubling $\omega_z = 2\omega_j$ as well as additional differential frequencies $\omega_\pm = \omega_s \pm \omega_j$. Those frequencies can be understood as, for instance, the S_z component does not couple to the magnetic field but is a product of $J_x(t)$ and $S_y(t)$. Ideally, those components develop as a superposition of sinusoidal functions of frequencies ω_s and ω_j, namely $J_x^{\text{eff}}(t) = b_s \sin(\omega_s t + \theta_s) + b_j \sin(\omega_j t + \theta_j)$ and $S_y^{\text{eff}}(t) = a_s \sin(\omega_s t + \phi_s) + a_j \sin(\omega_j t + \phi_j)$, respectively. The frequency ω_j describes an enveloping oscillation of the faster ω_s oscillations, while, the back-action from $\vec{S}$ to $\vec{J}$ is typically very small ($b_s \ll b_j$). Assuming, further, in-phase oscillations with respect to ω_j, i.e. $\phi_j = \theta_j = 0$ formal integration yields ($\lambda = 1$)

$$\begin{aligned} S_z^{\text{eff}}(t) &= \int_0^t dt' S_y^{\text{eff}}(t') J_x^{\text{eff}}(t') \\ &= -\frac{a_j b_j \sin(2\omega_j t)}{4\omega_j} + \frac{a_s b_j \sin(\phi_s - \omega_- t)}{2\omega_-} + \frac{a_s b_j \sin(\phi_s + \omega_+ t)}{2\omega_+} + \text{const}\,. \end{aligned} \tag{3.56}$$

The frequency doubling $\omega_z = 2\omega_j$ is often termed parametric resonance. The exact frequencies and amplitudes depend on the system parameters and the initial conditions, which have to be in proximity to the fixed point.

The system exhibits further fixed points, namely

$$\mathcal{P}^y = \left(0, \pm\sqrt{s^2 - \frac{B^2}{\lambda^2}}, -\frac{B}{\lambda}, 0, \pm\sqrt{j^2 - \frac{B^2}{\lambda^2}}, -\frac{B}{\lambda}\right). \tag{3.57}$$

These can be understood in terms of the anisotropic exchange coupling, since the x and z components of one and the same spin decouple, having either the trivial consequence of complete spin polarization ($\mathcal{P}^\pm$) or the z components being determined by the ratio $-B/\lambda$ and vanishing x components. It is obvious that this fixed point is only existing for $B \leq \lambda s$. If the initial conditions are close to the fixed point all components oscillate periodically with the same frequency, determined by the initial conditions. The further away from the fixed point the initial conditions are, the more we observe the separation of frequencies.
Moreover, there is a third set of fixed points,

$$\mathcal{P}^x = \left(\pm\frac{\mathcal{B}_1}{2B\lambda}, 0, -\frac{B^2 - \lambda^2(j^2 - s^2)}{2B\lambda}, \mp\frac{\mathcal{B}_1}{2B\lambda}, 0, -\frac{B^2 - \lambda^2(s^2 - j^2)}{2B\lambda}\right), \tag{3.58}$$

with $\mathcal{B}_1 = \sqrt{-\left[B^2 - \lambda^2(j-s)^2\right]\left[B^2 - \lambda^2(j+s)^2\right]}$ that occur only for nonvanishing magnetic fields that meet the condition $|B - \lambda j| < \lambda s$, i.e. for very large magnetic fields. Therefore, we will omit further analysis of this fixed point.
We verify that for fixed parameters B, λ the system exhibits regular and chaotic dynamics depending on the chosen initial conditions. We illustrate this by plotting the trajectories for different initial condition in terms of the Cartesian coordinates S_i and J_i with $i \in \{x, y, z\}$ on the Bloch sphere. As the spins' lengths are conserved, $\left\{\vec{S}^2, H\right\} = \left\{\vec{J}^2, H\right\} = 0$, the trajectories are restricted to the surface of Bloch spheres. Figure 3.2 displays that there are islands of regular dynamics around the fixed points that are not reached by quasiperiodic or chaotic trajectories. Note that while the small spin's chaotic trajectories reach nearly every point on the Bloch sphere the large spin is confined to a smaller region of the phase-space.

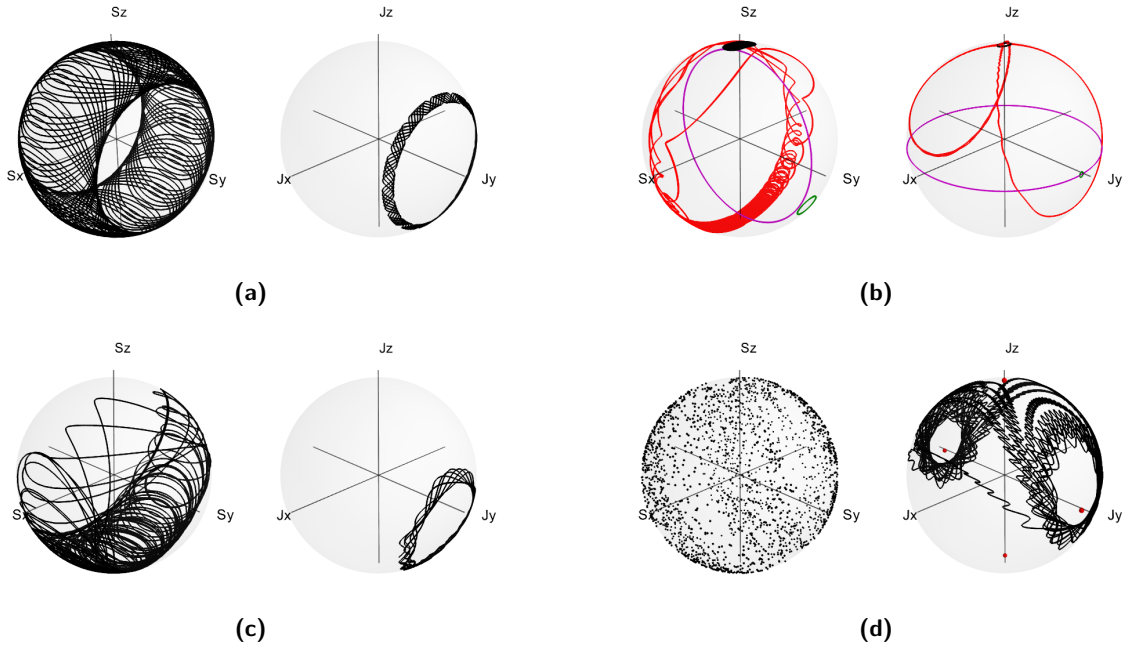

Figure 3.2.: Plots of the spins' dynamics in terms of Bloch sphere vectors for different parameters and initial conditions [small spin $\vec{S}$ on the left and large spin $\vec{J}$ on the right hand side of the respective panel]. For all plots the ratio of the spins' magnitude is set to $r = 20$. Panel (a) depicts the dynamics for the completely integrable system, $B = 0$, started at $S_x^{(0)} = s, S_y^{(0)} = S_z^{(0)} = 0, J_x^{(0)} = j/2, J_y^{(0)} = \sqrt{3}/2j, J_z^{(0)} = 0$. The magnetic fields for the solutions in panels (b) to (d) was $B/\lambda = 0.2$. In (b) the behavior close to the fixed points is depicted: the black trajectory shows the stable limit cycles with initial conditions close to $\mathcal{P}^+$. The red trajectories are obtained when starting close to $\mathcal{P}^-$. The dynamics depicted in magenta started at the fixed point $\mathcal{P}^y$ with opposite signs for the y components, i.e. $\operatorname{sgn} S_y^* = -\operatorname{sgn} J_y^*$; the trajectories are restricted to the S_y-S_z and J_x-J_y planes, respectively. The green line shows the rotation around the stable center $\mathcal{P}^y$ for $\operatorname{sgn} S_y^* = \operatorname{sgn} J_y^*$. In (c) and (d) the system parameters are identical but the dynamics are started from different initial conditions, i.e. the system is in its mixed phase. In (c) the dynamics are still periodic but with a number of frequencies involved; the initial conditions were the same as for (a). Panel (d) shows the PSS for $\vec{S}$. It reveals that the small spin covers the whole Bloch sphere except for the region around the fixed points. The large spins dynamics are restricted to the upper hemisphere and quasi-periodic, the region around the fixed points (red dots) is not covered. The initial conditions for (d) are $\theta_S = \frac{8}{9}\pi, \phi_S = \frac{2}{9}\pi, \theta_J = 0.416\pi, \phi_J = 0.573\pi$.

3.3.2. Quantum-to-Classical transition

Up to now, we have treated the two spin model classically. However, we want to show, briefly, that certain signatures of chaos can be revealed also in a quantum treatment. We follow the idea of Peres [107], which was also carried out by Srivastava *et al.* [108, 100] and Robb *et al.* [101] to compute and depict the simultaneous eigenvalues of the Hamiltonian and a second commuting operator.

Quantum webs of simultaneous eigenstates. This approach is based on the notion that it is difficult to attribute quantum numbers to the various energy levels in the complicated energy

spectra of highly excited quantum systems.
Let us consider a system of N degrees of freedom, described by a, in general, nonseparable Hamiltonian. In the so called Einstein-Brillouin-Keller (EBK) quantization method one looks for canonical invariants $I_1, \dots I_N$ of the Hamiltonian, that are called action variables [100, 107, 109]. As already stated above, a system with N degrees of freedom is called integrable (its quantum analogue is called *regular*) if invariants can be found everywhere in the phase-space and its orbits lie on N-dimensional tori. We can draw N topologically independent closed curves γ_k on each of those tori, which define the N action variables

$$I_k = \frac{1}{2\pi} \sum_k \oint_{\gamma_k} p_k dq_k \,. \tag{3.59}$$

The action variables label the tori and, therefore, any constant of motion C_A with respect to the dynamical variable A is a function $C_A(I_1, \dots, I_N)$.
In the EBK quantization the action variables evaluate to

$$I_k = a_k + m_k \hbar \,, \tag{3.60}$$

where a_k are constants and m_k are integers. Moreover, when expanding the C_A in powers of $\hbar$ it is straightforward to show that for any constant of motion of the system the eigenvalues differ by multiples of $\hbar$, i.e. $\hbar \sum_k m_k \partial C_A / \partial I_k$.

However, when a system becomes *irregular* (classically *nonintegrable*) there is no unambiguous way to label the energy levels by quantum numbers, that are related to constants of motion [110]. Moreover, the energies of the irregular spectrum are much more sensitive to slight changes or fixed perturbation.
Consequently, it would be useful to find a criterion to decide whether one can find "good" quantum numbers other than the energy, in order to distinguish regular from irregular quantum systems.
Often it is not known whether a system is integrable, such that we can cannot determine whether an arbitrary function $A(p, q)$ of the canonical variables is an invariant, i.e. has a vanishing Poisson bracket with the Hamiltonian.
Nonetheless, for any bounded variable A, which is independent of the Hamiltonian function H, we can determine its time average over the phase-space trajectory specified by the initial condition $(\theta_1^{(0)}, \phi_1^{(0)}, \theta_2^{(0)}, \phi_2^{(0)})$, or $(\vec{S}_1^{(0)}, \vec{S}_2^{(0)})$ respectively. Obviously, it is invariant and it reads

$$\langle A \rangle = \lim_{T \to \infty} \frac{1}{T} \int_0^T dt A\left(t; \vec{S}_1^{(0)}, \vec{S}_2^{(0)}\right) = C_A\left(\vec{S}_1^{(0)}, \vec{S}_2^{(0)}\right) . \tag{3.61}$$

This nonanalytic invariants are defined everywhere in phase-space except for a set of points with measure zero [100].
Let us transfer the last statements to the quantum language: We take any bounded operator $\hat{A}$ that represents a dynamical variable independent of $\hat{H}$ with $\left[\hat{A}, \hat{H}\right] \neq 0$. Then, we consider the operator $\hat{A}(t)$ in its spectral decomposition

$$\hat{A}(t) = \sum_{ij} \langle E_i | \hat{A}(0) | E_j \rangle \exp\left[\mathbf{i} (E_i - E_j) t/\hbar\right] |E_i\rangle \langle E_j| \,. \tag{3.62}$$

When taking the time average $\hat{A}_T$ of $\hat{A}(t)$, all off-diagonal elements are eliminated and one obtains (for a nondegenerate Hamiltonian)

$$\hat{A}_T = \lim_{T\to\infty} \frac{1}{T} \int_0^T dt\, \hat{A}(t) = \sum_i \langle E_i| \hat{A}(t) |E_j\rangle |E_i\rangle \langle E_j| \,. \tag{3.63}$$

Since $\hat{A}_T$ is diagonal in the energy representation it is possible to assign an eigenvalue to operator $\hat{A}_T$ for each eigenvalue of $\hat{H}$.
Let us assume that the considered system has $N = 2$ degrees of freedom and that we can find two good quantum numbers, m_1 and m_2, which correspond in the classical limit to two actions I_1 and I_2. Then the quantities $E(m_1, m_2) = \langle E| \hat{H} |E\rangle$ and $A_T(m_1, m_2) = \langle E| \hat{A}_T |E\rangle$ are expected to be smooth analytic functions of the quantum numbers m_1 and m_2. Reichl argues, that if $E(m_1, m_2)$ and $A_T(m_1, m_2)$ are known for a rather large range of m_1 and m_2 one can find a functional form for them for (large) sections of the spectrum [111]. The plot of $\langle E| \hat{A}_T |E\rangle$ versus E, on the other hand, gives a lattice of discrete points, which is called the *quantum web* [107, 100, 101, 111].

Srivastava *et al.* consider different two-spin XY models (coupling between the x and y components of the two spins), with either single-site anisotropy or exchange anisotropy, cf. [100]

$$\begin{aligned} \hat{H}_\gamma &= -\hbar^2 \left[(1+\gamma)\, \hat{\sigma}_1^x\, \hat{\sigma}_2^x + (1-\gamma)\, \hat{\sigma}_1^y\, \hat{\sigma}_2^y \right] , \\ \hat{H}_a &= -\hbar^2 \left(\hat{\sigma}_1^x\, \hat{\sigma}_2^x + \hat{\sigma}_1^y\, \hat{\sigma}_2^y \right) - \frac{1}{2} a \hbar^2 \left[(\hat{\sigma}_1^x)^2 + (\hat{\sigma}_2^x)^2 - \left(\hat{\sigma}_1^y\right)^2 - \left(\hat{\sigma}_2^y\right)^2 \right] . \end{aligned} \tag{3.64}$$

They studied their energy-spectra and analyzed how they are changed when the second constant of motion disappears [100]. The spectra can be decomposed with respect to invariant subspaces of different symmetry groups. For the XY models it is easy to show that they are invariant under the symmetry group $D_2 \otimes S_2$, i.e. the direct product of the group of rotations by an angle π about the x, y and z axes (D_2) and the group of permutations of two particles (S_2) [100, 111], which yields eight invariant subspaces. In [100] quantum webs are constructed from the Hamiltonian and the time average $(M_z^2)_T$ of the square of the sum $\hat{M}_z = \hat{\sigma}_1^z + \hat{\sigma}_2^z$ with respect to just two invariant subspaces. They show, that although the web exhibits some folds it is regular for $\hat{H}_\gamma$ in (3.64), as the classical counterpart is proven to be integrable. On the other hand, $\hat{H}_a$ is not integrable and for parts of the web the analytic structure is lost for higher a, which can be interpreted as signs of quantum chaos, cf. plots in [100].

We now want to turn back to our quantum two-spin system, eq. (3.46), with the spin quantum numbers σ_1, σ_2. For vanishing magnetic fields $B = 0$ in eq. (3.46) the 2nd constant of motion is trivial, namely, $\hat{\sigma}_y = \hat{\sigma}_1^y + \hat{\sigma}_2^y$. If a nonvanishing magnetic field is applied, we need to construct a second invariant using eqs. (3.62) and (3.63). Similarly to References [100, 101] we choose the time average of $\hat{A} = \sqrt{\hat{\sigma}_y^2}$ to construct a quantum web.
The Hamiltonian in eq. (3.46) is invariant with respect to the interchange of the two spins, $\hat{P}$, and the rotation of the spins by π about the z axis, i.e. operator

$$\hat{R}_2^z(\pi) = \mathrm{e}^{\mathbf{i}\pi\hat{\sigma}_z} \,, \tag{3.65}$$

where $\hat{\sigma}_z = \hat{\sigma}_1^z + \hat{\sigma}_2^z$. We, thus, form the quantum webs from the values $\sqrt{\langle E| \hat{\sigma}_y^2 |E\rangle}$ versus the values of E, for the class of states for which the permutation $\hat{P}$ and $\hat{R}_2^z(\pi)$, respectively, have the eigenvalues $(+1, -1)$. The quantum webs obtained for two spins with quantum numbers

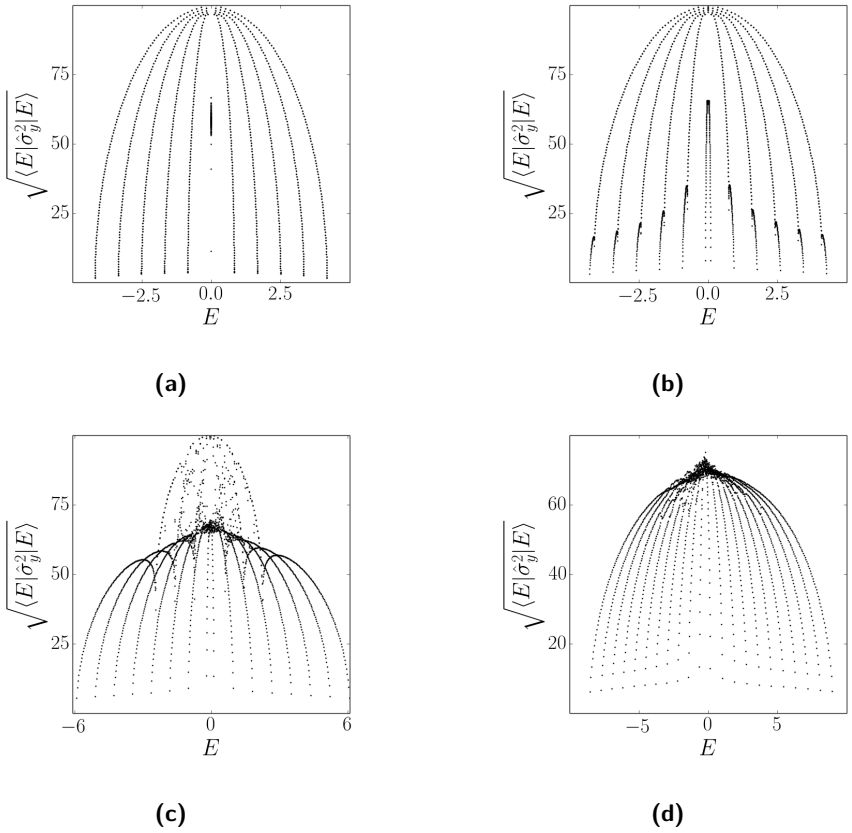

Figure 3.3.: Quantum webs formed from values of $\sqrt{\langle E|\,\hat{\sigma}_y^2\,|E\rangle}$ versus the values of E for a system with Hamiltonian in eq. (3.46). (a) $B/\lambda = 0$; (b) $B/\lambda = 0.01$; (c) $B/\lambda = 0.2$; (d) $B/\lambda = 0.5$. The two spins have quantum numbers $\sigma_1 = 5, \sigma_2 = 100$, such that we obtain $r = s_2/s_1 = 20$ in the classical limit.

$\sigma_1 = 5, \sigma_2 = 100$ (in classical limit this yields $r = 20 \gg 1$) and different magnetic fields B are depicted in fig. 3.3. The web is completely regular for a vanishing magnetic field. For small fields of $B/\lambda = 0.01$ a fold is developing, the model is predominantly integrable with this parameters, which the PSS depicted in fig. 3.1a already suggested. However, for intermediate fields $B/\lambda = 0.2$ the folds become more pronounced and the structure of the web is disrupted by many pairs of eigenvalues that are no longer part of the lattice, which we interpret as signatures of quantum chaotic behavior. This resembles, also in terms of the amount of chaos, what we have found for the classical case, cf. the PSS in fig. 3.1c.

The quantum-classical correspondence of two interacting spins was also investigated by Emerson and Ballentine for a model with a spin-spin coupling that is described by a sequence of δ-functions, i.e. a kicked interaction [112]. Their model allows for a treatment with Floquet operators in its quantum version and stroboscopic maps in its classical version. For both classical and quantum models they also find that for different parameters mixed phase-space regimes are developing as well as regimes where chaos is dominating. Further, they investigate the differences between quantum expectation values and classical Liouville averages for both regular

and chaotic dynamics beyond the short-time regime. For chaotic states the differences initially grow exponentially with an exponent that is larger than the largest Lyapunov exponent.
Emerson and Balletine have demonstrated that the exponent λ_{qc} which governs the initial growth rate of quantum-classical differences is not dependent on the quantum numbers (i.e. quantum spin lengths s and j, where $s \leq j$) and the effective prefactor of the growth scales with $1/j$, which is termed the logarithmic break-time rule [112]. The *break time* $t_b(j, p)$ determines the time at which quantum-classical differences go beyond some fixed tolerance p, with classical parameters and initial conditions kept constant.
On the other hand, it turns out that over long times the quantum observables remain well approximated by classical Liouville averages even for chaotic motions of few degree-of-freedom systems.

4. Transport through a single quantum dot coupled to a large external spin

[K. Mosshammer and T. Brandes. "Semiclassical spin-spin dynamics and feedback control in transport through a quantum dot". *Phys. Rev. B* 90 (13 2014), 134305]

4.1. Introduction

Of particular interest for the electronic dynamics of QD electrons is the coupling to external degrees of freedom. In serial semiconductor QDs the coupling to a phononic bath can give rise to spontaneous emission and absorption of phonons [114, 115], electronic decoherence [116, 34], or phonon replica in the transport characteristics [117]. Moreover, electrons tunneling to a QD device experience, for instance, a hyperfine and spin-orbit interaction with the nuclear spins of the host material [118, 82, 92]. Particularly, large Overhauser fields [119] are experienced by the electrons.
This interaction enables spin-flip transfer between the electronic and the nuclear spin system, which resolves the current in the spin-blockade regime of serially coupled QDs.
Transport experiments with QDs show that the hyperfine interaction can lift spin blockades and even induce self-sustained oscillations in currents with a period in the order of seconds [120] which is believed due to dynamical polarization of the nuclear spins addressed theoretically in Ref. [121, 122, 123, 124, 125, 126]. The hyperfine interaction in QDs has also been studied theoretically in detail [82, 122, 123, 127].
Similar to a previous work [128] our model is inspired by experiments on the hyperfine interaction with QDs without transport where electronic spins in single QDs [70, 73] or double QDs [129, 42] are considered in terms of spin relaxation and decoherence. There are also intriguing transport experiments where nonlinear behavior due to hyperfine interaction is induced: singlet-triplet state mixing in double QDs that leads to transport bistabilities [84], the single-electron spin manipulation in a double QD [130] or the lifting of spin blockades that leads to current fluctations driven by nuclear dynamics [127].
Exchange interactions that induce complex spin-spin dynamics also occur in molecular QDs. For the transport through molecular QDs [131] two types of degrees of freedom are relevant: molecule vibrations [132, 133, 134, 135, 136, 137, 138, 139, 140, 141, 142] or local magnetic moments in single molecular magnets [67, 143], which establish the research field of molecular spintronics [144, 145, 74]. In the last couple of years a number of theoretical works have been done on models with a single orbital as current-carrying channel [146, 147, 49, 148, 149, 150, 151, 152, 128, 153].
For example, Bode *et al.* [152] have derived Landau-Lifshitz-Gilbert-type equations of motion for the molecular spin based on a nonequilibrium Born-Oppenheimer-approximation, which assumes that the time scale of the dynamics of the local magnetic moment is much larger than the dwell time of the electrons. In Ref. [128] we have treated the dynamics of the average electron spin semiclassically in the infinite bias limit.

The host material of QDs often contains a huge number of spins (nuclear or molecular) and can be described by one large effective spin. Interacting spins in transport models with isotropic exchange coupling have been studied recently, where a characteristic current induced switching of magnetic layers [154, 155] or the external spin in QD setups [152, 156] was found as well as superradiant-like behavior in a single QD [157]. If the exchange coupling is anisotropic more involved nonlinear dynamics are spawned, that even contain chaos and which have been studied in detail for closed systems [98, 99, 100, 101, 158]. The nonlinear dynamics of anisotropically exchange coupled spins with connections to electronic reservoirs show intriguing features like self-sustained current oscillations, parametric oscillations, and chaotic dynamics. This has been addressed within different theoretical frameworks: In Refs. [128, 156] a quantum master equation with a classical large spin was used in an infinite bias limit to study the transport characteristics of single- and double-QD setups. Metelmann *et al.*[105] derived the equations of motion by Keldysh-Green functions.
We are particularly interested in controlling the spin interactions by intervening in the transport process, i.e. applying a closed-loop feedback to our model. The goal of such an intervention is to prevent the system from running into chaotic regimes or fixed points. The feedback we think of is included on the level of the master equation and inspired by the notion of Maxwell's demon, capable of sorting particles by conditionally inserting/removing a wall. This mechanism ideally does not require work to insert or remove the wall, which modifies the entropy balance (i.e. the second law of thermodynamics) while not affecting the energy balance (first law)[65]. A transport analog to the Maxwell demon is a device that is capable of generating electronic currents even against a bias voltage or thermal gradient by changing the energy barriers based solely on information about the current QD occupation. As an interesting application we show that our feedback scheme is capable of generating spin-currents of opposite directions.
Our Ref. [43] demonstrates the implementation of a demon-like feedback in a single-electron transistor and Ref. [44] provides an insight on the thermodynamics of a physical implementation. Recent experiments also show that it is, in fact, possible to transform information about particles into free energy [159, 160, 161]. For a transport setup the experimental difficulty is, clearly, to strongly modify the single-electron tunneling rates without changing the QD levels. However, investigations on quantum turnstile setups show that one can pump electrons by invoking a pump cycle based on the modulation of tunneling barriers by conventional electronics [162, 163]. Within these cycles electronic levels are not changed.

The remainder of this chapter starts in Sec. 4.2 with a detailed description of the model with the Hamiltonian (Sec. 4.2.1), the master equation (Sec. 4.3) and the introduction of the feedback mechanism (Sec. 4.5). The final equations of motion (EOMs) are presented in Sec. 4.6 and their resulting dynamics are discussed in Sec. 4.8. First we discuss the results for the transport without spin-spin interactions (Sec. 4.8.1). We proceed with discussing the results of solutions for the full system for infinite bias voltages (Sec. 4.8.2) and the results for the finite-bias regime are provided in Secs. 4.8.3 and 4.8.4. Finally, we conclude in Sec. 4.9.

4.2. Model

4.2.1. Hamiltonian

We consider a system of a single quantum dot (SQD) with one orbital level that is subject to an external magnetic field $\vec{B}$ in the z-direction which splits the quantum dot level. The SQD is coupled to electronic leads and without any further interaction the coupling leads to

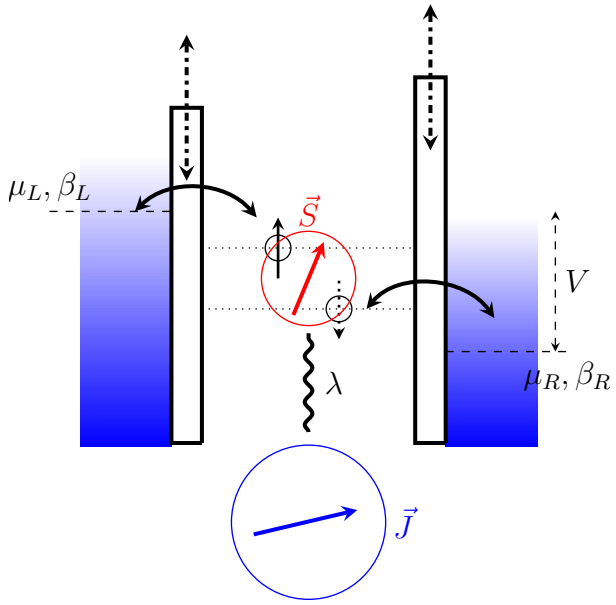

Figure 4.1.: Setup of the investigated system. An electronic spin $\vec{\hat{S}}$ (red) in a single quantum dot (SQD) is coupled to an external spin $\vec{\hat{J}}$ (blue) via an exchange interaction λ (wiggly line). The SQD level is split up by an external magnetic field $\vec{B}$ in z-direction. Due to coupling to the leads l (characterized by inverse temperatures β_l and chemical potentials μ_l) electronic transport is taking place on and off the SQD (solid arrows). The feedback mechanism, introduced in section 4.5, instantaneously modifies the tunneling barriers conditioned on the system states (dashdotted arrows).

the formation of two distinct spin-dependent current channels, since the spin of the tunneling electrons is assumed to be invariable while tunneling.
Moreover the model consists of a large spin $\vec{\hat{J}}$ with length j given by $\vec{\hat{J}}^2 |m,j\rangle = j(j+1)\,|m,j\rangle$, the z-component of which couples to the magnetic field as well and which is exchange-coupled with the electron-spin. For simplicity we comprise the g-factors of the electronic spin and the large spin and the Bohr magneton in our definition of B and assume the g-factors to be the same for electronic and large spin.
The full Hamiltonian reads as follows [cf. similar models [128, 156, 105]]

$$\hat{H} = \hat{H}_{\mathrm{SQD}} + \hat{H}_{\mathrm{J}} + \hat{H}_{\mathrm{int}} + \hat{H}_{\mathrm{leads}} + \hat{H}_{\mathrm{T}} \ , \tag{4.1}$$

and its components read

$$\begin{aligned}
\hat{H}_{\mathrm{SQD}} &= \sum_{\sigma=\uparrow,\downarrow} \varepsilon\, \hat{d}_\sigma^\dagger\, \hat{d}_\sigma + B\, \hat{S}_z \ , \\
\hat{H}_{\mathrm{J}} &= B\, \hat{J}_z \ , \quad \hat{H}_{\mathrm{int}} = \sum_{i=x,y,z} \lambda_i\, \hat{S}_i\, \hat{J}_i \ , \\
\hat{H}_{\mathrm{leads}} &= \sum_{kl\sigma} \varepsilon_{kl\sigma}\, \hat{c}_{kl\sigma}^\dagger\, \hat{c}_{kl\sigma} \qquad (l = L/R) \, , \\
\hat{H}_{\mathrm{T}} &= \sum_{kl\sigma} \left(\gamma_{kl\sigma}\, \hat{c}_{kl\sigma}^\dagger\, \hat{d}_\sigma + \mathrm{H.c.} \right) .
\end{aligned} \tag{4.2}$$

The operators $\hat{d}_\sigma^\dagger\,(\hat{d}_\sigma)$ describe the creation (annihilation) of an electron with spin $\sigma = \uparrow, \downarrow$ on the dot, $\hat{n}_\sigma$ is the related occupation number operator, $\hat{S}_i$ are the components of the electronic

spin operators in second quantization and can be written in terms of the creation/annihilation operators

$$\begin{aligned}\hat{S}_x &= \frac{1}{2}\Big(\hat{d}_\uparrow^\dagger \hat{d}_\downarrow + \hat{d}_\downarrow^\dagger \hat{d}_\uparrow\Big) = \frac{1}{2}\Big(\hat{S}_+ + \hat{S}_-\Big),\\ \hat{S}_y &= \frac{1}{2\mathbf{i}}\Big(\hat{d}_\uparrow^\dagger \hat{d}_\downarrow - \hat{d}_\downarrow^\dagger \hat{d}_\uparrow\Big) = \frac{1}{2\mathbf{i}}\Big(\hat{S}_+ - \hat{S}_-\Big),\\ \hat{S}_z &= \frac{1}{2}\Big(\hat{n}_\uparrow - \hat{n}_\downarrow\Big),\end{aligned} \tag{4.3}$$

with the usual commutation relations for angular momentum operators $(i,j,k = x,y,z, \hbar = 1)$

$$\big[\hat{S}_i\,, \hat{S}_j\big] = \mathbf{i}\sum_k \varepsilon_{ijk}\,\hat{S}_k\ , \tag{4.4}$$

where ε_{ijk} is the Levi-Civita-Symbol.
The electronic leads are assumed to be noninteracting. Electrons of momentum k and spin σ in the l-th lead are created(annihilated) by the corresponding operators $\hat{c}_{kl\sigma}^\dagger$ ($\hat{c}_{kl\sigma}$). The transitions between a state in the leads and the electronic levels are described by $\hat{H}_{\mathrm{T}}$, the tunneling amplitudes for these transitions are $\gamma_{kl\sigma}$.

4.3. Master equation for exchange coupling-assisted transport

The microscopic dynamics of the system described by the Hamiltonian (4.1) is involved. In particular, we are interested in the dynamics of single-particle observables such as components of the average electron and large spin and we will consider the reduced density-matrix of electrons dwelling in the dots.
The system's dynamics are governed by different time scales. First of all, we assume that the electronic leads are in thermal equilibrium and we have the time scale τ_{B} on which the bath correlations decay during a tunneling event. The second time scale is set by the electron tunneling, which we assume is much faster than the precession of the large spin; that implies that electron spin fluctuations do not affect the large spin dynamics and vice versa, which is reflected by a mean-field approximation. Another time scale is set by the instantaneous feedback mechanism that depends only on the occupation of the SQD.
We derive a Born-Markov master equation that governs the evolution of density operator $\hat{\rho}_{\mathrm{S}}$, for the SQD degrees of freedom. The resulting Liouvillian superoperator $\hat{\mathcal{L}}$ derived in the following is not only parametrized by the Markovian system-bath tunneling rates $\Gamma_{l\sigma}(\omega) = 2\pi\sum_k |\gamma_{kl\sigma}|^2\delta(\varepsilon_{kl\sigma} - \omega)$ and the lead Fermi functions $f_l(\omega) = [\mathrm{e}^{\beta(\omega-\mu_l)}+1]^{-1}$ but also by the (slow) dynamics of the large spin $\vec{\hat{J}}$ and in particular by its interaction with the electrons in the SQD. Within the derivation a mean-field approach, that neglects the (fast) fluctuations of the large spin, has been made. Therefore, the influence of the large spin is reflected by the effective Zeeman splitting $\varepsilon_z(t) = B + \lambda_z\langle\hat{J}_z\rangle_t$ that has a contribution coming from the large spin's polarisation. On the other hand the exchange coupling induces flips of the electronic spins driven by the parameter $\Lambda(t) = \frac{\lambda_x}{2}\langle\hat{J}_x\rangle_t + \mathbf{i}\frac{\lambda_y}{2}\langle\hat{J}_y\rangle_t$.

4.4. Derivation of the master equation

In terms of a system bath theory, as carried out in chapter 2 the total Hamiltonian (4.1) consists of three parts, namely

$$\hat{H} = \hat{H}_{\mathrm{S}} + \hat{H}_{\mathrm{B}} + \hat{H}_{\mathrm{I}}\ , \tag{4.5}$$

where the system part $\hat{H}_{\mathrm{S}} = \hat{H}_{\mathrm{SQD}} + \hat{H}_{\mathrm{J}} + \hat{H}_{\mathrm{int}}$ comprises the dynamics of the system, i.e. the SQD and the large spin and the interaction between them. The electronic leads form the bath described by $\hat{H}_{\mathrm{B}} = \hat{H}_{\mathrm{leads}}$ and the coupling between system and bath degrees of freedom is denoted by the interaction Hamiltonian $\hat{H}_{\mathrm{I}} = \hat{H}_{\mathrm{T}}$.
Along the lines of our derivation in chapter 2 we derive the dynamics of the system density matrix. Carrying out the Born- and Markov-approximations we obtain the Born-Markov master-equation in the Schrödinger picture, eq. (2.30)

$$\begin{aligned}\frac{\partial}{\partial t}\hat{\rho}_{\mathrm{S}} = &-\mathbf{i}\left[\hat{H}_{\mathrm{S}}, \hat{\rho}_{\mathrm{S}}(t)\right] - \sum_{\alpha\beta}\int_0^\infty d\tau \Big\{ C_{\alpha\beta}(\tau)\left[\hat{A}_\alpha, \mathrm{e}^{-\mathbf{i}\hat{H}_{\mathrm{S}}\tau}\,\hat{A}_\beta\,\mathrm{e}^{+\mathbf{i}\hat{H}_{\mathrm{S}}\tau}\,\hat{\rho}_{\mathrm{S}}(t)\right] \\ &+ C_{\beta\alpha}(-\tau)\left[\hat{\rho}_{\mathrm{S}}(t)\,\mathrm{e}^{-\mathbf{i}\hat{H}_{\mathrm{S}}\tau}\,\hat{A}_\beta\,\mathrm{e}^{+\mathbf{i}\hat{H}_{\mathrm{S}}\tau}, \hat{A}_\alpha\right]\Big\}. \end{aligned} \tag{4.6}$$

4.4.1. Mean-field approximation

We want to treat the interaction of electronic and large spin in a semiclassical manner, which should be valid as long as the external spin is sufficiently large ($j \gg 1$) and we can neglect its fluctuations. Consequently, there is no decay of the large spin due to dissipation and the length of the large spin will be conserved on the microscopic level,

$$\left[\vec{\hat{J}}^2, \hat{H}\right] = 0\,. \tag{4.7}$$

In a mean-field approach we rewrite the Hamiltonian describing the spin-spin interaction, $\hat{H}_{\mathrm{int}}$, by substituting the quantum operators $\hat{S}_i$, $\hat{J}_i$ by the sum of their expectation values and their fluctuation around the expectation values

$$\hat{S}_i = \langle\hat{S}_i\rangle + \delta\,\hat{S}_i\ , \quad \hat{J}_i = \langle\hat{J}_i\rangle + \delta\,\hat{J}_i\ , \tag{4.8}$$

which implies

$$\hat{S}_i\,\hat{J}_i = \left(\langle\hat{S}_i\rangle + \delta\,\hat{S}_i\right)\left(\langle\hat{J}_i\rangle + \delta\,\hat{J}_i\right) = \langle\hat{S}_i\rangle\,\hat{J}_i + \hat{S}_i\,\langle\hat{J}_i\rangle + \delta\,\hat{S}_i\,\delta\,\hat{J}_i - \langle\hat{S}_i\rangle\,\langle\hat{J}_i\rangle\ . \tag{4.9}$$

Within the mean-field approximation products of spin fluctuators $\delta\,\hat{S}_i\,\delta\,\hat{J}_i$ are neglected, and we obtain

$$\hat{H}_{\mathrm{int}}^{\mathrm{MF}} = \sum_i \lambda_i\left(\hat{S}_i\,\langle\hat{J}_i\rangle + \langle\hat{S}_i\rangle\,\hat{J}_i - \langle\hat{S}_i\rangle\,\langle\hat{J}_i\rangle\right)\ . \tag{4.10}$$

The system Hamiltonian in the unitary part of (4.6) is, accordingly,

$$\hat{H}_{\mathrm{S}} = \varepsilon\,(\hat{n}_\uparrow + \hat{n}_\downarrow) + \frac{B}{2}\,(\hat{n}_\uparrow - \hat{n}_\downarrow) + \hat{H}_{\mathrm{int}}^{\mathrm{MF}} + \hat{H}_{\mathrm{J}}\ , \tag{4.11}$$

where we find the following vanishing commutators

$$\left[\langle\hat{S}_i\rangle\,\hat{J}_i, \hat{\rho}_{\mathrm{S}}\right] = \left[\langle\hat{S}_i\rangle\,\langle\hat{J}_i\rangle\,\mathbb{1}, \hat{\rho}_{\mathrm{S}}\right] = \left[\hat{H}_{\mathrm{J}}, \hat{\rho}_{\mathrm{S}}\right] = 0\,. \tag{4.12}$$

As a consequence we rewrite the system Hamiltonian as an effective Hamiltonian by comprising all terms contributing to electronic level shifts and all terms that participate in the spin-flip processes

$$\begin{aligned}\hat{H}_{\mathrm{S}}^{\mathrm{eff}}(t) &= \sum_\sigma \varepsilon_\sigma(t)\,\hat{n}_\sigma + \Lambda^*(t)\,\hat{S}_+ + \Lambda(t)\,\hat{S}_- \\ &= \frac{\varepsilon_z(t)}{2}\,\hat{S}_z + \Lambda^*(t)\,\hat{S}_+ + \Lambda(t)\,\hat{S}_-\ , \end{aligned} \tag{4.13}$$

where we have set the absolute electronic levels to $\varepsilon = 0$ for convenience and defined

$$\varepsilon_\sigma(t) = \varepsilon \pm \frac{B}{2} \pm \frac{\lambda_z}{2} \langle \hat{J}_z \rangle_t \,, \tag{4.14}$$

$$\varepsilon_z(t) = \varepsilon_\uparrow(t) - \varepsilon_\downarrow(t) = B + \lambda_z \langle \hat{J}_z \rangle_t \,, \tag{4.15}$$

$$\Lambda(t) = \frac{\lambda_x}{2} \langle \hat{J}_x \rangle_t + \mathbf{i} \frac{\lambda_y}{2} \langle \hat{J}_y \rangle_t \,. \tag{4.16}$$

Note that the parameters are explicitly time-dependent, although we assume the time scale set by $\varepsilon_\sigma(t)$ and $\Lambda(t)$ to be much slower than the time scale of the lead-correlations τ_B and as well slower than the time scale of the electronic tunneling. However, for convenience, we will not always write these time-dependencies in the following.

4.4.2. System and bath coupling operators

In order to evaluate the master equation (4.6) we have to identify system operators $\hat{A}_\alpha$ and the corresponding bath operators $\hat{B}_\alpha$ that define the bath correlation functions.
The system-bath coupling operator reads

$$\hat{H}_\mathrm{T} = \sum_{kl\sigma} \gamma_{kl\sigma}\, \hat{c}^\dagger_{kl\sigma}\, \hat{d}_\sigma + \sum_{kl\sigma} \gamma^*_{kl\sigma}\, \hat{d}^\dagger_\sigma\, \hat{c}_{kl\sigma} = \sum_\sigma \hat{d}^\dagger_\sigma \sum_{kl} \gamma^*_{kl\sigma}\, \hat{c}_{kl\sigma} - \sum_\sigma \hat{d}_\sigma \sum_{kl} \gamma_{kl\sigma}\, \hat{c}^\dagger_{kl\sigma} \,. \tag{4.17}$$

This form, obviously, does not comply with the form we postulated in (2.3). We tackle this problem, by decomposing fermionic operators as tensor products of Pauli matrices σ_i and the 2-dimensional identity matrix $\mathbb{1}$, which is called Jordan-Wigner-transformation [164, 165]. We may, thus, define the fermionic coupling operators in a form that satisfies (2.3). We introduce the operators

$$\begin{aligned}
\tilde{d}_\uparrow &= \sigma_- \otimes \mathbb{1} \,, \quad \tilde{d}^\dagger_\uparrow = \sigma_+ \otimes \mathbb{1} \,, \\
\tilde{d}_\downarrow &= \sigma_z \otimes \sigma_- \,, \quad \tilde{d}^\dagger_\downarrow = \sigma_z \otimes \sigma_+ \,, \\
\tilde{c}_{kl\sigma} &= \underbrace{\sigma_z \otimes \cdots \otimes \sigma_z}_{k-1 \text{ times}} \otimes \sigma_- \otimes \mathbb{1} \otimes \cdots \otimes \mathbb{1} \,, \\
\tilde{c}^\dagger_{kl\sigma} &= \sigma_z \otimes \cdots \otimes \sigma_z \otimes \sigma_+ \otimes \mathbb{1} \otimes \cdots \otimes \mathbb{1} \,.
\end{aligned} \tag{4.18}$$

Here we used the auxiliary adjoint matrices $\sigma_\pm = \frac{1}{2}(\sigma_x \pm \mathbf{i}\sigma_y)$, with $(\sigma_+)^\dagger = \sigma_-$. As σ_z is self-adjoint and we have $\sigma_-\sigma_z = \sigma_-$ and $\sigma_+\sigma_z = -\sigma_+$ it is apparent that the interaction Hamiltonian has the desired form, namely

$$\hat{H}_\mathrm{I} = \sum_\sigma \left[\tilde{d}^\dagger_\sigma \otimes \sum_{kl} \gamma^*_{kl\sigma} \tilde{c}_{kl\sigma} + \tilde{d}_\sigma \otimes \sum_{kl} \gamma_{kl\sigma} \tilde{c}^\dagger_{kl\sigma} \right] . \tag{4.19}$$

We assume that the fermionic operators are given in the Jordan-Wigner-representation and go back to our old notation.
When comparing (4.19) and (2.3), it is straightforward to identify the following system operators

$$\begin{aligned}
\hat{A}_1 = \hat{A}_5 = \hat{A}^\dagger_2 = \hat{A}^\dagger_6 = \hat{d}_\uparrow \,, \\
\hat{A}_3 = \hat{A}_7 = \hat{A}^\dagger_4 = \hat{A}^\dagger_8 = \hat{d}_\downarrow \,,
\end{aligned} \tag{4.20}$$

while the corresponding bath coupling operators are identified as

$$\hat{B}_1 = \sum_k \gamma^*_{kR\uparrow}\,\hat{c}^\dagger_{kR\uparrow}\,, \quad \hat{B}_2 = \sum_k \gamma_{kR\uparrow}\,\hat{c}_{kR\uparrow}\,, \quad \hat{B}_3 = \sum_k \gamma^*_{kR\downarrow}\,\hat{c}^\dagger_{kR\downarrow}\,, \quad \hat{B}_4 = \sum_k \gamma_{kR\downarrow}\,\hat{c}_{kR\downarrow}\,,$$
$$\hat{B}_5 = \sum_k \gamma^*_{kL\uparrow}\,\hat{c}^\dagger_{kL\uparrow}\,, \quad \hat{B}_6 = \sum_k \gamma_{kL\uparrow}\,\hat{c}_{kL\uparrow}\,, \quad \hat{B}_7 = \sum_k \gamma^*_{kL\downarrow}\,\hat{c}^\dagger_{kL\downarrow}\,, \quad \hat{B}_8 = \sum_k t_{kL\downarrow}\,\hat{c}_{kL\downarrow}\,. \tag{4.21}$$

In a next step we will calculate the interaction picture for the system operators $\hat{A}_\alpha$ by neglecting the spin-flip terms in the effective Hamiltonian and use the free Hamiltonian instead, which reads

$$\hat{H}_{\mathrm{S}}^{\mathrm{free}}(t) = \sum_\sigma \varepsilon_\sigma(t)\,\hat{d}^\dagger_\sigma\,\hat{d}_\sigma\,. \tag{4.22}$$

The effective Hamiltonian $\hat{H}_{\mathrm{S}}^{\mathrm{eff}}(t)$, where the large spin only enters in form of parameters has block-diagonal form in the local basis $|a\rangle$ with $a \in \{0,\uparrow,\downarrow,d\}$. The labels $\uparrow$ / $\downarrow$ denote that either the $\uparrow$- or the $\downarrow$-level is filled, while labels 0 and d denote an empty or an doubly (i.e. by a $\uparrow$ and a $\downarrow$-electron) occupied QD. Along its diagonal $\hat{H}_{\mathrm{S}}^{\mathrm{eff}}(t)$ has two 1×1 blocks, that correspond to the states $|0\rangle$ and $|d\rangle$, the third block is of dimension 2×2 associated to the situation where the QD is occupied either by a $\uparrow$- or a $\downarrow$-electron. The energies $\varepsilon_{\uparrow/\downarrow}$ are the diagonal elements and the spin-flip contributions $\Lambda^{(*)}$ the off-diagonal elements. Contrarily, $\hat{H}_{\mathrm{S}}^{\mathrm{free}}(t)$ is already diagonal in the local basis, as we do not take into account the coupling of the two levels. As a consequence we do not have to perform the secular approximation explicitly, as there are only terms rotating with respect to τ in eq. (2.32).

In the following paragraphs we discuss how eq. (4.6) is evaluated with the replacement $\hat{H}_{\mathrm{S}}(t) \to \hat{H}_{\mathrm{S}}^{\mathrm{eff}}(t) \to \hat{H}_{\mathrm{S}}^{\mathrm{free}}(t)$ in the integral and under which conditions this is justified. We calculate the interaction picture terms, $\mathrm{e}^{-\mathbf{i}\hat{H}_{\mathrm{S}}^{\mathrm{free}}\tau}\,\hat{d}^{(\dagger)}_\sigma\,\mathrm{e}^{+\mathbf{i}\hat{H}_{\mathrm{S}}^{\mathrm{free}}\tau}$, by employing the Baker-Campbell-Hausdorff-formula, i.e.

$$\mathrm{e}^{X}\,Y\,\mathrm{e}^{-X} = \sum_{m=0}^{\infty}\frac{1}{m!}\,[X,Y]_m\,, \tag{4.23}$$

where $[X,Y]_m = [X,[X,Y]_{m-1}]$ is defined recursively and $[X,Y]_0 = Y$. Thus, we have to find the commutators $[X,Y]$ and use the fermionic (anti-)commutation relations

$$\begin{aligned}[X,Y] &= \left[-\mathbf{i}\,\hat{H}_{\mathrm{S}}^{\mathrm{free}}\tau, \hat{d}_\sigma\right] = -\mathbf{i}\sum_\mu \varepsilon_\mu\tau\left[\hat{d}^\dagger_\mu\,\hat{d}_\mu\,,\hat{d}_\sigma\right] = -\mathbf{i}\sum_\mu \varepsilon_\mu\tau\left[\hat{d}^\dagger_\mu\left\{\hat{d}_\mu\,,\hat{d}_\sigma\right\} - \left\{\hat{d}^\dagger_\mu\,,\hat{d}_\mu\right\}\hat{d}_\sigma\right]\\ &= \mathbf{i}\sum_\mu \varepsilon_\mu\tau\delta_{\mu\sigma}\,\hat{d}_\sigma = \mathbf{i}\varepsilon_\sigma\tau\,\hat{d}_\sigma\,.\end{aligned} \tag{4.24}$$

Applied recursively, we get

$$\mathrm{e}^{-\mathbf{i}\hat{H}_{\mathrm{S}}^{\mathrm{free}}\tau}\,\hat{d}_\sigma\,\mathrm{e}^{+\mathbf{i}\hat{H}_{\mathrm{S}}^{\mathrm{free}}\tau} = \mathrm{e}^{\mathbf{i}\varepsilon_\sigma\tau}\,\hat{d}_\sigma\,, \tag{4.25}$$
$$\mathrm{e}^{-\mathbf{i}\hat{H}_{\mathrm{S}}^{\mathrm{free}}\tau}\,\hat{d}^\dagger_\sigma\,\mathrm{e}^{+\mathbf{i}\hat{H}_{\mathrm{S}}^{\mathrm{free}}\tau} = \mathrm{e}^{-\mathbf{i}\varepsilon_\sigma\tau}\,\hat{d}^\dagger_\sigma\,. \tag{4.26}$$

Justification for the use of the free Hamiltonian

For a convenient notation we split up the effective system Hamiltonian $\hat{H}_{\mathrm{S}}^{\mathrm{eff}} = \hat{H}_0 + \hat{H}_1$, where $\hat{H}_0 = \hat{H}_{\mathrm{S}}^{\mathrm{free}}$ contains the two SQD levels and $\hat{H}_1 = \hat{H}_{\mathrm{S}}^{\mathrm{SF}}$ describes the spin-flips due to the exchange

interaction. The transformation of an arbitrary system operator $\hat{A}$ to the interaction picture can be written in terms of the Schwinger-Dyson identity involving superoperators $\hat{\mathcal{L}}_x \cdot = \left[\hat{H}_x\,, \cdot\right]$

$$\mathrm{e}^{-\mathbf{i}\hat{\mathcal{L}}_\mathrm{S}\tau} = \mathrm{e}^{-\mathbf{i}(\hat{\mathcal{L}}_0+\hat{\mathcal{L}}_1)\tau} = \mathrm{e}^{-\mathbf{i}\hat{\mathcal{L}}_0\tau} \sum_{n=0}^{\infty} (-\mathbf{i})^n \int_0^\tau d\tau_1 \int_0^{\tau_1} d\tau_2 \ldots \int_0^{\tau_{n-1}} d\tau_n \hat{\boldsymbol{\mathcal{L}}}_{\mathbf{1}}(\tau_1)\hat{\boldsymbol{\mathcal{L}}}_{\mathbf{1}}(\tau_2)\cdots\hat{\boldsymbol{\mathcal{L}}}_{\mathbf{1}}(\tau_n)\,, \tag{4.27}$$

where for any operator $\hat{A}$

$$\hat{\boldsymbol{\mathcal{L}}}_{\mathbf{1}}(\tau)\,\hat{A} = \mathrm{e}^{\mathbf{i}\hat{\mathcal{L}}_0\tau}\,\hat{\mathcal{L}}_1\,\mathrm{e}^{-\mathbf{i}\hat{\mathcal{L}}_0\tau}\,\hat{A} = \left[\mathrm{e}^{\mathbf{i}\hat{H}_0\tau}\,\hat{H}_1\,\mathrm{e}^{-\mathbf{i}\hat{H}_0\tau}, \hat{A}\right] = \left[\hat{\boldsymbol{H}}_{\mathbf{1}}(\tau), \hat{A}\right]. \tag{4.28}$$

The interaction picture operator in terms of this expansion up to the first order reads

$$\mathrm{e}^{-\mathbf{i}\hat{H}_\mathrm{S}\tau}\,\hat{A}\,\mathrm{e}^{\mathbf{i}\hat{H}_\mathrm{S}\tau} = \mathrm{e}^{-\mathbf{i}(\hat{\mathcal{L}}_0+\hat{\mathcal{L}}_1)\tau}\,\hat{A} = \mathrm{e}^{-\mathbf{i}\hat{\mathcal{L}}_0\tau}\,\hat{A} - \mathbf{i}\,\mathrm{e}^{-\mathbf{i}\hat{\mathcal{L}}_0\tau}\int_0^\tau d\tau_1 \left[\hat{\boldsymbol{H}}_{\mathbf{1}}(\tau_1), \hat{A}\right] + \ldots\,. \tag{4.29}$$

where we have to write the spin-flip Hamiltonian $\hat{H}_1$ in the interaction picture by applying, again, the Baker-Campbell-Hausdorff-formula

$$\hat{\boldsymbol{H}}_{\mathbf{1}}(\tau) = \mathrm{e}^{\mathbf{i}\varepsilon_z\tau}\,\Lambda^*\,\hat{S}_+ + \mathrm{e}^{-\mathbf{i}\varepsilon_z\tau}\,\Lambda\,\hat{S}_-\,, \tag{4.30}$$

which introduces the effective Zeeman-splitting $\varepsilon_z(t) = \varepsilon_\uparrow(t) - \varepsilon_\downarrow(t) = B + \lambda_z\,\langle \hat{J}_z \rangle_t$.
The integrals in (4.6) then read

$$\begin{aligned}
(*) &= \int_0^\infty d\tau C_{\alpha\beta}(\tau)\left[\hat{A}_\alpha\,, \mathrm{e}^{-\mathbf{i}\hat{H}_\mathrm{S}\tau}\,\hat{A}_\beta\,\mathrm{e}^{+\mathbf{i}\hat{H}_\mathrm{S}\tau}\,\hat{\rho}_\mathrm{S}(t)\right] \\
&= \int_0^\infty d\tau C_{\alpha\beta}(\tau)\left[\hat{A}_\alpha\,, \mathrm{e}^{-\mathbf{i}\hat{H}_0\tau}\,\hat{A}_\beta\,\mathrm{e}^{+\mathbf{i}\hat{H}_0\tau}\,\hat{\rho}_\mathrm{S}(t)\right] + (*^{(1)})\,, \qquad (4.31)\\
(*^{(1)}) &= \int_0^\infty d\tau C_{\alpha\beta}(\tau)\left[\hat{A}_\alpha\,, -\mathbf{i}\,\mathrm{e}^{-\mathbf{i}\hat{\mathcal{L}}_0\tau}\int_0^\tau d\tau_1 \left\{\mathrm{e}^{\mathbf{i}\varepsilon_z\tau_1}\,\Lambda^*\left[\hat{S}_+\,, \hat{A}_\beta\right] + \mathrm{e}^{-\mathbf{i}\varepsilon_z\tau_1}\,\Lambda\left[\hat{S}_-\,, \hat{A}_\beta\right]\right\}\hat{\rho}_\mathrm{S}(t)\right] \\
&= \int_0^\infty d\tau C_{\alpha\beta}(\tau) \\
&\qquad \times\left[\hat{A}_\alpha\,, -\mathbf{i}\,\mathrm{e}^{-\mathbf{i}\hat{\mathcal{L}}_0\tau}\left\{\frac{\Lambda^*}{\varepsilon_z}\left(\mathrm{e}^{\mathbf{i}\varepsilon_z\tau} - 1\right)\left[\hat{S}_+\,, \hat{A}_\beta\right] + \frac{\Lambda}{\varepsilon_z}\left(1 - \mathrm{e}^{-\mathbf{i}\varepsilon_z\tau}\right)\left[\hat{S}_-\,, \hat{A}_\beta\right]\right\}\hat{\rho}_\mathrm{S}(t)\right].
\end{aligned}$$

Here we have to consider two different time scales: the time scale τ_B set by the decay of the bath correlations that is in general much faster than the time scale set by the Zeeman splitting ε_z, i.e. $\varepsilon_z\tau_\mathrm{B} \ll 1$. We can thus perform an expansion in the parameter $\varepsilon_z\tau$: $\frac{\Lambda}{\varepsilon_z}\left(1 - \mathrm{e}^{-\mathbf{i}\varepsilon_z\tau}\right) \approx -\mathbf{i}\Lambda\tau$. As a consequence, it is justified to neglect the first-order corrections, $(*^{(1)})$ in (4.31), if the bath correlation time τ_B is sufficiently short compared to the time scale of the spin-flip dynamics, i.e. $\Lambda\tau_\mathrm{B} \ll 1$. Note that Schuetz *et al.* have provided a calculation for higher order corrections in a similar setup which suggests that the n-th order correction scales with $(\Lambda\tau_\mathrm{B})^n$.[157]

4.4.3. Transition rates

In order to calculate the transition rates we first recall the half-sided Fourier transformation of the bath-correlation functions and its splitting into hermitian and anti-hermitian parts, compare eqs. (2.34), (2.35) and (2.44).
With the identified system and bath operators, (4.20) and (4.21), we can exemplarily calculate the dissipator with respect to tunneling between the right lead and the ↑-state

$$\begin{aligned}(\star) = &\int_0^\infty d\tau C_{12}(\tau)\,\mathrm{e}^{-\mathbf{i}\varepsilon_\uparrow\tau}\left[\hat{d}_\uparrow\,,\hat{d}_\uparrow^\dagger\,\hat{\rho}_\mathrm{S}(t)\right] + \int_0^\infty d\tau C_{21}(-\tau)\,\mathrm{e}^{-\mathbf{i}\varepsilon_\uparrow\tau}\left[\hat{d}_\uparrow^\dagger\,\hat{\rho}_\mathrm{S}(t),\hat{d}_\uparrow\right]\\ &+\int_0^\infty d\tau C_{21}(\tau)\,\mathrm{e}^{\mathbf{i}\varepsilon_\uparrow\tau}\left[\hat{d}_\uparrow^\dagger\,,\hat{d}_\uparrow\,\hat{\rho}_\mathrm{S}(t)\right] + \int_0^\infty d\tau C_{12}(-\tau)\,\mathrm{e}^{\mathbf{i}\varepsilon_\uparrow\tau}\left[\hat{d}_\uparrow\,\hat{\rho}_\mathrm{S}(t),\hat{d}_\uparrow^\dagger\right],\end{aligned} \tag{4.32}$$

which reads with the definition for the half-sided Fourier transformations (2.34)

$$\begin{aligned}(\star) &= \Gamma_{12}^+(-\varepsilon_\uparrow)\left[\hat{d}_\uparrow\,,\hat{d}_\uparrow^\dagger\,\hat{\rho}_\mathrm{S}(t)\right] + \Gamma_{12}^-(-\varepsilon_\uparrow)\left[\hat{d}_\uparrow\,\hat{\rho}_\mathrm{S}(t),\hat{d}_\uparrow^\dagger\right]\\ &\quad+\Gamma_{21}^+(\varepsilon_\uparrow)\left[\hat{d}_\uparrow^\dagger\,,\hat{d}_\uparrow\,\hat{\rho}_\mathrm{S}(t)\right] + \Gamma_{21}^-(\varepsilon_\uparrow)\left[\hat{d}_\uparrow^\dagger\,\hat{\rho}_\mathrm{S}(t),\hat{d}_\uparrow\right]\\ &= \frac{1}{2}\gamma_{12}(-\varepsilon_\uparrow)\left(\left\{\hat{d}_\uparrow\,\hat{d}_\uparrow^\dagger\,,\hat{\rho}_\mathrm{S}\right\} - 2\,\hat{d}_\uparrow^\dagger\,\hat{\rho}_\mathrm{S}(t)\,\hat{d}_\uparrow\right) + \frac{1}{2}\gamma_{21}(\varepsilon_\uparrow)\left(\left\{\hat{d}_\uparrow^\dagger\,\hat{d}_\uparrow\,,\hat{\rho}_\mathrm{S}\right\} - 2\,\hat{d}_\uparrow\,\hat{\rho}_\mathrm{S}(t)\,\hat{d}_\uparrow^\dagger\right)\\ &\quad+\frac{1}{2}\left(\sigma_{21}(\varepsilon_\uparrow)-\sigma_{12}(-\varepsilon_\uparrow)\right)\left[\hat{d}_\uparrow^\dagger\,\hat{d}_\uparrow\,,\hat{\rho}_\mathrm{S}(t)\right].\end{aligned} \tag{4.33}$$

This equation is actually equivalent to the dissipator in eq. (2.48). Therefore, the use of the interaction free Hamiltonian to evaluate the dissipators of the master equation yields essentially the same results as the secular approximation.

In order to evaluate the coefficient $\gamma_{12}(\omega)$ and $\gamma_{21}(\omega)$ we need to calculate the respective bath correlations $C_{12}(\tau)$ and $C_{21}(\tau)$. We use the definition (2.25) and obtain

$$\begin{aligned}C_{12}(\tau) &= \sum_k |\gamma_{kR\uparrow}|^2 \mathrm{Tr}\left\{\hat{\boldsymbol{c}}_{\boldsymbol{kR\uparrow}}^\dagger(\tau)\,\hat{c}_{kR\uparrow}\,\hat{\rho}_\mathrm{B}^{\mathrm{eq},R}\right\}\\ &= \sum_k |\gamma_{kR\uparrow}|^2 \mathrm{Tr}\left\{\mathrm{e}^{\mathbf{i}\hat{H}_\mathrm{B}\tau}\,\hat{c}_{kR\uparrow}^\dagger\,\mathrm{e}^{-\mathbf{i}\hat{H}_\mathrm{B}\tau}\,\hat{c}_{kR\uparrow}\,\hat{\rho}_\mathrm{B}^{\mathrm{eq},R}\right\}\\ &= \sum_k |\gamma_{kR\uparrow}|^2 \mathrm{Tr}\left\{\mathrm{e}^{\mathbf{i}\varepsilon_{kR\uparrow}\tau}\,\hat{c}_{kR\uparrow}^\dagger\,\hat{c}_{kR\uparrow}\,\hat{\rho}_\mathrm{B}^{\mathrm{eq},R}\right\}\\ &= \sum_k |\gamma_{kR\uparrow}|^2 \mathrm{Tr}\left\{\hat{c}_{kR\uparrow}^\dagger\,\hat{c}_{kR\uparrow}\,\hat{\rho}_\mathrm{B}^{\mathrm{eq},R}\right\}\mathrm{e}^{\mathbf{i}\varepsilon_{kR\uparrow}\tau},\end{aligned} \tag{4.34}$$

$$\begin{aligned}C_{21}(\tau) &= \sum_k |\gamma_{kR\uparrow}|^2 \mathrm{Tr}\left\{\hat{\boldsymbol{c}}_{\boldsymbol{kR\uparrow}}(\tau)\,\hat{c}_{kR\uparrow}^\dagger\,\hat{\rho}_\mathrm{B}^{\mathrm{eq},R}\right\}\\ &= \sum_k |\gamma_{kR\uparrow}|^2 \mathrm{Tr}\left\{\hat{c}_{kR\uparrow}\,\hat{c}_{kR\uparrow}^\dagger\,\hat{\rho}_\mathrm{B}^{\mathrm{eq},R}\right\}\mathrm{e}^{-\mathbf{i}\varepsilon_{kR\uparrow}\tau},\end{aligned} \tag{4.35}$$

We assume that each of the leads l is in its respective thermal equilibrium state with $\hat{\rho}_\mathrm{B}^{\mathrm{eq},l}$ with the corresponding temperature β_l and chemical potential μ_l

$$\hat{\rho}_\mathrm{B}^{\mathrm{eq},l} = \frac{\mathrm{e}^{-\beta_l\left(\hat{H}_\mathrm{B}^{(l)}-\mu_l\hat{N}_\mathrm{B}^{(l)}\right)}}{Z_l}, \tag{4.36}$$

introduces the partition function for the grand-canonical ensemble ($\hat{N}_{\mathrm{B}}^{(l)} = \sum_j \hat{n}_j = \sum_j \hat{c}_j^\dagger \hat{c}_j$, where the index j comprises the energy k and the spin σ)

$$\begin{aligned} Z_l &= \mathrm{Tr}\left\{\mathrm{e}^{-\beta_l(\hat{H}_{\mathrm{B}}-\mu_l\hat{N}_{\mathrm{B}})}\right\} = \mathrm{Tr}\left\{\mathrm{e}^{-\beta_l\sum_j(\varepsilon_{j,l}-\mu_l)n_j}\right\} \\ &= \prod_{j=1}^{m}\sum_{n_j=0}^{1}\mathrm{e}^{-\beta_l(\varepsilon_{j,l}-\mu_l)n_j} = \prod_{j=1}^{m}\left[1+\mathrm{e}^{-\beta_l(\varepsilon_{j,l}-\mu_l)}\right], \end{aligned} \tag{4.37}$$

where we eliminated the $\sum_j$ by writing products of exponentials and substitute the trace by $\sum_{n_j}$ with $n_j = \{0,1\}$ as micro-state j can only by occupied by 0 or 1 fermion. That means for the bath correlation functions with respect to lead l

$$\begin{aligned} \mathrm{Tr}\left\{\hat{c}_{j'}^\dagger\,\hat{c}_j\,\hat{\rho}_{\mathrm{B}}^{\mathrm{eq},l}\right\} &= \delta_{j,j'}\mathrm{Tr}\left\{\hat{c}_j^\dagger\,\hat{c}_j\,\hat{\rho}_{\mathrm{B}}^{\mathrm{eq},l}\right\} = \delta_{j,j'}\frac{1}{Z_l}\prod_{j=1}^{m}\sum_{n_j=0}^{1} n_j\,\mathrm{e}^{-\beta_l(\varepsilon_{j,l}-\mu_l)n_j} \\ &= \delta_{j,j'}\frac{\mathrm{e}^{-\beta_l(\varepsilon_{j,l}-\mu_l)}}{1+\mathrm{e}^{-\beta_l(\varepsilon_{j,l}-\mu_l)}} = \delta_{j,j'}\frac{1}{1+\mathrm{e}^{\beta_l(\varepsilon_{j,l}-\mu_l)}} \\ &= \delta_{k,k'}\delta_{\sigma,\sigma'}\frac{1}{1+\mathrm{e}^{\beta_l(\varepsilon_{kl\sigma}-\mu_l)}} = \delta_{k,k'}\delta_{\sigma,\sigma'}f_l(\varepsilon_{kl\sigma}), \end{aligned} \tag{4.38}$$

$$\mathrm{Tr}\left\{\hat{c}_{j'}\,\hat{c}_j^\dagger\,\hat{\rho}_{\mathrm{B}}^{\mathrm{eq},l}\right\} = \delta_{k,k'}\delta_{\sigma,\sigma'}\left[1-f_l(\varepsilon_{kl\sigma})\right], \tag{4.39}$$

with eqs. (4.34) and (4.35) this yields

$$C_{12}(\tau) = \sum_k f_R(\varepsilon_{kR\uparrow})|\gamma_{kR\uparrow}|^2\,\mathrm{e}^{\mathbf{i}\varepsilon_{kR\uparrow}\tau}, \tag{4.40}$$

$$C_{21}(\tau) = \sum_k \left[1-f_R(\varepsilon_{kR\uparrow})\right]|\gamma_{kR\uparrow}|^2\,\mathrm{e}^{-\mathbf{i}\varepsilon_{kR\uparrow}\tau}\,. \tag{4.41}$$

Here the mean number of quanta in the bath l with energy ω is given by the Fermi-Dirac statistics, i.e.

$$f_l(\omega) = \frac{1}{\mathrm{e}^{\beta_l(\omega-\mu_l)}+1}\,. \tag{4.42}$$

Furthermore, we introduce the spectral density $J_{l\sigma}(\omega) = \sum_{k=1}^{M}|\gamma_{kl\sigma}|^2\delta(\omega-\varepsilon_{kl\sigma})$. As we take the baths to have a continuous spectrum we take $M\to\infty$ and obtain for the correlations

$$C_{12}(\tau) = \int_{-\infty}^{\infty} d\omega J_{R\uparrow}(-\omega)f_R(-\omega)\,\mathrm{e}^{\mathbf{i}\omega\tau}, \tag{4.43}$$

$$C_{21}(\tau) = \int_{-\infty}^{\infty} d\omega J_{R\uparrow}(\omega)\left[1-f_R(\omega)\right]\mathrm{e}^{-\mathbf{i}\omega\tau}\,. \tag{4.44}$$

Finally, we obtain γ_{12},γ_{21} by Fourier transforming eqs. (4.43) and (4.44), which yields

$$\gamma_{12}(\omega) = \Gamma_{R\uparrow}(-\omega)f_R(-\omega), \qquad \gamma_{21}(\omega) = \Gamma_{R\uparrow}(\omega)\left[1-f_R(\omega)\right], \tag{4.45}$$

where we introduced for convenience the spin-resolved tunneling rates

$$\Gamma_{l\sigma}(\omega) = 2\pi J_{l\sigma}(\omega)\,. \tag{4.46}$$

Analogously, we find the following nonvanishing coefficients governing the rate of dissipation with the electronic contacts

$$\begin{aligned} &\gamma_{34}(\omega) = \Gamma_{R\downarrow}(-\omega)f_R(-\omega), \qquad \gamma_{43}(\omega) = \Gamma_{R\downarrow}(\omega)(1-f_R(\omega)), \\ &\gamma_{56}(\omega) = \Gamma_{L\uparrow}(-\omega)f_L(-\omega), \qquad \gamma_{65}(\omega) = \Gamma_{L\uparrow}(\omega)(1-f_L(\omega)), \\ &\gamma_{78}(\omega) = \Gamma_{L\downarrow}(-\omega)f_L(-\omega), \qquad \gamma_{87}(\omega) = \Gamma_{L\downarrow}(\omega)(1-f_L(\omega)). \end{aligned} \tag{4.47}$$

Lambshift terms

Additionally, the odd Fourier transforms of the bath correlations functions, called Lamb-shift terms, are calculated from the even Fourier transforms by using the Cauchy principal value integral (2.47)

$$\sigma_{\alpha\beta}(\omega) = \frac{\mathbf{i}}{\pi}\mathrm{P.V.}\int_{-\infty}^{\infty}\frac{\gamma_{\alpha\beta}(\Omega)}{\omega-\Omega}d\Omega\,. \tag{4.48}$$

We show, straightforwardly, that the Lamb-shift contributions vanish

$$\begin{aligned}\sigma_{21}(\omega)-\sigma_{12}(-\omega) &= \frac{\mathbf{i}}{\pi}\mathrm{P.V.}\int_{-\infty}^{\infty}\frac{\Gamma_{R\uparrow}\left[f_R(\Omega)+1-f_R(\Omega)\right]}{\omega-\Omega}d\Omega\\ &= \frac{\mathbf{i}}{\pi}\mathrm{P.V.}\int_{-\infty}^{\infty}\frac{\Gamma_{R\uparrow}}{\omega-\Omega}d\Omega = \frac{\mathbf{i}}{\pi}\lim_{\omega'\to\infty}\mathrm{P.V.}\int_{-\omega'}^{\omega'}\frac{\Gamma_{R\uparrow}}{\omega-\Omega}d\Omega\\ &= \frac{\mathbf{i}}{\pi}\Gamma_{R\uparrow}\lim_{\omega'\to\infty}\ln\left(\frac{|\omega-\omega'|}{|\omega+\omega'|}\right)=0\,,\end{aligned} \tag{4.49}$$

where we set energy independent tunneling rates

$$\Gamma_{l\sigma}(\omega)\to\Gamma_{l\sigma} \tag{4.50}$$

i.e. the density of states around the transition frequencies is assumed to be flat, which is usually termed *wide-band limit*.

The final master equation has Lindblad form, i.e. preserves trace, hermiticity and the positivity of the reduced density matrix as it is of Lindblad form (compare (2.80)).

$$\frac{\partial}{\partial t}\hat{\rho}_{\mathrm{S}}(t) = \hat{\mathcal{L}}_t\left[\hat{\rho}_{\mathrm{S}}(t)\right] = -\mathbf{i}\left[\hat{H}_{\mathrm{S}}^{\mathrm{eff}}(t),\hat{\rho}_{\mathrm{S}}(t)\right]+\sum_{k=1}^{N^2-1}\gamma_k(t)\left(\hat{A}_k\,\hat{\rho}_{\mathrm{S}}(t)\,\hat{A}_k^\dagger-\frac{1}{2}\left\{\hat{A}_k^\dagger\,\hat{A}_k\,,\hat{\rho}_{\mathrm{S}}(t)\right\}\right), \tag{4.51}$$

where $N=3$ is the dimension of the SQD Hilbert space and we used (4.20). The nonnegative eigenvalues of the generator $\hat{\mathcal{L}}_t$ are the rates

$$\begin{aligned}&\gamma_1(t)=\gamma_{21}(\varepsilon_\uparrow(t))\,, \quad \gamma_2(t)=\gamma_{12}(-\varepsilon_\uparrow(t))\,,\\ &\gamma_3(t)=\gamma_{43}(\varepsilon_\downarrow(t))\,, \quad \gamma_4(t)=\gamma_{34}(-\varepsilon_\downarrow(t))\,,\\ &\gamma_5(t)=\gamma_{65}(\varepsilon_\uparrow(t))\,, \quad \gamma_6(t)=\gamma_{56}(-\varepsilon_\uparrow(t))\,,\\ &\gamma_7(t)=\gamma_{87}(\varepsilon_\downarrow(t))\,, \quad \gamma_8(t)=\gamma_{78}(-\varepsilon_\downarrow(t))\,.\end{aligned} \tag{4.52}$$

4.4.4. Complete Liouvillian

We now take matrix elements in an arbitrary basis, $\rho_{ij}=\langle i|\,\hat{\rho}_{\mathrm{S}}\,|j\rangle$, such that

$$\dot{\rho}_{ij} = -\mathbf{i}\,\langle i|\left[\hat{H}_{\mathrm{S}}^{\mathrm{eff}}(t),\hat{\rho}_{\mathrm{S}}\right]|j\rangle+\sum_{k=1}^{8}\gamma_k(t)\left(\langle i|\,\hat{A}_k\,\hat{\rho}_{\mathrm{S}}(t)\,\hat{A}_k^\dagger\,|j\rangle-\frac{1}{2}\,\langle i|\left\{\hat{A}_k^\dagger\,\hat{A}_k\,,\hat{\rho}_{\mathrm{S}}(t)\right\}|j\rangle\right), \tag{4.53}$$

and obtain in the local basis $(i,j \in 0,\downarrow,\uparrow)$. Taking the expectation values for the relevant observables $\frac{d}{dt}\langle\hat{O}\rangle = \mathrm{Tr}_\mathrm{S}\left\{\hat{O}\,\hat{\mathcal{L}}_t\left[\hat{\rho}_\mathrm{S}(t)\right]\right\}$ and writing the vector

$$\vec{\rho} = \left(\langle\rho_{00}\rangle, \langle\hat{n}_\downarrow\rangle, \langle\hat{n}_\uparrow\rangle, \langle\hat{S}_+\rangle, \langle\hat{S}_-\rangle\right)^\mathrm{T}, \tag{4.54}$$

we, finally, obtain the rate equations describing the dynamics of the interesting observables interested in

$$\frac{\partial}{\partial t}\vec{\rho} = \mathcal{L}_t\vec{\rho}\,. \tag{4.55}$$

The Liouvillian is represented by the rate matrix $\mathcal{L}_t = \sum_l \mathcal{L}_t^{(l)}$

$$\mathcal{L}_t^{(l)} = \begin{pmatrix} -\sum_\sigma \Gamma_{l\sigma} f_{l\sigma} & \Gamma_{l\downarrow}\overline{f_{l\downarrow}} & \Gamma_{l\uparrow}\overline{f_{l\uparrow}} & 0 & 0 \\ \Gamma_{l\downarrow} f_{l\downarrow} & -\Gamma_{l\downarrow}\overline{f_{l\downarrow}} & 0 & \frac{\mathrm{i}}{2}\Lambda^* & -\frac{\mathrm{i}}{2}\Lambda \\ \Gamma_{l\uparrow} f_{l\uparrow} & 0 & -\Gamma_{l\uparrow}\overline{f_{l\uparrow}} & -\frac{\mathrm{i}}{2}\Lambda^* & \frac{\mathrm{i}}{2}\Lambda \\ 0 & \frac{\mathrm{i}}{2}\Lambda & -\frac{\mathrm{i}}{2}\Lambda & \frac{\mathrm{i}}{2}\varepsilon_z - \frac{1}{2}\sum_\sigma \Gamma_{l\sigma}\overline{f_{l\sigma}} & 0 \\ 0 & -\frac{\mathrm{i}}{2}\Lambda^* & \frac{\mathrm{i}}{2}\Lambda^* & 0 & -\frac{\mathrm{i}}{2}\varepsilon_z - \frac{1}{2}\sum_\sigma \Gamma_{l\sigma}\overline{f_{l\sigma}} \end{pmatrix}. \tag{4.56}$$

The Fermi functions are evaluated at the transition frequencies $\varepsilon = \varepsilon_\sigma(t)$, thus $f_{l\sigma} = f_l(\varepsilon_\sigma)$ and we define $\overline{f_{l\sigma}} = [1 - f_{l\sigma}]$.

4.5. Introducing feedback

For small bias voltages across the SQD a device that yields information about its instantaneous occupation, such as an quantum point contact (QPC), cannot resolve to which of the attached electron reservoirs an electron has tunneled. Therefore, the simplest feedback mechanisms can only be conditioned on the occupation of the SQD itself or whether an electron has tunneled in or out, without knowing the direction. Recent experiments show that the random telegraph signals of QPCs contains information about the spin-state of electrons in monitored quantum dots [166]. Now the Maxwell demon feedback is implemented as suggested in Ref. [43]. We apply different Liouvillians conditioned on whether the SQD is empty(E), populated in $\uparrow$-state or populated in the $\downarrow$-state, i.e. we construct new rate matrices by taking the rate matrix (4.56) and multiplying it by the dimensionless feedback parameters $\delta_{l\nu} \in \mathbb{R}; \nu \in \{E,\uparrow,\downarrow\}$, that encode the modification of the tunneling rates (with $\delta_{l\nu} = 0$ recovering the case without feedback)

$$\mathcal{L}_\nu \equiv \sum_{l=L/R} \mathrm{e}^{\delta_{l\nu}}\,\mathcal{L}^{(l)}\,. \tag{4.57}$$

We construct the effective feedback generator by projecting on the empty and filled dot states and on the two interesting coherences

$$\mathcal{L}_{\mathrm{fb}} = \mathcal{L}_E \begin{pmatrix} 1 & 0 & 0 & 0 & 0 \\ 0 & 0 & 0 & 0 & 0 \\ 0 & 0 & 0 & 0 & 0 \\ 0 & 0 & 0 & 0 & 0 \\ 0 & 0 & 0 & 0 & 0 \end{pmatrix} + \mathcal{L}_{\downarrow} \begin{pmatrix} 0 & 0 & 0 & 0 & 0 \\ 0 & 1 & 0 & 0 & 0 \\ 0 & 0 & 0 & 0 & 0 \\ 0 & 0 & 0 & 0 & 0 \\ 0 & 0 & 0 & 0 & 0 \end{pmatrix}$$
$$+ \mathcal{L}_{\uparrow} \begin{pmatrix} 0 & 0 & 0 & 0 & 0 \\ 0 & 0 & 0 & 0 & 0 \\ 0 & 0 & 1 & 0 & 0 \\ 0 & 0 & 0 & 0 & 0 \\ 0 & 0 & 0 & 0 & 0 \end{pmatrix} + \mathcal{L}_{\mathrm{nofb}} \begin{pmatrix} 0 & 0 & 0 & 0 & 0 \\ 0 & 0 & 0 & 0 & 0 \\ 0 & 0 & 0 & 0 & 0 \\ 0 & 0 & 0 & 1 & 0 \\ 0 & 0 & 0 & 0 & 1 \end{pmatrix}, \tag{4.58}$$

where $\mathcal{L}_{\mathrm{nofb}} = \mathcal{L}$ is the nonmodified Liouvillian, (4.56), where we dropped, again, the index t for better readability.
This feedback scheme has been named "Maxwell demon feedback" by Schaller and Esposito in Refs. [43, 65] as one can think of a Maxwell demon that is able to instantaneously alter the tunneling amplitudes for the hopping on and off the SQD only based on the information about the current state of the system.

4.6. Final EOM of interacting spin system with demon like feedback

The final equations that are the subject of our investigation read

$$\frac{\partial}{\partial t}\vec{\rho} = \mathcal{L}_{\mathrm{fb}}\vec{\rho}\,. \tag{4.59}$$

where the vector $\vec{\rho}$ comprises the relevant observables we need to describe the nonlinear spin-spin dynamics under feedback.
We now can reduce the amount of equations by eliminating the equation for $d/dt\,\langle\rho_{00}\rangle$ by using $\mathrm{Tr}\{\rho\} = 1$, which is possible because the transport rate matrix $\mathcal{L}_{\mathrm{fb}}$ has rank 4. We obtain with (4.3) (for the sake of readability we omit the time dependences, here)

$$\begin{aligned}
\frac{d}{dt}\langle\hat{S}_x\rangle &= +\lambda_y\langle\hat{J}_y\rangle\langle\hat{S}_z\rangle - \varepsilon_z\langle\hat{S}_y\rangle - \sum_{l\sigma}\frac{\Gamma_{l\sigma}}{2}\overline{f_{l\sigma}}\langle\hat{S}_x\rangle\,, \\
\frac{d}{dt}\langle\hat{S}_y\rangle &= -\lambda_x\langle\hat{J}_x\rangle\langle\hat{S}_z\rangle + \varepsilon_z\langle\hat{S}_x\rangle - \sum_{l\sigma}\frac{\Gamma_{l\sigma}}{2}\overline{f_{l\sigma}}\langle\hat{S}_y\rangle\,, \\
\frac{d}{dt}\langle\hat{S}_z\rangle &= \sum_l\left\{\mathrm{e}^{\delta_{lE}}\left[\frac{\Gamma_{l\uparrow}}{2}f_{l\uparrow} - \frac{\Gamma_{l\downarrow}}{2}f_{l\downarrow}\right](1 - \langle\hat{n}_\uparrow\rangle - \langle\hat{n}_\downarrow\rangle) - \mathrm{e}^{\delta_{l\uparrow}}\frac{\Gamma_{l\uparrow}}{2}\overline{f_{l\uparrow}}\langle\hat{n}_\uparrow\rangle + \mathrm{e}^{\delta_{l\downarrow}}\frac{\Gamma_{l\downarrow}}{2}\overline{f_{l\downarrow}}\langle\hat{n}_\downarrow\rangle\right\} \\
&\quad + \lambda_x\langle\hat{J}_x\rangle\langle\hat{S}_y\rangle - \lambda_y\langle\hat{J}_y\rangle\langle\hat{S}_x\rangle\,, \\
\frac{d}{dt}\langle\hat{n}_\sigma\rangle &= \sum_l \mathrm{e}^{\delta_{lE}}\Gamma_{l\sigma}f_{l\sigma}(1 - \langle\hat{n}_\uparrow\rangle - \langle\hat{n}_\downarrow\rangle) - \sum_l \mathrm{e}^{\delta_{l\sigma}}\Gamma_{l\sigma}\overline{f_{l\sigma}}\langle\hat{n}_\sigma\rangle \\
&\quad + \left(\lambda_x\langle\hat{J}_x\rangle\langle\hat{S}_y\rangle - \lambda_y\langle\hat{J}_y\rangle\langle\hat{S}_x\rangle\right)(\delta_{\sigma\uparrow} - \delta_{\sigma\downarrow})\,.
\end{aligned} \tag{4.60}$$

These equations are strongly nonlinear and we need to generate EOM for the components of the large spin to complete the set of equations.
The large spin components obey the commutation relations $\left[\hat{J}_i\,,\hat{J}_j\right] = \mathbf{i}\sum_k \varepsilon_{ijk}\,\hat{J}_k$.

As already stated, we implemented a mean-field approximation, which implies that the large spin is not decaying due to the electronic leads, i.e. its length j is conserved, and $\vec{\hat{J}}$ is essentially treated as a classical object. Therefore, we can use the mean-field interaction Hamiltonian, (4.10), to calculate the Ehrenfest EOM

$$\frac{d}{dt}\langle \hat{J}_i \rangle = -\mathbf{i}\left\langle \left[\hat{J}_i \,, \hat{H}_{\mathrm{J}} + \hat{H}_{\mathrm{int}}^{\mathrm{MF}} \right] \right\rangle + \left\langle \frac{\partial \hat{J}_i}{\partial t} \right\rangle . \tag{4.61}$$

We obtain the EOM of the expectation values of the large spin's degrees of freedom $\langle \hat{J}_i \rangle$

$$\begin{aligned}
\frac{d}{dt}\langle \hat{J}_x \rangle &= +\lambda_y \langle \hat{S}_y \rangle \langle \hat{J}_z \rangle - \left(B + \lambda_z \langle \hat{S}_z \rangle \right) \langle \hat{J}_y \rangle \,, \\
\frac{d}{dt}\langle \hat{J}_y \rangle &= -\lambda_x \langle \hat{S}_x \rangle \langle \hat{J}_z \rangle + \left(B + \lambda_z \langle \hat{S}_z \rangle \right) \langle \hat{J}_x \rangle \,, \\
\frac{d}{dt}\langle \hat{J}_z \rangle &= +\lambda_x \langle \hat{S}_x \rangle \langle \hat{J}_y \rangle - \lambda_y \langle \hat{S}_y \rangle \langle \hat{J}_x \rangle \,.
\end{aligned} \tag{4.62}$$

This equations have the form of Hasegawa-Bloch equations, [167, 168] completed by the electronic back-action.

4.7. Alternative derivations of the EOM

In our derivation we implicitly applied an adiabatic approach when we assumed that the large spin enters the effective transport Hamiltonian in form of parameters that change on a much slower time scale than the tunneling time scale.
The model, without the feedback part, (4.1) has been studied before by López-Monís *et al.* [128] and Metelmann *et al.* [105]. López-Monís and coworkers derived mean-field EOM restricting themselves to the infinite bias voltages across the device and an adiabatic treatment of the large spin's motion. The resulting EOM conincide with (4.60) in the infinite bias limit, except for the fact, that we explicitly ruled out double occupation of the QD. Metelmann *et al.* show that the nonadiabatic approach developed in Ref. [105] includes the short-time dynamics as well as the level-broadening effects that arise from the coupling of the large spin to the transport leads. They introduce lead-transition functions, $B^l_{\sigma\sigma'}(\omega, t) = \mathbf{i} \sum_k \gamma_{kl\sigma} \delta(\omega - \varepsilon_{lk\sigma})\, \mathrm{e}^{\mathbf{i}\varepsilon_{kl\sigma} t} \langle \hat{c}^\dagger_{kl\sigma}(t)\, \hat{d}_{\sigma'}(t) \rangle$ that explicitly couple the EOM for the spin correlators $\langle \hat{d}^\dagger_\sigma(t)\, \hat{d}_{\sigma'}(t) \rangle$ with the QD-lead correlators $\langle \hat{c}^\dagger_{kl\sigma}(t)\, \hat{d}_{\sigma'}(t) \rangle$. This increases the amount of equations to solve drastically and, thus, the numerical effort. However, the study shows that the nonadiabatic corrections are important in the regime of low magnetic fields. Metelmann also provides analytic solutions for the adiabatic approach via Green's functions.

4.8. Analysis and Numerical results

4.8.1. System without exchange-interaction ($\lambda_i = 0$)

If the exchange-interaction is ineffective we do not need to consider any coherences as the ↑- and ↓-transport channels do not mix. With the new vector of probabilities p_ν to find the system in states $\nu = \{E, \downarrow, \uparrow\}$, $\vec{\rho}_{\text{noint}} = (p_E, p_\downarrow, p_\uparrow)^{\mathrm{T}} = (\langle\rho_{00}\rangle, \langle\hat{n}_\downarrow\rangle, \langle\hat{n}_\uparrow\rangle)^{\mathrm{T}}$ Eq. (4.59) reduces to $\frac{\partial}{\partial t}\vec{\rho}_{\text{noint}} = \mathcal{L}_{\text{fb}}^{(\text{noint})}\vec{\rho}_{\text{noint}}$, where the rate matrix is merely the 3×3 submatrix of (4.58) with respect to the occupations, i.e.

$$\mathcal{L}_{\text{fb}}^{(\text{noint})} = \sum_l \begin{pmatrix} -\sum_\sigma W_{\sigma E}^{(l)} & W_{E\downarrow}^{(l)} & W_{E\uparrow}^{(l)} \\ W_{\downarrow E}^{(l)} & -W_{E\downarrow}^{(l)} & 0 \\ W_{\uparrow E}^{(l)} & 0 & -W_{E\uparrow}^{(l)} \end{pmatrix}. \tag{4.63}$$

Here the rates for transitions between unoccupied SQD ("E") and spin-σ states induced by the coupling to lead l read

$$W_{\sigma E}^{(l)} = \mathrm{e}^{\delta_{lE}}\,\Gamma_{l\sigma} f_l(\varepsilon_\sigma)\,, \quad W_{E\sigma}^{(l)} = \mathrm{e}^{\delta_{l\sigma}}\,\Gamma_{l\sigma}\overline{f_{l\sigma}(\varepsilon_\sigma)}\,. \tag{4.64}$$

Along the lines of Ref. [65] it can be shown straightforwardly, that the local detailed balance condition, (2.142), of our device is modified once the feedback is applied; i.e. constants $\Delta_{l\sigma} \equiv \delta_{l\sigma} - \delta_{lE}$ are nonzero,

$$\ln\frac{W_{\sigma E}^{(l)}}{W_{E\sigma}^{(l)}} = -\beta_l(\varepsilon_\sigma - \mu_l) - \Delta_{l\sigma}\,. \tag{4.65}$$

A detailed discussion of the stochastic thermodynamics of the Maxwell demon feedback has been provided in Refs. [65, 43, 44]. The crucial point is that the feedback mechanism does not affect the energy and matter balances of the system but does alter the entropy balance; i.e, besides the matter and energy currents I_{M} and I_{E}, an information current I_{F} is introduced, that changes the second law of the system. In chapter 5 we will a study a generic model for a microscopic implementation of Maxwell-demon like feedback, that will shed some more light on the thermodynamical properties of this kind of feedback.
The currents from lead l read

$$\begin{aligned} I_{\text{E}}^{(l)} &= \sum_{\nu\neq\nu'} W_{\nu\nu'}^{(l)} p_{\nu'}(\varepsilon_\nu - \varepsilon_{\nu'}) \\ I_{\text{M}}^{(l)} &= \sum_{\nu\neq\nu'} W_{\nu\nu'}^{(l)} p_{\nu'}(N_\nu - N_{\nu'}) \\ I_{\text{F}}^{(l)} &= \sum_{\nu\neq\nu'} W_{\nu\nu'}^{(l)} p_{\nu'}(\delta_{l\nu} - \delta_{l\nu'})\,, \end{aligned} \tag{4.66}$$

where ε_ν, N_ν are the respective energies and particle numbers. Since we restrict the number of particles on the SQD to 1, the matter and energy currents are proportional to each other. The electron tunneling is spin preserving and, thus, we can treat the ↑ / ↓-channels separately and find (note that, due to particle conservation, $I_{\text{M}\sigma} = I_{\text{M}\sigma}^{(L)} = -I_{\text{M}\sigma}^{(R)}$)

$$I_{\text{M}\sigma} = W_{\sigma E}^{(L)} p_E - W_{E\sigma}^{(L)} p_\sigma = I_\sigma = I_{\text{E}\sigma}/\varepsilon_\sigma\,. \tag{4.67}$$

If the system is in its stationary state the spin-σ currents read

$$I_\sigma = \frac{\left(\mathrm{e}^{(\delta_{LE}+\delta_{R\sigma})}\, f_{L\sigma}\overline{f_{R\sigma}} - \mathrm{e}^{(\delta_{L\sigma}+\delta_{RE})}\,\overline{f_{L\sigma}} f_{R\sigma}\right)\Gamma_{L\sigma}\Gamma_{R\sigma}}{\sum_l \left(\mathrm{e}^{\delta_{lE}}\, f_{l\sigma} + \mathrm{e}^{\delta_{l\sigma}}\,\overline{f_{l\sigma}}\right)\Gamma_{l\sigma} + C_\sigma}\,,$$
$$C_\sigma = \frac{\left(\sum_l \mathrm{e}^{\delta_{lE}}\, f_{l\bar{\sigma}}\Gamma_{l\bar{\sigma}}\right)\left(\sum_l \mathrm{e}^{\delta_{l\sigma}}\,\overline{f_{l\sigma}}\Gamma_{l\sigma}\right)}{\left(\sum_l \mathrm{e}^{\delta_{l\bar{\sigma}}}\,\overline{f_{l\bar{\sigma}}}\Gamma_{l\bar{\sigma}}\right)}\,, \tag{4.68}$$

where negative currents are effective currents from the right to the left lead and positive ones vice versa. The information current, on the other hand, evaluates to

$$I_{\mathrm{F}} = \sum_\sigma (\Delta_{L\sigma} - \Delta_{R\sigma}) I_\sigma\,. \tag{4.69}$$

The system entropy is given in terms of the Shannon entropy, (2.122),

$$S = -\sum_\nu p_\nu \ln p_\nu\,. \tag{4.70}$$

Consequently, $\dot{S}$ is the entropy change in the system and after some algebra we can define the total entropy production [65],

$$\dot{S}_{\mathrm{i}} = \dot{S} - \sum_l \frac{\dot{Q}^{(l)}}{T_l} + I_{\mathrm{F}}\,, \tag{4.71}$$

which is nonnegative definite and where $\dot{Q}^{(l)} = I_{\mathrm{E}}^{(l)} - \mu_l I_{\mathrm{M}}^{(l)}$ is the heat flow with the l-th reservoir. In the absence of feedback ($I_{\mathrm{F}} = 0$) the entropy production is just the sum of entropy change in the system and the reservoirs. The nonnegativity of $\dot{S}_{\mathrm{i}}$ implies that $\dot{S} \geq \sum_l \dot{Q}^{(l)}/T_l$, which is the second law of thermodynamics. The presence of feedback may change this, depending on the sign of I_{F}. The entropy change provided by the feedback mechanism adds to the total entropy. Once the system reaches its steady state the system entropy remains constant ($\dot{S} = 0$) and the entropy production becomes

$$\dot{S}_{\mathrm{i}} = \left(\frac{1}{T_R} - \frac{1}{T_L}\right) I_{\mathrm{E}} - \left(\frac{\mu_R}{T_R} - \frac{\mu_L}{T_L}\right) I_{\mathrm{M}} + I_{\mathrm{F}} \geq 0. \tag{4.72}$$

If the leads are held at the same temperature $T_R = T_L = T$ and a chemical potential gradient is established ($\mu_R - \mu_L \geq 0$), the extracted power becomes $\mathcal{P} = (\mu_R - \mu_L)\, I_{\mathrm{M}}$; cf. eq. (2.146). In the absence of feedback I_{F} the matter flux can only flow with the gradient ($I_{\mathrm{M}} \leq 0$). If the feedback mechanism is effective and if the feedback current is sufficiently positive, particles can be transferred against the chemical potential gradient ($I_{\mathrm{M}} \geq 0$).
If the device can discriminate spin directions of electrons we can implement the following feedback schemes.

Feedback schemes. In this paper we investigate the effect of two feedback parameter choices. First is scheme A with parameters chosen as

$$\delta_{L\uparrow} = \delta_{RE} = -\delta, \delta_{R\uparrow} = \delta_{LE} = \delta\,, \quad \delta_{L\downarrow} = \delta_{R\downarrow} = 0\,, \tag{4.73}$$

where δ is positive. In scheme A currents of both ↑- and ↓-electrons can be transported against a chemical bias, but the ↑-currents are preferred. The second scheme, B, implements a spin filter,

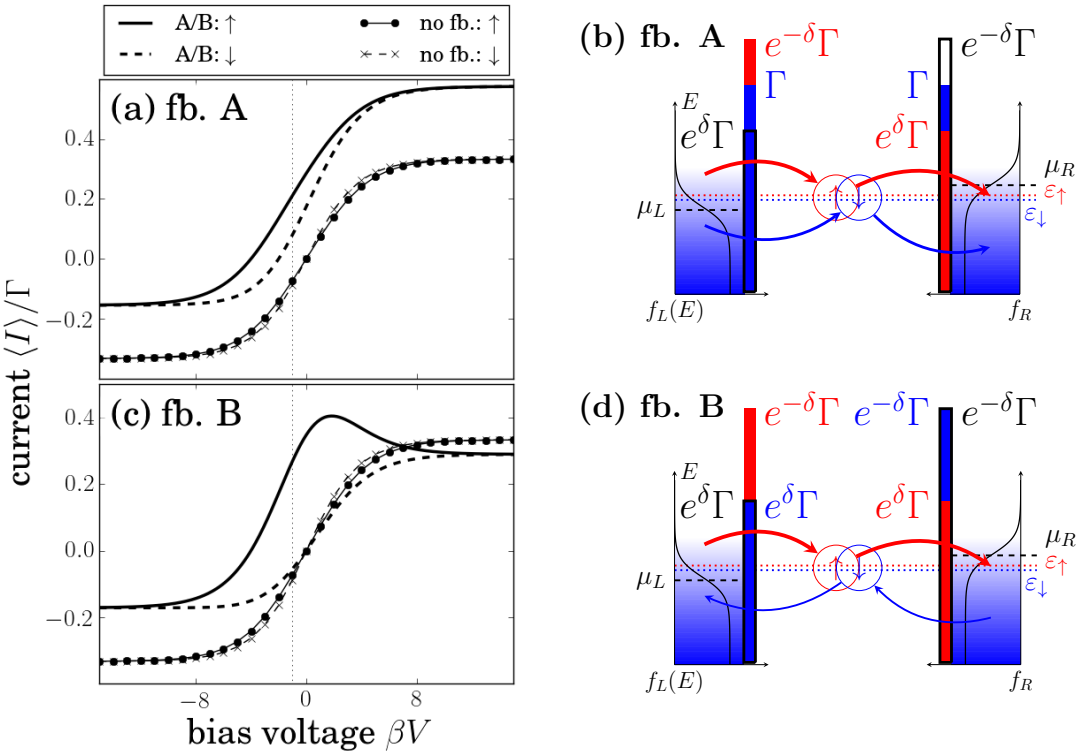

Figure 4.2.: Plots (a) and (c) show the spin-dependent currents as function of the applied bias voltage V between the left and right transport leads, plotted for different feedback schemes and compared to the nonfeedback case. ↑(↓)-currents are depicted as solid (dashed) lines. Scheme B can act as a spin filter, as depicted in (c), where only ↑-electrons are transported against the bias. For scheme A, shown in (a), all electrons are transported against the bias, but ↑-currents are preferred. Plots (b) and (d) show a sketch of the SQD with the respective tunneling rates if the system is empty(black) or occupied by an ↑(red) or ↓(blue)-electron. Thickness and directions of the red/blue tunneling arrows show which net currents are reached. The setup is sketched for fixed bias voltages, $V/\lambda = -1$, shown by the dotted vertical lines in plots (a) and (c).

where ↑-currents are pumped against the bias and ↓-currents are transported with the bias, by applying the parameters

$$\delta_{L\uparrow} = \delta_{RE} = \delta_{R\downarrow} = -\delta\,, \quad \delta_{L\downarrow} = \delta_{LE} = \delta_{R\uparrow} = \delta\,, \tag{4.74}$$

The physical effect of the two schemes can be seen best in Fig. 4.2, where in subplots (a) and (c) the current-bias voltage characteristics are plotted and in panels (b) and (d) the tunneling processes are sketched. Without feedback, all tunneling rates are equal, $\Gamma_{l\sigma} = \Gamma$. Due to the feedback the rates are changed according to the schemes. The averaged tunneling is depicted by the red and blue arrows, the thickness and direction of which indicate the direction and strength, respectively, of the resulting spin-σ currents (red arrows show ↑-currents, while blue ones show ↓-currents).
The spin filter effects can be used to generate oscillating currents with or against the bias depending on the electron spin in the interacting setup, as shown in Sec. 4.8.4.

4.8.2. Dynamics in the Infinite Bias Regime

Throughout this analysis we consider an anisotropic coupling between the spins, namely, $\lambda_y = 0$ and $\lambda_x = \lambda_z = \lambda$ (compare Refs. [128, 105]). The qualitative system dynamics for double and single QD systems with isotropic coupling has been investigated in Ref. [156]. For the sake of clarity we choose the QD level to be $\varepsilon = 0$. Furthermore, we choose the leads to be at equal temperatures β. The chemical potentials allow for tunneling from left to right only ($\mu_{L,R} \to \pm\infty$). In the following we discuss the difficult nonlinear dynamics occurring in our setup. In particular, we are interested in the average spin σ-electron current through the barrier l, i.e.

$$\langle I_{l\sigma} \rangle (t) = e\Gamma_{l\sigma} \left(\mathrm{e}^{\delta_{l\sigma}} \overline{f_{l\sigma}} \langle \hat{n}_\sigma \rangle - \mathrm{e}^{\delta_{lE}} f_{l\sigma} \left(1 - \langle \hat{n}_\sigma \rangle - \langle \hat{n}_{\bar{\sigma}} \rangle \right) \right) , \tag{4.75}$$

where, by convention, net flux off the SQD is positive. Further, we are interested in the backaction on the large spin and what the influence of the applied feedback mechanisms is. As stated above, we consider quantum expectation values of the electronic spin's components $\langle \hat{S}_i \rangle$, while the large spin $\vec{\hat{J}}$ is treated as a classical object, which is justified and motivated as we remain in a limit where $s \ll j$.

Analytic fixed points

To describe the domain of regular motion it is of particular interest to investigate whether there are fixed points. We denote the fixed points introducing the notation [cf. section 3.3.1]

$$\mathcal{P} = \left(\langle \hat{S}_x^* \rangle , \langle \hat{S}_y^* \rangle , \langle \hat{S}_z^* \rangle , \langle \hat{J}_x^* \rangle , \langle \hat{J}_y^* \rangle , \langle \hat{J}_z^* \rangle \right) . \tag{4.76}$$

For a general choice of parameters it might become difficult to calculate the fixed points straightforwardly, since the introduction of the Fermi function renders the equations transcendental. For special infinite bias setups, nonetheless, it is possible to calculate them directly, by setting Eqs. (4.60) to zero and solving them.
However, due to the nature of the exchange interaction one can easily see that there exist trivial fixed points when the large spin is aligned (anti-)parallel with the magnetic field since the spins decouple then. If there is no coupling to the leads, the electronic spin is conserved and will be aligned with the magnetic field. However, contrasting the spin-conserving setup we have to take into account what happens to the electronic spin, once the exchange interaction is ineffective. This, of course, depends on the dissipative setup, i.e. on $\Gamma_{l\sigma}$. The most trivial dissipative setup consists of setting all tunneling rates to Γ and applying an infinite bias voltage, so that the electronic spin will simply decay, all further electrons tunnel through the device without being flipped, and the transport channels are decoupled.
If the setup is changed in a way that tunneling between the right contact and the SQD is only possible for $\uparrow$-electrons, in terms of the tunneling rates $\Gamma_{R\downarrow} = 0, \Gamma_{L\uparrow} = \Gamma_{R\uparrow} = \Gamma_{L\downarrow} = \Gamma$, $\downarrow$-electrons will be trapped in the system and can only leave the SQD after being flipped. Note that in this setup (labeled "IB"), which we consider throughout this section, the two feedback schemes introduced above are identical, which can be verified by applying the scheme to Eqs. (4.60), and thus the feedback strength enters the equation by the dimensionless parameter δ.
The respective fixed points are, accordingly,

$$\mathcal{P}_{\mathrm{IB}}^{\pm} = \left(0, 0, -\frac{1}{2}, 0, 0, \pm j \right) . \tag{4.77}$$

These fixed points are independent of the parameters B, λ and, therefore, exist in the whole parameter regime. The fixed points can be investigated further using linear stability analysis.

Such analysis requires the knowledge of the partial derivatives of spin components with respect to other components, which are, in general, not accessible.
There is a second set of fixed points,

$$\mathcal{P}_{\mathrm{IB}}^{-y,\pm} = \left(0, -\mathcal{B}_3, -\frac{B}{\lambda}, -\frac{\Gamma}{2B}\mathcal{B}_3, \pm\mathcal{B}_2, -\frac{B}{\lambda}\right),$$
$$\mathcal{P}_{\mathrm{IB}}^{+y,\pm} = \left(0, +\mathcal{B}_3, -\frac{B}{\lambda}, +\frac{\Gamma}{2B}\mathcal{B}_3, \pm\mathcal{B}_2, -\frac{B}{\lambda}\right), \tag{4.78}$$

with

$$\mathcal{B}_2 = \sqrt{j^2 - \left(\frac{B}{\lambda}\right)^2 - \frac{\mathrm{e}^{\delta}}{5}\left(\frac{\Gamma}{\lambda}\right)^2\left(\frac{\lambda}{2B} - 1\right)},$$
$$\mathcal{B}_3 = \mathrm{e}^{\delta/2}\,\frac{2}{\sqrt{5}}\sqrt{\frac{B}{\lambda}\left(\frac{1}{2} - \frac{B}{\lambda}\right)}. \tag{4.79}$$

This fixed point can be understood in terms of the anisotropic exchange coupling, since the x- and z-components of one and the same spin decouple, having either the trivial consequence of complete spin polarization ($\mathcal{P}_{\mathrm{IB}}^{\pm}$) or the z-components being determined by the ratio $-B/\lambda$ and vanishing x-components.
These results are very similar to the findings in Refs. [128, 105], only differing due to different choices of the transport rates and the introduction of the feedback parameter. Note that we explicitly restricted the number of allowed electrons in the SQD at a time to one, which is not the case for Ref. [128].
The quantities $\mathcal{B}_2$, $\mathcal{B}_3$ can assume finite imaginary values. The fixed points $\mathcal{P}_{\mathrm{IB}}^{\pm y,\pm}$, therefore, only have a physical meaning in the region of the parameter space where they remain real valued. The parameter space can thus be separated into different regions whose boundaries are obtained by solving $\mathcal{B}_2 = 0$ and $\mathcal{B}_3 = 0$. We obtain the critical values

$$\mathcal{B}_2 = 0 \to \Gamma_c = \mathrm{e}^{-\delta/2}\sqrt{10\frac{(B^3 - Bj^2\lambda^2)}{2B - \lambda}},$$
$$\mathcal{B}_3 = 0 \to B_c = \frac{\lambda}{2}. \tag{4.80}$$

A projection of the three-dimensional parameter space (λ, B, Γ) for different feedback parameters δ with fixed λ on the $\Gamma - B$ plane is, therefore, divided into three regions as plotted in Fig. 4.3. $\mathcal{P}_{\mathrm{IB}}^{\pm}$ are physical fixed points for all possible parameters.
The labels 1 to 4 in Fig. 4.3 mark the parameters for which we solve the numerics and plot the results in Figs. 4.4 to 4.7. The specific dynamics are discussed in the following.

Region I: damped oscillations

In region I with weak magnetic fields $B < B_c$ and very fast tunneling processes, i.e. rates $\Gamma > \Gamma_c$, the time scale of electronic transport is much faster than that of the exchange interaction; therefore, the rate equations results only show damped oscillations in the current and evolution towards $\mathcal{P}_{\mathrm{IB}}^{\pm}$. The resulting stationary current will be obviously zero, since the spin-spin interaction is ineffective once either of the fixed points is reached and a ↓-electron is trapped in the QD. The origin of the often complicated transient oscillations is the interplay between the modulation of the electronic current by the large spin and the electronic feedback on the large spin. Different initial conditions decide which of the two fixed points is reached. Turning on the demon feedback does not change the behavior qualitatively, but only the shape of the transient oscillations; their frequency and the damping is increased.

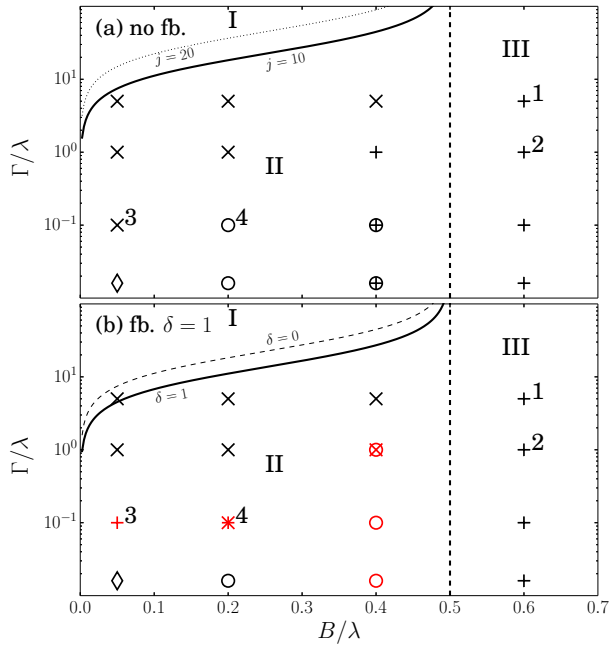

Figure 4.3.: Parameter regions I,II and III in the infinite bias (IB) setup. Solid lines show the region-I-II-border [as a reference the borders for larger j (dotted) in (a) or the nonfeedback case (dashed) in (b) are shown]. The thick dashed lines show the transition from region II to region III, which is determined by the critical magnetic field $B_c = \lambda/2$. In region I the system always runs into either of the fixed points $\mathcal{P}^{\pm}_{\mathrm{IB}}$ performing damped oscillations. If the magnetic field is stronger than $\lambda/2$ (region III) the system performs self-sustained oscillations, either according to the effective model (4.81) or around the polar fixed points $\mathcal{P}^{\pm}_{\mathrm{IB}}$. For region II, we plot exemplarily which dynamics the system exhibits with respect to parameters B and Γ. We find not only damped oscillations towards the system's fixed points (marked by "×") and ongoing oscillations ("+") but also quasiperiodic ("∘") or chaotic oscillations ("⋄"). Plot (a) shows the typical behavior for the nonfeedback case. In plot (b) we show how and in which parameter regions the system's behavior is changed qualitatively if feedback is applied ($\delta/\lambda = 1$). The red labels show the regions in parameter space, where the dynamics are changed significantly. Labels 1–4 show the parameters for which we plotted solutions in Figs. 4.4 to 4.7.

Region III: self-sustained oscillations, parametric resonance and an effective model

If the magnetic field is increased beyond B_c (parameter region III), however, the numerical results exhibit solely self-sustained oscillations in the electronic current and both electronic and large spin.

The system oscillates on orbits around the stable fixed points $\mathcal{P}^{\pm}_{\mathrm{IB}}$, with the large spin performing periodic oscillations close to full polarization $\pm j$, driving the electronic spin to a periodic orbit close to $\langle \hat{S}^{\star}_z \rangle = -1/2$.

A second type of self-sustained oscillation can be described by an effective model, where $\langle \hat{J}_z \rangle = -B/\lambda$, and $\langle \hat{S}_x \rangle = 0$ remain constant and the oscillation of $\langle \hat{J}_{x,y} \rangle$ is driving the periodic

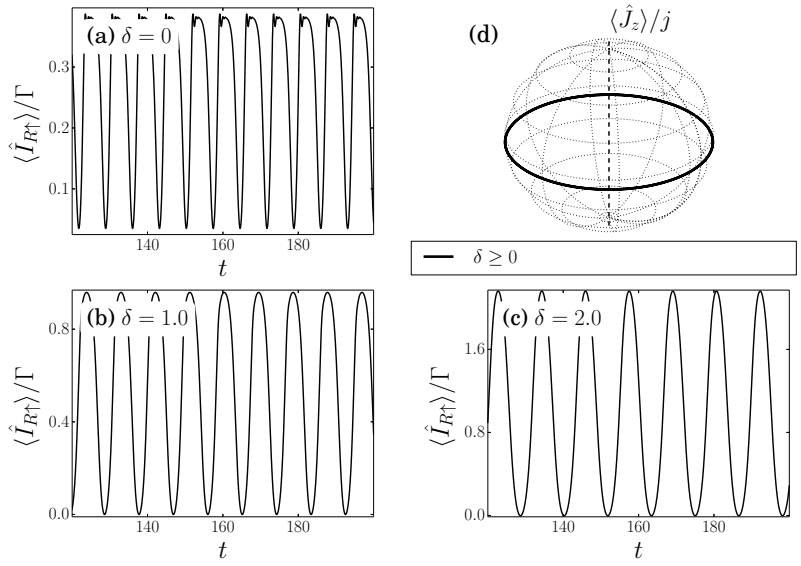

Figure 4.4.: (a)–(c) Electronic currents and (d) the dynamics of $\vec{\hat{J}}$ for parameters from region III with respect to different feedback strengths δ. The current becomes more sinusoidal, while the frequency is decreased; the rotation of $\vec{\hat{J}}$ remains in the $x-y$-plane. Parameters: $B/\lambda = 0.6, \Gamma/\lambda = 5, j/\lambda = 10$.

oscillation of the small spin, which reduces the system to

$$\begin{aligned}
\frac{d}{dt}\langle \hat{S}_x \rangle &= -\frac{\Gamma}{2}\langle \hat{S}_x \rangle \\
\frac{d}{dt}\langle \hat{S}_y \rangle &= -\frac{1}{2}B_x(t)\left(\langle \hat{n}_\uparrow \rangle - \langle \hat{n}_\downarrow \rangle\right) - \frac{\Gamma}{2}\langle \hat{S}_y \rangle \\
\frac{d}{dt}\langle \hat{n}_\uparrow \rangle &= B_x(t)\langle \hat{S}_y \rangle + \mathrm{e}^{\delta}\,\Gamma - \mathrm{e}^{\delta}\,\Gamma\left(2\langle \hat{n}_\uparrow \rangle + \langle \hat{n}_\downarrow \rangle\right) \\
\frac{d}{dt}\langle \hat{n}_\downarrow \rangle &= -B_x(t)\langle \hat{S}_y \rangle + \mathrm{e}^{\delta}\,\Gamma - \mathrm{e}^{\delta}\,\Gamma\left(\langle \hat{n}_\uparrow \rangle + \langle \hat{n}_\downarrow \rangle\right),
\end{aligned} \tag{4.81}$$

with the oscillating effective magnetic $B_x(t) = \frac{1}{\sqrt{2}}\sqrt{j^2 - \frac{B^2}{\lambda^2}}\lambda\left(\cos\left(B_{\mathrm{eff}}t\right) - \sin\left(B_{\mathrm{eff}}t\right)\right)$. Thus, the oscillation of the electronic plane is taking place in the $y-z$ plane, while the large spin rotates in the $x-y$ plane. The derivation of this model in Appendix A.1 makes use of the rotational invariance of the large spin. The effective precession frequency, B_{eff} is decreasing with increasing Γ, as well as with increasing δ. Due to the term $B + \lambda\langle \hat{S}_z \rangle$ and the fact that $\langle \hat{S}_z \rangle < 0$ is, on average, the effective precession frequency B_{eff} is smaller than B for all cases we examined. We find $B_{\mathrm{eff}} \approx B$ for very small Γ. The same consideration gives rise to the discovery that for the orbits around the fixed points $\mathcal{P}^{\pm}_{\mathrm{IB}}$ the effective precession frequency is much smaller than B.
In section 3.3 we stated that the regular motion in large parts of the phase-space is dominated by parametric resonances, cf. eq. (3.56). This effect is also important in the dissipative setup. However, the larger the dissipation gets, the more the electronic spin assumes the large spin's frequency, which is due to the faster decay of SQD states. The initial conditions of the large spin also play an important role since the exchange interaction is enhanced the more $\vec{\hat{J}}$ is perpendicular to the magnetic field.
Note also that a frequency doubling for the oscillation of the z-components of the spins and the electronic currents occur for every periodic oscillation, damped and undamped. Before reaching

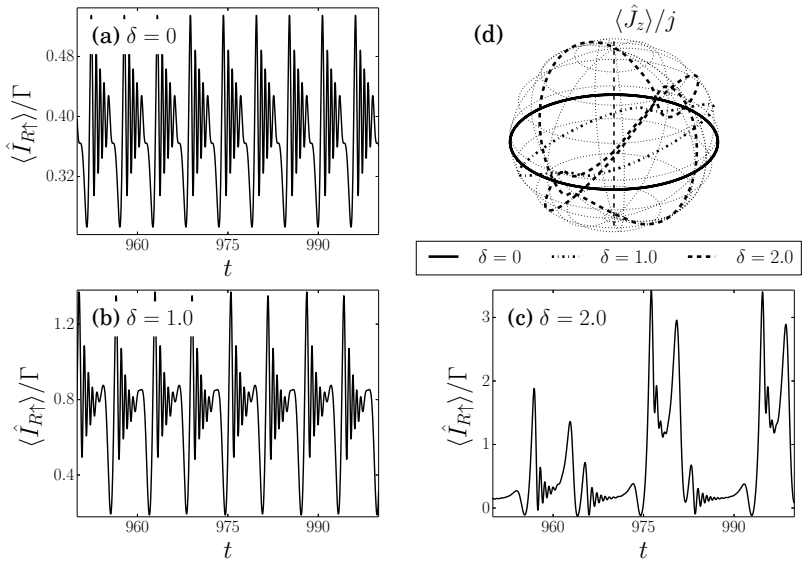

Figure 4.5.: (a)–(c) Electronic currents and (d) the dynamics of $\vec{\hat{J}}$ for parameters from region III with respect to different feedback strengths δ. The current oscillations become slower and turn to quasiperiodic oscillations. The oscillation of $\vec{\hat{J}}$ is not planar anymore and the limit cycles become more complicated. Parameters: $B/\lambda = 0.6, \Gamma/\lambda = 1, j/\lambda = 10$.

stationary cycles the system often undergoes transient oscillations.

As long as the feedback mechanism is switched off this holds for the whole parameter region. Once the feedback is switched on, for instance, with a feedback constant δ in the order of magnitude of λ, region III exhibits subregions with respect to the magnitude of Γ.

For $\Gamma \gg \lambda$ the large spin oscillates in the $\langle \hat{J}_z^* \rangle = -B/\lambda$ plane, independent of δ. The corresponding currents are regularized to become almost sinusoidal; cf. Fig. 4.4.

With much slower electronic transport $\Gamma \ll \lambda$ the oscillation plane of $\vec{\hat{J}}$ is tilted by an angle ϕ around the x-axis and we find even more complicated orbits for the oscillation of $\vec{\hat{J}}$ that is not restricted to a plane anymore if Γ is close to λ. Since δ enters exponentially into the equations the tunneling setup is, thus, detuned drastically if the feedback parameter δ is increased. For some parameters the dynamics change towards quasiperiodic oscillations or even chaos. In Fig. 4.5 we have plotted the currents and the large spin's cycles for different δ. We see that the regular motion becomes quasiperiodic for increasing feedback strength. For intermediate δ the $\vec{\hat{J}}$ rotation stays planar, but the rotation plane is tilted. This kind of limit cycle oscillation where the plane of oscillation through $\langle \hat{J}_z \rangle = -B/\lambda$ is tilted by an angle ϕ around the x-axis may be described by an effective model similarly to (4.81), if one found the angle ϕ and adjusted the transformation in Appendix A.1 accordingly.

In Fig. 4.8 we compare the solutions for our effective model to the full solutions for different Γ and, if possible, for different δ.

One further remark should be given on the periodic orbits. The oscillation around the polarization fixed point $\mathcal{P}_{\mathrm{IB}}^{\pm}$ is undamped and the magnitude of the electronic spin is nearly constant. In this case the two interacting spins can be considered as a system of two interacting undamped Bloch equations. Those could be recast in the form of coupled complex Riccati equations [168, 169]. Unfortunately, to the best of our knowledge these Riccati equations can only be solved for

special setups, e.g., isotropic coupling.

Region II: mixed dynamics

We observe the full variety of the possible dynamics, in regime II. All fixed points are real valued, but $\mathcal{P}_{\mathrm{IB}}^{\pm}$ are unstable while $\mathcal{P}_{\mathrm{IB}}^{\pm y,\pm}$ are stable. We find many parameter settings and initial conditions where the system will oscillate strongly damped to run into $\mathcal{P}_{\mathrm{IB}}^{\pm y,\pm}$. Once one of the fixed points $\mathcal{P}_{\mathrm{IB}}^{\pm y,\pm}$ is reached, a stationary current is established that follows straightforwardly from (4.60). We find the stationary state of the total SQD occupancy $\hat{N} = \sum_\sigma \hat{n}_\sigma$ by solving

$$0 = -\mathrm{e}^{\delta}\,\Gamma\left(5\,\langle \hat{n}_\uparrow^* \rangle - 4\,\langle \hat{S}_z^* \rangle - 2\right), \tag{4.82}$$

which provides the stationary current of ↑-electrons leaving the SQD ($\langle \hat{S}_z^* \rangle \to -B/\lambda$)

$$\frac{\langle I_{R\uparrow} \rangle}{e\Gamma} = \frac{2}{5}\,\mathrm{e}^{\delta}\left(1 - 2\frac{B}{\lambda}\right). \tag{4.83}$$

On the other hand, the current will vanish when the system reaches the full polarization fixed point $\mathcal{P}_{\mathrm{IB}}^{\pm}$, as the SQD is found in a Coulomb blockade then.
Additionally, we find quasiperiodic or even chaotic oscillations and two kinds of self-sustained oscillations as we have found for region III.
If the feedback mechanism is switched on and the system is started from the same initial conditions we often find the system to respond in a way that an oscillation vanishes and the system runs into fixed points $\mathcal{P}_{\mathrm{IB}}^{\pm y,\pm}$. Periodic oscillations for magnetic fields close to B_c are often changed to run into fixed points or detuned into quasiperiodic oscillations.
Nonetheless, the numerical results show that there are parts of the parameter space where feedback turns quasiperiodic oscillations into regular self-sustained, though not planar, oscillations; compare Fig. 4.7 and labels 3 and 4 in Fig. 4.3. It is possible as well to prevent the system from running into its fixed points and induce periodic oscillations instead; compare Fig. 4.6.
Chaotic behavior in region II is dominant in parameter regimes where the exchange interaction is much stronger than the tunnel coupling, i.e. $\Gamma \ll \lambda$ and small magnetic field $B \ll \lambda$. As a consequence the feedback effect is rather small in these regimes, at least with feedback parameters δ in the order of magnitude of λ.

4.8.3. Finite bias regime: fixed points and parameter regions

In the finite-bias (FB) regime we choose the tunneling rates asymmetrically as or the infinite bias setup, because of the richness of the occurring dynamics. In the following we assume a symmetric detuning of the chemical potentials with respect to the SQD level ($\varepsilon = 0$), i.e. $\mu_L = -\mu_R = V/2$. In the limit of vanishing temperatures only electrons with energies between the leads' chemical potentials can participate in transport. This so-called transport window is smeared out due to thermal melting of the Fermi edges if the temperatures are finite. We, however, consider equal finite temperatures $\beta_l = \beta$ and choose the bias voltage in a manner that for given parameters B, λ, j the energies $\varepsilon_\sigma(t)$ lie between the chemical potentials for all times. The maximum detuning between the ↑- and ↓-levels is $\varepsilon_z^{\max} = B + \lambda_z j$, and accordingly we choose $\beta V > \beta\varepsilon_z^{\max}$.
We have to remark that bidirectional tunneling for this parameters is only possible for finite temperatures, obviously.

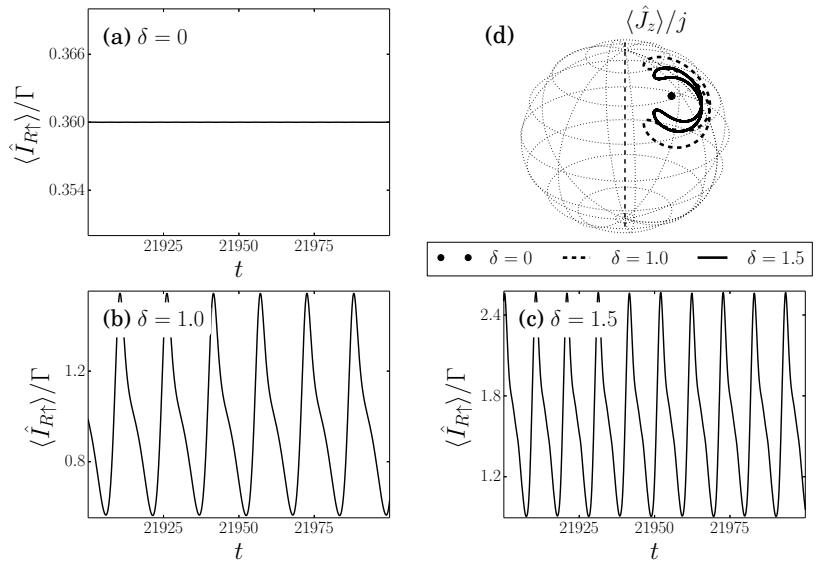

Figure 4.6.: (a)–(c) Electronic currents and (d) the dynamics of $\vec{\hat{J}}$ for parameters from region II with respect to different feedback strengths δ. The evolution towards the fixed point $\mathcal{P}^y$ [with a corresponding current (4.83)] is changed into self-sustained oscillations via feedback. Parameters: $B/\lambda = 0.05, \Gamma/\lambda = 0.1, j/\lambda = 10$.

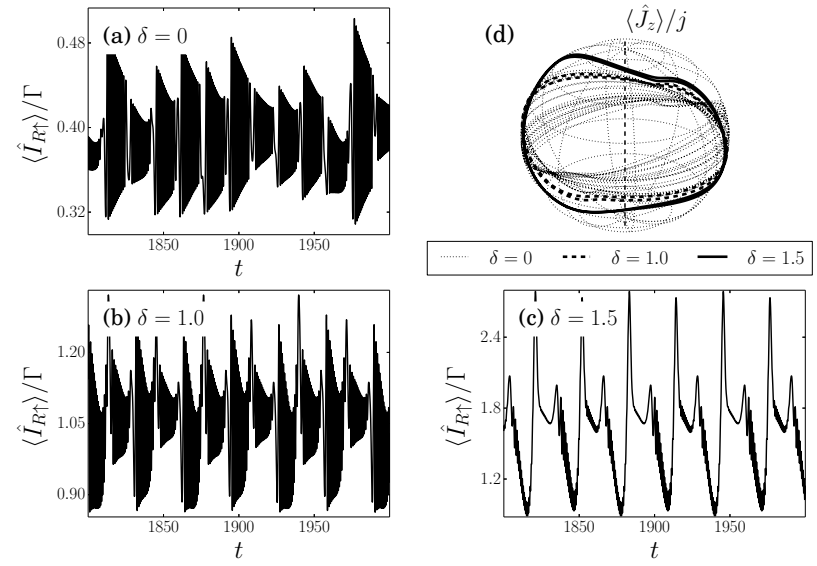

Figure 4.7.: (a)–(c) Electronic currents and (d) the dynamics of $\vec{\hat{J}}$ for parameters from region II with respect to different feedback strengths δ. Irregular oscillations are regularized for both electronic and large spin. Parameters: $B/\lambda = 0.2, \Gamma/\lambda = 0.1, j/\lambda = 10$.

Fixed points

As in the previous sections, we find fixed points, where the dynamics of the spins are decoupled and $\vec{\hat{J}}$ is fully polarized,

$$\mathcal{P}^{\pm}_{\mathrm{FB}} = \left(0, 0, +\mathcal{B}^{\mathrm{A,B}}_{4\pm}, 0, 0, \pm j\right) \tag{4.84}$$

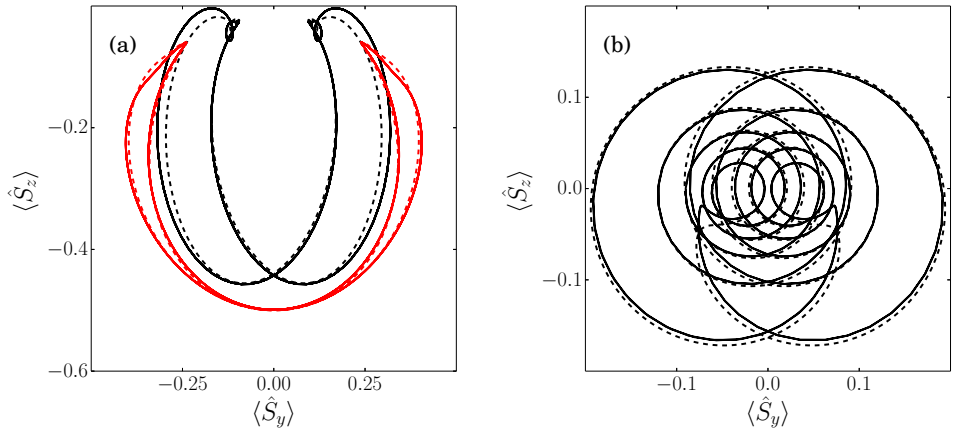

Figure 4.8.: Comparison between solutions to the full set of Eqs. (4.60) and (4.62) (dashed lines) and solutions to the effective model (4.81) (solid lines) for different setups. Parameters (a) $B/\lambda = 0.6$, $\Gamma/\lambda = 5$, $j/\lambda = 10$, $\delta/\lambda = 1$ (red) and $\delta = 0$ (black). Parameters (b) $B/\lambda = 0.6$, $\Gamma/\lambda = 1$, $j/\lambda = 10$, $\delta = 0$.

The values $\mathcal{B}_{4\pm}^{\mathrm{A,B}}$ are dependent on the respective feedback scheme. They are denoted in Appendix A.2. The alignment of the electronic spin is not only asymmetric with respect to the detuning of the leads' chemical potentials, but also with respect to the large spin polarization, i.e. for increasing λ and a large j we find trapped electrons with its spin antiparallel to the polarization of the large spin: $\langle \hat{S}_z^* \rangle (\pm j, \lambda \gg 0, V = 0) \to \mp 1/2$. In Fig. 4.9 we plot $\langle \hat{S}_z^* \rangle$ and the stationary states that are established once the spins decouple; compare Appendix A.2.
As in the infinite bias setup there is a second set of fixed points, with $\langle \hat{S}_z^* \rangle = \langle \hat{J}_z^* \rangle = -B/\lambda$, namely,

$$\mathcal{P}_{\mathrm{FB}}^{\pm y,\pm} = \left(0, \pm\sqrt{\frac{2B}{\lambda}} \frac{1 + \mathrm{e}^{\frac{\beta V}{2}}}{2 + \mathrm{e}^{\frac{\beta V}{2}}} \mathcal{B}_6^{\mathrm{A/B}}, -\frac{B}{\lambda}, \pm \frac{\Gamma}{\sqrt{2B\lambda}} \mathcal{B}_6^{\mathrm{A/B}}, \pm \mathcal{B}_7^{\mathrm{A/B}}, -\frac{B}{\lambda}\right), \tag{4.85}$$

with the parameters

$$\begin{aligned}
\mathcal{B}_6^{\mathrm{A}} &= \sqrt{-\frac{\left(4B + \mathrm{e}^{\delta + \frac{\beta V}{2}} (2B - \lambda) + \lambda\right)}{\lambda \left(3 + \mathrm{e}^{\delta} + 5\,\mathrm{e}^{2\delta + \frac{\beta V}{2}}\right)} C}\,, \\
\mathcal{B}_6^{\mathrm{B}} &= \sqrt{-\frac{\mathrm{e}^{\delta} \left(4B + \mathrm{e}^{\frac{\beta V}{2}} (2B - \lambda) + \lambda\right)}{\lambda \left(3 + \mathrm{e}^{2\delta} \left(1 + 5\,\mathrm{e}^{\frac{\beta V}{2}}\right)\right)} C}\,, \\
\mathcal{B}_7^{\mathrm{A/B}} &= \sqrt{j^2 - \left(\frac{B}{\lambda}\right)^2 - \frac{\Gamma^2}{2B\lambda} \left(\mathcal{B}_6^{\mathrm{A/B}}\right)^2}\,, \\
C &= \left(2 + \mathrm{e}^{\frac{\beta V}{2}}\right) \frac{1 + \mathrm{e}^{2\delta + \frac{\beta V}{2}}}{\left(1 + \mathrm{e}^{\frac{\beta V}{2}}\right)^2}\,.
\end{aligned} \tag{4.86}$$

We can, once again, identify a region, where the fixed points $\mathcal{P}_{\mathrm{FB}}^{\pm y,\pm}$ assume finite real values for all components (region II) and regions (I,III) where they have no physical meaning. We solve

the equations $\mathcal{B}_6 = 0$ and $\mathcal{B}_7 = 0$ and obtain the critical values

$$
\begin{aligned}
B_c^{\mathrm{A}} &= \frac{\lambda}{2}\left(1 - \frac{3}{2 + \mathrm{e}^{\delta + \frac{\beta V}{2}}}\right), \\
B_c^{\mathrm{B}} &= \frac{\lambda}{2}\left(1 - \frac{3}{2 + \mathrm{e}^{\frac{\beta V}{2}}}\right), \\
\Gamma_c^{\mathrm{A}} &= \sqrt{\frac{2B\left(5\,\mathrm{e}^{2\delta + \frac{\beta V}{2}} + \mathrm{e}^{\delta} + 3\right)(B - \lambda j)(B + \lambda j)}{\left((2B - \lambda)\,\mathrm{e}^{\delta + \frac{V}{2}} + 4B + \lambda\right)}\frac{1}{C}}, \\
\Gamma_c^{\mathrm{B}} &= \sqrt{\frac{2B\left(5\,\mathrm{e}^{2\delta + \frac{\beta V}{2}} + \mathrm{e}^{2\delta} + 3\right)(B - \lambda j)(B + \lambda j)}{\mathrm{e}^{\delta}\left((2B - \lambda)\,\mathrm{e}^{\frac{V}{2}} + 4B + \lambda\right)}\frac{1}{C}}.
\end{aligned}
\tag{4.87}
$$

Interestingly, the border between regimes II and III for the feedback scheme B is the same as for the nonfeedback case. Thus, switching between the two considered feedback schemes might go along with transitions between the parameter regions.
The dynamics for the three parameter regions are quite similar to that in the infinite bias regime. Though, there are some special features.
The dominant behaviors in region I are damped oscillations towards the polarization of spins $\mathcal{P}_{\mathrm{FB}}^{\pm}$. There exist additional fixed points where $\langle \hat{J}_y^* \rangle \to 0$ for intermediate bias voltages. It is not possible to calculate them analytically, since $\langle \hat{J}_z \rangle$ couples to $\langle \hat{S}_x \rangle$ and $\langle \hat{S}_y \rangle$ via hyperbolic functions.
In region II the system can – depending on the tunneling rate Γ and the initial conditions – run into one of the fixed points $\mathcal{P}_{\mathrm{FB}}^{\pm y,\pm}$. For smaller Γ the spins may as well perform periodic oscillations or even chaotic ones, similar to the behavior for the infinite bias case.
We find dynamics that are very similar to the infinite bias case in region III. Nevertheless, additional oscillations occur, where $\vec{\hat{J}}$ is only partially polarized antiparallel to the external magnetic field and its magnitude is increased with increased bias voltage. This partial polarization is accompanied by the decay of the the electronic states and coherences and, thus, constant average currents. It takes place for intermediate bias voltage of $\beta V/\lambda \approx 5$. If the bias voltage is increased and given suitable initial conditions the system ends up completely polarized and electrons get trapped while the energy level for electrons of the opposite spin is shifted outside the transport window. The partial polarization is $P_\kappa = |\langle \hat{J}_z^{*\kappa} \rangle|$ with κ denoting the feedback scheme A,B, or 0 (no feedback applied). It is of magnitude $P_\kappa/\beta V \approx 1$ and is unique for all tuples (B, λ, V, δ) and the respective feedback scheme and we find $P_{\mathrm{A}} > P_{\mathrm{B}} > P_0$.

4.8.4. Typical feedback trajectories, spin filter setups

In the following we want to sketch typical trajectories found for a spin filter setup that makes use of the demon feedback. As stated above, the setup without interaction with the external spin generates currents even against small bias voltages (compare Sec. 4.8.1). To demonstrate the spin filtering effect, while the interaction with the large spin is effective we suggest a small negative bias voltage with $|V| > B + \lambda j$. For small ratios λ/j the electronic backaction on $\vec{\hat{J}}$ is very small and for suitable initial conditions the large spin stabilizes at $\langle \hat{J}_z \rangle = -B/\lambda$ and precesses freely. In this special case the energies ε_σ coincide and become constant in time. Due to the anisotropic exchange interaction the occupations of the ↑- and ↓-levels oscillate with the doubled precession frequency, and we find regularly oscillating currents accordingly.

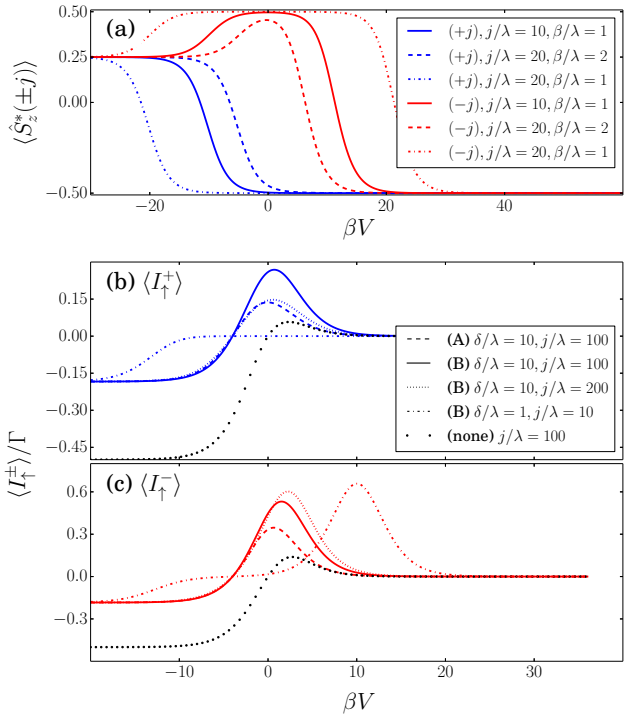

Figure 4.9.: (a) The values of the S_z-component of the global fixed point $\mathcal{P}_{\mathrm{FB}}^{\pm}$ vs the bias voltage. The spin-dependent stationary currents after the system reaches the fixed point $\mathcal{P}_{\mathrm{FB}}^{+}$ (b) or $\mathcal{P}_{\mathrm{FB}}^{-}$ (c) are shown for feedback schemes A and B and the nonfeedback case.

If no feedback takes place, the currents are flowing with the bias, i.e. from the right to the left. Due to the spin interactions the averaged ↑-influx through the right lead splits up to generate oscillating ↑- and ↓-currents from the SQD to the left reservoir, as we depict in Fig. 4.10(a).
It is due to our feedback scheme B that the direction of the influx is reversed. The inflowing current, again, is split up and the ↑-electrons are transported to the right while the ↓-electrons are released to the left; compare Fig. 4.10(c).
Interestingly, for scheme A and for the same parameters we find that the two transport channels decouple and the expectation values $\langle \hat{S}_i \rangle$ decay; the averaged probabilities to find the SQD empty or occupied by an electron of spin σ are equal. As a consequence, the ↓-current through the left barrier vanishes, i.e. with Eq. (4.75) becomes $\langle I_{L\downarrow} \rangle = (1 - f_{L\downarrow})/3 - \exp[\delta] f_{L\downarrow}/3 = 0$. At the same time a constant net ↑-current from the left to the right lead builds up. This critical point is characterized by the ratio of $V/\delta = -2$. If the ratio is smaller than -2 a net outflux of ↓-electrons to the left lead is generated while the ↑-current flows from left to right. For bias voltages $V > -2\delta$ ↓-electrons are trapped in the SQD and only leave it after being flipped. In Fig. 4.10(e) we depicted the corresponding currents at and close to the critical parameters.
It is obvious that $V = 0$ is the critical bias voltages for the nonfeedback and scheme B as well, where the two transport channels decouple. If one can prepare the large spin to have a polarization of $\langle \hat{J}_z \rangle$ the energies ε_σ are constant and equal to the chemical potentials of the reservoirs. It is due to the thermal melting of the Fermi edges that transport is still possible, and therefore we get the net currents (4.68) evaluated for $B = 0$ since the level splitting is compensated by the large spin polarization.
We should also mention, that the opposite oscillating currents can as well be generated when the

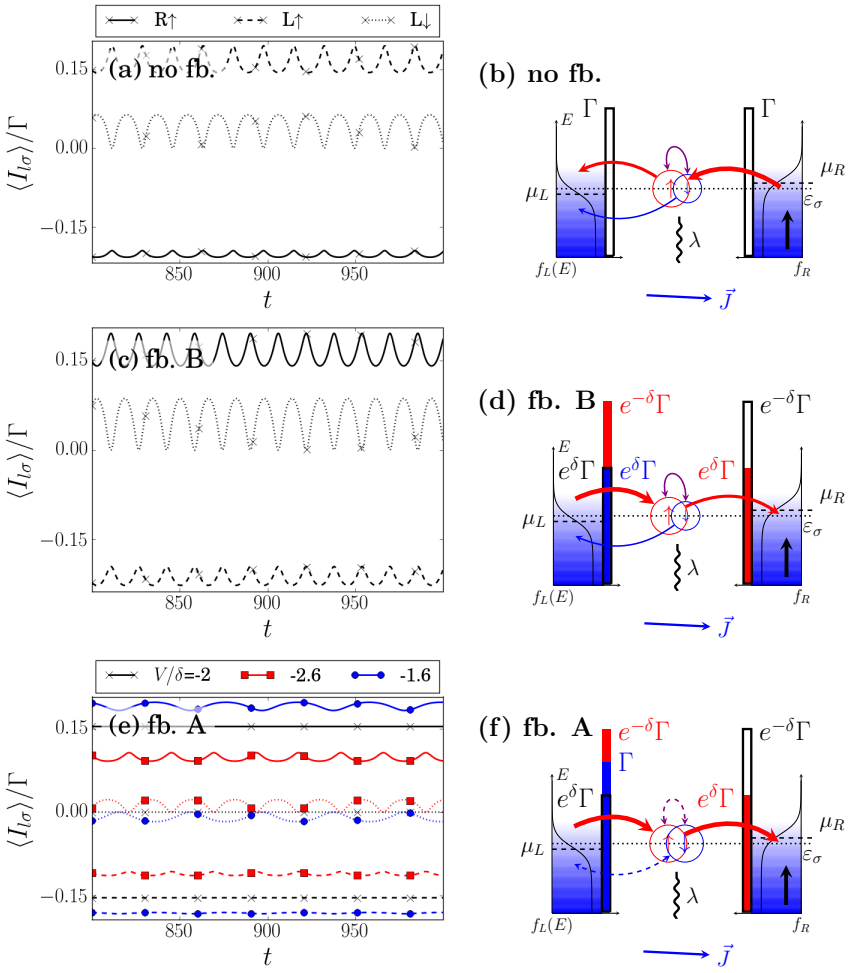

Figure 4.10.: Average spin-σ currents through barrier l for small negative biases and different feedback schemes. Without feedback (a) the currents flow according to the applied bias voltage from the right lead to the left lead. For feedback scheme B (c) an oscillating ↑-current against the bias is building up, and ↓-electrons are ejected with the bias, the device is acting as a spin filter. With the given parameters the two transport channels decouple for feedback scheme A (e). A little detuning of the bias voltage leads to the oscillating ↑-currents against the bias. ↓-electrons are either ejected to the left reservoir(red squares) or trapped (blue circles). Images (b),(d) and (f) show the SQD with the respective tunneling rates if the system state is empty (black), ↑ (red) or ↓ (blue). Thickness and direction of the arrows show which net currents are reached. Level transitions (spin flips) are shown in violet. In (f) the transport channels decouple, no spin flips occur, and the ↓-current vanishes (dashed lines). Parameters: $B/\lambda = 0.1$, $\Gamma/\lambda = 10$,$\delta/\lambda = 10$ and $\beta V/\lambda = -20$.

tunneling rates are chosen symmetrically ($\Gamma_{l\sigma} = \Gamma$), and therefore, spin filter behavior is possible in setups without polarized leads.

4.9. Conclusions

In this chapter we have studied the complex dynamics of electronic transport through a SQD when interacting with a large external spin. We use semiclassical EOM for the large external spin together with a quantum master equation technique for the dynamics of the SQD. This method works well if we assume that the large spin precession is taking place on a much slower time scale than the electronic tunneling. The treatment allows for the introduction of a Maxwell-demon-like feedback. This feedback uses occupation-dependent alternation of the transport Liouvillian and can generate currents even against a moderate bias voltage.
We restricted ourselves to studying the special case of an anisotropic exchange interaction and a polarized right transport lead, since this setup generates a variety of interesting dynamics, such as parametric oscillation of both electron spin and large spin or complete polarization. We can calculate a number of fixed points analytically, for both finite and infinite bias and under the influence of our demon's feedback.
Furthermore, we studied the effect of two different feedback schemes, which can work as an effective spin filter for small bias voltages, that "sort" electrons by its spin and generate oscillating currents in opposite directions.
For the infinite bias regime both feedback schemes are identical. The numerical solutions of the highly nonlinear equations are very sensitive to the change of initial conditions and the parameters (B, Γ, δ) with respect to λ.
On the one hand, the asymmetric transport setup as a consequence of the applied feedback can transfer periodic motions to quasiperiodic dynamics or even chaos, e.g., for magnetic fields close to B_c and small tunneling rates $\Gamma \lessapprox \lambda$.
On the other hand, we have found that for small magnetic fields $B \lessapprox 0.2\lambda$ and tunneling rates $\Gamma \approx 0.1\lambda$ quasiperiodic oscillations are changed to undamped periodic oscillations when applying feedback of moderate strengths ($\delta \approx \lambda$).

As experimental realizations for the large external spin we think of magnetic impurities in semiconductor QDs or magnetic moments in single molecules (single molecular magnets). A possible realization where the mean-field approach is justified might be the hyperfine interaction with an ensemble of nuclear spins, where the number of spins is reasonably high. Although experiments suggest that it is possible to determine the spin state of electrons in a device it still is an open question as to how the spin-dependent tunneling rates can be modified conditionally in experiments.
On the other hand, the usage of conventional electronic circuits to control the tunneling setup seems also feasible. In experiments it is possible to measure single electron tunneling events accurately and is possible to modify tunneling rates on very fast time scales, by detuning gate voltages [59] to access feedback parameters $\ln[\Gamma_{\text{filled}}/\Gamma_{\text{empty}}] = \delta \approx 1$, which lead to the mentioned feedback effect.

5. Generic model for a Maxwell demon

5.1. Model Hamiltonian

In this chapter we want to discuss a generic model that implements a Maxwell-demon-like feedback mechanism, acting on a transport system. The model and the approach is strongly inspired by the seminal work of Strasberg *et al.* [44], who first discussed a physical implementation of a Maxwell-demon like feedback [43, 65] applied with a single electron transistor (SET) system, which they describe in terms of stochastic thermodynamics [41]. Strasberg also discussed a similar implementation for two serially coupled QDs [170].

The model consists of two parallel QDs, labeled A and B, with one orbital level each that are coupled coherently. The so formed double QD (DQD) is interacting capacitively to an additional single-level QD. We will label the latter as demon or detector QD, respectively, and equip it with the index d. The parallel DQD is weakly coupled to ideal reservoirs L (left) and R (right), and the demon QD is coupled to a single reservoir D. The electronic reservoirs $\nu \in \{D, L, R\}$ are characterized by their respective temperatures T_ν and their chemical potentials μ_ν.

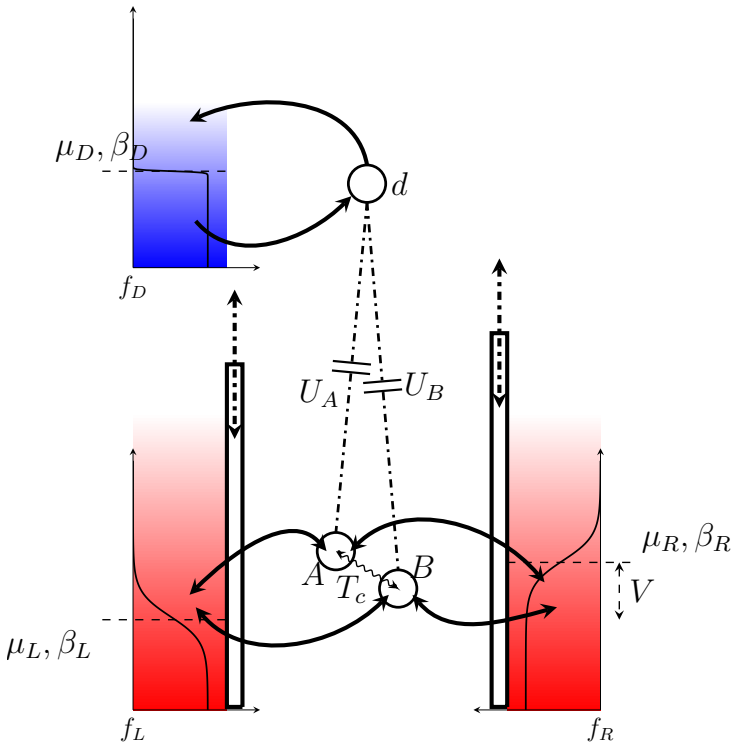

Figure 5.1.: Setup of the investigated toymodel system.

The system Hamiltonian reads

$$\hat{H}_{\mathrm{S}} = \varepsilon_A \hat{d}_A^\dagger \hat{d}_A + \varepsilon_B \hat{d}_B^\dagger \hat{d}_B + \varepsilon_d \hat{e}^\dagger \hat{e} + T_c(\hat{d}_A^\dagger \hat{d}_B + \hat{d}_B^\dagger \hat{d}_A) + \sum_x U_x \hat{e}^\dagger \hat{e} \hat{d}_x^\dagger \hat{d}_x \,, \quad x \in \{A, B\}\,, \tag{5.1}$$

where $\hat{d}_x$ and $\hat{e}$ denote the fermionic annihilation operators for the QDs A,B and the demon dot, respectively. The parameter T_c denotes the strength of the coherent coupling.
For later convenience we introduce a few definitions to rewrite the Hamiltonian

$$2U_0 \equiv U_A + U_B\,, \quad 2\Delta \equiv U_B - U_A \Longleftrightarrow U_A = U_0 - \Delta\,, \quad U_B = U_0 + \Delta\,,$$
$$\Omega \equiv \varepsilon_A - \varepsilon_B \Longleftrightarrow \varepsilon_A = \varepsilon + \Omega\,, \varepsilon_B = \varepsilon\,. \tag{5.2}$$

where we choose $\Delta, \Omega \geq 0$.
Equation (5.1) can, thus, be rewritten as follows:

$$\hat{H}_{\mathrm{S}} = (\varepsilon + \Omega)\, \hat{d}_A^\dagger \hat{d}_A + \varepsilon\, \hat{d}_B^\dagger \hat{d}_B + \varepsilon_d\, \hat{e}^\dagger \hat{e} + T_c(\hat{d}_A^\dagger \hat{d}_B + \hat{d}_B^\dagger \hat{d}_A) + (U_0 - \Delta)\, \hat{e}^\dagger \hat{e}\, \hat{d}_A^\dagger \hat{d}_A + (U_0 + \Delta)\, \hat{e}^\dagger \hat{e}\, \hat{d}_B^\dagger \hat{d}_B\,. \tag{5.3}$$

Note that the DQD part of $\hat{H}_{\mathrm{S}}$ is effectively equivalent to a charge qubit Hamiltonian $\hat{H}_{\mathrm{QB}} = \frac{\Omega}{2}\hat{\sigma}_z + T_c \hat{\sigma}_x$, when we disregard the absolute energy levels of QDs A and B. This qubit Hamiltonian, on the other hand, is equivalent to the effective Hamiltonian, (4.13), we studied in chapter 4. Let us assume very slow dynamics of the large spin, i.e. constant level splittings ε_z in (4.15) and constant coefficients for the spin-flip terms in (4.16). Given, additionally, an anisotropic coupling (e.g., $\lambda_y = 0$) in (4.16), we can identify $\varepsilon_z \leftrightarrow \Omega$ and $\Lambda \leftrightarrow T_c$.

The Hamiltonian for the reservoirs and the system-bath coupling read, respectively

$$\hat{H}_{\mathrm{leads}} = \sum_k \sum_{l\in\{L,R\}} \sum_{x\in\{A,B\}} \varepsilon_{klx}\, \hat{c}_{klx}^\dagger \hat{c}_{klx} + \sum_k \varepsilon_{kD}\, \hat{c}_{kD}^\dagger \hat{c}_{kD}\,,$$
$$\hat{H}_{\mathrm{T}} = \sum_k \sum_l \sum_x \left(t_{klx}\, \hat{c}_{klx}^\dagger \hat{d}_x + \mathrm{H.c.}\right) + \sum_k \left(t_{kD}\, \hat{c}_{kD}^\dagger \hat{e} + \mathrm{H.c.}\right). \tag{5.4}$$

Here we treat the reservoirs L, R incoherently, i.e. effectively as four different baths lx where operators $\hat{c}_{klx}^\dagger$ create electrons in the mode k and bath lx and the respective couplings to the DQD levels are $t_{klx}^{(*)}$. Note, however, that, in the course of this chapter we will assume that the effective leads LA and LB assume the same temperatures β_L and chemical potentials μ_L, respectively, which renders them in fact indistinguishable [and similar for leads RA and RB]. Nevertheless, for later convenience we treat them as separate reservoirs.
As we have done before, we use the Jordan-Wigner transformation to map the fermionic operators on spin operators; we have three sites where an electron can stay, which yields for the fermionic annihilation operators

$$\hat{d}_A = \hat{\sigma}_- \otimes \mathbb{1} \otimes \mathbb{1}\,,$$
$$\hat{d}_B = \hat{\sigma}_z \otimes \hat{\sigma}_- \otimes \mathbb{1}\,,$$
$$\hat{e} = \hat{\sigma}_z \otimes \hat{\sigma}_z \otimes \hat{\sigma}_-\,. \tag{5.5}$$

Obviously, we use the Hermitian conjugates for the creation operators. Note that we assume that the DQD is operated in a Coulomb blockade regime, i.e. the electron number in the DQD is either 0 or 1.

In the next step, we obtain the following eigenenergies

$$
\begin{aligned}
E_0^0 &= 0\,,\\
E_0^1 &= \varepsilon_d\,,\\
E_\pm^0 &= \varepsilon + \frac{\Omega}{2} \pm \frac{1}{2}\sqrt{\Omega^2 + 4T_c^2}\,,\\
E_\pm^1 &= \varepsilon + \frac{\Omega}{2} + \varepsilon_d + U_0 \pm \frac{1}{2}\sqrt{\Omega_1^2 + 4T_c^2}\,, \quad \Omega_1 = \Omega - 2\Delta\,,
\end{aligned}
\tag{5.6}
$$

The system Hamiltonian is already diagonal in the local basis, which we introduce in the form

$$
|d,s\rangle = |d\rangle \otimes |s\rangle\ , \quad \text{with } d \in \{0,1\}\,, \quad s \in \{0,A,B\}\,. \tag{5.7}
$$

In this basis the eigenstates read:

$$
\begin{aligned}
&|0,0\rangle\,, \qquad |1,0\rangle\ ,\\
&|0,-_0\rangle = \frac{1}{N_-^0}\left[-\eta_-^0\,|0,A\rangle - |0,B\rangle\right]\,, \quad |1,-_1\rangle = \frac{1}{N_-^1}\left[-\eta_-^1\,|1,A\rangle - |1,B\rangle\right]\,,\\
&|0,+_0\rangle = \frac{1}{N_+^0}\left[-\eta_+^0\,|0,A\rangle - |0,B\rangle\right]\,, \quad |1,+_1\rangle = \frac{1}{N_+^1}\left[-\eta_+^1\,|1,A\rangle - |1,B\rangle\right]\,.
\end{aligned}
\tag{5.8}
$$

The coefficients and the normalizations are parametrized by the occupations of the demon dot, which is reflected by the index $d \in \{0,1\}$

$$
\eta_\pm^d = \frac{\Omega_d \pm \sqrt{\Omega_d^2 + 4T_c^2}}{2T_c}\,, \quad N_\pm^d = \sqrt{1 + (\eta_\pm^d)^2} = \left[1 + \frac{\left(\Omega_d \pm \sqrt{\Omega_d^2 + 4T_c^2}\right)^2}{4T_c^2}\right]^{-1/2}\ , \tag{5.9}
$$

with Ω_d with $\Omega_0 = \Omega, \Omega_1 = \Omega - 2\Delta$.
The local basis vectors can be written in terms of eigenvectors. Therefore, we introduce the transformation matrix $\mathbf{T}_d$, and its inverse

$$
\mathbf{T}_d = \begin{pmatrix} -\frac{\eta_+^d}{N_+^d} & \frac{1}{N_+^d} \\ -\frac{\eta_-^d}{N_+^d} & \frac{1}{N_-^d} \end{pmatrix} \Longrightarrow \mathbf{T}_d^{-1} = \begin{pmatrix} \alpha_+^d & \alpha_-^d \\ \beta_+^d & \beta_-^d \end{pmatrix}\,. \tag{5.10}
$$

Thus, we obtain for the local basis vectors

$$
\begin{pmatrix} |d,A\rangle \\ |d,B\rangle \end{pmatrix} = \mathbf{T}_d^{-1} \begin{pmatrix} |d,+_d\rangle \\ |d,-_d\rangle \end{pmatrix}\,, \tag{5.11}
$$

where the overlap matrix elements read

$$
\begin{aligned}
\alpha_-^d &= \langle d,A|d,-_d\rangle = -\frac{N_-^d}{\eta_-^d - \eta_+^d}\,, \quad \alpha_+^d = \langle d,A|d,-_d\rangle = \frac{N_+^d}{\eta_-^d - \eta_+^d}\,,\\
\beta_-^d &= \langle d,B|d,-_d\rangle = -\frac{N_-^d \eta_+^d}{\eta_-^d - \eta_+^d}\,, \quad \beta_+^d = \langle d,B|d,+_d\rangle = \frac{N_+^d \eta_-^d}{\eta_-^d - \eta_+^d}\,.
\end{aligned}
\tag{5.12}
$$

It is obvious, that these coefficients are real-valued. Later on we need their squares which read

$$
\begin{aligned}
|\alpha_-^d|^2 = |\beta_+^d|^2 &= \frac{1}{2}\left(1 - \frac{\Omega_d}{\sqrt{\Omega_d^2 + 4T_c^2}}\right) = \frac{(\eta_-^d)^2}{1+(\eta_-^d)^2} = \frac{1}{1+(\eta_+^d)^2}\,, \\
|\alpha_+^d|^2 = |\beta_-^d|^2 &= \frac{1}{2}\left(1 + \frac{\Omega_d}{\sqrt{\Omega_d^2 + 4T_c^2}}\right) = \frac{(\eta_+^d)^2}{1+(\eta_+^d)^2} = \frac{1}{1+(\eta_-^d)^2}\,,
\end{aligned}
\tag{5.13}
$$

with $|\alpha_-^d|^2 + |\beta_-^d|^2 = |\alpha_+^d|^2 + |\beta_+^d|^2 = |\alpha_+^d|^2 + |\alpha_-^d|^2 = |\beta_+^d|^2 + |\beta_-^d|^2 = 1$.

5.2. Rate equations

Along the lines of section 2.8 we can now derive rate equations for the populations of the eigenstates of our model. To start with, we first identify the system and bath coupling operators. These are

$$
\begin{aligned}
&\hat{A}_1 = \hat{A}_5 = \hat{A}_2^\dagger = \hat{A}_6^\dagger = \hat{d}_A\,, \\
&\hat{A}_3 = \hat{A}_7 = \hat{A}_4^\dagger = \hat{A}_8^\dagger = \hat{d}_B\,, \\
&\hat{A}_9 = \hat{A}_{10}^\dagger = \hat{e}\,, \\
&\hat{B}_1 = \sum_k t_{kRA}^*\,\hat{c}_{kRA}^\dagger\,, \qquad \hat{B}_2 = \sum_k t_{kRA}\,\hat{c}_{kRA}\,, \\
&\hat{B}_3 = \sum_k t_{kRB}^*\,\hat{c}_{kRB}^\dagger\,, \qquad \hat{B}_4 = \sum_k t_{kRB}\,\hat{c}_{kRB}\,, \\
&\hat{B}_5 = \sum_k t_{kLA}^*\,\hat{c}_{kLA}^\dagger\,, \qquad \hat{B}_6 = \sum_k t_{kLA}\,\hat{c}_{kLA}\,, \\
&\hat{B}_7 = \sum_k t_{kLB}^*\,\hat{c}_{kLB}^\dagger\,, \qquad \hat{B}_8 = \sum_k t_{kLB}\,\hat{c}_{kLB}\,, \\
&\hat{B}_9 = \sum_k t_{kD}^*\,\hat{c}_{kD}^\dagger\,, \qquad \hat{B}_{10} = \sum_k t_{kD}\,\hat{c}_{kD}\,.
\end{aligned}
\tag{5.14}
$$

With the assumption that the electronic reservoirs are in thermal equilibrium it is straightforward to calculate the rates for the transitions induced by the coupling between system and baths. Using the definition of the bath correlation functions eq. (2.23) and its even Fourier transformation eq. (2.45) we obtain the rates [cf. section 4.4.3]

$$
\begin{aligned}
\gamma_{12}(\omega) &= \Gamma_{RA}(-\omega) f_R(-\omega)\,, \quad \gamma_{21}(\omega) = \Gamma_{RA}(\omega)\,[1 - f_R(\omega)]\,, \\
\gamma_{34}(\omega) &= \Gamma_{RB}(-\omega) f_R(-\omega)\,, \quad \gamma_{43}(\omega) = \Gamma_{RB}(\omega)\,[1 - f_R(\omega)]\,, \\
\gamma_{56}(\omega) &= \Gamma_{LA}(-\omega) f_L(-\omega)\,, \quad \gamma_{65}(\omega) = \Gamma_{LA}(\omega)\,[1 - f_L(\omega)]\,, \\
\gamma_{78}(\omega) &= \Gamma_{LB}(-\omega) f_L(-\omega)\,, \quad \gamma_{87}(\omega) = \Gamma_{LB}(\omega)\,[1 - f_L(\omega)]\,, \\
\gamma_{9,10}(\omega) &= \Gamma_{D}(-\omega) f_D(-\omega)\,, \quad \gamma_{10,9}(\omega) = \Gamma_{D}(\omega)\,[1 - f_D(\omega)]\,,
\end{aligned}
\tag{5.15}
$$

where the effective tunneling rates evaluated at the energy ω yield

$$
\begin{aligned}
\Gamma_D(\omega) &= 2\pi \sum_k |t_{kD}|^2 \delta\left(\omega - \varepsilon_{kD}\right)\,, \\
\Gamma_{lx}(\omega) &= 2\pi \sum_k |t_{klx}|^2 \delta\left(\omega - \varepsilon_{klx}\right)\,.
\end{aligned}
\tag{5.16}
$$

The rate equations are then calculated according to (2.84) and (2.85). Their coefficients can be written in the form of a rate matrix, which represents the Liouvillian generator of the master equations $\partial_t \hat{\rho} = \hat{\mathcal{L}}\hat{\rho}$. We rearrange the populations in the density matrix $\hat{\rho}$ as a vector,

$$\hat{\rho} \to \rho = (p_{00}, p_{0-}, p_{0+}, p_{10}, p_{1-}, p_{1+})^{\mathrm{T}}\,, \tag{5.17}$$

and decompose the corresponding rate matrix $\mathcal{L}$ into parts, that describe the dynamics due to the reservoirs $\nu \in \{L, R, D\}$. They read

$$\mathcal{L} = \sum_{\nu} \mathcal{L}^{(\nu)}\,, \tag{5.18}$$

$$\mathcal{L}^{(l)} = \begin{pmatrix} \mathcal{L}^{(l),0} & \mathbf{0} \\ \mathbf{0} & \mathcal{L}^{(l),1} \end{pmatrix}, \quad \mathcal{L}^{(l),d} = \begin{pmatrix} -\sum_\sigma \gamma^d_{l\sigma} & \overline{\gamma}^d_{l-} & \overline{\gamma}^d_{l+} \\ \gamma^d_{l-} & -\overline{\gamma}^d_{l-} & 0 \\ \gamma^d_{l+} & 0 & -\overline{\gamma}^d_{l+} \end{pmatrix}, \quad d \in \{0,1\}\,, \quad l \in \{L, R\}\,,$$

$$\mathcal{L}^{(D)} = \begin{pmatrix} -(\cdots) & 0 & 0 & \overline{\gamma}_D(\varepsilon_d) & 0 & 0 \\ 0 & -(\cdots) & 0 & 0 & \kappa_{--}\overline{\gamma}_D(\varepsilon_{--}) & \kappa_{-+}\overline{\gamma}_D(\varepsilon_{-+}) \\ 0 & 0 & -(\cdots) & 0 & \kappa_{+-}\overline{\gamma}_D(\varepsilon_{+-}) & \kappa_{++}\overline{\gamma}_D(\varepsilon_{++}) \\ \gamma_D(\varepsilon_d) & 0 & 0 & -(\cdots) & 0 & 0 \\ 0 & \kappa_{--}\gamma_D(\varepsilon_{--}) & \kappa_{+-}\gamma_D(\varepsilon_{+-}) & 0 & -(\cdots) & 0 \\ 0 & \kappa_{-+}\gamma_D(\varepsilon_{-+}) & \kappa_{++}\gamma_D(\varepsilon_{++}) & 0 & 0 & -(\cdots) \end{pmatrix}.$$

The diagonal elements of the submatrices, denoted by $-(\cdots)$ are given by the other elements such that the column sums of the respective sub-Liouvillian yield Null. The specific block structure of the rate matrix is due to the ordering eq. (5.17).
The blocks $\mathcal{L}^{(l),d}$ contain the rates for the tunneling into qubit eigenstates $|\sigma_d\rangle$, with $\sigma \in \{+,-\}$, that are conditioned on the state of the detector QD. We, therefore, introduced the composed rates for the hopping of an electron onto the lead l from state $|\sigma_d\rangle$ and vice versa

$$\begin{aligned} \overline{\gamma}_{l\sigma} &= \left|\alpha^0_\sigma\right|^2 \overline{\gamma}_{lA}\left(E^0_\sigma\right) + \left|\beta^0_\sigma\right|^2 \overline{\gamma}_{lB}\left(E^0_\sigma\right)\,, \quad \gamma_{l\sigma} = \left|\alpha^0_\sigma\right|^2 \gamma_{lA}\left(E^0_\sigma\right) + \left|\beta^0_\sigma\right|^2 \gamma_{lB}\left(E^0_\sigma\right)\,, \\ \overline{\gamma}^U_{l\sigma} &= \left|\alpha^1_\sigma\right|^2 \overline{\gamma}_{lA}\left(\Delta E^1_\sigma\right) + \left|\beta^1_\sigma\right|^2 \overline{\gamma}_{lB}\left(\Delta E^1_\sigma\right)\,, \quad \gamma^U_{l\sigma} = \left|\alpha^1_\sigma\right|^2 \gamma_{lA}\left(\Delta E^1_\sigma\right) + \left|\beta^1_\sigma\right|^2 \gamma_{lB}\left(\Delta E^1_\sigma\right)\,, \\ \overline{\gamma}_{lx}(\omega) &= \Gamma_{lx}(\omega)\overline{\gamma}_l(\omega)\,, \quad \gamma_{lx}(\omega) = \Gamma_{lx}(\omega) f_l(\omega)\,, \end{aligned} \tag{5.19}$$

where γ_{lx} are the contributions to the rates with respect to the tunneling processes between leads l and dots $x \in \{A, B\}$. Note that we have two transport channels through dots x, that decouple in the limit $T_c \to 0$. Thus, this further splitting of the rates is useful as we want to investigate how the currents through the distinct channels is influenced by different feedback schemes, later on.
It is crucial to note that the bare tunneling rates $\Gamma_{lx}(\omega)$ are in general energy-dependent as well as the Fermi energies $f(\omega)$. Therefore, the transition rates γ have to be evaluated at the transition energies E^0_σ and $\Delta E^1_\sigma = E^1_\sigma - E^1_0$.
The dissipation rates with respect to the demon dot reservoir D are

$$\overline{\gamma}_D(\omega) = \Gamma_D \overline{\gamma}_D(\omega)\,, \quad \gamma_D(\omega) = \Gamma_D f_D(\omega)\,, \tag{5.20}$$

and in $\mathcal{L}^{(D)}$ we introduced for the sake of a shorter notation

$$\kappa_{\sigma\sigma'} = |\beta^0_\sigma|^2 |\beta^1_{\sigma'}|^2 \left(1 + \eta^0_\sigma \eta^1_{\sigma'}\right)^2\,. \tag{5.21}$$

Additionally we use the new compact notation for the transition energies due to the coupling to reservoir D, i.e.

$$\varepsilon_{\sigma\sigma'} = E^1_{\sigma'} - E^0_\sigma\,. \tag{5.22}$$

In fig. 5.2 the tunneling processes are sketched in a graph plot.

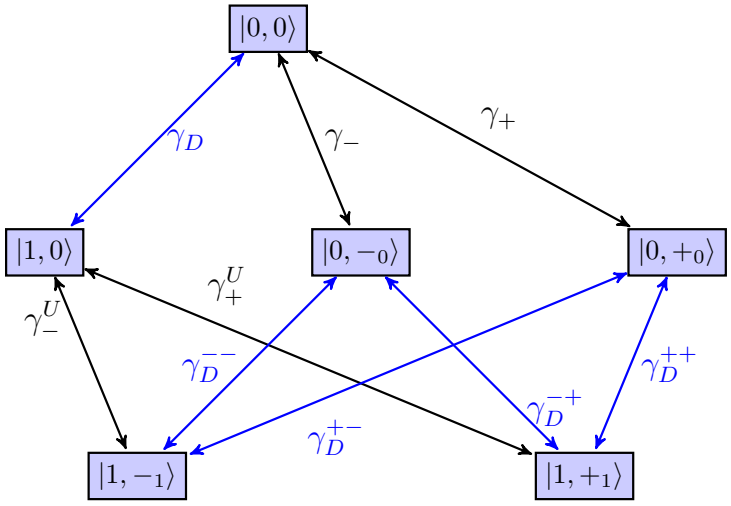

Figure 5.2.: Transitions between eigenstates of the model. Blue arrows depict transitions with respect to reservoir D, black ones those with respect to the contacts L, R. The compact rates for the tunneling from reservoir D are defined as follows: $\gamma_D = \gamma_D(\varepsilon_d)$, $\gamma_D^{\sigma\sigma'} = \kappa_{\sigma\sigma'}\gamma_D(\varepsilon_{\sigma\sigma'})$, $\gamma_\sigma = \sum_l \gamma_{l\sigma}(E_\sigma^0)$ and $\gamma_\sigma^U = \sum_l \gamma_{l\sigma}(\Delta E_\sigma^1)$. Note that for the sake of clearness we do not note down the rates of the reverse processes, which of course go with $\overline{\gamma} = 1 - \gamma$.

5.2.1. Currents and entropy production

We can now directly calculate the (nonequilibrium) steady-state particle and energy currents with respect to terminal $\nu \in \{L, R, D\}$ according to eqs. (2.125) and (2.126)

$$\bar{I}_{\mathrm{M}}^{(\nu)} = \sum_{ij}^{6} \mathcal{L}_{ij}^{(\nu)} \bar{p}_j \Delta n_{i,j} \,, \tag{5.23}$$

$$\bar{I}_{\mathrm{E}}^{(\nu)} = \sum_{ij}^{6} \mathcal{L}_{ij}^{(\nu)} \bar{p}_j \Delta E_{i,j} \tag{5.24}$$

where $\mathcal{L}\bar{\rho} = 0$ defines the system's steady-state, and $\bar{p}_j, j \in \{1 \dots 6\}$ are its components. We obtain the following particle currents ($l \in \{L, R\}$),

$$\bar{I}_{\mathrm{M}}^{(l)} = -\sum_{\sigma} \left[\overline{\gamma}_{l\sigma}(E_\sigma^0)\bar{p}_{0\sigma} - \gamma_{l\sigma}(E_\sigma^0)\bar{p}_{00} + \overline{\gamma}_{l\sigma}(\Delta E_\sigma^1)\bar{p}_{1\sigma} - \gamma_{l\sigma}(\Delta E_\sigma^1)\bar{p}_{10} \right] , \tag{5.25}$$

$$\begin{aligned} \bar{I}_{\mathrm{M}}^{(D)} = {} & -\overline{\gamma}_D(\varepsilon_d)\bar{p}_{10} + \gamma_D(\varepsilon_d)\bar{p}_{00} \\ & - \kappa_{--}\left[\overline{\gamma}_D(\varepsilon_{--})\bar{p}_{1-} - \gamma_D(\varepsilon_{--})\bar{p}_{0-}\right] - \kappa_{-+}\left[\overline{\gamma}_D(\varepsilon_{-+})\bar{p}_{1+} - \gamma_D(\varepsilon_{-+})\bar{p}_{0-}\right] \\ & - \kappa_{+-}\left[\overline{\gamma}_D(\varepsilon_{+-})\bar{p}_{1-} - \gamma_D(\varepsilon_{+-})\bar{p}_{0+}\right] - \kappa_{++}\left[\overline{\gamma}_D(\varepsilon_{++})\bar{p}_{1+} - \gamma_D(\varepsilon_{++})\bar{p}_{0+}\right] . \end{aligned} \tag{5.26}$$

Consequently, the corresponding energy currents read

$$\bar{I}_{\mathrm{E}}^{(l)} = -\sum_{\sigma} \left[E_\sigma^0 \left(\overline{\gamma}_{l\sigma}(E_\sigma^0)\bar{p}_{0\sigma} - \gamma_{l\sigma}(E_\sigma^0)\bar{p}_{00} \right) + \Delta E_\sigma^1 \left(\overline{\gamma}_{l\sigma}(\Delta E_\sigma^1)\bar{p}_{1\sigma} - \gamma_{l\sigma}(\Delta E_\sigma^1)\bar{p}_{10} \right) \right] , \tag{5.27}$$

$$\begin{aligned} \bar{I}_{\mathrm{E}}^{(D)} = {} & -\varepsilon_d \left[\overline{\gamma}_D(\varepsilon_d)\bar{p}_{10} - \gamma_D(\varepsilon_d)\bar{p}_{00}\right] \\ & - \varepsilon_{--}\kappa_{--}\left[\overline{\gamma}_D(\varepsilon_{--})\bar{p}_{1-} - \gamma_D(\varepsilon_{--})\bar{p}_{0-}\right] - \varepsilon_{-+}\kappa_{-+}\left[\overline{\gamma}_D(\varepsilon_{-+})\bar{p}_{1+} - \gamma_D(\varepsilon_{-+})\bar{p}_{0-}\right] \\ & - \varepsilon_{+-}\kappa_{+-}\left[\overline{\gamma}_D(\varepsilon_{+-})\bar{p}_{1-} - \gamma_D(\varepsilon_{+-})\bar{p}_{0+}\right] - \varepsilon_{++}\kappa_{++}\left[\overline{\gamma}_D(\varepsilon_{++})\bar{p}_{1+} - \gamma_D(\varepsilon_{++})\bar{p}_{0+}\right] . \end{aligned} \tag{5.28}$$

In general the steady-state is rather difficult to calculate analytically, which is a motivation for an analysis with respect to the separation of time scales. Note, however, that a numerical evaluation confirms that the energy and the particle numbers are conserved, in the system's nonequilibrium steady-state.
At this steady-state the energy balance (i.e. the first law of thermodynamics), eq. (2.128) becomes

$$0 = \sum_{\nu} \dot{Q}^{(\nu)} + \sum_{\nu} \mu_{\nu} \bar{I}_{\mathrm{M}}^{(\nu)} \,, \tag{5.29}$$

where we assumed that there are no external sources of work. With the definition of the heat flow, eq. (2.130), the first law leads to energy conservation,

$$0 = \sum_{\nu} \bar{I}_{\mathrm{E}}^{(\nu)} \Longleftrightarrow \bar{I}_{\mathrm{E}}^{(D)} = -\bar{I}_{\mathrm{E}}^{(L)} - \bar{I}_{\mathrm{E}}^{(R)} \,. \tag{5.30}$$

With the matter balance, eq. (2.124), we can easily confirm that the particle number is also conserved, i.e.

$$0 = \sum_{\nu} \bar{I}_{\mathrm{M}}^{(\nu)} \,. \tag{5.31}$$

It is trivial, that there is no net particle current across the junction between the demon dot and the reservoir D: $I_{\mathrm{M}}^{(D)} = 0$. As a consequence we can explicitly state

$$0 = \bar{I}_{\mathrm{M}}^{(L)} + \bar{I}_{\mathrm{M}}^{(R)} \Longleftrightarrow \bar{I}_{\mathrm{M}} \equiv \bar{I}_{\mathrm{M}}^{(L)} = -\bar{I}_{\mathrm{M}}^{(R)} \,. \tag{5.32}$$

Furthermore, we recall that the entropy production in the system is a nonnegative quantity, which in nonequilibrium steady-states ($\dot{S} = 0$) is compensated by the entropy flow to the environment, as we have shown in eq. (2.145). We have

$$\bar{\dot{S}}_{\mathrm{i}} = -\bar{\dot{S}}_{\mathrm{e}} = -\sum_{\nu} \frac{\dot{Q}^{(\nu)}}{T_{\nu}} \geq 0 \,. \tag{5.33}$$

Physically, the DQD is connected to two terminals L and R with temperatures T_L and T_R and chemical potentials μ_L and μ_R. Let's assume that the terminals L and R are kept at the same temperature $T = T_L = T_R$. With the results from eqs. (5.30) and (5.32) and the definition of the heat flow, we can, thus, rewrite the entropy production, (5.33).
We obtain

$$\bar{\dot{S}}_{\mathrm{i}} = \frac{1}{T} \left(\mu_L - \mu_R\right) \bar{I}_{\mathrm{M}} + \left(\frac{1}{T} - \frac{1}{T_D}\right) \bar{I}_{\mathrm{E}}^{(D)} = \beta \left(\mu_L - \mu_R\right) \bar{I}_{\mathrm{M}} + \left(\beta - \beta_D\right) \bar{I}_{\mathrm{E}}^{(D)} \geq 0 \,. \tag{5.34}$$

The latter inequation formulates the condition that has to be met in order to pump electrons through the DQD against a chemical bias. In order to achieve that we need to have $(\mu_L - \mu_R)\bar{I}_{\mathrm{M}} \leq 0$. This yields the condition

$$\left(1 - \frac{\beta_D}{\beta}\right) \bar{I}_{\mathrm{E}}^{(D)} \geq -(\mu_L - \mu_R)\bar{I}_{\mathrm{M}} \geq 0 \,, \tag{5.35}$$

which, clearly, imposes bounds on the possible values for the temperature of the bath and the energy current. We can read off two immediate consequences: pumping against bias is not possible if either the temperature of the demon reservoir equals the temperature of the DQD

contacts, $\beta_D = \beta$, or if the energy current vanishes $\bar{I}_{\mathrm{E}}^{(D)} = 0$. Equation (5.35) means in terms of the extracted power [cf. eq. (2.146)]

$$\left(1 - \frac{\beta_D}{\beta}\right) \bar{I}_{\mathrm{E}}^{(D)} \geq \mathcal{P} \geq 0\,. \tag{5.36}$$

Thus, a suitable nonvanishing imbalance of the energy currents may lead to positive extracted power.

5.3. Coarse graining dynamics

Along the lines of the theory presented in section 2.13 we briefly recall how a system with two distinct time scales can be simplified.
The key to the coarse-grained description is to decompose the microscopic probabilities as

$$\mathbb{P}_{d|s}(t) = \frac{p_{ds}(t)}{P_s}\,, \tag{5.37}$$

where $\mathbb{P}_{d|s}(t)$ denotes the conditional probability to find the demon in state $d \in \{0, 1\}$ provided that the DQD is in state $s \in \{0, -, +\}$. On the other hand $P_s = \sum_d p_{ds}$ is the mesoscopic probability to find the DQD in state s.
In order to reduce the number of rate equations we adiabatically eliminate the faster degrees of freedom, i.e. the demon degrees. Within the elimination we assume that the mesoscopic probability distributions P_s are essentially fixed, i.e. time-independent.
We write with eqs. (2.149) to (2.151)

$$\dot{P}_s = \sum_{s'} V_{s,s'} P_{s'}\,, \tag{5.38}$$

$$V_{s,s'} = \sum_{d,d'} W_{ds,d's'} \mathbb{P}_{d'|s'}\,, \tag{5.39}$$

where the mesoscopic rates $V_{s,s'}$ depend on the dynamics of the microstates through the conditional probabilities $\mathbb{P}_{d|s}$.
The rate matrices obey the conditions $\sum_s V_{s,s'} = 0$, $\sum_{ds} W_{ds,d's'} = 0$ and the rates denoted by $W_{ds,d's'}$ are to be identified with the elements of the rate matrix $\mathcal{L}$, eq. (5.18), that can be written in terms of new submatrices as follows

$$\mathcal{L} = \begin{pmatrix} \mathcal{L}_{00} & \mathcal{L}_{01} \\ \mathcal{L}_{10} & \mathcal{L}_{11} \end{pmatrix}, \quad \text{with} \quad \mathcal{L}_{dd'} = \begin{pmatrix} W_{d0,d'0} & W_{d0,d'-} & W_{d0,d'+} \\ W_{d-,d'0} & W_{d-,d'-} & W_{d-,d'+} \\ W_{d+,d'0} & W_{d+,d'-} & W_{d+,d'+} \end{pmatrix}, \tag{5.40}$$

which enables us to simply read off the rates W.
In order to close eq. (5.39) we need to find the stationary states of the conditional probabilities. We thus have to compute [compare eq. (2.153)]

$$\sum_{d'} W_{ds,d's} \overline{\mathbb{P}}_{d'|s} = 0\,. \tag{5.41}$$

A further approximation is obvious: Given that the tunneling processes in the demon happen on a much faster time scale (τ_{mic}) than the hopping on/off the DQD (τ_{mes}), i.e. provided that the relation $\Gamma_D \gg \Gamma_{lx}(\omega)$ holds for all transition energies ω, it is justified to approximate $\mathcal{L}$ by $\mathcal{L}^{(D)}$, which is the *fast demon* condition introduced by Strasberg *et al.* in [44]. The extreme limit of

this condition is $\Gamma_D \to \infty$, which means – given an appropriate tuning of the chemical potential of the demon dot junction – that the demon dot is repopulated immediately after the DQD is emptied. In other words, the lifetime of states $|0,0\rangle$ goes to 0.
We then can solve eq. (5.41) for the conditional probabilities, where we have to take into account the normalization condition for the conditional probabilities $\mathbb{P}_{1|s} + \mathbb{P}_{0|s} = 1$.

5.4. Reduction for noninteracting DQD, $T_c \to 0$

The model reduces drastically if the coherent coupling between the two system quantum dots is switched off, i.e. if we consider the limit $T_c \to 0$. In this limit we obtain two distinct transport channels through the DQD, namely either through dot A or through dot B.
At first, we study how the rate matrix $\mathcal{L}$ reduces. With the assumption that $\Omega - 2\Delta \leq 0$ we find the following parameter reductions

$$\begin{aligned}
\lim_{T_c\to\infty} \left(|\alpha_-^0|^2, |\alpha_+^0|^2, |\beta_-^0|^2, |\beta_+^0|^2\right) &= (0,1,1,0)\,, \\
\lim_{T_c\to\infty} \left(|\alpha_-^1|^2, |\alpha_+^1|^2, |\beta_-^1|^2, |\beta_+^1|^2\right) &= (1,0,0,1)\,, \\
\lim_{T_c\to\infty} \left(\kappa_{--}, \kappa_{-+}, \kappa_{+-}, \kappa_{++}\right) &= (0,1,1,0)\,.
\end{aligned} \tag{5.42}$$

Consequently, the nontrivial eigenstates become

$$\lim_{T_c\to\infty} \left(|0,-_0\rangle, |0,+_0\rangle, |-,1\rangle, |1,+_1\rangle\right) = \left(|0,B\rangle, |0,A\rangle, |1,A\rangle, |1,B\rangle\right)\,. \tag{5.43}$$

And finally, the energy arguments in the transition rates transform to

$$\begin{aligned}
\lim_{T_c\to\infty} \left(E_-^0, E_+^0, \Delta E_+^1, \Delta E_-^1\right) &= \left(\varepsilon, \varepsilon+\Omega, \varepsilon+U_0+\Omega-\Delta, \varepsilon+U_0+\Delta\right), \\
\lim_{T_c\to\infty} \left(\varepsilon_{--}, \varepsilon_{++}, \varepsilon_{-+}, \varepsilon_{+-}\right) &= \left(\varepsilon_d+U_0+\Omega-\Delta, \varepsilon_d+U_0-\Omega+\Delta, \varepsilon_d+U_0+\Delta, \varepsilon_d+U_0-\Delta\right)\,.
\end{aligned} \tag{5.44}$$

Therefore, the rate matrix in the master equation assumes, with respect to the basis $(p_{00}, p_{0B}, p_{0A}, p_{10}, p_{1A}, p_{1B})$, the form

$$\begin{aligned}
\mathcal{L}_{T_c\to 0} &= \mathcal{L}^{(L)}_{T_c\to 0} + \mathcal{L}^{(R)}_{T_c\to 0} + \mathcal{L}^{(D)}_{T_c\to 0} \\
&= \begin{pmatrix}
-(\cdots) & \overline{\gamma}_B(E_-^0) & \overline{\gamma}_A(E_+^0) & \overline{\gamma}_D(\varepsilon_d) & 0 & 0 \\
\gamma_B(E_-^0) & -(\cdots) & 0 & 0 & 0 & \overline{\gamma}_D(\varepsilon_{-+}) \\
\gamma_A(E_+^0) & 0 & -(\cdots) & 0 & \overline{\gamma}_D(\varepsilon_{+-}) & 0 \\
\gamma_D(\varepsilon_d) & 0 & 0 & -(\cdots) & \overline{\gamma}_A(\Delta E_-^1) & \overline{\gamma}_B(\Delta E_+^1) \\
0 & 0 & \gamma_D(\varepsilon_{+-}) & \gamma_A(\Delta E_-^1) & -(\cdots) & 0 \\
0 & \gamma_D(\varepsilon_{-+}) & 0 & \gamma_B(\Delta E_+^1) & 0 & -(\cdots)
\end{pmatrix},
\end{aligned} \tag{5.45}$$

$$\gamma_x(\varepsilon) = \sum_l \gamma_{lx}(\varepsilon)\,, \quad \overline{\gamma}_x(\varepsilon) = \sum_l \overline{\gamma}_{lx}(\varepsilon)\,. \tag{5.46}$$

Having reduced the full rate matrix we can now compute the stationary conditional probabilities, i.e. evaluate eq. (5.41) by identifying the respective rates of $\mathcal{L}^{(D)}_{T_c\to 0}$ in eq. (5.45).
We obtain

$$\begin{aligned}
\overline{\mathbb{P}}_{1|0} &= \gamma_D(\varepsilon_d)\,, \\
\overline{\mathbb{P}}_{1|A} &= \gamma_D(\varepsilon_{+-}) = \gamma_D(\varepsilon_d + U_0 - \Delta)\,, \\
\overline{\mathbb{P}}_{1|B} &= \gamma_D(\varepsilon_{-+}) = \gamma_D(\varepsilon_d + U_0 + \Delta)\,.
\end{aligned} \tag{5.47}$$

In the next step we need to tune the demon dot chemical potential μ_D in a way that the detector can reliably discriminate between the states in the DQD. We have three possible transition energies for the tunneling between the reservoir D and the detector dot, namely ε_d, ε_{+-} and ε_{-+}. For $U_0, \Delta > 0$ and $U_0 > \Delta$ we have $\varepsilon_d < \varepsilon_{+-} < \varepsilon_{-+}$.
Recall that ε_d is the transition energy for hopping on/off the demon dot while the DQD is empty, $|1,0\rangle \leftrightarrow |0,0\rangle$. On the other hand ε_{+-} is the energy for transitions $|1,-_1\rangle = |1,A\rangle \leftrightarrow |0,+_0\rangle = |0,A\rangle$, i.e. tunneling with respect to reservoir D while the DQD is in $|A\rangle$. Analogously, ε_{-+} accounts for transitions $|1,+_1\rangle = |1,B\rangle \leftrightarrow |0,-_0\rangle = |0,B\rangle$.
The reduced graph of transitions is shown in fig. 5.3, which clearly discloses that two noninteracting transport channels through the QDs A and B, respectively, are formed.
Note that with two distinct channels the currents can be split up, explicitly. Therefore, we can also formulate condition (5.35) for each transport channel, separately.

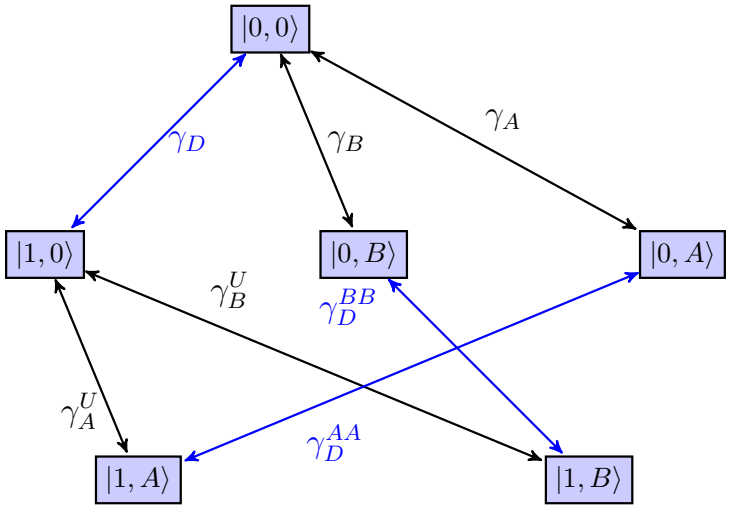

Figure 5.3.: Transitions between eigenstates of the model in the limit $T_c \to 0$. Blue arrows depict transitions induced by the coupling to reservoir D, black ones those with respect to the contacts L, R. The compact rates for the tunneling from reservoir D are defined as follows: $\gamma_D = \gamma_D(\varepsilon_d)$, $\gamma_D^{AA/BB} = \gamma_D(\varepsilon_{-+/+-})$, $\gamma_{A/B} = \sum_l \gamma_{lA/B}(E^0_{+/-})$ and $\gamma^U_{A/B} = \sum_l \gamma_{lA/B}(\Delta E^1_{-/+})$. Note that for the sake of clearness we do not note down the rates of the reverse processes, which of course go with $\overline{\gamma} = 1 - \gamma$. One can easily see, that the transport channels through dots A and B decouple.

5.4.1. Detection schemes

This considerations give rise to possible detection schemes, two of which we want to discuss and apply here. Let us start with scheme I, where the detector discriminates between $s \in \{0, A\}$ and $s = B$, which can be achieved if the chemical potential μ_D is chosen such that

$$\varepsilon_d < \varepsilon_{+-} = \varepsilon_d + U_0 - \Delta < \mu_D < \varepsilon_{-+} = \varepsilon_d + U_0 + \Delta\,. \tag{5.48}$$

We choose $\mu_D = \varepsilon_d + U_0$ which satisfies condition (5.48) as long as $\Delta > 0$. With the assumption that $\Gamma_D(\varepsilon_d) = \Gamma_D(\varepsilon_{+-}) = \Gamma_D(\varepsilon_{-+}) = \Gamma_D$, i.e. that the tunneling rates with respect to reservoir D

are energy independent. We divide eq. (5.47) by Γ_D and find for the conditional probabilities

$$\begin{aligned}
\overline{\mathbb{P}}_{1|0} &= f_D(\varepsilon_d) = \left(\exp\left[-\beta_D U_0\right] + 1\right)^{-1} , \\
\overline{\mathbb{P}}_{1|A} &= f_D(\varepsilon_d + U_0 + \Delta) = \left(\exp\left[-\beta_D \Delta\right] + 1\right)^{-1} , \\
\overline{\mathbb{P}}_{1|B} &= f_D(\varepsilon_d + U_0 - \Delta) = \left(\exp\left[\beta_D \Delta\right] + 1\right)^{-1} .
\end{aligned} \tag{5.49}$$

In the limit $\beta_D U_0, \beta_D \Delta \to \infty$, which was introduced as *precise demon limit* in [44], we finally obtain

$$\overline{\mathbb{P}}_{1|0} \to 1 , \quad \overline{\mathbb{P}}_{1|A} \to 1 , \quad \overline{\mathbb{P}}_{1|B} \to 0 . \tag{5.50}$$

In scheme II we want to discriminate between empty and occupied DQD states, i.e. between $s = 0$ and $s \in \{A, B\}$. In analogy to scheme I we formulate a condition for the chemical potential, μ_D

$$\varepsilon_d < \mu_D < \varepsilon_{+-} < \varepsilon_{-+} . \tag{5.51}$$

We fix the chemical potential at $\mu_D = \varepsilon_d + \frac{(U_0 - \Delta)}{2}$ and see immediately, that the conditional probabilities now reduce to (recall that we need $U_0 > \Delta$ and the precise demon limit)

$$\begin{aligned}
\overline{\mathbb{P}}_{1|0} &= \left(\exp[-\beta_D (U_0 - \Delta)/2] + 1\right)^{-1} \to 1 , \\
\overline{\mathbb{P}}_{1|A} &= \left(\exp[\beta_D (U_0 + 3\Delta)/2] + 1\right)^{-1} \to 0 , \\
\overline{\mathbb{P}}_{1|B} &= \left(\exp[\beta_D (U_0 - \Delta)/2] + 1\right)^{-1} \to 0 .
\end{aligned} \tag{5.52}$$

We can of course design additional detection schemes by detuning U_0, Δ and μ_D, but these two will suffice for the following elaborations.

5.4.2. Mesoscopic description

Now that we have shed some light onto the conditional probabilities in eq. (5.37), we can turn our focus on the dynamics of the mesoscopic probabilities P_s of finding the DQD in state $s \in \{0, A, B\}$.
Thus, we yield for the dynamics of the mesoscopic probabilities

$$\begin{aligned}
\dot{P}_0 = &- \left\{ \left[\gamma_A(\varepsilon + \Omega) + \gamma_B(\varepsilon)\right] \overline{\mathbb{P}}_{0|0} + \left[\gamma_A(\varepsilon + \Omega + U_0 - \Delta) + \gamma_B(\varepsilon + U_0 + \Delta)\right] \overline{\mathbb{P}}_{1|0} \right\} P_0 \\
&+ \left\{ \overline{\gamma}_A(\varepsilon + \Omega) \overline{\mathbb{P}}_{0|A} + \overline{\gamma}_A(\varepsilon + \Omega + U_0 - \Delta) \overline{\mathbb{P}}_{1|A} \right\} P_A \\
&+ \left\{ \overline{\gamma}_B(\varepsilon) \overline{\mathbb{P}}_{0|B} + \overline{\gamma}_B(\varepsilon + U_0 + \Delta) \overline{\mathbb{P}}_{1|B} \right\} P_B , \\
\dot{P}_B = &- \left\{ \overline{\gamma}_B(\varepsilon) \overline{\mathbb{P}}_{0|B} + \overline{\gamma}_B(\varepsilon + U_0 + \Delta) \overline{\mathbb{P}}_{1|B} \right\} P_B \\
&+ \left\{ \gamma_B(\varepsilon) \overline{\mathbb{P}}_{0|0} + \gamma_B(\varepsilon + U_0 + \Delta) \overline{\mathbb{P}}_{1|0} \right\} P_0 , \\
\dot{P}_A = &- \left\{ \overline{\gamma}_A(\varepsilon + \Omega) \overline{\mathbb{P}}_{0|A} + \overline{\gamma}_A(\varepsilon + \Omega + U_0 - \Delta) \overline{\mathbb{P}}_{1|A} \right\} P_A \\
&+ \left\{ \gamma_A(\varepsilon + \Omega) \overline{\mathbb{P}}_{0|0} + \gamma_A(\varepsilon + \Omega + U_0 - \Delta) \overline{\mathbb{P}}_{1|0} \right\} P_0 .
\end{aligned} \tag{5.53}$$

Consequently, we find the following effective rate matrices for the dynamics of the mesoscopic

states (P_0, P_B, P_A) in the limit of detection schemes I and II

$$\begin{aligned}\mathcal{V}^{\mathrm{I}} &= \begin{pmatrix} -\gamma_A(\varepsilon+\Omega+U_0-\Delta)-\gamma_B(\varepsilon+U_0+\Delta) & \overline{\gamma}_B(\varepsilon) & \overline{\gamma}_A(\varepsilon+\Omega+U_0-\Delta) \\ \gamma_B(\varepsilon+U_0+\Delta) & -\overline{\gamma}_B(\varepsilon) & 0 \\ \gamma_A(\varepsilon+\Omega+U_0-\Delta) & 0 & -\overline{\gamma}_A(\varepsilon+\Omega+U_0-\Delta) \end{pmatrix} \\ &= \begin{pmatrix} -(\cdots) & \overline{\gamma}_{LB}+\overline{\gamma}_{RB} & \overline{\gamma}^U_{LA}+\overline{\gamma}^U_{RA} \\ \gamma^U_{LB}+\gamma^U_{RB} & -(\cdots) & 0 \\ \gamma^U_{LA}+\gamma^U_{RA} & 0 & -(\cdots) \end{pmatrix}, \end{aligned} \tag{5.54}$$

$$\begin{aligned}\mathcal{V}^{\mathrm{II}} &= \begin{pmatrix} -\gamma_A(\varepsilon+\Omega+U_0-\Delta)-\gamma_B(\varepsilon+U_0+\Delta) & \overline{\gamma}_B(\varepsilon) & \overline{\gamma}_A(\varepsilon+\Omega) \\ \gamma_B(\varepsilon+U_0+\Delta) & -\overline{\gamma}_B(\varepsilon) & 0 \\ \gamma_A(\varepsilon+\Omega+U_0-\Delta) & 0 & -\overline{\gamma}_A(\varepsilon+\Omega) \end{pmatrix} \\ &= \begin{pmatrix} -(\cdots) & \overline{\gamma}_{LB}+\overline{\gamma}_{RB} & \overline{\gamma}_{LA}+\overline{\gamma}_{RA} \\ \gamma^U_{LB}+\gamma^U_{RB} & -(\cdots) & 0 \\ \gamma^U_{LA}+\gamma^U_{RA} & 0 & -(\cdots) \end{pmatrix}, \end{aligned} \tag{5.55}$$

where we introduced a more compact notation for the transition rates

$$\begin{aligned}\gamma_{lA} &= \Gamma_{lA} f_{lA} = \Gamma_{lA}(\varepsilon+\Omega) f_l(\varepsilon+\Omega)\,, \\ \gamma^U_{lA} &= \Gamma^U_{lA} f^U_{lA} = \Gamma_{lA}(\varepsilon+\Omega+U_0-\Delta) f_l(\varepsilon+\Omega+U_0-\Delta)\,, \\ \gamma_{lB} &= \Gamma_{lB} f_{lB} = \Gamma_{lB}(\varepsilon) f_l(\varepsilon)\,, \\ \gamma^U_{lB} &= \Gamma^U_{lB} f^U_{lB} = \Gamma_{lB}(\varepsilon+U_0+\Delta) f_l(\varepsilon+U_0+\Delta)\,. \end{aligned} \tag{5.56}$$

Thermodynamics for detection scheme I

Let us now take a closer look on the thermodynamics of the reduced dynamics with respect to the detection scheme I. First of all, we find the steady-state mesostate probabilities, which read

$$\begin{aligned}\bar{P}_0 &= \frac{\overline{\gamma}^U_A \overline{\gamma}_B}{\overline{\gamma}^U_A \overline{\gamma}_B + \overline{\gamma}^U_A \gamma^U_B + \gamma^U_A \overline{\gamma}_B}\,, \\ \bar{P}_B &= \frac{\overline{\gamma}^U_A \gamma^U_B}{\overline{\gamma}^U_A \overline{\gamma}_B + \overline{\gamma}^U_A \gamma^U_B + \gamma^U_A \overline{\gamma}_B}\,, \\ \bar{P}_A &= \frac{\gamma^U_A \overline{\gamma}_B}{\overline{\gamma}^U_A \overline{\gamma}_B + \overline{\gamma}^U_A \gamma^U_B + \gamma^U_A \overline{\gamma}_B}\,. \end{aligned} \tag{5.57}$$

The steady-state entropy production, corresponding to eq. (2.165), yields

$$\bar{\dot{S}}^{\star}_{\mathrm{i}} = \sum_{l,i,j} \mathcal{V}^{(l)}_{ij} \bar{P}_j \ln \frac{\mathcal{V}^{(l)}_{ij}}{\mathcal{V}^{(l)}_{ji}}\,. \tag{5.58}$$

With respect to the detection scheme I we obtain

$$\bar{\dot{S}}^{\star}_{\mathrm{i}} = \bar{I}^{\star(LA)}_{\mathrm{M}} \ln \frac{\gamma^U_{LA}}{\overline{\gamma}^U_{LA}} + \bar{I}^{\star(RA)}_{\mathrm{M}} \ln \frac{\gamma^U_{RA}}{\overline{\gamma}^U_{RA}} + \bar{I}^{\star(LB)}_{\mathrm{M}} \ln \frac{\gamma^U_{LB}}{\overline{\gamma}_{LB}} + \bar{I}^{\star(RB)}_{\mathrm{M}} \ln \frac{\gamma^U_{RB}}{\overline{\gamma}_{RB}}\,. \tag{5.59}$$

We verify analytically that in the stationary state the particle number is conserved, $\bar{I}^{\star(L)}_{\mathrm{M}} + \bar{I}^{\star(R)}_{\mathrm{M}} = 0$, compare eq. (5.32). Moreover, due to the decoupling of the transport channels through QDs A and B particle number conservation holds channel-wise

$$\bar{I}^{\star(x)}_{\mathrm{M}} = \bar{I}^{\star(Lx)}_{\mathrm{M}} = -\bar{I}^{\star(Rx)}_{\mathrm{M}}\,, \quad x \in \{A, B\}\,, \tag{5.60}$$

and we can identify the two contributions to the entropy production. We rearrange eq. (5.59) in terms of affinities $\mathcal{F}$, i.e. generalized forces that drive the irreversible transport processes [171], and obtain

$$\bar{\dot{S}}_{\mathrm{i}}^{*} = \mathcal{F}_A^{*}\bar{I}_{\mathrm{M}}^{*(A)} + \mathcal{F}_B^{*}\bar{I}_{\mathrm{M}}^{*(B)}\,. \tag{5.61}$$

Let us start by analyzing the affinity with respect to the transport through A

$$\mathcal{F}_A^{*} = \ln\left[\frac{\gamma_{LA}^{U}}{\overline{\gamma}_{LA}^{U}}\frac{\overline{\gamma}_{RA}^{U}}{\gamma_{RA}^{U}}\right] = \ln\left[\frac{\Gamma_{LA}^{U}}{\Gamma_{LA}^{U}}\frac{\Gamma_{RA}^{U}}{\Gamma_{RA}^{U}}\right] + \ln\left[\frac{f_{LA}^{U}(1-f_{RA}^{U})}{(1-f_{LA}^{U})f_{RA}^{U}}\right]. \tag{5.62}$$

which evaluates to

$$\mathcal{F}_A^{*} = \left(\varepsilon + \Omega + U_0 - \Delta\right)\left[\beta_R - \beta_L\right] + \beta_L\mu_L - \beta_R\mu_R\,. \tag{5.63}$$

We assume, again, that the reservoirs L and R have the same temperature and therefore we find that the transport through channel A contributes to the entropy production

$$\bar{\dot{S}}_{\mathrm{i}}^{*(A)} = \mathcal{F}_A^{*}\bar{I}_{\mathrm{M}}^{*(A)} = \beta(\mu_L - \mu_R)\bar{I}_{\mathrm{M}}^{*(A)}\,. \tag{5.64}$$

Here, one can immediately notice that the energy currents at the left and right contact with respect to A are balanced,

$$\bar{I}_{\mathrm{E}}^{*(LA)} = -\bar{I}_{\mathrm{E}}^{*(RA)} = \left(\varepsilon + \Omega + U_0 - \Delta\right)\bar{I}_{\mathrm{M}}^{*(A)}\,, \tag{5.65}$$

and proportional to the matter current

$$\bar{I}_{\mathrm{M}}^{*(A)} = \gamma_{LA}^{U}\bar{P}_0 - \overline{\gamma}_{LA}^{U}\bar{P}_A\,. \tag{5.66}$$

This means that the detector does not extract energy from transport through A. As a consequence we ascertain that pumping against a chemical bias $V = \mu_L - \mu_R$ is not possible in this detection scheme, as the condition (5.35) cannot be met.

Let's inspect what happens with respect to the transfer of electrons via B. The affinity yields

$$\begin{aligned}\mathcal{F}_B^{*} &= \ln\left[\frac{\gamma_{LB}^{U}}{\overline{\gamma}_{LB}}\frac{\overline{\gamma}_{RB}}{\gamma_{RB}^{U}}\right] = \ln\left[\frac{\Gamma_{LB}^{U}\Gamma_{RB}}{\Gamma_{LB}\Gamma_{RB}^{U}}\frac{f_{LB}^{U}(1-f_{RB})}{(1-f_{LB})f_{RB}^{U}}\right] \\ &= \ln\left[\frac{f_{LB}(1-f_{RB})}{(1-f_{LB})f_{RB}}\right] + \ln\left[\frac{\Gamma_{LB}^{U}\Gamma_{RB}}{\Gamma_{LB}\Gamma_{RB}^{U}}\frac{f_{LB}^{U}f_{RB}}{f_{LB}f_{RB}^{U}}\right].\end{aligned} \tag{5.67}$$

In the last step we included a "1" and, thus, we can now identify two contributions to the entropy production that are induced by tunneling onto/from B. Thus, we find

$$\begin{aligned}\bar{\dot{S}}_{\mathrm{i}}^{*(B)} &= \mathcal{F}_B^{*}\bar{I}_{\mathrm{M}}^{*(B)} \\ &= \left(\varepsilon\left[\beta_R - \beta_L\right] + \beta_L\mu_L - \beta_R\mu_R\right)\bar{I}_{\mathrm{M}}^{*(B)} + \ln\left[\frac{\Gamma_{LB}^{U}\Gamma_{RB}}{\Gamma_{LB}\Gamma_{RB}^{U}}\frac{f_{LB}^{U}f_{RB}}{f_{LB}f_{RB}^{U}}\right]\bar{I}_{\mathrm{M}}^{*(B)} \\ &= \beta(\mu_L - \mu_R)\bar{I}_{\mathrm{M}}^{*(B)} + \bar{I}_{\mathrm{F}}^{*(B)}\,,\end{aligned} \tag{5.68}$$

with the particle current

$$\bar{I}_{\mathrm{M}}^{*(B)} = \gamma_{LB}^{U}\bar{P}_0 - \overline{\gamma}_{LB}\bar{P}_B\,. \tag{5.69}$$

In the last step we set $\beta_L = \beta_R = \beta$ and introduced the so called information current $\bar{I}_{\mathrm{F}}^{*(B)}$. These results are very similar to those found by Strasberg *et al.* in [44], who only considered one transport channel. The first contribution is just the entropy production of the isolated transport through B while the contribution is to be interpreted as information transferred between the system and the demon, that modifies the entropy balance of the system (i.e. its second law). Although we eliminated the very fast dynamics of the detector dot, the demon effectively extracts energy from channel B. That can be quantified as follows

$$\begin{aligned}
\bar{I}_{\mathrm{E}}^{*(LB)} &= \varepsilon \bar{I}_{\mathrm{M}}^{*(LB)} + (U_0 + \Delta)\gamma_{LB}^{U} \bar{P}_0 \,, \\
\bar{I}_{\mathrm{E}}^{*(RB)} &= \varepsilon \bar{I}_{\mathrm{M}}^{*(RB)} + (U_0 + \Delta)\gamma_{RB}^{U} \bar{P}_0 \,, \\
\bar{I}_{\mathrm{E}}^{*(B)} &= -\bar{I}_{\mathrm{E}}^{*(LB)} - \bar{I}_{\mathrm{E}}^{*(RB)} = -(U_0 + \Delta)\gamma_{B}^{U} \bar{P}_0 \,.
\end{aligned} \tag{5.70}$$

A proper Maxwell demon, however, does not alter the energy balance of the system. Therefore, we employ another limit, the *true Maxwell demon limit*, according to Ref. [44]. In this limit we assume that the temperatures of the reservoirs coupling to the DQD are sufficiently low compared to the energy scale set by the capacitive couplings U_0, Δ, i.e. that we can set $\beta U_0, \beta\Delta \to 0$. As a consequence we find that the Fermi functions evaluated at different transition energies yield the same values

$$\lim_{\beta U_0, \beta\Delta \to 0} f_{lx}^{U} = f_{lx} \,. \tag{5.71}$$

As a consequence the above energy imbalance for the transport through B vanishes.
In this limit the information current $\bar{I}_{\mathrm{F}}^{*(B)} \to \bar{I}_{\mathrm{F}}^{\mathrm{eff}(B)}$ becomes

$$\bar{I}_{\mathrm{F}}^{\mathrm{eff}(B)} = \ln\left[\frac{\Gamma_{LB}^{U}\Gamma_{RB}}{\Gamma_{LB}\Gamma_{RB}^{U}}\right] \bar{I}_{\mathrm{M}}^{\mathrm{eff}(B)} \,, \tag{5.72}$$

which vanishes if the tunneling rates are chosen symmetrically. In other words our setup does not change the energetics of the system, on the one hand, but at the same time has to change the energy barriers between the system states in order to modify the entropy production and generate currents against a chemical bias.

Note that the effective matter currents read

$$\begin{aligned}
\bar{I}_{\mathrm{M}}^{\mathrm{eff}(A)} &= \Gamma_{LA}^{U} f_{LA} \bar{P}_0^{\mathrm{eff}} - \Gamma_{LA}^{U} \overline{f}_{LA} \bar{P}_A^{\mathrm{eff}} \,, \\
\bar{I}_{\mathrm{M}}^{\mathrm{eff}(B)} &= \Gamma_{LB}^{U} f_{LB} \bar{P}_0^{\mathrm{eff}} - \Gamma_{LB} \overline{f}_{LB} \bar{P}_B^{\mathrm{eff}} \,,
\end{aligned} \tag{5.73}$$

where the stationary probabilities to find the DQD in states $0, A, B$ in the ideal Maxwell demon limit are

$$\begin{aligned}
\bar{P}_0^{\mathrm{eff}} &= \frac{1}{N}\Big(\sum_l \Gamma_{lA}^{U} \overline{f}_{lA}\Big)\Big(\sum_l \Gamma_{lB} \overline{f}_{lB}\Big) \,, \\
\bar{P}_B^{\mathrm{eff}} &= \frac{1}{N}\Big(\sum_l \Gamma_{lA}^{U} \overline{f}_{lA}\Big)\Big(\sum_l \Gamma_{lB}^{U} f_{lB}\Big) \,, \\
\bar{P}_A^{\mathrm{eff}} &= \frac{1}{N}\Big(\sum_l \Gamma_{lA}^{U} f_{lA}\Big)\Big(\sum_l \Gamma_{lB} \overline{f}_{lB}\Big) \,, \\
N &= \Big(\sum_l \Gamma_{lA}^{U} \overline{f}_{lA}\Big)\Big(\sum_l \Gamma_{lB} \overline{f}_{lB}\Big) + \Big(\sum_l \Gamma_{lA}^{U} \overline{f}_{lA}\Big)\Big(\sum_l \Gamma_{lB}^{U} f_{lB}\Big) + \Big(\sum_l \Gamma_{lA}^{U} f_{lA}\Big)\Big(\sum_l \Gamma_{lB} \overline{f}_{lB}\Big) \,.
\end{aligned} \tag{5.74}$$

Remarks on the Maxwell demon limit

Let us consider, again, the Maxwell demon limit introduced in eq. (5.71); in this limit we distinguish between the two transport channels, i.e. f_{lA} evaluates differently than f_{lB}. This, however, is particularly useful in setups, where $\Omega \gg U_0, \Delta$. If this is not the case, one can evaluate all Fermi functions at the same energy E, that might be chosen somewhere between $E^0_-, E^0_+, \Delta E^1_-$ and ΔE^1_+. Then we obtain $f_{lA} = f_{lB} = f_l(E)$. Numerically, we get slightly differing values for the currents. The scaling of the information current in (5.72), however, is not affected, as one can easily verify, and thus, the resulting entropy is very close to that one obtained when applying the limit (5.71). In the course of this section we stick to the distinction of the Fermi energies f_{lA} and f_{lB}.

We now want to summarize briefly how the entropy production is written with respect to different levels of description. Recall, that we demand the lead temperatures for the left and the right lead to be equal ($\beta_L = \beta_R = \beta$). We have found for the entropy productions

$$\bar{\dot{S}}_{\mathrm{i}} = \beta V \bar{I}_{\mathrm{M}} + (\beta - \beta_D)\bar{I}^{(D)}_E = -\beta \mathcal{P} + (\beta - \beta_D)\bar{I}^{(D)}_E \quad \text{(microscopic)}\,, \tag{5.75}$$

$$\bar{\dot{S}}^{*}_{\mathrm{i}} = \beta V \bar{I}^{*}_{\mathrm{M}} + \bar{I}^{*}_{\mathrm{F}} = -\beta \mathcal{P}^{*} + \bar{I}^{*}_{\mathrm{F}} \quad \text{(mesoscopic)}\,, \tag{5.76}$$

$$\bar{\dot{S}}^{\mathrm{eff}}_{\mathrm{i}} = \beta V \bar{I}^{\mathrm{eff}}_{\mathrm{M}} + \bar{I}^{\mathrm{eff}}_{\mathrm{F}} = -\beta \mathcal{P}^{\mathrm{eff}} + \bar{I}^{\mathrm{eff}}_{\mathrm{F}} \quad \text{(ideal Maxwell demon)}\,. \tag{5.77}$$

In the microscopic description we have to explicitly take into account the energy currents, while for the mesoscopic description the information current enters. The numerical investigation shows that, the currents extracted from the solution to the six microscopic rate equations is converging to the mesoscopic solutions even if Γ_D, β_D are finite as long as $\Gamma_D \gg \max\{\Gamma^U_{lx}, \Gamma_{lx}\}$ and $\beta_D U_0, \beta_D \Delta \gg 1$. Note also that, in the error free limit ($\beta_D \to \infty$) the microscopic entropy production diverges.
For the ideal Maxwell demon the reformulated condition for pumping against bias, eq. (5.35), reads in terms of the information current

$$\bar{I}^{\mathrm{eff}}_{\mathrm{F}} \geq -\beta V \bar{I}^{\mathrm{eff}}_{\mathrm{M}} = \beta \mathcal{P}^{\mathrm{eff}} \geq 0\,. \tag{5.78}$$

Thus, pumping against the chemical bias V is only possible if the information current is sufficiently positive. This, once again, confirmes that the extracted power of the device remains nonpositive as long as the information current is not sufficiently positive.

One last remark should be made concerning the energy currents in the Maxwell demon limit. In this limit we assume that the dominating contribution to the energy that is exchanged between the electronic leads l and the DQD is set by ε_x. This is reflected in the so called *tight coupling* property; i.e. the energy and matter currents are proportional [cf. [41]]

$$\bar{I}^{\mathrm{eff}(x)}_{\mathrm{E}} = \varepsilon_x \bar{I}^{\mathrm{eff}(x)}_{\mathrm{M}}\,. \tag{5.79}$$

The same holds for the information current, as we can read off from eq. (5.72).

5.4.3. Nontrivial effects, pumping against a chemical bias

With the results we found up to now, we can make sure that the detector QD in the proposed setup can in fact distinguish between different states in the transport DQD. However, in order to achieve any nontrivial effect such as pumping electrons against a chemical bias we need to

have energy-dependent tunneling rates $\Gamma_{\nu x}(\omega)$. Thus, the wide-band limit that is often assumed cannot be adopted here.
Instead, let us assume tunneling rates of Lorentzian shape, as done for single electron transistor models in [172], i.e.

$$\Gamma(\omega) = \frac{a}{b^2 + (\omega - \omega_0)^2}\Gamma\,, \quad (a > 0)\,. \tag{5.80}$$

This enables us to model the energy-dependence of the tunneling according to our needs. Let us choose, for example, the energy $\omega_0 = E_A^0$, where the bare tunneling rate Γ_{RA} reaches its maximum and the tunneling rate at the transition energy ΔE_A^1 as

$$\begin{aligned}\Gamma_{RA} &= \Gamma_{RA}(E_A^0) = \frac{a}{b^2} = \mathrm{e}^{+\delta}\,\Gamma\,,\\ \Gamma_{RA}^U &= \Gamma_{RA}(\Delta E_A^1) = \frac{a}{b^2 + (\Delta E_A^1 - E_A^0)^2} = \mathrm{e}^{-\delta}\,\Gamma\,,\end{aligned} \tag{5.81}$$

we can determine the parameters as $a = \Gamma(U_0 - \Delta)^2/2\,\mathrm{csch}(\delta)$ and $b = (U_0 - \Delta)^2/2[\coth(\delta) - 1]$. Provided, that we have specific tunneling coefficients $t_{k\nu x}$ we assume that we can define the remaining tunneling rates analogously, i.e.

$$\begin{aligned}\Gamma_{RB} &= \mathrm{e}^{+\delta}\,\Gamma\,, \qquad \Gamma_{RB}^U = \mathrm{e}^{-\delta}\,\Gamma\,,\\ \Gamma_{LA} &= \mathrm{e}^{-\delta}\,\Gamma\,, \qquad \Gamma_{LA}^U = \mathrm{e}^{+\delta}\,\Gamma\,,\\ \Gamma_{LB} &= \mathrm{e}^{-\delta}\,\Gamma\,, \qquad \Gamma_{LB}^U = \mathrm{e}^{+\delta}\,\Gamma\,.\end{aligned} \tag{5.82}$$

Throughout, we choose the parameter δ to be nonnegative.

Likely trajectories

Which trajectories become likely with this choice of tunneling rates for the two detection schemes we probe above?
Recall, that our detection scheme I implies that if QD A is populated the demon dot remains occupied; i.e. the relevant rates with respect to transport through A are Γ_{lA}^U. For transport through QD A we thus find that a trajectory $|1,0\rangle \longrightarrow |1,A\rangle \longrightarrow |1,0\rangle$ is most likely, where the effective transport direction is determined by the sign of the chemical bias with $V > 0$ inducing transport from the left to the right lead. However, invoking transport against the bias is not possible, although the above choice of the tunneling rates leads to higher net currents for positive V:

$$|\bar{I}_{\mathrm{M}}^{(A)}(V)| > |\bar{I}_{\mathrm{M}}^{(A)}(-V)|\,, \quad \delta, V > 0\,. \tag{5.83}$$

Contrarily, for the transport via B we have the following trajectory $|1,0\rangle \longrightarrow |1,B\rangle \Rightarrow |0,B\rangle \longrightarrow |0,0\rangle \Rightarrow |1,0\rangle$, where the double arrows depict the transitions that happen very fast and in the error-free instantaneous limit, immediately. Assuming rates according to eqs. (5.81) and (5.82) with $\delta > 0$ we obtain steady-state currents that are pumping electrons through B against the chemical bias.
Figure 5.4 show the steady-state currents with respect to the distinct transport channels and the corresponding coarse-grained entropy productions $\dot{S}_{\mathrm{i}}^*$. One can clearly see that even if the strict Maxwell demon limit is not met the mesostate entropy production is approaching that of the ideal demon as the ratio U_0/Ω decreases. For $\varepsilon \gg U_0$ the energy imbalance $\bar{I}_{\mathrm{E}}^*$, i.e. the modification of the first law (5.70), becomes negligible, cf. [44].

The entropy production with respect to the two transport channels becomes minimal, for bias voltages V where the net steady-state current through the respective channel vanishes, as can be seen in the inset of fig. 5.4b. Accordingly, the overall entropy production becomes minimal where the sum of the currents vanishes.

Moreover, the numerics show that the solution to the full microscopic model coincide with the mesoscopic solutions even for finite temperatures $\beta_D U_0 \approx 20$. To obtain reasonable results for the microscopic solutions it is of course necessary to increase β_D when lowering the capacitive coupling between DQD and detector.

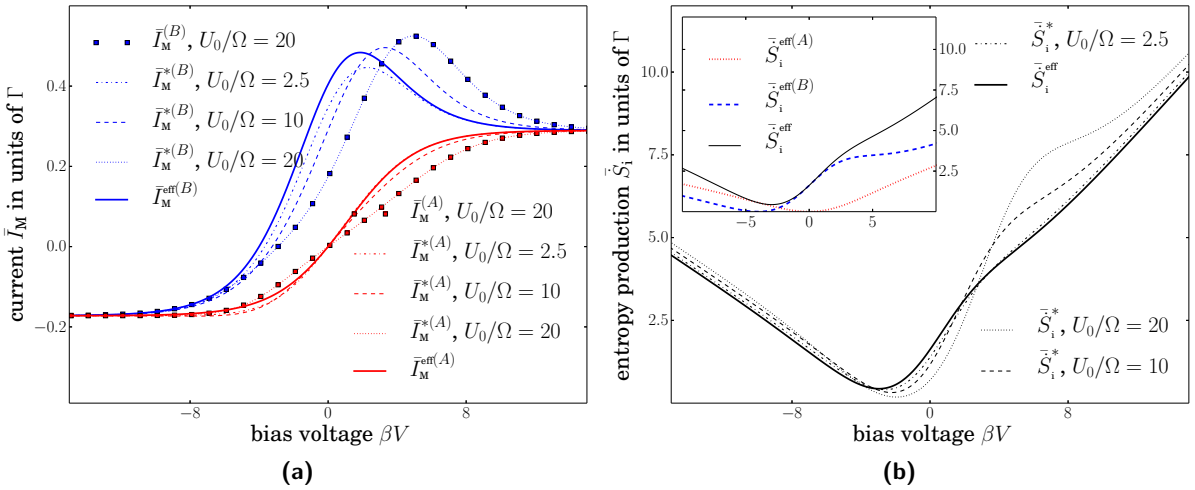

Figure 5.4.: Steady state currents (a) and entropy production (b) of the system for detection scheme I and rates chosen according to eqs. (5.81) and (5.82); Parameters: $\Delta/\Omega = 2$, $\delta/\Omega = 10$. In subplot (a) also the microscopic currents for one set of parameters are depicted (red and blue squares, respectively), where the temperature is $\beta_D = 10\beta$.

When applying the second detection scheme the trajectories taken are the same for both transport channels: $|1,0\rangle \longrightarrow |1,x\rangle \Rightarrow |0,x\rangle \longrightarrow |0,0\rangle \Rightarrow |1,0\rangle$ with $x \in \{A,B\}$. Thus, with the above nontrivial choice of the tunneling rates, (5.81) and (5.82), we obtain the stationary currents and entropy productions plotted in fig. 5.5. In the limit of an ideal Maxwell demon currents are only differing due to the small level splitting Ω. Therefore, the channel-wise entropy productions become minimal for nearly the same bias voltages.

Let us, briefly, consider the power extraction of the device when operated in either of the detection schemes. To bound the Liouvillian we assume the feedback parameter δ in eqs. (5.81) and (5.82) to be finite. Then for a fixed δ and equal lead temperatures $\beta_L = \beta_R = \beta$ the extracted power $\mathcal{P} = -V\bar{I}_M$ can be evaluated (channel-wise) as $\beta\mathcal{P}^{\mathrm{eff}(x)} = -\beta V \bar{I}_M^{\mathrm{eff}(x)}$, where the parameter $\beta V = \ln\left[\frac{f_{Lx}\bar{f}_{Rx}}{\bar{f}_{Lx}f_{Rx}}\right]$ parametrizes the expression for the current, which can be used to find the bias voltage where $\mathcal{P}$ becomes maximal, cf. [43]. In fig. 5.6 we show contour plots of the power for fixed parameters U_0, Δ and varying bias voltage V and feedback parameters δ, where black solid lines shows the border between positive and negative power extraction. We also depict the voltages for maximum power for varying δ (black dotted lines).

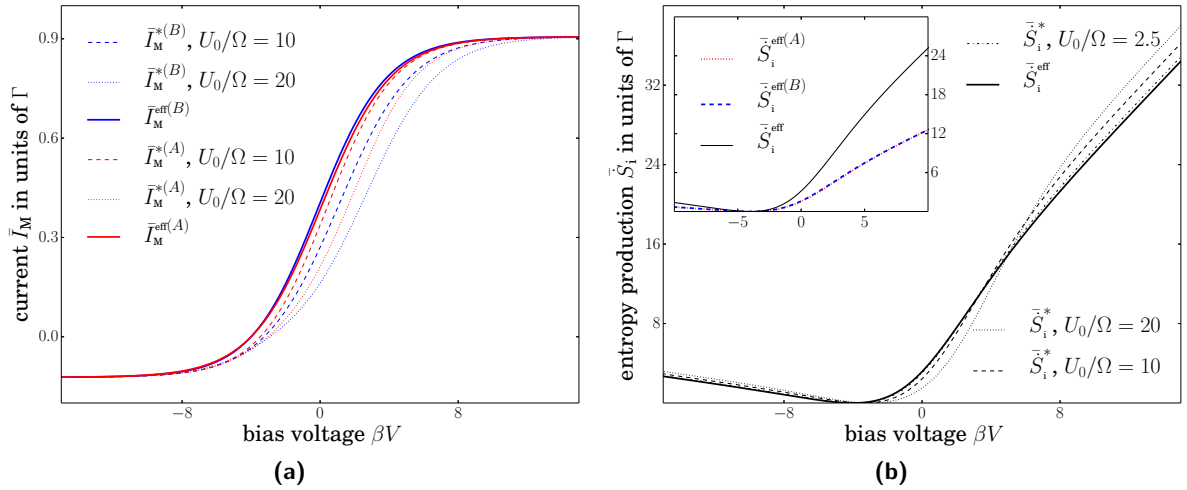

Figure 5.5.: Steady state currents (a) and entropy production (b) of the system for detection scheme II and rates chosen according to eqs. (5.81) and (5.82); Parameters: $\Delta/\Omega = 2$, $\delta/\Omega = 10$.

5.4.4. Spin-filter reloaded

We now want to take a look at the explicit expressions for the effective steady-state currents we obtained in the previous section. Recall, exemplarily, the mesoscopic version of the steady-state currents for detection scheme I, eqs. (5.66) and (5.69) and the respective steady states eq. (5.57). In the strict Maxwell demon limit, the rates $\gamma_{lx}^{(U)}$ and $\overline{\gamma}_{lx}^{(U)}$ become

$$\begin{aligned}\gamma_{lx}^{(U)} &= \Gamma_{lx}^{(U)} f_{lx}\,,\\ \overline{\gamma}_{lx}^{(U)} &= \Gamma_{lx}^{(U)} \overline{f}_{lx}\,.\end{aligned} \tag{5.84}$$

In section 4.5 we have implemented the feedback in terms of a state-dependent modification of the tunneling rates, i.e. without a microscopic mechanism. The system of two parallel QDs is equivalent to the spin-qubit Hamiltonian in chapter 4. In the noninteracting case, with $T_c \to 0$, we can identify the states $|\uparrow\rangle \leftrightarrow |B\rangle$, $|\downarrow\rangle \leftrightarrow |A\rangle$ and the magnetic field $B \leftrightarrow \Omega$. Thus, we can rewrite the rates for transitions from an unoccupied DQD ("E") to state $|x\rangle$ as $\mathrm{e}^{\delta_{lE}}\,\Gamma f_{lx}$ and the reverse rates as $\mathrm{e}^{\delta_{lx}}\,\Gamma \overline{f}_{lx}$. The effective currents eq. (5.73), therefore, become

$$\begin{aligned}\bar{I}_{\mathrm{M}}^{\mathrm{eff}(A)} &= \mathrm{e}^{\delta_{LE}}\,\Gamma f_{LA} \bar{P}_0^{\mathrm{eff}} - \mathrm{e}^{\delta_{LA}}\,\Gamma \overline{f}_{LA} \bar{P}_A^{\mathrm{eff}}\,,\\ \bar{I}_{\mathrm{M}}^{\mathrm{eff}(B)} &= \mathrm{e}^{\delta_{LE}}\,\Gamma f_{LB} \bar{P}_0^{\mathrm{eff}} - \mathrm{e}^{\delta_{LB}}\,\Gamma \overline{f}_{LB} \bar{P}_B^{\mathrm{eff}}\,.\end{aligned} \tag{5.85}$$

When replacing the rates in the expression for the steady-state probabilities, (5.74), the resulting current confirms the results from eq. (4.68) (where we set $\Gamma_{l\sigma} = \Gamma$).
Finally, comparing the current expressions (5.73) and (5.85) and taking into account the specific parametrization of the tunneling amplitudes (5.81) and (5.82), we find the following mapping

$$\delta \leftrightarrow \delta_{LE}\,,\quad -\delta \leftrightarrow \delta_{RE}\,,\quad \delta \leftrightarrow \delta_{LA}\,,\quad -\delta \leftrightarrow \delta_{LB}\,,\quad -\delta \leftrightarrow \delta_{RA}\,,\quad \delta \leftrightarrow \delta_{RB}\,, \tag{5.86}$$

which corresponds to the feedback scheme B, (4.74), from section 4.8.1. Hence, in the special case of noninteracting transport channels ($T_c \to 0$) the ideal Maxwell-demon dynamics of our

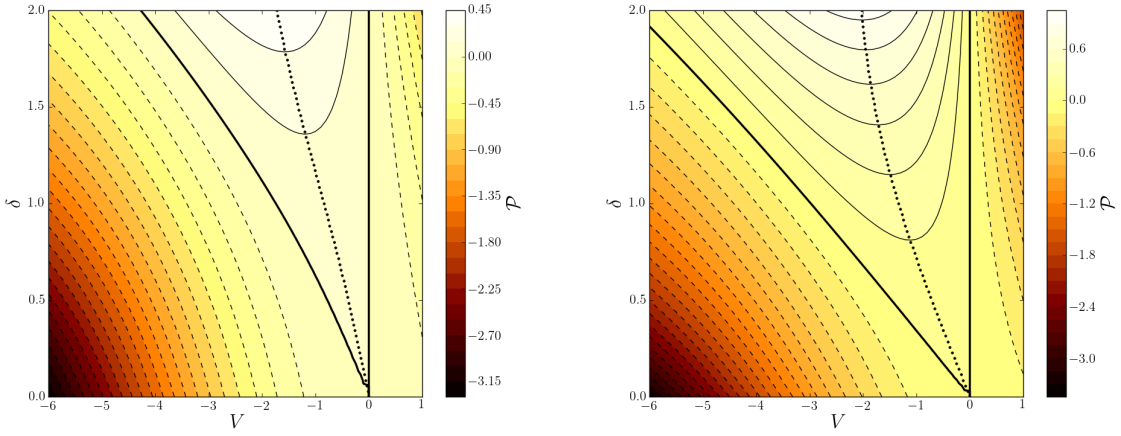

Figure 5.6.: Contour plots of the power extraction $\mathcal{P}$ for varying bias voltages V and feedback parameters δ. Panel (a) shows the contour for detection scheme I, eq. (5.48), and (b) the contour for detection scheme II, eq. (5.51). For both panels the parameters are $U_0/\Omega = 20, \Delta/\Omega = 2$ and the tunneling rates chosen according to eqs. (5.81) and (5.82). The black dotted lines show the numerically obtained voltages where the power is maximal.

generic model reproduces the dynamics for the closed-loop feedback operations we applied to the exchange-free transport model in chapter 4.
This can be also be seen when comparing the currents in Figures 4.2(c) and 5.4. The filtering effect can be even more pronounced when tuning the tunneling amplitudes differently, as shown in fig. 5.7.

5.5. Coarse grained dynamics for arbitrary T_c

Once we allow for interacting transport channels the coarse graining will in general fail, because the separation of the microstate probabilities into conditional probabilities and mesoscopic probabilities is not possible anymore. Naively, one could assign indices $d \in \{0, 1\}$ to microstates and indices $s \in \{0, +, -\}$ to mesostates. In fact, each of the 4 microstates $|0, -_0\rangle, |0, +_0\rangle, |1, -_1\rangle$ and $|1, +_1\rangle$ belong to different mesostates. This can be understood as there are transitions with rates $\mathcal{W}_{ds,d's'}, (s \neq s')$ that are proportional to Γ_D and, therefore, determined by a much faster time scale than the population of the DQD. Contrarily, in the limit $T_c \to 0$ these transitions vanish.
Thus, the condition eq. (2.152) is not fullfilled and an important requirement for the adiabatic elimination is not met. However, we still can separate the probabilities for states $|0, 0\rangle$ and $|1, 0\rangle$, which read $p_{00} = \mathbb{P}_{0|0} P_0$ and $p_{10} = \mathbb{P}_{1|0} P_0$, without any ambiguity. It follows directly that we can identify the mesostate 0. In the steady-state we get

$$\bar{\mathbb{P}}_{0|0} = 1 - f_D(\varepsilon_d), \bar{\mathbb{P}}_{1|0} = f_D(\varepsilon_d)\,, \tag{5.87}$$

where we already divided the expression by Γ_D.

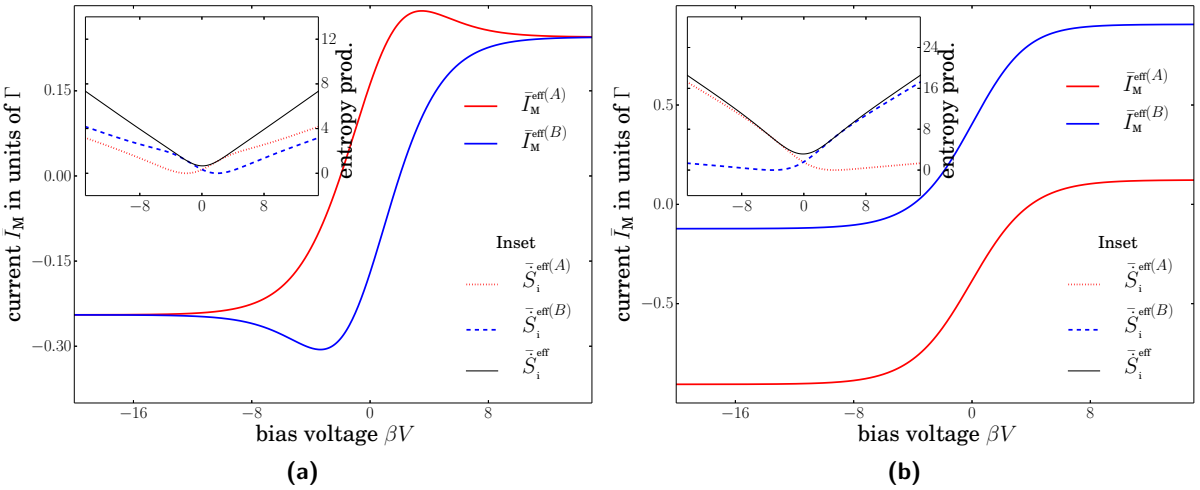

Figure 5.7.: Steady state currents and entropy production (insets) of the system. (a) Detection scheme II, the rates are $\Gamma_{RA} = \mathrm{e}^{+\delta}\Gamma, \Gamma^U_{RA} = \Gamma, \Gamma_{RB} = \mathrm{e}^{-\delta}\Gamma, \Gamma^U_{RB} = \Gamma, \Gamma_{LA} = \mathrm{e}^{-\delta}\Gamma, \Gamma^U_{LA} = \Gamma, \Gamma_{LB} = \mathrm{e}^{+\delta}\Gamma, \Gamma^U_{LB} = \Gamma$. (b) Detection scheme II, the rates are $\Gamma_{RA} = \mathrm{e}^{-\delta}\Gamma, \Gamma^U_{RA} = \mathrm{e}^{+\delta}\Gamma, \Gamma_{RB} = \mathrm{e}^{+\delta}\Gamma, \Gamma^U_{RB} = \mathrm{e}^{-\delta}\Gamma, \Gamma_{LA} = \mathrm{e}^{+\delta}\Gamma, \Gamma^U_{LA} = \mathrm{e}^{-\delta}\Gamma, \Gamma_{LB} = \mathrm{e}^{-\delta}\Gamma, \Gamma^U_{LB} = \mathrm{e}^{+\delta}\Gamma$. System parameters: $\Delta/\Omega = 2$, $\delta/\Omega = 10$.

The remaining equations of $\mathcal{L}^{(D)}\bar{\rho} = 0$ read

$$
\begin{aligned}
0 &= -\left[\kappa_{--}\gamma_D(\varepsilon_{--}) + \kappa_{-+}\gamma_D(\varepsilon_{-+})\right]\bar{p}_{0-} + \kappa_{--}\overline{\gamma}_D(\varepsilon_{--})\bar{p}_{1-} + \kappa_{-+}\overline{\gamma}_D(\varepsilon_{-+})\bar{p}_{1+}\,,\\
0 &= -\left[\kappa_{+-}\gamma_D(\varepsilon_{+-}) + \kappa_{++}\gamma_D(\varepsilon_{++})\right]\bar{p}_{0+} + \kappa_{+-}\overline{\gamma}_D(\varepsilon_{+-})\bar{p}_{1-} + \kappa_{++}\overline{\gamma}_D(\varepsilon_{++})\bar{p}_{1+}\,,\\
0 &= \kappa_{--}\gamma_D(\varepsilon_{--})\bar{p}_{0-} + \kappa_{+-}\gamma_D(\varepsilon_{+-})\bar{p}_{0+} - \left[\kappa_{--}\overline{\gamma}_D(\varepsilon_{--}) + \kappa_{+-}\overline{\gamma}_D(\varepsilon_{+-})\right]\bar{p}_{1-}\,,\\
0 &= \kappa_{-+}\gamma_D(\varepsilon_{-+})\bar{p}_{0-} + \kappa_{++}\gamma_D(\varepsilon_{++})\bar{p}_{0+} - \left[\kappa_{-+}\overline{\gamma}_D(\varepsilon_{-+}) + \kappa_{++}\overline{\gamma}_D(\varepsilon_{++})\right]\bar{p}_{1+}\,.
\end{aligned}
\tag{5.88}
$$

P. Strasberg [170] points out that in order achieve a unique decomposition of the microstate probabilities according to eq. (5.37) and to reduce the amount of equations, i.e. to adiabatically eliminate the demon dot degrees of freedom we need further considerations. The decomposition is only possible in the extreme case of the fast and precise demon limits; i.e. when we have a) infinitely fast tunneling to the demon dot $\Gamma_D \to \infty$ and b) zero temperature for the demon dot reservoir $\beta_D \to \infty$.

It is important to assume that when taking the limit $\beta_D, \Gamma_D \to \infty$ the scaling of Γ_D is only polynomially and not exponentially. Otherwise all rates $\gamma_D(\omega)$ and $\overline{\gamma_D}(\omega)$ for any energy ω would diverge. When Γ_D scales polynomially we find without any ambiguity [170]

$$
\lim_{\beta_D,\Gamma_D\to\infty} \gamma_D(\omega) = \lim_{\beta_D,\Gamma_D\to\infty} \Gamma_D f_D(\omega) = \begin{cases} 0\,, & \omega > 0 \\ \infty\,, & \omega < 0 \end{cases}, \quad \text{where}\, \Gamma_D = a\beta_D^b\,, \quad (a, b > 0)\,.
\tag{5.89}
$$

The numerical solutions to the microscopic rate equations suggests that the transition from finite tunneling rates and temperatures to infinitely fast tunneling and zero temperature is smooth. With the above considerations we can divide eq. (5.88) by Γ_D, solve them for the probabilities and proceed with calculating reduced dynamics.

5.5.1. Tuning the detector

Before defining a detection scheme we need to impose some restrictions on the choice of parameters. Let us assume that $U_0, \Omega, \Delta > 0$, and

$$U_0 > \frac{1}{2}\sqrt{4T_c^2 + \Omega^2} + \frac{1}{2}\sqrt{4T_c^2 + (\Omega - 2\Delta)^2}\,,$$
$$\frac{1}{2}\sqrt{4T_c^2 + (\Omega - 2\Delta)^2} \geq \frac{1}{2}\sqrt{4T_c^2 + \Omega^2} \Leftrightarrow \Omega \leq \Delta\,. \tag{5.90}$$

These conditions imply a ordering of transition energies $\varepsilon_d < \varepsilon_{+-} < \varepsilon_{--} \leq \varepsilon_{++} < \varepsilon_{-+}$.
The only adjustment of the chemical potential of the detector junction that leads to a proper state reduction in the extreme limit ($\beta_D, \Gamma_D \to 0$) is [170]

$$\varepsilon_d < \mu_D < \varepsilon_{+-} < \varepsilon_{--} \leq \varepsilon_{++} < \varepsilon_{-+}\,, \tag{5.91}$$

which corresponds to the detector tuning, eq. (5.51), we used before.
The condition eq. (5.90) is, of course, arbitrary. We also could adjust the parameters to meet, e.g., (with $\Omega < \Delta$)

$$-\frac{1}{2}\sqrt{4T_c^2 + \Omega^2} + \frac{1}{2}\sqrt{4T_c^2 + (\Omega - 2\Delta)^2} > U_0 > \frac{1}{2}\sqrt{4T_c^2 + \Omega^2} - \frac{1}{2}\sqrt{4T_c^2 + (\Omega - 2\Delta)^2}\,, \tag{5.92}$$

which leads to a different ordering of the transition energies, namely $\varepsilon_{+-} < \varepsilon_{--} < \varepsilon_d < \varepsilon_{++} < \varepsilon_{-+}$.
Figure 5.8 shows that – when tuning the detector differently than according to (5.91) – the system reduces such that only two states "survive", i.e. have nonvanishing lifetime and population probability. In fact the states $|d, +\rangle$ are no longer reached in the long term. This restriction can also be seen when numerically solving the microscopic equations. As a consequence, with (5.91), the setup in the extreme limit of the fast demon along with error-free detection is restricted to the detection whether the DQD is populated or not.

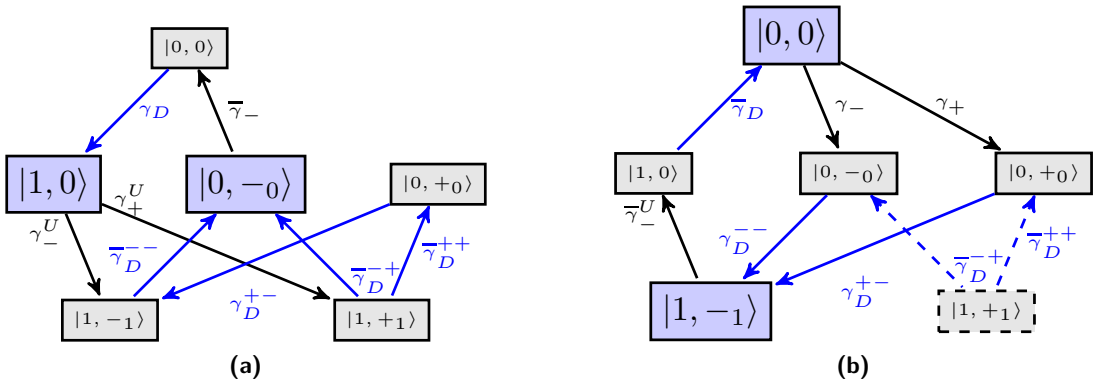

Figure 5.8.: The stategraph shows which states "survive" (blue blackground) and which not (gray background), when tuning the detector (a) such that $\varepsilon_d < \varepsilon_{+-} < \mu_D < \varepsilon_{--} \leq \varepsilon_{++} < \varepsilon_{-+}$. Tuning for (b) is $\varepsilon_{+-} < \varepsilon_{--} < \mu_D < \varepsilon_d < \varepsilon_{++} < \varepsilon_{-+}$. In the extreme limit of the fast demon dot the state $|1, +_1\rangle$ is only populated when it is the initial state.

5.5.2. Mesoscopic dynamics

The procedure to generate reduced rate equations is now somewhat different to that in section 5.4.2 [170]. We start by writing the full system density matrix (DQD and demon dot) in terms of the energy eigenstates and obtain

$$\begin{aligned}\rho = {} & p_{00}\left|0,0\right\rangle\left\langle 0,0\right| + p_{10}\left|1,0\right\rangle\left\langle 1,0\right| \\ & + p_{0-}\left|0,-_0\right\rangle\left\langle 0,-_0\right| + p_{1-}\left|1,-_1\right\rangle\left\langle 1,-_1\right| + p_{0+}\left|0,+_0\right\rangle\left\langle 0,+_0\right| + p_{1+}\left|1,+_1\right\rangle\left\langle 1,+_1\right| . \end{aligned} \tag{5.93}$$

To get rid of the detector's degree of freedom we take the partial trace

$$\begin{aligned}\mathrm{Tr}_{\mathrm{D}}\left\{\rho\right\} \equiv \rho_{\mathrm{DQD}} = {} & \left(p_{00}+p_{10}\right)\left|0\right\rangle_{\mathrm{DQD}}\left\langle 0\right| \\ & + p_{0-}\left|-_0\right\rangle_{\mathrm{DQD}}\left\langle -_0\right| + p_{0+}\left|+_0\right\rangle_{\mathrm{DQD}}\left\langle +_0\right| + p_{1-}\left|-_1\right\rangle_{\mathrm{DQD}}\left\langle -_1\right| + p_{1+}\left|+_1\right\rangle_{\mathrm{DQD}}\left\langle +_1\right| . \end{aligned} \tag{5.94}$$

The Hilbert space for the empty DQD is spanned by the eigenvector $\left|0\right\rangle_{\mathrm{DQD}}$; the one-particle Hilbert space is spanned by two vectors of the overcomplete set of the remaining eigenstates $\left|-_0\right\rangle_{\mathrm{DQD}}, \left|+_0\right\rangle_{\mathrm{DQD}}, \left|-_1\right\rangle_{\mathrm{DQD}}, \left|+_1\right\rangle_{\mathrm{DQD}}$. We, therefore, choose two states of the 1-electron Hilbert space as basis and express the other two vectors in terms of them, namely,

$$\begin{aligned}\mathbb{1} &= \left|-_0\right\rangle\left\langle -_0\right| + \left|+_0\right\rangle\left\langle +_0\right| , \\ \left|-_1\right\rangle &= \left\langle -_0|-_1\right\rangle\left|-_0\right\rangle + \left\langle +_0|-_1\right\rangle\left|+_0\right\rangle , \\ \left|+_1\right\rangle &= \left\langle -_0|+_1\right\rangle\left|-_0\right\rangle + \left\langle +_0|+_1\right\rangle\left|+_0\right\rangle , \end{aligned} \tag{5.95}$$

where we omitted the index "DQD".
Therefore, we obtain for the remaining states

$$\begin{aligned}\left|-_1\right\rangle\left\langle -_1\right| = {} & \underbrace{\left|\left\langle -_0|-_1\right\rangle\right|^2}_{\kappa_{--}}\left|-_0\right\rangle\left\langle -_0\right| + \underbrace{\left|\left\langle +_0|-_1\right\rangle\right|^2}_{\kappa_{+-}}\left|+_0\right\rangle\left\langle +_0\right| \\ & + \underbrace{\left\langle -_0|-_1\right\rangle\left\langle -_1|+_0\right\rangle}_{\sqrt{\kappa_{--}\kappa_{+-}}}\left|-_0\right\rangle\left\langle +_0\right| + \underbrace{\left\langle +_0|-_1\right\rangle\left\langle -_1|-_0\right\rangle}_{\sqrt{\kappa_{+-}\kappa_{--}}}\left|+_0\right\rangle\left\langle -_0\right| , \\ \left|+_1\right\rangle\left\langle +_1\right| = {} & \underbrace{\left|\left\langle -_0|+_1\right\rangle\right|^2}_{\kappa_{-+}}\left|-_0\right\rangle\left\langle -_0\right| + \underbrace{\left|\left\langle +_0|+_1\right\rangle\right|^2}_{\kappa_{++}}\left|+_0\right\rangle\left\langle +_0\right| \\ & + \underbrace{\left\langle -_0|+_1\right\rangle\left\langle +_1|+_0\right\rangle}_{-\sqrt{\kappa_{-+}\kappa_{++}}}\left|-_0\right\rangle\left\langle +_0\right| + \underbrace{\left\langle +_0|+_1\right\rangle\left\langle +_1|-_0\right\rangle}_{-\sqrt{\kappa_{++}\kappa_{-+}}}\left|+_0\right\rangle\left\langle -_0\right| . \end{aligned} \tag{5.96}$$

Note that the wavefunction overlaps fulfill $\sqrt{\kappa_{--}\kappa_{+-}} = \sqrt{\kappa_{+-}\kappa_{--}} = \sqrt{\kappa_{-+}\kappa_{++}} = \sqrt{\kappa_{++}\kappa_{-+}} = \kappa$.

Then the DQD density matrix in the basis $\left\{\left|0\right\rangle, \left|-_0\right\rangle, \left|+_0\right\rangle\right\}$ reads with eq. (5.96)

$$\begin{aligned}\rho_{\mathrm{DQD}} = {} & \left(p_{00}+p_{10}\right)\left|0\right\rangle\left\langle 0\right| + \left(p_{0-}+\kappa_{--}p_{1-}+\kappa_{-+}p_{1+}\right)\left|-_0\right\rangle\left\langle -_0\right| \\ & + \left(p_{0+}+\kappa_{+-}p_{1-}+\kappa_{++}p_{1+}\right)\left|+_0\right\rangle\left\langle +_0\right| \\ & + \kappa\left(p_{1-}-p_{1+}\right)\left(\left|-_0\right\rangle\left\langle +_0\right| + \left|+_0\right\rangle\left\langle -_0\right|\right) . \end{aligned} \tag{5.97}$$

Taking the time derivatives yields

$$\begin{aligned}\dot{\rho}_{\mathrm{DQD}} = {} & \left(\dot{p}_{00}+\dot{p}_{10}\right)\left|0\right\rangle\left\langle 0\right| + \left(\dot{p}_{0-}+\kappa_{--}\dot{p}_{1-}\kappa_{-+}\dot{p}_{1+}\right)\left|-_0\right\rangle\left\langle -_0\right| \\ & + \left(\dot{p}_{0+}+\kappa_{+-}\dot{p}_{1-}+\kappa_{++}\dot{p}_{1+}\right)\left|+_0\right\rangle\left\langle +_0\right| \\ & + \kappa\left(\dot{p}_{1-}-\dot{p}_{1+}\right)\left(\left|-_0\right\rangle\left\langle +_0\right| + \left|+_0\right\rangle\left\langle -_0\right|\right) . \end{aligned} \tag{5.98}$$

We now can plug the master equations $\partial_t \vec{\rho} = \mathcal{L}\vec{\rho}$ derived in section 5.2 into eq. (5.98).
Furthermore, we can always write the following decomposition for the microstate probabilities, which use just the formal definition of conditional probability

$$\begin{aligned}
p_{00} &= \mathbb{P}_{0|0} P_0 \,, \\
p_{10} &= \mathbb{P}_{1|0} P_0 \,, \\
p_{0-} &= p_{0-_0} = \mathbb{P}_{0|-_0} P_{-_0} \,, \\
p_{0+} &= p_{0+_0} = \mathbb{P}_{0|+_0} P_{+_0} \,, \\
p_{1-} &= p_{1-_1} = \mathbb{P}_{1|-_1} P_{-_1} = \mathbb{P}_{1|-_1} \left[\kappa_{++} P_{-_0} + \kappa_{+-} P_{+_0} + \kappa \left((\rho_{\mathrm{DQD}})_{+_0,-_0} + (\rho_{\mathrm{DQD}})_{-_0,+_0} \right) \right] \,, \\
p_{1+} &= p_{1+_1} = \mathbb{P}_{1|+_1} P_{+_1} = \mathbb{P}_{1|+_1} \left[\kappa_{-+} P_{-_0} + \kappa_{--} P_{+_0} - \kappa \left((\rho_{\mathrm{DQD}})_{+_0,-_0} + (\rho_{\mathrm{DQD}})_{-_0,+_0} \right) \right] \,.
\end{aligned} \tag{5.99}$$

That defines formally five mesoscopic probabilities $P_0, P_{-_0}, P_{+_0}, P_{-_1}$ and P_{+_1}, where the first three are the diagonal elements of ρ_{DQD} and the remaining are given by them and the off-diagonal elements.
In the extreme limit the solution to eqs. (5.87) and (5.88) yields for the detection scheme (5.91)

$$\bar{p}_{00} = \bar{p}_{1-_1} = \bar{p}_{1+_1} = 0 \,, \quad \bar{p}_{10} + \bar{p}_{0-_0} + \bar{p}_{0+_0} = 1 \,. \tag{5.100}$$

Therefore, we can identify three effective mesostates

$$\begin{aligned}
&\bar{\mathbb{P}}_{0|0} = \bar{\mathbb{P}}_{1|-_1} = \bar{\mathbb{P}}_{1|+_1} = 0 \,, \quad \bar{\mathbb{P}}_{1|0} = \bar{\mathbb{P}}_{0|-_0} = \bar{\mathbb{P}}_{0|+_0} = 1 \,, \\
&p_{10} \equiv P_0 \,, \quad p_{0-_0} \equiv P_- \,, \quad p_{0+_0} \equiv P_+ \,.
\end{aligned} \tag{5.101}$$

With this identities we obtain

$$\dot{\rho}_{\mathrm{DQD}} = \dot{P}_0 \left|0\right\rangle \left\langle 0\right| + \dot{P}_- \left|-_0\right\rangle \left\langle -_0\right| + \dot{P}_+ \left|+_0\right\rangle \left\langle +_0\right| \,. \tag{5.102}$$

Equivalently, we can write down the effective mesoscopic rate matrix. With our definition (5.19) it reads

$$\mathcal{V} = \begin{pmatrix} -\gamma^U_{L-} - \gamma^U_{L+} - \gamma^U_{R-} - \gamma^U_{R+} & \overline{\gamma}_{L-} + \overline{\gamma}_{R-} & \overline{\gamma}_{L+} + \overline{\gamma}_{R+} \\ \kappa_{--}(\gamma^U_{L-} + \gamma^U_{R-}) + \kappa_{-+}(\gamma^U_{L+} + \gamma^U_{R+}) & -\overline{\gamma}_{L-} - \overline{\gamma}_{R-} & 0 \\ \kappa_{+-}(\gamma^U_{L-} + \gamma^U_{R-}) + \kappa_{++}(\gamma^U_{L+} + \gamma^U_{R+}) & 0 & -\overline{\gamma}_{L+} - \overline{\gamma}_{R+} \end{pmatrix} . \tag{5.103}$$

We verify $\sum_s \mathcal{V}_{s,s'} = 0$ as $\kappa_{\sigma\sigma'} + \kappa_{\sigma\sigma} = 1$ holds for $\sigma \neq \sigma'$. This implies, howbeit, $\kappa_{++} = \kappa_{--}$ and $\kappa_{+-} = \kappa_{-+}$. Figure 5.9 shows the reduction of the stategraph if we tune the demon dot chemical potential according to (5.91).

The resulting currents to/from mesostates $|\sigma\rangle$ with respect to lead l read [recall the rates defined in eq. (5.19)]

$$\begin{aligned}
\bar{I}^{*(l-)}_{\mathrm{M}} &= \left[\kappa_{--} \gamma_{l-}(\Delta E^1_-) + \kappa_{-+} \gamma_{l+}(\Delta E^1_+) \right] \bar{P}^*_0 - \overline{\gamma}_{l-}(E^0_-) \bar{P}^*_- \,, \\
\bar{I}^{*(l+)}_{\mathrm{M}} &= \left[\kappa_{+-} \gamma_{l-}(\Delta E^1_-) + \kappa_{++} \gamma_{l+}(\Delta E^1_+) \right] \bar{P}^*_0 - \overline{\gamma}_{l+}(E^0_+) \bar{P}^*_+ \,.
\end{aligned} \tag{5.104}$$

As a sanity check we first make sure that for the limit of noninteracting QDs ($T_c \to 0$) the latter currents coincide with

$$\begin{aligned}
\bar{I}^{*(l-)}_{\mathrm{M}} \to \bar{I}^{*(lB)}_{\mathrm{M}} &= \gamma_{lB}(\varepsilon + U_0 + \Omega - \Delta) \bar{P}^*_0 - \overline{\gamma}_{lB}(\varepsilon) \bar{P}^*_B \,, \\
\bar{I}^{*(l+)}_{\mathrm{M}} \to \bar{I}^{*(lA)}_{\mathrm{M}} &= \gamma_{lA}(\varepsilon + U_0 + \Delta) \bar{P}^*_0 - \overline{\gamma}_{lA}(\varepsilon + \Omega) \bar{P}^*_A \,,
\end{aligned} \tag{5.105}$$

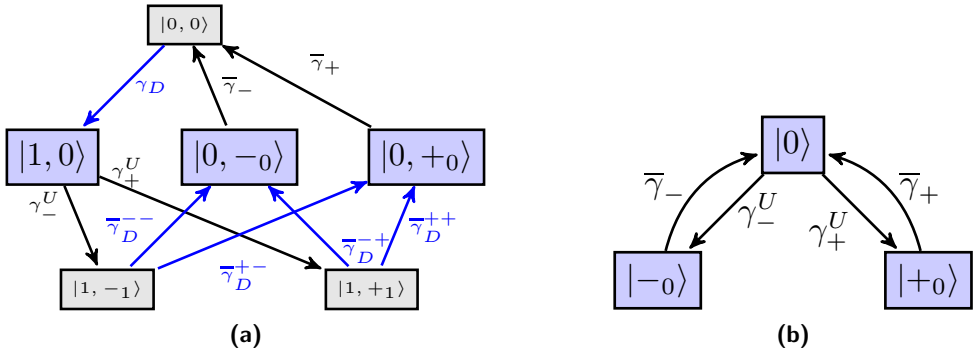

Figure 5.9.: Stategraph for detection scheme (5.91) in the extreme limit. (a) shows which states "survive" (blue blackground) and which not (gray background). The reduction of degrees of freedom leads to the reduced stategraph (b).

which are the currents we obtained in the previous section for detection scheme II. We verify numerically that $\bar{I}_{\mathrm{M}}^{*(L\sigma)} = -\bar{I}_{\mathrm{M}}^{*(R\sigma)}$. The net current through the device [and, thus, also the power extraction] slightly decreases for increasing T_c and is, therefore, always smaller than for the case of noninteracting transport channels.
Let us now, briefly, inspect the entropy production for arbitrary couplings T_c. It reads with (5.58),

$$\bar{\dot{S}}_{\mathrm{i}}^{*} = \sum_{l} \left\{ \bar{I}_{\mathrm{M}}^{*(l+)} \ln \frac{\kappa_{+-}\gamma_{l-}^{U} + \kappa_{++}\gamma_{l+}^{U}}{\overline{\gamma}_{l+}} + \bar{I}_{\mathrm{M}}^{*(l-)} \ln \frac{\kappa_{--}\gamma_{l-}^{U} + \kappa_{-+}\gamma_{l+}^{U}}{\overline{\gamma}_{l-}} \right\} . \tag{5.106}$$

When taking into account the definitions for the transition rates, (5.19), and if we further assume that the bare tunneling coefficients fulfill $\Gamma_{lA}^{(U)} = \Gamma_{lB}^{(U)} = \Gamma_{l}^{(U)}$, which is also assumed in eqs. (5.81) and (5.82), (5.106) yields

$$\begin{aligned} \bar{\dot{S}}_{\mathrm{i}}^{*} = \sum_{l} \Bigg\{ & \bar{I}_{\mathrm{M}}^{*(l+)} \ln \frac{\kappa_{+-}\Gamma_{l}^{U} f_l(\Delta E_{-}^{1}) + \kappa_{++}\Gamma_{l}^{U} f_l(\Delta E_{+}^{1})}{\Gamma_l \overline{f}_l(E_{+}^{0})} \\ & + \bar{I}_{\mathrm{M}}^{*(l-)} \ln \frac{\kappa_{--}\Gamma_{l}^{U} f_l(\Delta E_{-}^{1}) + \kappa_{-+}\Gamma_{l}^{U} f_l(\Delta E_{+}^{1})}{\Gamma_l \overline{f}_l(E_{-}^{0})} \Bigg\} . \end{aligned} \tag{5.107}$$

This expression cannot be simplified further unless we take additional limits into account. As previously done we implement the Maxwell-demon limit, where we assume that all the Fermi energies are evaluated at the same energy E, e.g., the arithmetic average of $E_{-}^{0}, E_{+}^{0}, \Delta E_{-}^{1}$ and ΔE_{+}^{1}. Thus, the effective entropy production becomes ($\beta_L = \beta_R = \beta$)

$$\bar{\dot{S}}_{\mathrm{i}}^{\mathrm{eff}} = \beta V \bar{I}_{\mathrm{M}}^{\mathrm{eff}} + \ln \left[\frac{\Gamma_{L}^{U}\Gamma_{R}}{\Gamma_{L}\Gamma_{R}^{U}} \right] \bar{I}_{\mathrm{M}}^{\mathrm{eff}} , \tag{5.108}$$

where the information currents resembles the channelwise information current, eq. (5.72). Note also that the currents eq. (5.104) become identical in the Maxwell-demon limit.

Serial setup. To end the study of this model, we take a look at the thermodynamics when we switch off the couplings $t_{kLB} \to 0$ and $t_{kRA} \to 0$, or in terms of the rates $\Gamma_{LA}^{(U)} \to \Gamma_{L}^{(U)}$, $\Gamma_{RB}^{(U)} \to \Gamma_{R}^{(U)}$ and $\Gamma_{LB}^{(U)}, \Gamma_{RA}^{(U)} \to 0$. Thus, the model is effectively a *model of serially coupled QDs*, cf. [170].

That implies for the currents (already in the Maxwell-demon limit)

$$\begin{aligned}\bar{I}_{\mathrm{M}}^{\mathrm{eff}(l-)} &= \left[\kappa_{--}|\alpha_-^1|^2 + \kappa_{-+}|\alpha_+^1|^2\right]\gamma_l(E)\bar{P}_0 - |\alpha_-^0|^2\overline{\gamma}_l(E)\bar{P}_-\,,\\ \bar{I}_{\mathrm{M}}^{\mathrm{eff}(l+)} &= \left[\kappa_{+-}|\alpha_-^1|^2 + \kappa_{++}|\alpha_+^1|^2\right]\gamma_l(E)\bar{P}_0 - |\alpha_+^0|^2\overline{\gamma}_l(E)\bar{P}_+\,.\end{aligned} \tag{5.109}$$

The entropy production evaluates to

$$\begin{aligned}\bar{\dot{S}}_{\mathrm{i}}^{\mathrm{eff}} &= \beta V\bar{I}_{\mathrm{M}}^{\mathrm{eff}} + \ln\left[\frac{\Gamma_L^U\Gamma_R}{\Gamma_L\Gamma_R^U}\right]\bar{I}_{\mathrm{M}}^{\mathrm{eff}} + \bar{I}_{\mathrm{M}}^{\mathrm{eff}(L+)}\ln C_1 + \bar{I}_{\mathrm{M}}^{\mathrm{eff}(L-)}\ln C_2 + \bar{I}_{\mathrm{M}}^{\mathrm{eff}(R+)}\ln C_2 + \bar{I}_{\mathrm{M}}^{\mathrm{eff}(R-)}\ln C_1\,,\\ C_1 &\equiv \frac{\kappa_{+-}|\alpha_-^1|^2 + \kappa_{++}|\alpha_+^1|^2}{|\alpha_+^0|^2} = \frac{\kappa_{--}|\beta_-^1|^2 + \kappa_{-+}|\beta_+^1|^2}{|\beta_-^0|^2}\,,\\ C_2 &\equiv \frac{\kappa_{--}|\alpha_-^1|^2 + \kappa_{-+}|\alpha_+^1|^2}{|\alpha_-^0|^2} = \frac{\kappa_{+-}|\beta_-^1|^2 + \kappa_{++}|\beta_+^1|^2}{|\beta_+^0|^2}\,.\end{aligned} \tag{5.110}$$

The particle conservation $\sum_{l\sigma}\bar{I}_{\mathrm{M}}^{l\sigma} \equiv 0$ implies further [confirming [170]]

$$\begin{aligned}\bar{\dot{S}}_{\mathrm{i}}^{\mathrm{eff}} &= \beta V\bar{I}_{\mathrm{M}}^{\mathrm{eff}} + \ln\left[\frac{\Gamma_L^U\Gamma_R}{\Gamma_L\Gamma_R^U}\right]\bar{I}_{\mathrm{M}}^{\mathrm{eff}} + \left(\bar{I}_{\mathrm{M}}^{\mathrm{eff}(L-)} - \bar{I}_{\mathrm{M}}^{\mathrm{eff}(L+)}\right)\ln\left[\frac{C_2}{C_1}\right],\\ \ln\left[\frac{C_2}{C_1}\right] &= \ln\left[\frac{4T_c^2 + \Omega^2 - 2\Omega\Delta + 2\Delta\left(\sqrt{4T_c^2+\Omega^2} + 2\Delta\right)}{4T_c^2 + \Omega^2 - 2\Omega\Delta - 2\Delta\left(\sqrt{4T_c^2+\Omega^2} - 2\Delta\right)}\right].\end{aligned} \tag{5.111}$$

Note that the expression $\ln[C_2/C_1]$ is always positive, given that $\Omega, \Delta > 0$. If we assume $\Gamma_l = \Gamma_l^U$, i.e. no explicit rate modification scheme is applied, the positivity of the entropy production implies that the current through $|-\rangle$ overevaluates that one through $|+\rangle$ at least at small bias voltages, which we verify numerically. Contrarily to the model of parallel QDs, the serial configuration, thus, introduces a strictly positive entropy production even if no modification of the tunneling rates is taking place. One could argue that the current via $|-\rangle$ is pumped against the bias due to the wave function overlaps, when considering this current as isolated. However, as we have to consider the net current in order to calculate the power, we need to take into account as well the current through $|+\rangle$, which compensates that through $|-\rangle$. We find that in the Maxwell-demon limit for all T_c the power $\mathcal{P} = -VI_{\mathrm{M}}^{\mathrm{eff}}$ is strictly nonpositive and therefore the thermoelectric device is in average not transporting electrons against the chemical bias unless the tunnel couplings are modified appropriately.
In fig. 5.10 we depict the steady state currents and the respective entropy production as a function of the bias voltage.

5.6. Conclusions

In this chapter we have derived the dynamics for a generic model that implements a Maxwell-demon like feedback for transport through two parallel QDs. The model is an extension of the implementation investigated by Strasberg *et al.* [44]. Its feedback mechanism is based on the interplay of a fast detector quantum dot and the transport system. The different time scales give rise to carrying out a coarse graining procedure along the lines of the theory introduced in section 2.13 to reduce the model. The model of two noninteracting channels ($T_c \to 0$) is a microscopic implementation for the phenomenological feedback introduced in chapter 4 and we reproduce the effects we discovered when switching off the interaction with the external spin, cf.

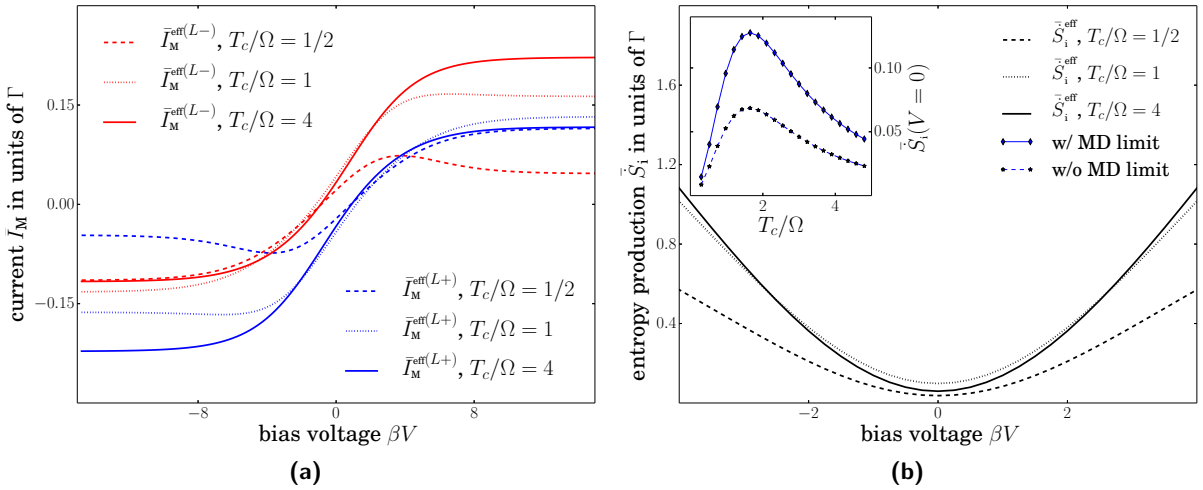

Figure 5.10.: Steady state currents (a) and entropy productions (b) for the model of serially coupled QDs for different parameters for the coherent coupling. The entropy production is always strictly positive and symmetric with respect to V, while the power remains negative. System parameters: $\Delta/\Omega = 2$, $\delta/\Omega = 0$. The inset in (b) shows the entropy production vs T_c evaluated at zero bias voltage (with and without considering the Maxwell-demon limit (MD)). The maximum entropy is reached for $T_c \approx 1.65\Omega$.

section 4.8.1. We showed that nontrivial effects in the current only emerge when the tunneling is energy dependent, such that the interaction with the detector triggers different strengths of the tunnel coupling.

When the coherent coupling is present ($T_c \neq 0$) the coarse graining procedure is restricted, such that the detector can only distinguish between an empty and an occupied DQD and we have to imply the extreme limit of very fast detector tunneling. The resulting currents are slightly decreased compared to the noninteracting case. Although the generic model Hamiltonian can be mapped onto the Hamiltonian for anisotropic exchange interaction in chapter 4 we cannot reproduce the complex dynamics discussed in section 4.8.4 as the parameters are strongly time-dependent and nonlinear. It would be interesting to tackle this problem in the future using, e.g., Floquet theory or other suitable time-dependent theories.

6. Transport and semiclassical dynamics of coupled quantum dots interacting with a local magnetic moment

[K. Mosshammer, G. Kiesslich, and T. Brandes. "Transport and semiclassical dynamics of coupled quantum dots interacting with a local magnetic moment". *Phys. Rev. B* 86 (16 2012), 165447]

6.1. Introduction

In this chapter, we will extend the method used in chapter 4 and Ref. [128] for the description of an electronic setup with two serially coupled QDs, which interact with the same magnetic moment. We will show that in contrast to the single-QD case, the derived equations of motion for the electronic part will possess a much more involved structure due to the inclusion of coherences. The resulting coupling of the semiclassical dynamics of the attached magnetic moment with the spin dynamics of the nonequilibrium electrons gives rise to complex transient dynamics, such as chaos, and peculiar steady-state dependencies on the initial conditions. Furthermore, we find the phenomenon of parametric resonance in the current oscillations. We compare the current-induced switching behavior of the attached magnetic moment in our coupled setup with the single-QD setup in Refs. [152, 128].

The remainder of this chapter is organized as follows: Sec. 6.2 contains the model with the Hamiltonian (6.2.1), with a discussion of the level of description in Sec. 6.2.2, with the semiclassical approximation and derivation of the Ehrenfest equations of motion (6.2.3), and with the final equations of motion containing the transport dissipator in Sec. 6.2.4. In Sec. 6.3 the results will be discussed: steady-state currents (6.3.1), isotropic coupling and current-induced switching of the large spin (6.3.2), and anisotropic coupling (6.3.4). Finally, we will conclude in Sec. 6.4.

6.2. Model

6.2.1. Hamiltonian

We consider a system of two serially coupled QDs with one orbital level each (see Fig. 6.1). The system is subject to an external magnetic field B in the $z-$direction, which splits the QD spin levels. Moreover, the system is coupled to electronic leads, as well as to a large spin $\vec{J}$ with length j given by $\vec{J}^2 |m, j\rangle = j(j+1) |m, j\rangle$. The total system Hamiltonian reads as follows:

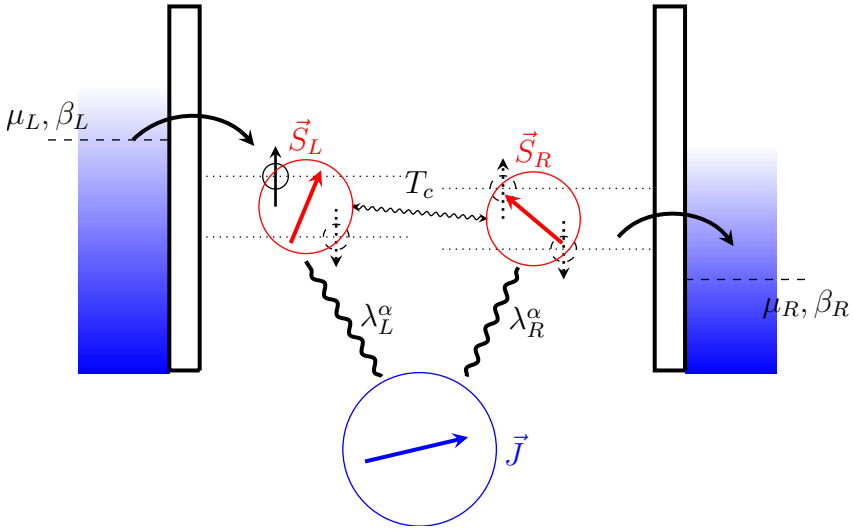

Figure 6.1.: Setup of two QDs mutually tunnel-coupled with strength T_c. The electron spins $\vec{\hat{S}}_i$ interact with a common large spin $\vec{\hat{J}}$ via λ_i^α. The QDs are attached to ferromagnetic electronic reservoirs with spin-dependent tunneling rates $\Gamma_{i\sigma}$.

$$
\begin{aligned}
\hat{H} &= \hat{H}_{\mathrm{DQD}} + \hat{H}_{\mathrm{J}} + \hat{H}_{\mathrm{leads}} + \hat{H}_{\mathrm{int}} \ , \\
\hat{H}_{\mathrm{DQD}} &= \sum_{\substack{i=L,R \\ \sigma=\uparrow,\downarrow}} \varepsilon_i \, \hat{d}_{i\sigma}^\dagger \, \hat{d}_{i\sigma} + T_c \sum_{i\neq j,\sigma} \hat{d}_{i\sigma}^\dagger \, \hat{d}_{j\sigma} + B \sum_i \hat{S}_i^z \ , \\
\hat{H}_{\mathrm{J}} &= B \, \hat{J}^z \ , \qquad \hat{H}_{\mathrm{int}} = \sum_{\substack{\alpha=x,y,z \\ i}} \lambda_i^\alpha \, \hat{S}_i^\alpha \, \hat{J}^\alpha \ , \\
\hat{H}_{\mathrm{leads}} &= \sum_{l,p,\sigma} \varepsilon_{lp\sigma} \, \hat{c}_{lp\sigma}^\dagger \, \hat{c}_{lp\sigma} + \sum_{lp} t_{lp} \sum_\sigma \hat{c}_{lp\sigma}^\dagger \, \hat{d}_{l\sigma} + \mathrm{H.c.} \, .
\end{aligned}
\tag{6.1}
$$

Here $\hat{H}_{\mathrm{DQD}}$ describes the double-QD system (DQD), with the tunnel coupling T_c between the left and the right dot, and the energies of the orbital levels $\varepsilon_L, \varepsilon_R$, respectively. Note that our definition of B comprises the Bohr magneton and g factors. For the sake of simplicity we assume identical g factors for electron and large spin throughout the following. The Coulomb repulsion between excess electrons within the QD system is assumed to be much larger than all other system and bath energies to constrain their maximal number to one (i.e. the system is operated in the Coulomb blockade regime).

The operators $\hat{d}_{i\sigma}^\dagger(\hat{d}_{i\sigma})$ describe the creation(annihilation) of an electron with spin $\sigma = \uparrow, \downarrow$ on the ith dot $(i, j, l = L, R)$; the occupation operator is defined by $\hat{n}_{i\sigma} = \hat{d}_{i\sigma}^\dagger \, \hat{d}_{i\sigma}$. The relationship between these electronic operators and the αth component of the spin operator $\vec{\hat{S}}_i$ is given by

$$
\begin{aligned}
\hat{S}_i^x &= \frac{1}{2}\left(\hat{d}_{i\uparrow}^\dagger \, \hat{d}_{i\downarrow} + \hat{d}_{i\downarrow}^\dagger \, \hat{d}_{i\uparrow}\right) = \frac{1}{2}\left(\hat{S}_i^+ + \hat{S}_i^-\right) , \\
\hat{S}_i^y &= \frac{1}{2\mathbf{i}}\left(\hat{d}_{i\uparrow}^\dagger \, \hat{d}_{i\downarrow} - \hat{d}_{i\downarrow}^\dagger \, \hat{d}_{i\uparrow}\right) = \frac{1}{2\mathbf{i}}\left(\hat{S}_i^+ - \hat{S}_i^-\right) , \\
\hat{S}_i^z &= \frac{1}{2}\left(\hat{n}_{i\uparrow} - \hat{n}_{i\downarrow}\right) .
\end{aligned}
\tag{6.2}
$$

with the usual commutation relations $\left[\hat{S}_i^+, \hat{S}_j^-\right] = \delta_{ij} 2\,\hat{S}_j^z$ and $\left[\hat{S}_i^z, \hat{S}_j^\pm\right] = \pm\delta_{ij}\,\hat{S}_j^\pm$.
In contrast to most of other related studies, here we also allow for anisotropic coupling between electronic and large spin: $\lambda_i^\alpha \neq \lambda_i^\beta$ for $\alpha \neq \beta$.
The lead electrons are assumed to be noninteracting; the corresponding operator $\hat{c}_{lp\sigma}^\dagger\,(\hat{c}_{lp\sigma})$ creates (annihilates) an electron of momentum p and spin σ in the lth lead, while t_{lp} is the spin-independent coupling strength between lth lead and lth dot.

6.2.2. Level of description and time scale separation

The microscopic dynamics of the system described by (6.1) is involved and contains a lot of information, which we are not interested in. Therefore we will choose a level of description, where only the dynamics of single-particle observables such as components of the average electron and large spin and the reduced density matrix of electrons dwelling in the dots will be considered.
A rigorous derivation of the corresponding equations of motion in a controlled manner can be performed, e.g., by projective methods [173] or by Keldysh-Green functions [105]. The price one has to pay for projecting out some "irrelevant" (microscopic) information is the occurence of non-Markovian terms and residual forces in the equations of motion. One typical way to retain Markovian (time local) dynamics may be the separation of time scales present in the considered problem.
In this work we avoid this derivation path and gain the dynamics of the relevant observables by a simple semiclassical approximation instead (see section 6.2.3 and chapter 4). We argue phenomenologically that the time scale of the large spin precession is much slower than the electron dwell time; i.e. electron spin fluctuations do not affect the large spin dynamics and *vice versa*. Those electron spin fluctuations arise from the tunnel coupling to the electron reservoirs, which we are going to treat in the standard Born-Markov approximation.
In our Ref. [128] we have used a technique based on Laplace transform (see Appendix A of that reference) to combine the semiclassical Ehrenfest equations of motion for the spin observables with the reduced density matrix for the electrons. The same final equations of motions can be simply obtained by adding the terms based on the Lindblad master equation for dot-lead coupling to the spin dynamics as we have proven for the single-QD setup in Ref. [128]. Here, we take advantage of this observation and employ this simplified method to set up our final equations of motion (see Sec. 6.2.4).

6.2.3. Semiclassical approximation and Ehrenfest equations of motion

In order to investigate the dynamics of the coupled spin system we employ an equations of motion (EOM) technique for the expectation values of the involved spin operators. We recall that, in general, the EOM for the expectation value of an arbitrary operator $\hat{O}$ reads

$$\frac{d}{dt}\langle\hat{O}\rangle = \frac{1}{\mathbf{i}}\langle\left[\hat{O}, \hat{H}\right]\rangle + \left\langle\frac{\partial\hat{O}}{\partial t}\right\rangle . \tag{6.3}$$

Due to the interaction between electrons and large spin in (6.1) an infinite series of coupled EOM of higher-order spin correlators will be obtained. In order to truncate this hierarchy we implement a semiclassical approximation on the level of the interaction Hamiltonian: We substitute $\hat{S}_i^\alpha = \langle\hat{S}_i^\alpha\rangle + \delta\,\hat{J}^\alpha$ and $\hat{J}^\alpha = \langle\hat{J}^\alpha\rangle + \delta\,\hat{J}^\alpha$ into the interaction Hamiltonian $\hat{H}_{\rm int}$ and obtain the already used mean-field interaction [cf. eq. (4.10)]

$$\hat{H}_{\rm int}^{\rm MF} = \sum_{\alpha,i}\lambda_i^\alpha\left(\hat{S}_i^\alpha\,\langle\hat{J}^\alpha\rangle + \langle\hat{S}_i^\alpha\rangle\,\hat{J}^\alpha - \langle\hat{S}_i^\alpha\rangle\,\langle\hat{J}^\alpha\rangle\right), \tag{6.4}$$

where the product of the spin fluctuators $\delta\hat{S}_i^\alpha\,\delta\hat{J}^\alpha$ is neglected, which is justified for $j \gg 1$ and $\lambda_i^\alpha/B \ll 1$ $(\forall\alpha, i)$. Thus, we essentially treat $\vec{\hat{J}}$ as a classical object. Note, that since the Hamiltonian (6.1) does not contain any interaction of the large spin with the lead electrons or with an additional bath its length j will be conserved on the microscopic level ($\left[\vec{\hat{J}}^2, \hat{H}\right] = 0$). Nevertheless, later on we will introduce a way of damping in the large spin EOMs, which is not microscopically motivated.
Using the semiclassical interaction Hamiltonian (6.4) yields the following correlators [cf. section A.3] for the electronic part of EOM (for the sake of clarity we omit the time dependencies)

$$\begin{aligned}
\frac{d}{dt}\langle\hat{d}_{i\sigma}^\dagger\,\hat{d}_{j\sigma'}\rangle = \frac{\mathbf{i}}{2}\Big[&(\delta_{\sigma\uparrow}-\delta_{\sigma\downarrow})\left(B+\lambda_i^z\langle\hat{J}^z\rangle\right)+(\delta_{\sigma'\downarrow}-\delta_{\sigma'\uparrow})\left(B+\lambda_j^z\langle\hat{J}^z\rangle\right)+2(\varepsilon_i-\varepsilon_j)\Big]\langle\hat{d}_{i\sigma}^\dagger\,\hat{d}_{j\sigma'}\rangle\\
&+\mathbf{i}T_c\left(\langle\hat{d}_{\bar{i}\sigma}^\dagger\,\hat{d}_{j\sigma'}\rangle-\langle\hat{d}_{i\sigma}^\dagger\,\hat{d}_{\bar{j}\sigma'}\rangle\right)\\
&+\frac{\mathbf{i}}{2}\left[\lambda_i^x\langle\hat{J}^x\rangle-\mathbf{i}(\delta_{\sigma\uparrow}-\delta_{\sigma\downarrow})\lambda_i^y\langle\hat{J}^y\rangle\right]\langle\hat{d}_{i\bar{\sigma}}^\dagger\,\hat{d}_{j\sigma'}\rangle\\
&-\frac{\mathbf{i}}{2}\left[\lambda_j^x\langle\hat{J}^x\rangle-\mathbf{i}(\delta_{\sigma'\downarrow}-\delta_{\sigma'\uparrow})\lambda_j^y\langle\hat{J}^y\rangle\right]\langle\hat{d}_{i\sigma}^\dagger\,\hat{d}_{j\bar{\sigma}'}\rangle\\
&-\mathbf{i}\sum_p\Big[\gamma_{Lp\sigma'}^*\delta_{Lj}\langle\hat{d}_{i\sigma}^\dagger\,\hat{c}_{Lp\sigma'}\rangle+\gamma_{Rp\sigma'}^*\delta_{Rj}\langle\hat{d}_{i\sigma}^\dagger\,\hat{c}_{Rp\sigma'}\rangle\\
&\qquad-\gamma_{Lp\sigma}\delta_{Li}\langle\hat{c}_{Lp\sigma}^\dagger\,\hat{d}_{j\sigma'}\rangle-\gamma_{Rp\sigma}\delta_{Ri}\langle\hat{c}_{Rp\sigma}^\dagger\,\hat{d}_{j\sigma'}\rangle\Big],
\end{aligned}\tag{6.5}$$

where $\bar{i} = L(R)$ for $i = R(L)$, $\bar{\sigma} = \downarrow(\uparrow)$ for $\sigma = \uparrow(\downarrow)$.
The EOM for the expectation values of the large spin's degree of freedom take the form of a Bloch equation completed by the electronic back-action and the phenomenological damping:

$$\frac{d}{dt}\langle\vec{\hat{J}}\rangle(t) = \left[B\vec{e}_z+\sum_i\langle\vec{\hat{S}}_i'\rangle(t)\right]\times\langle\vec{\hat{J}}\rangle(t)-\gamma_J\langle\vec{\hat{J}}\rangle(t),\tag{6.6}$$

with $\langle\vec{\hat{S}}_i'\rangle(t) \equiv \sum_\alpha\lambda_i^\alpha\langle\hat{S}_i^\alpha\rangle(t)\vec{e}_\alpha$.
So far we have derived the Ehrenfest EOM for the closed coupled spin system. In order to pursue a microscopic derivation of spin-dependent rates for the transport between the electronic contacts and the system we could follow the method proposed in Ref. [128]. This technique requires the direct computation of all dot-lead correlators appearing in Eq. (6.5): $\langle\hat{d}_{i\sigma}^\dagger\,\hat{c}_{jp\sigma'}\rangle$ and $\langle\hat{c}_{ip\sigma'}^\dagger\,\hat{d}_{j\sigma}\rangle$, respectively. However, the number of relevant dynamical variables in the DQD $\langle\hat{d}_{i\sigma}^\dagger\,\hat{d}_{j\sigma'}\rangle(t)$ is far too large for the analytical derivation along the lines of Appendix A in Ref. [128]. Instead we make use of the fact that for the single-QD the same EOM can be obtained alternatively by replacing the last term of the right-hand side of (6.5) with terms originating from the Lindblad-type master equation [cf. chapter 4]. Even though there is no proof of equivalence we believe that those aproaches lead to the same results in the case of DQD. The corresponding derivation will be provided in the following section.

6.2.4. Transport master equation

Here, we will combine the Ehrenfest EOM (6.5) with the quantum master equation of the DQD that is not coupled to the large spin. Specifically, we use the Lindblad-type master equation for the

system density matrix $\hat{\rho}$, which is derived by means of the standard Born-Markov-approximation in the infinite bias limit:

$$\begin{aligned}\frac{d}{dt}\,\hat{\rho}\,(t) = -\mathbf{i}\left[\hat{H}_{\mathrm{DQD}}\,,\hat{\rho}\,(t)\right] \\ -\frac{1}{2}\sum_{\sigma}\Bigg[\Gamma_{L\sigma}\Bigg(\left\{\hat{d}_{L\sigma}\,\hat{d}^{\dagger}_{L\sigma}\,,\hat{\rho}\,(t)\right\} - 2\,\hat{d}^{\dagger}_{L\sigma}\,\hat{\rho}\,(t)\,\hat{d}_{L\sigma}\Bigg) \\ +\Gamma_{R\sigma}\left(\left\{\hat{d}^{\dagger}_{R\sigma}\,\hat{d}_{R\sigma}\,,\hat{\rho}(t)\right\} - 2\,\hat{d}_{R\sigma}\,\hat{\rho}\,(t)\,\hat{d}^{\dagger}_{R\sigma}\right)\Bigg].\end{aligned} \tag{6.7}$$

The matrix elements of $\hat{\rho}$ are $\langle \hat{d}^{\dagger}_{i\sigma}\,\hat{d}_{j\sigma'}\rangle$. The tunnel rates are given by $\Gamma_{l\sigma} = 2\pi|t_l|^2\rho_{l\sigma}$ with the spin-dependent density of states $\rho_{l\sigma}$ in the lth lead, which is approximated to be energy-independent. The asymmetry in the density of states will be parametrized by the degree of spin polarization (see also [174])

$$p_l \equiv \frac{\rho_{l\uparrow} - \rho_{l\downarrow}}{\rho_{l\uparrow} + \rho_{l\downarrow}}\,, \tag{6.8}$$

with $p_l \in [-1,1]$; $p_l = 0$ corresponds to a nonmagnetic lead and $p_l = \pm\,1$ describes a spin up/down-polarized half-metallic ferromagnetic contact, respectively. The tunneling rates then read $\Gamma_{l\uparrow} = \frac{1}{2}\Gamma_l(1+p_l)$, $\Gamma_{l\downarrow} = \frac{1}{2}\Gamma_l(1-p_l)$, and $\Gamma_l = \Gamma_{l\uparrow} + \Gamma_{l\downarrow}$.
Now we define the density matrix $\hat{\rho}$ in vector form with the following subvectors (omitting the time dependence):

$$\begin{aligned}\vec{\rho}^{\,\sigma} &\equiv \left(\langle\hat{\rho}^{\sigma}_{L}\rangle\,,\langle\hat{\rho}^{\sigma}_{R}\rangle\,,\langle\hat{\rho}^{\sigma}_{LR}\rangle\,,\langle\hat{\rho}^{\sigma}_{RL}\rangle\right)^{\mathrm{T}} \\ &= \left(\langle\hat{n}_{L\sigma}\rangle\,,\langle\hat{n}_{R\sigma}\rangle\,,\langle\hat{d}^{\dagger}_{L\sigma}\,\hat{d}_{R\sigma}\rangle\,,\langle\hat{d}^{\dagger}_{R\sigma}\,\hat{d}_{L\sigma}\rangle\right)^{\mathrm{T}}\,, \\ \vec{\xi}_e &\equiv \left(\langle\hat{S}^{+}_{L}\rangle\,,\langle\hat{S}^{-}_{L}\rangle\,,\langle\hat{S}^{+}_{R}\rangle\,,\langle\hat{S}^{-}_{R}\rangle\right)^{\mathrm{T}}\,, \\ \vec{\xi}_u &\equiv \left(\langle\hat{d}^{\dagger}_{L\uparrow}\,\hat{d}_{R\downarrow}\rangle\,,\langle\hat{d}^{\dagger}_{R\downarrow}\,\hat{d}_{L\uparrow}\rangle\,,\langle\hat{d}^{\dagger}_{R\uparrow}\,\hat{d}_{L\downarrow}\rangle\,,\langle\hat{d}^{\dagger}_{L\downarrow}\,\hat{d}_{R\uparrow}\rangle\right)^{\mathrm{T}}\,,\end{aligned} \tag{6.9}$$

and the vacuum operator $\hat{\rho}_0 \equiv \mathbb{1} - \hat{N}$ with the total electron number operator $\hat{N} = \sum_{l\sigma}\hat{n}_{l\sigma}$; its EOM is obtained by (6.8) and reads

$$\frac{d}{dt}\,\langle\hat{\rho}_0\rangle\,(t) = -\Gamma_L\,\langle\hat{\rho}_0\rangle\,(t) + \Gamma_{R\uparrow}\,\langle\hat{\rho}^{\uparrow}_{R}\rangle\,(t) + \Gamma_{R\downarrow}\,\langle\hat{\rho}^{\downarrow}_{R}\rangle\,(t)\,. \tag{6.10}$$

Eventually, the combination of (6.5), (6.8), and (6.10) results in the EOM of the electronic part, which we provide in a compact vector form

$$\frac{d}{dt}\hat{\rho}(t) = \mathcal{M}\Big(\,\langle\hat{J}^{x}\rangle\,,\langle\hat{J}^{y}\rangle\,,\langle\hat{J}^{z}\rangle\,\Big)\hat{\rho}(t)\,, \tag{6.11}$$

with $\hat{\rho}(t) \equiv \big(\,\langle\hat{\rho}_0\rangle\,(t),\vec{\rho}^{\uparrow}(t),\vec{\rho}^{\downarrow}(t),\vec{\xi}_e(t),\vec{\xi}_u(t)\big)^{\mathrm{T}}$ and

$$\mathcal{M} \equiv \left(\begin{array}{ccc|cc} -\Gamma_L & \vec{r}^{\uparrow} & \vec{r}^{\downarrow} & \vec{0}_4^{\mathrm{T}} & \vec{0}_4^{\mathrm{T}} \\ \vec{l}^{\uparrow} & \mathbf{L}^{\uparrow} & \mathbf{0}_{4,4} & \mathbf{A} & \mathbf{B} \\ \vec{l}^{\downarrow} & \mathbf{0}_{4,4} & \mathbf{L}^{\downarrow} & -\mathbf{A} & \mathbf{C} \\ \hline \vec{0}_4 & -\mathbf{A}^{\dagger} & \mathbf{A}^{\dagger} & \mathbf{D} & \mathbf{E} \\ \vec{0}_4 & -\mathbf{B}^{\dagger} & -\mathbf{C}^{\dagger} & \mathbf{E} & \mathbf{F} \end{array}\right), \tag{6.12}$$

where $\mathbf{0}_{4,4}$ is the (4,4)-zero-matrix, $\vec{0}_4$ is the 4-dimensional zero-vector, $\vec{l}^{\sigma} \equiv (\Gamma_{L\sigma}, 0, 0, 0)^{\mathrm{T}}$, $\vec{r}^{\sigma} \equiv (0, \Gamma_{R\sigma}, 0, 0)^{\mathrm{T}}$.

Together with the modified Bloch equations (6.6) for the large spin $\langle \vec{\hat{J}} \rangle$ this forms an involved set of nonlinear differential equations, which describe the coupled dynamics of the nonequilibrium QD system and the large spin. Note that due to the internal tunnel coupling coherences between different spin directions in different QDs (ξ_e,ξ_u) also need to be considered in the EOM. The matrix on the right-hand side of (6.12) provides the coupling structure; the detailed definition of the 4×4 block matrices $\mathbf{L}^{\sigma}, \mathbf{A}, \mathbf{B}, \ldots \mathbf{F}$ can be found in Appendix A.4. In particular, for vanishing coupling $\lambda_i^{\alpha} = 0$ the $\hat{\rho}$ part decouples completely from the $\hat{\xi}$-part and from the large spin $\langle \vec{\hat{J}} \rangle$. The resulting master equation for $\hat{\rho}$ describes the unidirectional transport of electrons through two spin channels [175, 176]. Due to the strong Coulomb blockade the electron transfer in those channels is correlated and for finite coupling λ_i^{α} they mutually couple due to spin-flip transfer between electron and large spin.

Since we consider the QD system in the infinite bias limit the average time-dependent electron current through the DQD can be calculated by the product of occupations and tunnel rates of the right QD

$$\langle \hat{I} \rangle (t) = \Gamma_{R\uparrow} \langle \hat{n}_R^{\uparrow} \rangle (t) + \Gamma_{R\downarrow} \langle \hat{n}_R^{\downarrow} \rangle (t) \,. \tag{6.13}$$

6.3. Analysis and Numerical results

6.3.1. Steady-state currents

Before we will start with the discussions of the dynamics of large and electronic spin, we consider the steady-state currents in the uncoupled and coupled case. With the interaction to the large spin turned off (i.e. $\lambda = 0$) the steady-state current can be obtained analytically and reads

$$\frac{\langle \hat{I} \rangle}{e} = \frac{4T_c^2(\Gamma_{L\downarrow} + \Gamma_{L\uparrow})\Gamma_{R\downarrow}\Gamma_{R\uparrow}}{4a\,T_c^2 + b_{\downarrow} + b_{\uparrow}} \,, \tag{6.14}$$

where $a \equiv 2(\Gamma_{L\uparrow}\Gamma_{R\downarrow} + \Gamma_{L\downarrow}\Gamma_{R\uparrow}) + \Gamma_{R\downarrow}\Gamma_{R\uparrow}$, $b_{\sigma} \equiv \Gamma_{L\sigma}\Gamma_{R\bar{\sigma}}({\Gamma_{R\sigma}}^2 + 4\varepsilon^2)$, and $\varepsilon \equiv \varepsilon_L - \varepsilon_R$ denotes the level detuning between the left and right dot levels in the system. With the definition of the tunneling rates and the assumption of symmetric tunnel couplings $\Gamma_L = \Gamma_R \equiv \Gamma$ this can be rewritten as

$$\frac{\langle \hat{I} \rangle}{e\Gamma} = \frac{4T_c^2(1 - p_R^2)}{4T_c^2[5 - p_R(4p_L + p_R)] + 8\varepsilon^2(1 - p_L p_R) + c\Gamma^2} , \tag{6.15}$$

with $c \equiv (1 + p_L p_R)(1 - p_R^2)/2$. For symmetric polarizations $p \equiv p_L = p_R$ we further obtain

$$\frac{\langle \hat{I} \rangle}{e\Gamma} = \frac{4T_c^2}{20T_c^2 + 8\varepsilon^2 + (1 + p^2)\Gamma^2/2} \,, \tag{6.16}$$

which becomes maximal for nonmagnetic leads ($p = 0$). We need to note that this current expression is only valid for incomplete polarization ($|p| < 1$) since in the polarized case the steady-state version of the master equation (6.11) is not well defined: In particular, the relevant part of the coefficient matrix (Liouvillian superoperator) $\mathcal{M}$ (6.12) reduces to the left upper $N \times N$ submatrix (detached by lines) with $N = 9$. For $|p| < 1$ its rank is $(N - 1)$ and a unique steady state follows. In contrast for $|p| = 1$ when one spin channel is completely switched off

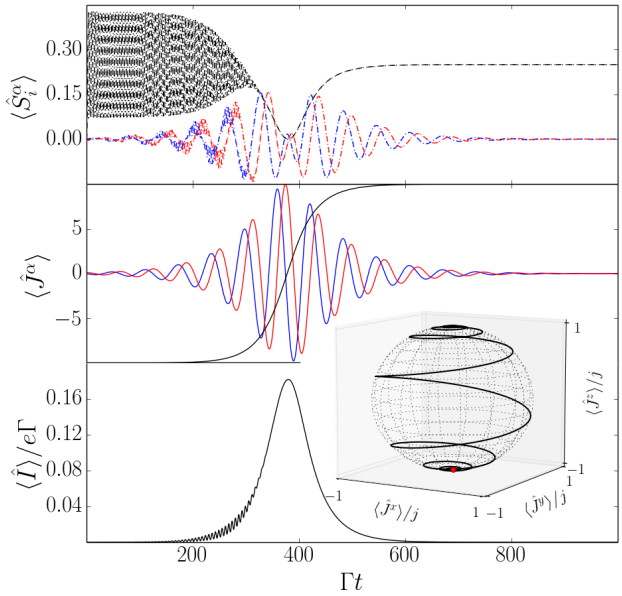

Figure 6.2.: Current-induced magnetization of the large spin. (Top) Components of the electron spin $\langle \hat{S}_L^x \rangle$ (blue, dotted), $\langle \hat{S}_R^x \rangle$ (blue, dashed) $\langle \hat{S}_L^y \rangle$ (red, dotted), $\langle \hat{S}_L^y \rangle$ (red, dashed), $\langle \hat{S}_L^z \rangle$ (black, dotted), $\langle \hat{S}_R^z \rangle$ (black, dashed). (Middle) Components of the large spin: $\langle \hat{J}^x \rangle$ (blue), $\langle \hat{J}^y \rangle$ (red), $\langle \hat{J}^z \rangle$ (black). (Bottom) Electronic current $\langle I \rangle (t)$ vs. time. In the long-term limit one observes $\langle \hat{J}^x \rangle = \langle \hat{J}^y \rangle = 0$, $\langle \hat{J}^z \rangle = j$ and the current vanishes. (Inset) Evolution of the large spin as trajectory in the Bloch sphere, where the red circle depicts the initial position. Note that the onset time depends on the initial orientation of the large spin, the more the large spin deviates from alignment with the magnetic field, the faster the switching process sets in. Parameters: $p_L = -p_R = 1$, $B/\Gamma = 0.1$, $T_c/\Gamma = 0.5$, $\lambda/\Gamma = 1$, $\varepsilon = 0$, $\gamma_J/\Gamma = 0$, large spin length $j = 10$.

the rank reduces and more than one steady state is obtained, which is clearly unphysical. The steady-state master equation is over-determined. In order to obtain the steady state for complete polarization we have to make use of the spin-polarized master equation considered in Refs. [176, 34] where $N = 5$. The corresponding current reads

$$\frac{\langle \hat{I} \rangle_p}{e\Gamma} = \frac{4T_c^2}{12T_c^2 + 8\varepsilon^2 + \Gamma^2}, \tag{6.17}$$

which significantly differs from (6.16) and leads to a discontinuity of the current when $|p|$ approaches one. Therefore, the complete symmetric lead polarization provides a singular case in our description, which has to be either excluded or treated with caution (see below).

Coupled spins. For arbitrary spin couplings we have not been able to derive an analytical expression for the current due to the high dimensionality of the EOM. However, when the large spin components $\langle \hat{J}^x \rangle$ and $\langle \hat{J}^y \rangle$ approach zero in the long-term limit, we again obtain the steady-state current (6.14). This either occurs when the large spin is damped ($\gamma_J > 0$) or for isotropic spin coupling ($\lambda_i^\alpha = \lambda$, $\forall i, \alpha$) as will be discussed in the next section.
As in the uncoupled case complete symmetric contact polarization ($|p| = 1$) causes pecularities, such as a dependency of the stationary current on initial conditions or multistable current

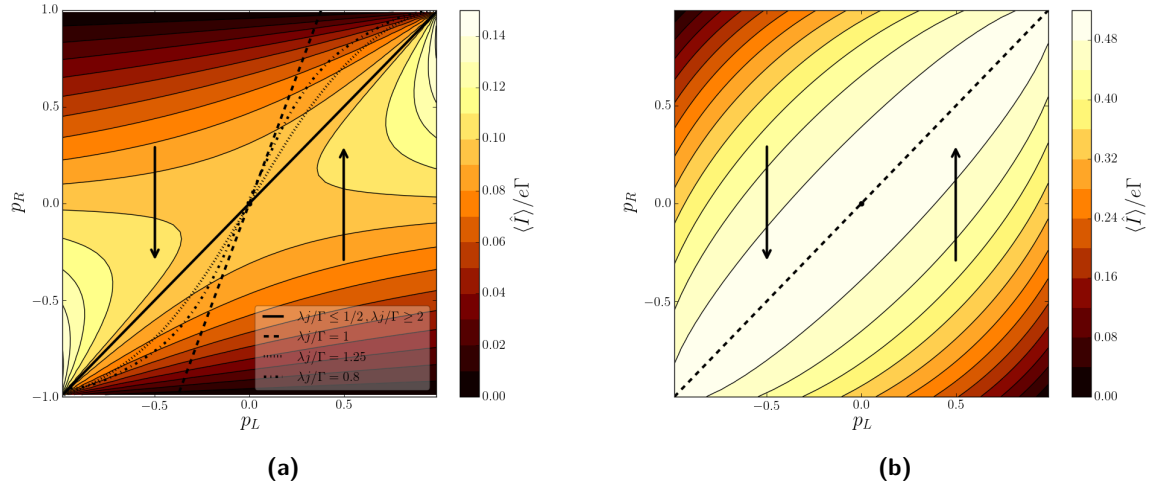

Figure 6.3.: Contour plots of the stationary currents vs p_L and p_R. (a) Coupled QDs with parameters $\varepsilon = 0$, $T_c/\Gamma = 0.5$, $B/\Gamma = 0.1$. (b) Single-QD with the same magnetic field B. The black vertical arrows denote switching directions in areas divided by the straight black lines. For $p_L = p_R = 0$, i.e. unpolarized contacts, and on the borders drawn as black lines no switching takes place. Note that for the DQD the transition between switching up and down depends on the product λj: For $\lambda j/\Gamma \leq 1/2$ and $\lambda j/\Gamma \geq 2$ the transition takes place along the line $p_R = p_L$ (solid); otherwise the transition line is located in the region bounded by $p_R \approx 2.6\, p_L$ for $\lambda j/\Gamma = 1$ (dashed). Note that those transitions are not linear with respect to p_L as shown, e.g., for $\lambda j/\Gamma = 1.25$ (dotted) of $\lambda j/\Gamma = 0.8$ (dashed-dotted).

behavior (see Sec. 6.3.4). We note, that this is also caused by the above mentioned failure of the electronic master equation and not by the semiclassical approximation of the spin interaction. However, the spin-polarized master equation can not be used here.

6.3.2. Isotropic coupling and current-induced magnetization of the large spin

In this section we consider isotropic coupling $\lambda_i^\alpha = \lambda$ $(\forall i, \alpha)$ between the electron spin and the large spin. We will discuss the dynamical behavior of both spins and the current for various lead polarizations p_L and p_R.

Reverse lead polarizations. For the sake of clarity we start our discussions with complete reverse polarization $p_L = -p_R = \pm 1$. An electron transfer through the QD system only takes place when each spin-up (spin-down) electron entering the left QD is able to down-flip (up-flip) its spin state, respectively. According to the microscopic spin coupling $\hat{H}_{\rm int} = \lambda \sum_j (\frac{1}{2}\hat{S}_j^+ \hat{J}^- + \frac{1}{2}\hat{S}_j^- \hat{J}^+ + \hat{S}_j^z \hat{J}^z)$ this electron spin-up (spin-down) flip is accompanied with the decrement (increment) of the large spin magnetic number by one: $m \mp 1$ $(\hat{J}^z |m, j\rangle = m |m, j\rangle$ with $|m| \leq j)$. Once the minimal (maximal) number $\mp j$ is reached, the large spin is completely aligned with the z–direction and the current vanishes. This process is independent of the external magnetic field and can be considered as current-induced switching [152] of the attached local magnetic moment. This effect is also known in magnetic layers described by a Landau-Lifshitz-Gilbert equation for the layer magnetization [154]. In this approach the current-induced magnetization has been interpreted as spin-transfer torque [154, 155] acting on the magnetic moment. Unfortunately, for our DQD

we are not able to identify analogous terms in Eq. 6.6 due to the complex coupling structure with the electronic part.

Figure 6.2 shows the dynamics of the current-induced switching of $\langle \hat{\vec{J}} \rangle$ for our DQD, in the case of $p_L = -p_R = \pm 1$ and no damping of the large spin $\gamma_J = 0$. In the transient regime, damped coherent oscillations of the electron between the QDs with frequency $2T_c$ ($\varepsilon = 0$) are visible in the current and in the electron spin evolution. For the sake of clear demonstration we have chosen the initial large spin to be reversely aligned to its final direction. According to our above explanation the current then is peaked around the time when the derivative of $\langle \hat{J}^z \rangle (t)$ is maximal, in the isotropic case when $\langle \hat{J}^z \rangle = 0$, as the spin-spin interaction and thus the spin-transfer becomes maximal there. In the long-term limit the current is given by (6.14). If one assumes a finite damping $\gamma_J > 0$ the $z-$component of the large spin will approach zero as well.

The inset of Fig. 6.2 contains the large spin evolution in the Bloch sphere – in addition to the large spin magnetization from $\langle \hat{J}^z \rangle = -j$ to $+j$ a precession with frequency B occurs. The time for the magnetization reversal (switching time), however, does not depend on the external magnetic field.

Since the coupling parameter λ provides the number of spin-flips per unit time and Γ the number of electrons entering the left QD per unit time the switching time is determined by their ratio: It diverges when $\lambda/\Gamma \to 0$ and saturates for $\lambda/\Gamma \simeq 1$ as long as the tunnel coupling T_c between the QDs is on the order of Γ. This provides a lower bound for the switching time, whereas for $T_c/\Gamma \gg 1$ and $\ll 1$ it increases.

Aside from the magnetization time scale, we observe that the onset of the switching process depends on the initial orientation of the large spin. In particular, if it is nearly aligned with magnetic field ($\langle \hat{J}^z \rangle_0 \approx j$) the spin-flip rate becomes significantly diminished, since the corresponding coupling is proportional to $\lambda(\langle \hat{J}^x \rangle + \langle \hat{J}^y \rangle)$ [see eq. (6.4)]. This leads to a slowing down of the magnetization onset; in the limit $\langle \hat{J}^z \rangle_0 = j$ the large spin keeps his initial orientation.

Arbitrary lead polarizations. So far we have addressed complete reverse lead polarizations. However, switching also takes place for arbitrary p_L and p_R as shown in fig. 6.3(a). The direction of the spin torque is schematically depicted by vertical arrows depending on p_L and p_R together with the steady-state current (6.14) as contour plot. For $p_L < p_R$ ($p_L > p_R$) the large spin will switch to the spin-down (spin-up) direction, respectively. Note that this holds only for parameters $\lambda j/\Gamma \leq \frac{1}{2}$ or $\lambda j/\Gamma \geq 2$, respectively. If $\frac{1}{2} < \lambda j/\Gamma < 2$ the transition between up- and down-switching lies in the region bounded by $p_R = p_L$ and $p_R \approx 2.6\, p_L$ for $\lambda j/\Gamma = 1$. In this area the transition lines are not linear with respect to p_L, as shown for $\lambda j/\Gamma = 1.25$ in fig. 6.3(a).

The switching time is also affected by the choice of lead polarizations. Given that $|p_L| = |p_R| = |p|$, the switching time decreases with decreasing $|p|$, as depicted in Fig.6.4. Given a fixed left lead polarization $|p_L| < 1$, while p_R is variable, the switching time has a lower bound for the minimum of $-p_L/p_R$. On the other hand the spin transfer is increased as the left lead polarization is increased. Thus, the switching time is minimized for complete reverse lead polarization $p_L = -p_R = \pm 1$.

In the nonmagnetic case $p_L = p_R = 0$ [origins in Figs. 6.3(a) and (b)] no switching takes place and the electron spin state ends up in a completely mixed state. When both QDs are presumed to be initially unoccupied the electronic spin state is completely mixed for the entire evolution. Consequently, the large spin evolves independently of the electron spins. This enables an effective description of the electron spin dynamics presented in Appendix A.5. The situation, however, changes when the QDs are initially occupied. During the decay of the electronic state into a complete mixture the large spin evolution becomes affected and possesses transient oscillations

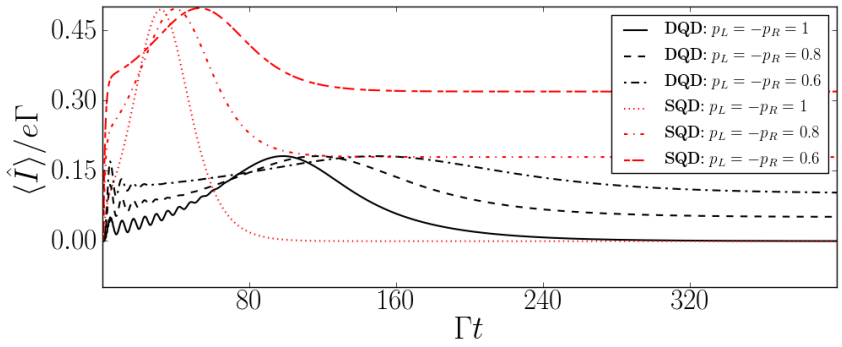

Figure 6.4.: Time-dependent currents in single-QD and DQD setup for different contact polarizations p_L and p_R during the process of magnetization reversal. The currents possess a maximum when $\langle \hat{J}^z \rangle = 0$. With decreasing $|p_L| = |p_R|$ the time for magnetization switching increases. In DQD the switching time is always larger than for the single-QD. Parameters: $\lambda/\Gamma = 1$, $T_c/\Gamma = 0.5$, $B/\Gamma = 0.1$

before it runs into the back-action free precession for $\gamma_J = 0$. The frequency of the transient oscillations depend on the parameter λ/Γ while their duration is governed by Γ. It follows that in the undamped case the large spin steady state depends on the initial QD occupation.

Isotropic coupling with difference between left and right site. For a coupling scheme where the components of one electronic spin are isotropic, i.e. $\lambda_i^\alpha = \lambda_i$ $(\forall \alpha)$ but the coupling differs between the two electronic sites, i.e, $\lambda_L \neq \lambda_R$, we observe in principle the same current-induced magnetization behavior as before. However, the difference $\Delta\lambda \equiv \lambda_L - \lambda_R$ has an impact on the specific behavior, for instance, on the switching times. The more the couplings differ, i.e. for increasing $|\Delta\lambda|$, the longer the switching takes. Given that the coupling strengths are on the order of magnitude of the tunneling rates, the sign of $\Delta\lambda$ is of subordinate importance.

6.3.3. Comparison with single-QD

In the following we will compare the phenomenon of current-induced switching in a single-QD and in the DQD in the same semiclassical description. Again, we consider the Hamiltonian $\hat{H} = \hat{H}_{\mathrm{SQD}} + \hat{H}_{\mathrm{J}} + \hat{H}_{\mathrm{int}} + \hat{H}_{\mathrm{leads}} + \hat{H}_{\mathrm{T}}$ with its components defined in eq. (4.2). Using the EOM technique introduced in Sec. 6.2.3 and the Lindblad master equation for the SQD setup

$$\begin{aligned}\frac{d}{dt}\hat{\rho}(t) = &-\mathbf{i}\left[\hat{H}_{\mathrm{SQD}}, \hat{\rho}(t)\right] \\ &-\frac{1}{2}\sum_\sigma \Bigg[\Gamma_{L\sigma}\left(\left\{\hat{d}_\sigma \hat{d}_\sigma^\dagger, \hat{\rho}(t)\right\} - 2\hat{d}_\sigma^\dagger \hat{\rho}(t)\hat{d}_\sigma\right) \\ &+\Gamma_{R\sigma}\left(\left\{\hat{d}_\sigma^\dagger \hat{d}_\sigma, \hat{\rho}(t)\right\} - 2\hat{d}_\sigma \hat{\rho}(t)\hat{d}_\sigma^\dagger\right)\Bigg],\end{aligned} \tag{6.18}$$

we obtain the following EOM for the QD occupations, the electron spin, and the large spin ($\Gamma \equiv \Gamma_L = \Gamma_R$, omitting the time dependence):

$$\frac{d}{dt}\langle\hat{n}^\sigma\rangle = \Big(\lambda^x\langle\hat{J}^x\rangle\langle\hat{S}^y\rangle - \lambda^y\langle\hat{J}^y\rangle\langle\hat{S}^x\rangle\Big)(\delta_{\sigma\uparrow}-\delta_{\sigma\downarrow}) - (\Gamma_{R\sigma}+\Gamma_{L\sigma})\langle\hat{n}^\sigma\rangle + \Gamma_{L\sigma}(1-\hat{n}_{\bar{\sigma}}) ,$$
$$\frac{d}{dt}\langle\hat{\vec{S}}\rangle = \big[\langle\hat{\vec{J}}'\rangle + B\vec{e}_z\big]\times\langle\hat{\vec{S}}\rangle - \frac{1}{2}\Gamma\langle\hat{\vec{S}}\rangle - \frac{1}{2}\Gamma(p_L+p_R)\langle\hat{N}\rangle\,\vec{e}_z + \frac{1}{2}\Gamma\,p_L\,\vec{e}_z ,$$
$$\frac{d}{dt}\langle\hat{\vec{J}}\rangle = \big[\langle\hat{\vec{S}}'\rangle + B\vec{e}_z\big]\times\langle\hat{\vec{J}}\rangle , \tag{6.19}$$

with $\langle\hat{\vec{S}}'\rangle \equiv \sum_\alpha \lambda^\alpha\langle\hat{S}^\alpha\rangle\vec{e}_\alpha$, $\langle\hat{\vec{J}}'\rangle \equiv \sum_\alpha \lambda^\alpha\langle\hat{J}^\alpha\rangle\vec{e}_\alpha$ and $\langle\hat{N}\rangle = \langle\hat{n}_\uparrow\rangle + \langle\hat{n}_\downarrow\rangle$, which is the infinite bias version of eq. (4.60). The anisotropic version of these equations ($\lambda^x = \lambda^z = \lambda$ and $\lambda^y = 0$) has been already studied in Ref. [128], but with a different focus. For isotropic coupling Fig. 6.3(b) presents the steady-state current and the final direction of the large spin depicted as vertical arrows in dependence on the lead polarizations p_L and p_R. The transition between the two directions occurs for $p_L = p_R$, which has been also obtained in Ref. [152]. There the magnetization change was discussed in terms of the sign of the spin-transfer torque, which is determined by $\mathrm{sgn}[\Gamma_{L\downarrow}\Gamma_{R\uparrow} - \Gamma_{L\uparrow}\Gamma_{R\downarrow}]$. In contrast to the switching in DQD [see Fig. 6.3(a)] the transition does not depend on λ or j. We further note that since the electrons are assumed to be noninteracting in the single-QD the current is symmetric with respect to an exchange of p_L and p_R. This does not hold for the DQD.
The comparison of the current evolutions for both setups (as shown in Fig. 6.4) reveals that the SQD switching occurs always faster for the same set of parameters. In other words the coherent electron transfer between the QDs slows down the switching.

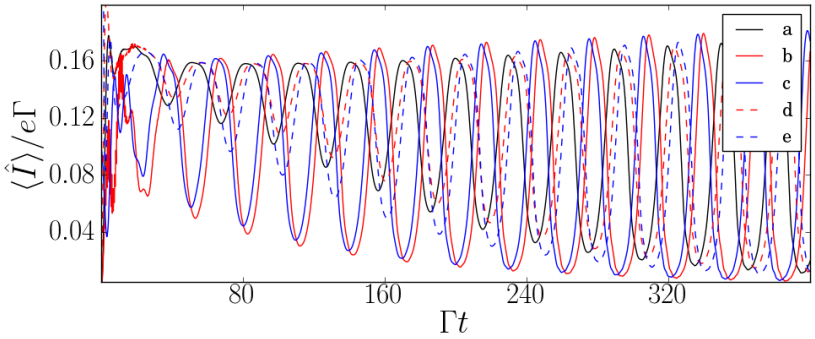

Figure 6.5.: Time-dependent currents in the case of undamped large spin for different initial system state: (a) empty DQD , (b) $n_{L\uparrow}(0) = 1$, (c) $n_{L\downarrow}(0) = 1$, (d) $n_{R\uparrow}(0) = 1$ and (e) $n_{R\downarrow}(0) = 1$. The dominating oscillation frequencies are multiples of $2B$ for all currents (parametric resonance; see text), but we observe phase shifts and different magnitudes. Parameters: $p_L = p_R = -0.9$, $B/\Gamma = 0.1$, $T_c/\Gamma = 0.4$, $\lambda_L^\alpha = \lambda_R^x = \lambda_R^z = \Gamma$, $\lambda_R^y = 0$.

6.3.4. Anisotropic coupling

Large spin switching. Given the investigations of the spin magnetization reversal in the isotropic case we probe for anisotropic coupling schemes that yield spin switching as well. In principle we observe that the switching process takes place as long as the x-and y-components of the spins are isotropically coupled ($\lambda_i^x \approx \lambda_i^y$, $\forall i$) and the leads polarized suitably. Taking into account the microscopic spin interaction [see Sec. 6.3.2] this becomes clear since the λ_i^z terms are not directly contributing in the spin-transfer process. However, the $z-$couplings affect

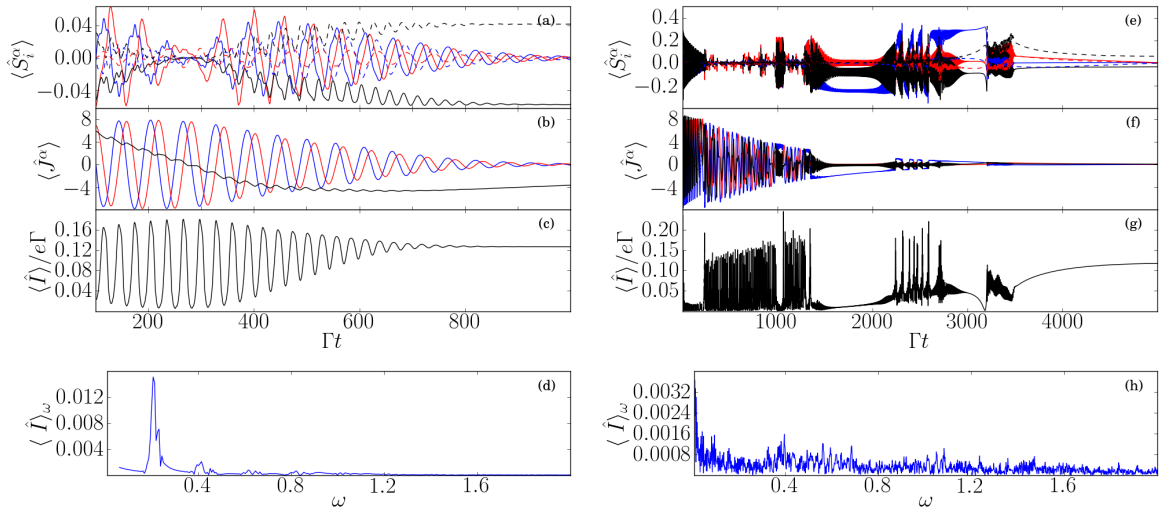

Figure 6.6.: Different transient currents for a setup with strongly polarized contacts ($p_L = p_R = -0.9$ and $T_c/\Gamma = 0.4$, $B/\Gamma = 0.1$, $\varepsilon = 0$, $\gamma_J/\Gamma = 10^{-3}$) and different couplings between spins: (Left) $\lambda_L^\alpha = \lambda_R^x = \lambda_R^z = \Gamma$, $\lambda_R^y = 0$ and (Right) $\lambda_L^x/\Gamma = 0.2$, $\lambda_L^y/\Gamma = 4.2$, $\lambda_L^z/\Gamma = 1.3$, $\lambda_R^x/\Gamma = 2.9\,, \lambda_R^y/\Gamma = 1.5$, $\lambda_R^z/\Gamma = 0.7$. (a) and (e) Components of the electron spin $\langle \hat{S}_L^x \rangle$ (blue, solid), $\langle \hat{S}_R^x \rangle$ (blue, dashed) $\langle \hat{S}_L^y \rangle$ (red, solid), $\langle \hat{S}_L^y \rangle$ (red, dashed), $\langle \hat{S}_L^z \rangle$ (black, solid), $\langle \hat{S}_R^z \rangle$ (black, dashed). (b) and (f) Components of the large spin: $\langle \hat{J}^x \rangle$ (blue), $\langle \hat{J}^y \rangle$ (red), $\langle \hat{J}^z \rangle$ (black). (c) and (g) Electronic current $\langle I \rangle (t)$ vs. time. The steady-state current is given by Eq. (6.14). (d) and (h) In the current spectrum of (c) the dominating frequencies are even multiples (2,4,6...) of the large spin Larmor frequency B, which refers to the phenomenon of parametric resonance (see text). The current spectrum of (g) is broad and noisy, which we attribute to chaotic behavior (see also Ref. [128]). For both cases holds: As the large spin is damped out, the current oscillations vanish, since no more spin-flips occur.

the speed of magnetization reversal: The magnetization process, e.g., can be slowed down by increasing the $z-$ couplings on both sites: $\lambda_L^z = \lambda_R^z \equiv \lambda^z > \lambda$. Contrariwise, decreasing λ^z steps up the switching. Even if the z-couplings are different switching occurs. The corresponding currents display a peak at the time when the derivative of $\langle \hat{J}^z \rangle (t)$ is maximal.

Nonmagnetic leads $p_L = p_R = 0$. Basically the same as for the isotropic coupling holds. In addition we find that the transient phase and, thus, the polar angle for the free precession depend crucially on the initial electronic states.

Undamped large spin $\gamma_J = 0$. We obtain various regimes with respect to lead polarization and spin coupling that exhibit limit cycles in the current, similar to Ref. [128] and chapter 4. The Fourier spectra of those current time evolutions exhibit peaks at well defined frequencies, confirming the periodicity of the system's evolution. We note that in contrast to the single-QD the initial system occupation plays an important rôle in the evolution of both the DQD and the large spin, which is illustrated in Fig. 6.5. A similar observation has been made in Ref. [122]. For a more detailed analysis the fix points of the EOM have to be determined. Unfortunately, due to the size and complexity of the EOM, we did not manage to find them analytically. Even their numerical computation provides a complicated task.

Parametric resonance. Studying the rich dynamics provided by the anisotropy, we can observe parametric resonance in the current oscillations, particularly. The evolutions exhibit current oscillations at multiples of the doubled Larmor frequency of the large spin, i.e. $2B$, as can be seen in Figs. 6.6(a)– 6.6(c). Although the periodic oscillations are in general very complicated, due to the nonlinearity in the equations, the dominating frequency of the oscillations of the x and y components of the electron spins, respectively, is B. The z component and consequently the current, on the other hand, oscillates with multiples of $2B$, which we reveal in the Fourier spectrum [Fig. 6.6(d)]. The same phenomenon has been observed in the single-QD, so that we can employ its model to provide an explanation. We assume anisotropic spin-spin coupling, i.e. $\lambda^x = \lambda^z = \lambda$ and $\lambda^y = 0$ and magnetic leads ($p_L, p_R \neq 0$). Given that $\lambda j \ll 1$ we can make use of the back-action free EOM for the large spin (A.20). It follows from Eqs. (6.19) that $\langle \hat{S}^x \rangle$ and $\langle \hat{S}^y \rangle$ oscillate with frequency B. We further recognize that the time derivative of $\langle \hat{n}^\sigma \rangle$ couples to the product $\langle \hat{S}^y \rangle \langle \hat{J}^x \rangle$. Integrating this product of sinusoidal oscillations both with frequency B leads us to the current and $\langle \hat{S}^z \rangle$ oscillating with frequency $2B$ [cf. section 3.3 and [105]].
Given that the large spin is damped by the rate γ_J the evolutions for different initial DQD occupations match in the long-time limit. Consequently, the periodic or nonperiodic oscillations are only present during the transients (as shown in the panels of Fig. 6.6). We observe different transient scenarios ranging from quasiperiodic [(a)–(d)] to chaotic motion [(e)–(h)]. In all cases the steady-state current is given by (6.14).

6.4. Conclusions

In this chapter we have studied electron transport through a DQD setup coupled to electronic contacts . The spin of the excess electrons in the DQD interacts with a large spin and an external magnetic field is applied. We use semiclassical Ehrenfest EOM together with a quantum master equation technique. This method works well if one assumes that the dwell time of the electrons is much smaller than the average large spin precession period.
We have found that the coupled dynamics of the large spin and the electron spins as well as the current through the DQD structure strongly depend on the polarization of the electronic leads and on the isotropy of the spin-spin coupling. Particularly, if the coupling between electron spin and large spin is isotropic with respect to x and y while the electronic leads are reversely polarized, a current-induced magnetization process of the large spin is obtained. The speed of this switching is always lower than for a single-QD setup and depends, most importantly, on the lead polarization.
On the other hand, a complete anisotropic coupling leads to a rich variety of different dynamical scenarios, which for an undamped large spin depend on the initial state. In particular, we have found that the electronic system may show self-sustained oscillations, either quasi-periodic or even chaotic. Introducing a large spin damping renders these dynamics to be transient. A remarkable feature of the undamped or damped dynamics is the occurence of parametric resonance, observable as frequency doubling in the current. Furthermore, we analytically have derived the stationary currents for the spin-dependent unidirectional single-electron transport, when no interactions with the external spin are present. It turns out that this current also applies for the case of current-polarized or damped large spin.
Experimental realizations for the large spin could be either the spin of magnetic impurities in semiconductor QDs or a net magnetic moment in single molecules (single molecular magnets). Whether our mean-field approach is applicable for these examples, where the spin typically is not very large, needs further investigations. However, one possible realization for the large spin,

that might justify the semiclassical treatment is the hyperfine interaction with an ensemble of nuclear spins, where the number of spins is reasonably high [157].

7. Summary

In this thesis we used a combined theory to study the complex dynamics of electronic transport through QD structures in an external magnetic field. We applied a Markovian master equation approach to model the transport and additionally exploited a semiclassical theory to model the nonlinear spin-dynamics that arise when the electron spins of the excess electrons in the QDs interact with external angular momenta via an exchange coupling. The semiclassical approach is particularly justified for large external spins, e.g., the collective nuclear spins of the surrounding material. Moreover, there is an implicit adiabatic approximation in the derivation as we assumed that the precession of the large external spin is significantly slower than the electronic tunneling. Thus, we obtain sets of equations of motion that can be solved numerically in an efficient way and disclose at least some analytic features, such as fixed points. As an extension to the method used in Ref. [128] our equations of motion for the SQD case work also for finite bias voltages. The numerical solutions provide the time traces of often complicated dynamics that are not only prone to the choice of parameters but also to the initial conditions.

Anisotropic couplings between electronic spins and the external spin give rise to different regimes of complex nonlinear dynamics. For the model of two coupled spins – with or without dissipation – we found fixed points, that are either stable centers or saddle points. Regular or quasi-periodic oscillations occur. The determining parameters are the strength of the external magnetic field and the dissipation rates in relation to the exchange coupling between the spins, which clearly separates the phase-space into distinct regions, where qualitatively different behaviors occur. The oscillations are damped if the dissipation exceeds a critical rate and if the magnetic field is smaller than a critical magnetic field. Above that critical field oscillations remain undamped and the system can be mapped on an effective model.
For both SQD and DQD setup as well as for nondissipative setups we have found common effects such as parametric resonance. If the exchange interaction is isotropic we observed that spin polarized currents switch the external spin to a position (anti-)parallel to the magnetic field, where the current polarization determines the speed of the switching. In the DQD setup the switching process is additionally slowed down due to the coherent coupling between the QDs.
Spin systems – particularly with anisotropic coupling – often display chaotic dynamics. The nondissipative system is completely integrable only if the magnetic field is vanishing. For higher magnetic fields chaos occurs for large parts of the phase-space of the semiclassical models, but signatures of chaos emerge also in the quantum versions, as the quantum webs of simultaneous eigenvalues are disrupted by higher fields. For the transport systems chaos is spotted the easiest when computing the Fourier analyses of the time traces of the spins' components or the currents. In transport systems chaos is most likely to appear for smaller magnetic fields and smaller tunneling rates. For magnetic fields higher than the critical field no chaos occurs. On the other hand, one has to be aware that especially for the regime of low magnetic fields higher-order transitions due to couplings of the external spin and the transport leads can be relevant and our approach might miss parts of the dynamics as A. Metelmann pointed out [105].

Furthermore, we equipped the SQD model with a Maxwell-demon like feedback that modifies the transport Liouvillian based on the measurement of the QD-occupation. Due to this modification

the device is useful to generate currents against a moderate chemical bias. We were able to define feedback schemes that implement a spin filter that generates currents where ↑- and ↓-currents have opposite directions. When the spin interaction is turned off one finds constant currents, but under certain conditions even periodically oscillating currents in opposite directions are possible when the spin interaction is present.
Finally, we were able to find a microscopic implementation for the Maxwell demon in terms of an extension of the model P. Strasberg introduced in Ref. [44]. In this model we mapped the spin-σ levels in the SQD on two parallel QDs that interact capacitively with a third QD, the detector. The interaction between DQD and detector than triggers different tunnel couplings. With this generic model we were able to reproduce the spin-filtering effects generated by the phenomenological feedback introduced in the SQD model. The derivation of the dynamics of the generic demon model makes use of the Markovian master equation theory we introduced and we, further, used a coarse graining approach to reduce the amount of equations that describe the transport characteristics under feedback.
The generic model also works for coherently coupled QDs, although, with some restrictions. In order to find a microscopic implementation of the feedback when the spin interaction is present one has to exploit time-dependent theories, as there are many oscillating parameters. This might be part of future research.

A. Appendix

A.1. Simplified model for limit oscillation around $\vec{J}_z = -B/\lambda$

For this model $\langle \hat{J}_z \rangle$ is fixed and we transform the equations to a rotation-invariant frame by using the rotation matrix around the z-axis to obtain a stationary $\vec{\tilde{J}}$ [cf. [128]]. Note that the effective rotation frequency B_{eff} is not B, since the backaction of the electronic system on the precessing large spin is changing this frequency. The transformation reads

$$\begin{aligned}
\langle \vec{\hat{S}} \rangle &= \mathrm{e}^{-\Gamma t}\, \mathbf{R}_S(t)\, \langle \vec{\tilde{S}} \rangle \,, \qquad \mathbf{R}_S(t) = \begin{pmatrix} \cos(B_{\text{eff}}t) & -\sin(B_{\text{eff}}t) & 0 & 0 \\ \sin(B_{\text{eff}}t) & \cos(B_{\text{eff}}t) & 0 & 0 \\ 0 & 0 & 1 & 0 \\ 0 & 0 & 0 & 1 \end{pmatrix}, \\
\langle \vec{\hat{J}} \rangle &= \mathbf{R}_J(t)\, \langle \vec{\tilde{J}} \rangle \,, \qquad \mathbf{R}_J(t) = \begin{pmatrix} \cos(B_{\text{eff}}t) & -\sin(B_{\text{eff}}t) & 0 \\ \sin(B_{\text{eff}}t) & \cos(B_{\text{eff}}t) & 0 \\ 0 & 0 & 1 \end{pmatrix}.
\end{aligned} \tag{A.1}$$

Using the inverse transformations $\langle \vec{\tilde{S}} \rangle = \mathrm{e}^{\Gamma t}\, \mathbf{R}_S^{-1}\, \langle \vec{\hat{S}} \rangle$ and $\langle \vec{\tilde{J}} \rangle = \mathbf{R}_J^{-1}\, \langle \vec{\hat{J}} \rangle$ we can calculate the eom for the spin components in the rotation invariant frame

$$\begin{aligned}
\frac{d}{dt} \langle \vec{\tilde{S}} \rangle &= \mathrm{e}^{\Gamma t}\, \mathbf{R}_S^{-1} \frac{d \langle \vec{\hat{S}} \rangle}{dt} + \frac{d\mathbf{R}_S^{-1}}{dt} \mathbf{R}_S \langle \vec{\tilde{S}} \rangle + \Gamma \mathbf{R}_S^{-1} \mathbf{R}_S \langle \vec{\tilde{S}} \rangle \,, \\
\frac{d}{dt} \langle \vec{\tilde{J}} \rangle &= \mathbf{R}_J^{-1} \frac{d \langle \vec{\hat{J}} \rangle}{dt} + \frac{d\mathbf{R}_J^{-1}}{dt} \mathbf{R}_J \langle \vec{\tilde{J}} \rangle \,.
\end{aligned} \tag{A.2}$$

Inserting Eqs. (4.60) and (4.62) and applying the spin-valve feedback scheme, anisotropic

coupling, and the infinite bias setup with tunneling rates $\Gamma_{R\downarrow}=0, \Gamma_{L\uparrow}=\Gamma_{R\uparrow}=\Gamma_{L\downarrow}=\Gamma$, we obtain

$$
\begin{aligned}
\frac{d}{dt}\langle\tilde{S}_x\rangle &= -\lambda\left(\langle\tilde{J}_x\rangle\cos(B_{\text{eff}}t)-\langle\tilde{J}_y\rangle\sin(B_{\text{eff}}t)\right)\sin(B_{\text{eff}}t)\langle\tilde{S}_z\rangle-\lambda\langle\tilde{J}_z\rangle\langle\tilde{S}_y\rangle+\frac{\Gamma}{2}\langle\tilde{S}_x\rangle\,,\\
\frac{d}{dt}\langle\tilde{S}_y\rangle &= -\lambda\left(\langle\tilde{J}_x\rangle\cos(B_{\text{eff}}t)-\langle\tilde{J}_y\rangle\sin(B_{\text{eff}}t)\right)\cos(B_{\text{eff}}t)\langle\tilde{S}_z\rangle+\lambda\langle\tilde{J}_z\rangle\langle\tilde{S}_x\rangle+\frac{\Gamma}{2}\langle\tilde{S}_y\rangle\,,\\
\frac{d}{dt}\langle\tilde{n}_\uparrow\rangle &= \lambda\left[\left(\langle\tilde{J}_x\rangle\cos(B_{\text{eff}}t)-\langle\tilde{J}_y\rangle\sin(B_{\text{eff}}t)\right)\left(\langle\tilde{S}_x\rangle\sin(B_{\text{eff}}t)+\langle\tilde{S}_y\rangle\cos(B_{\text{eff}}t)\right)\right]\,,\\
&\quad+\Gamma\left(1-2\,\mathrm{e}^{\delta}\right)\langle\tilde{n}_\uparrow\rangle-\mathrm{e}^{\delta}\,\Gamma\langle\tilde{n}_\downarrow\rangle+\mathrm{e}^{\delta-\Gamma t}\,\Gamma\,,\\
\frac{d}{dt}\langle\tilde{n}_\downarrow\rangle &= -\lambda\left[\left(\langle\tilde{J}_x\rangle\cos(B_{\text{eff}}t)-\langle\tilde{J}_y\rangle\sin(B_{\text{eff}}t)\right)\left(\langle\tilde{S}_x\rangle\sin(B_{\text{eff}}t)+\langle\tilde{S}_y\rangle\cos(B_{\text{eff}}t)\right)\right]\\
&\quad+\Gamma\left(1-\mathrm{e}^{\delta}\right)\langle\tilde{n}_\downarrow\rangle-\mathrm{e}^{\delta}\,\Gamma\langle\tilde{n}_\uparrow\rangle+\mathrm{e}^{\delta-\Gamma t}\,\Gamma\,,\\
\frac{d}{dt}\langle\tilde{J}_x\rangle &= -\lambda\,\mathrm{e}^{-\Gamma t}\left[\left(\langle\tilde{S}_x\rangle\cos(B_{\text{eff}}t)-\langle\tilde{S}_y\rangle\sin(B_{\text{eff}}t)\right)\sin(B_{\text{eff}}t)\langle\tilde{J}_z\rangle+\langle\tilde{S}_z\rangle\langle\tilde{J}_y\rangle\right]\,,\\
\frac{d}{dt}\langle\tilde{J}_y\rangle &= \lambda\,\mathrm{e}^{-\Gamma t}\left[-\left(\langle\tilde{S}_x\rangle\cos(B_{\text{eff}}t)-\langle\tilde{S}_y\rangle\sin(B_{\text{eff}}t)\right)\cos(B_{\text{eff}}t)\langle\tilde{J}_z\rangle+\langle\tilde{S}_z\rangle\langle\tilde{J}_x\rangle\right]\,,\\
\frac{d}{dt}\langle\tilde{J}_z\rangle &= \lambda\,\mathrm{e}^{-\Gamma t}\left[\left(\langle\tilde{S}_x\rangle\cos(B_{\text{eff}}t)-\langle\tilde{S}_y\rangle\sin(B_{\text{eff}}t)\right)\left(\langle\tilde{J}_x\rangle\sin(B_{\text{eff}}t)+\langle\tilde{J}_y\rangle\cos(B_{\text{eff}}t)\right)\right]\,.
\end{aligned}
\tag{A.3}
$$

In the long-time limit the equations for $\vec{\tilde{J}}$ are stationary; thus, $\tilde{J}_i$ are constants in the equations for $\vec{\tilde{S}}$, and thus the number of equations is reduced in this effective model. From the numerical solutions we know that the large spin's z-component assumes a characteristic value that is related two the fixed points $\mathcal{P}_{\text{IB}}^{\pm y,\pm}$, namely, $\langle\hat{J}_z\rangle=\langle\tilde{J}_z\rangle=-B/\lambda$, and since the large spin is precessing almost unperturbed we can further assume $\langle\tilde{J}_x\rangle=\langle\tilde{J}_y\rangle=\frac{1}{\sqrt{2}}\sqrt{j^2-\frac{B^2}{\lambda^2}}$. The reduced set of equations for the effective model is obtained by applying the inverse transformation. We get

$$
\frac{d}{dt}\langle\vec{\hat{S}}\rangle=\mathrm{e}^{-\Gamma t}\,\mathbf{R}_S\frac{\langle\vec{\tilde{S}}\rangle}{dt}+\frac{d\mathbf{R}_S}{dt}\mathbf{R}_S^{-1}\langle\vec{\hat{S}}\rangle-\Gamma\langle\vec{\hat{S}}\rangle\,,
\tag{A.4}
$$

which leads to (4.81).

A.2. Finite bias fixed points and stationary states

The $\langle\hat{S}_z^*\rangle$-components of the fixed points $\mathcal{P}_{\text{FB}}^{\pm}$ read for scheme A and B

$$
\begin{aligned}
\mathcal{B}_{4\pm}^{\text{A}} &= \frac{\mathrm{e}^{\tilde{V}/2}\left(-\mathrm{e}^{\delta+\tilde{\varepsilon}_z^{\pm}}+\mathrm{e}^{2\delta}+1\right)-\mathrm{e}^{3\delta+\tilde{\varepsilon}_z^{\pm}+\frac{3\tilde{V}}{2}}-\left(\mathrm{e}^{2\delta+\tilde{\varepsilon}_z^{\pm}}-\mathrm{e}^{\delta}+\mathrm{e}^{\tilde{\varepsilon}_z^{\pm}}\right)\mathrm{e}^{\delta+\frac{\tilde{\varepsilon}_z^{\pm}}{2}+\tilde{V}}+\mathrm{e}^{\tilde{\varepsilon}_z^{\pm}/2}}{2\left(\left(\mathrm{e}^{2\delta+\tilde{\varepsilon}_z^{\pm}}+2\,\mathrm{e}^{\delta}+\mathrm{e}^{\tilde{\varepsilon}_z^{\pm}}\right)\mathrm{e}^{\delta+\frac{\tilde{\varepsilon}_z^{\pm}}{2}+\tilde{V}}+\mathrm{e}^{3\delta+\tilde{\varepsilon}_z^{\pm}+\frac{3\tilde{V}}{2}}+\mathrm{e}^{\tilde{V}/2}\left(\left(\mathrm{e}^{\delta}+\mathrm{e}^{2\delta}+1\right)\mathrm{e}^{\tilde{\varepsilon}_z^{\pm}}+\mathrm{e}^{2\delta}+1\right)+2\,\mathrm{e}^{\tilde{\varepsilon}_z^{\pm}/2}\right)}\,,\\
\mathcal{B}_{4\pm}^{\text{B}} &= \frac{1}{2}\left(\frac{\left(\mathrm{e}^{2\delta}+1\right)\left(\mathrm{e}^{\tilde{\varepsilon}_z^{\pm}}+2\right)\mathrm{e}^{\tilde{V}/2}+3\,\mathrm{e}^{2\delta+\frac{\tilde{\varepsilon}_z^{\pm}}{2}+\tilde{V}}+3\,\mathrm{e}^{\tilde{\varepsilon}_z^{\pm}/2}}{\left(\mathrm{e}^{2\delta}+1\right)\mathrm{e}^{\frac{3}{2}\tilde{\varepsilon}_z^{\pm}+\tilde{V}}+\mathrm{e}^{2\delta+\tilde{\varepsilon}_z^{\pm}+\frac{\tilde{V}}{2}}+2\,\mathrm{e}^{2\delta+\frac{\tilde{\varepsilon}_z^{\pm}}{2}+\tilde{V}}+\mathrm{e}^{2\delta+\tilde{\varepsilon}_z^{\pm}+\frac{3\tilde{V}}{2}}+\mathrm{e}^{2\delta+\frac{\tilde{V}}{2}}+2\,\mathrm{e}^{\tilde{\varepsilon}_z^{\pm}+\frac{\tilde{V}}{2}}+2\,\mathrm{e}^{\tilde{\varepsilon}_z^{\pm}/2}+\mathrm{e}^{\tilde{V}/2}}-1\right)\,,
\end{aligned}
\tag{A.5}
$$

with the parameters

$$
\tilde{\varepsilon}_z^{\pm}\equiv\beta(B\pm\lambda j)\,,\quad \tilde{V}\equiv\beta V\,.
\tag{A.6}
$$

If one of the fixed points $\mathcal{P}_{\text{FB}}^{\pm}$ is reached the exchange interaction becomes ineffective and the two spin-current channels decouple. Due to the tunneling setup $\Gamma_{L\uparrow}=\Gamma_{L\downarrow}=\Gamma_{R\uparrow}=\Gamma, \Gamma_{R\downarrow}=0$, there is no net $\downarrow$-current ($\langle I_{L\downarrow}^{\pm}\rangle=-\langle I_{R\downarrow}^{\pm}\rangle=0$) and for $\uparrow$-current we obtain $\langle I_{R\uparrow}^{\pm}\rangle=-\langle I_{L\uparrow}^{\pm}\rangle=\langle I_{\uparrow}^{\pm}\rangle$,

which read with respect to the two feedback schemes

$$
\begin{aligned}
\frac{\langle I_{\uparrow}^{+\mathrm{A}}\rangle}{e\Gamma} &= \frac{\mathrm{e}^{\frac{\tilde{\varepsilon}_z^+}{2}-\delta}\left(\mathrm{e}^{4\delta+\tilde{V}}-1\right)}{\mathrm{e}^{\delta+\tilde{\varepsilon}_z^++\frac{\tilde{V}}{2}}+\mathrm{e}^{2\delta+\tilde{\varepsilon}_z^++\frac{\tilde{V}}{2}}+\mathrm{e}^{\delta+\frac{3\tilde{\varepsilon}_z^+}{2}+\tilde{V}}+\mathrm{e}^{3\delta+\frac{3\tilde{\varepsilon}_z^+}{2}+\tilde{V}}+\mathrm{e}^{3\delta+\tilde{\varepsilon}_z^++\frac{3\tilde{V}}{2}}+2\,\mathrm{e}^{2\delta+\frac{1}{2}(\tilde{\varepsilon}_z^++2\tilde{V})}+\mathrm{e}^{2\delta+\frac{\tilde{V}}{2}}+\mathrm{e}^{\tilde{\varepsilon}_z^++\frac{\tilde{V}}{2}}+2\,\mathrm{e}^{\tilde{\varepsilon}_z^+/2}+\mathrm{e}^{\tilde{V}/2}}\,,\\
\frac{\langle I_{\uparrow}^{-\mathrm{A}}\rangle}{e\Gamma} &= \frac{\mathrm{e}^{\tilde{a}-\delta}\left(\mathrm{e}^{4\delta+\tilde{V}}-1\right)}{\mathrm{e}^{2\delta}\left(\mathrm{e}^{\frac{1}{2}(\tilde{d}+V)}+2\,\mathrm{e}^{\tilde{a}+V}+\mathrm{e}^{\frac{\tilde{b}+\tilde{V}}{2}}\right)+\mathrm{e}^{3\delta}\left(\mathrm{e}^{\frac{1}{2}(\tilde{d}+3V)}+\mathrm{e}^{\tilde{c}+\tilde{V}}\right)+\mathrm{e}^{\frac{1}{2}(\tilde{d}+V)+\delta}+\mathrm{e}^{\frac{1}{2}(\tilde{d}+V)}+2\,\mathrm{e}^{\tilde{a}}+\mathrm{e}^{\frac{\tilde{b}+\tilde{V}}{2}}+\mathrm{e}^{\tilde{c}+\delta+\tilde{V}}}\,,\\
\frac{\langle I_{\uparrow}^{+\mathrm{B}}\rangle}{e\Gamma} &= \frac{\mathrm{e}^{\frac{\tilde{\varepsilon}_z^+}{2}-\delta}\left(\mathrm{e}^{4\delta+\tilde{V}}-1\right)}{\mathrm{e}^{2\delta}\left(\mathrm{e}^{\tilde{\varepsilon}_z^++\frac{\tilde{V}}{2}}+\mathrm{e}^{\tilde{\varepsilon}_z^++\frac{3\tilde{V}}{2}}+2\,\mathrm{e}^{\frac{1}{2}(\tilde{\varepsilon}_z^++2\tilde{V})}+\mathrm{e}^{\frac{1}{2}(3\tilde{\varepsilon}_z^++2\tilde{V})}+\mathrm{e}^{\tilde{V}/2}\right)+2\,\mathrm{e}^{\tilde{\varepsilon}_z^++\frac{\tilde{V}}{2}}+\mathrm{e}^{\frac{1}{2}(3\tilde{\varepsilon}_z^++2\tilde{V})}+2\,\mathrm{e}^{\tilde{\varepsilon}_z^+/2}+\mathrm{e}^{\tilde{V}/2}}\,,\\
\frac{\langle I_{\uparrow}^{-\mathrm{B}}\rangle}{e\Gamma} &= \frac{\mathrm{e}^{\tilde{a}-\delta}\left(\mathrm{e}^{4\delta+\tilde{V}}-1\right)}{\mathrm{e}^{2\delta}\left(\mathrm{e}^{\frac{1}{2}(\tilde{a}+\tilde{c}+\tilde{V})}+\mathrm{e}^{\frac{1}{2}(\tilde{a}+\tilde{c}+3\tilde{V})}+2\,\mathrm{e}^{\tilde{a}+\tilde{V}}+\mathrm{e}^{\frac{\tilde{b}+\tilde{V}}{2}}+\mathrm{e}^{\tilde{c}+\tilde{V}}\right)+2\,\mathrm{e}^{\frac{1}{2}(\tilde{a}+\tilde{c}+\tilde{V})}+2\,\mathrm{e}^{\tilde{a}}+\mathrm{e}^{\frac{\tilde{b}+\tilde{V}}{2}}+\mathrm{e}^{\tilde{c}+\tilde{V}}}\,,
\end{aligned}
\tag{A.7}
$$

where the parameters $\tilde{a}\equiv\beta(B/2+\lambda j)\,,\tilde{b}\equiv 3\beta\lambda j\,,\tilde{c}\equiv 3\beta B/2\,,\tilde{d}\equiv\tilde{a}+\tilde{c}$ have been introduced.

If the system has developed towards the fixed points $\mathcal{P}_{\mathrm{FB}}^{\pm y,\pm}$, we only need to consider the spin-dependent currents at the left lead since the currents are balanced ($\langle I_{L\uparrow}^{y}\rangle+\langle I_{L\downarrow}^{y}\rangle=-\langle I_{R\uparrow}^{y}\rangle$). We obtain

$$
\begin{aligned}
\frac{\langle I_{L\downarrow}^{y\mathrm{A}}\rangle}{e\Gamma}C_{\mathrm{A}} &= \left(\mathrm{e}^{2\delta+\frac{\tilde{V}}{2}}+1\right)\left((2B-\lambda)\,\mathrm{e}^{\delta+\frac{\tilde{V}}{2}}+4B+\lambda\right),\\
\frac{\langle I_{L\uparrow}^{y\mathrm{A}}\rangle}{e\Gamma}C_{\mathrm{A}} &= \mathrm{e}^{-\delta}\left((2B-\lambda)\,\mathrm{e}^{4\delta+\tilde{V}}+\mathrm{e}^{2\delta+\frac{\tilde{V}}{2}}\left(-\mathrm{e}^{\delta}(2B+\lambda)-2B+\lambda\right)-2B\left(\mathrm{e}^{\delta}+1\right)+\lambda\right),\\
C_{\mathrm{A}} &= \lambda\left(\mathrm{e}^{\tilde{V}/2}+1\right)\left(5\,\mathrm{e}^{2\delta+\frac{\tilde{V}}{2}}+\mathrm{e}^{\delta}+3\right),\\
\frac{\langle I_{L\downarrow}^{y\mathrm{B}}\rangle}{e\Gamma}C_{\mathrm{B}} &= \mathrm{e}^{\delta}\left(\mathrm{e}^{2\delta+\frac{\tilde{V}}{2}}+1\right)\left(\mathrm{e}^{\tilde{V}/2}(2B-\lambda)+4B+\lambda\right),\\
\frac{\langle I_{L\uparrow}^{y\mathrm{B}}\rangle}{e\Gamma}C_{\mathrm{B}} &= \mathrm{e}^{-\delta}\left((2B-\lambda)\,\mathrm{e}^{4\delta+\tilde{V}}-2\,\mathrm{e}^{3\delta+\frac{\tilde{V}}{2}}(2B\cosh(\delta)+\lambda\sinh(\delta))-2B\left(\mathrm{e}^{2\delta}+1\right)+\lambda\right),\\
C_{\mathrm{B}} &= \lambda\left(\mathrm{e}^{\tilde{V}/2}+1\right)\left(\mathrm{e}^{2\delta}\left(5\,\mathrm{e}^{\tilde{V}/2}+1\right)+3\right).
\end{aligned}
\tag{A.8}
$$

A.3. Commutators for general correlator operators

The most general correlator commutator used in section 6.2.3 reads

$$
\left[\hat{d}_{i\sigma}^{\dagger}\,\hat{d}_{i\sigma'}\,,\hat{d}_{js}^{\dagger}\,\hat{d}_{js'}\right]=\delta_{ij}\left(\delta_{s\sigma'}\,\hat{d}_{i\sigma}^{\dagger}\,\hat{d}_{js}-\delta_{s'\sigma}\,\hat{d}_{js}^{\dagger}\,\hat{d}_{i\sigma'}\right).
\tag{A.9}
$$

More specifically one needs

$$
\begin{aligned}
\left[\hat{n}_{i,\sigma}\,,\hat{S}_j^{+}\right] &= \delta_{ij}\left(\delta_{\sigma\uparrow}\,\hat{S}_i^{+}-\delta_{\sigma\downarrow}\,\hat{S}_i^{-}\right),\\
\left[\hat{n}_{i,\sigma}\,,\hat{S}_j^{-}\right] &= \delta_{ij}\left(\delta_{\sigma\downarrow}\,\hat{S}_i^{+}-\delta_{\sigma\uparrow}\,\hat{S}_i^{-}\right),\\
\left[\hat{S}_i^{+}\,,\hat{S}_j^{-}\right] &= \delta_{ij}\left(\hat{n}_{i\downarrow}-\hat{n}_{j\uparrow}\right),\\
[\hat{n}_{i,\sigma}\,,\hat{n}_{j,\sigma'}] &= \left[\hat{S}_i^{\pm}\,,\hat{S}_j^{\pm}\right]=0\,.
\end{aligned}
\tag{A.10}
$$

A.4. Block-matrices and parameters

Here, we provide the coupling matrices used in the EOM for the electronic part (6.11)

$$\mathbf{L}^{\sigma}\left(\langle\hat{J}^{z}\rangle\right)=\begin{pmatrix}0 & 0 & -\mathbf{i}T_c & \mathbf{i}T_c\\ 0 & -\Gamma_{R\sigma} & \mathbf{i}T_c & -\mathbf{i}T_c\\ -\mathbf{i}T_c & \mathbf{i}T_c & -\frac{\Gamma_{R\sigma}}{2}+\mathbf{i}\varepsilon^{\sigma} & 0\\ \mathbf{i}T_c & -\mathbf{i}T_c & 0 & -\frac{\Gamma_{R\sigma}}{2}-\mathbf{i}\varepsilon^{\sigma}\end{pmatrix}, \tag{A.11}$$

$$\mathbf{A}\left(\langle\hat{J}^{x}\rangle,\langle\hat{J}^{y}\rangle\right)=\begin{pmatrix}-\Lambda_L^- & \Lambda_L^+ & 0 & 0\\ 0 & 0 & -\Lambda_R^- & \Lambda_R^+\\ 0 & 0 & 0 & 0\\ 0 & 0 & 0 & 0\end{pmatrix}, \tag{A.12}$$

$$\mathbf{B}\left(\langle\hat{J}^{x}\rangle,\langle\hat{J}^{y}\rangle\right)=\begin{pmatrix}0 & 0 & 0 & 0\\ 0 & 0 & 0 & 0\\ -\Lambda_R^- & 0 & 0 & \Lambda_L^+\\ 0 & \Lambda_R^+ & -\Lambda_L^- & 0\end{pmatrix}, \tag{A.13}$$

$$\mathbf{C}\left(\langle\hat{J}^{x}\rangle,\langle\hat{J}^{y}\rangle\right)=\begin{pmatrix}0 & 0 & 0 & 0\\ 0 & 0 & 0 & 0\\ \Lambda_L^- & 0 & 0 & -\Lambda_R^+\\ 0 & -\Lambda_L^+ & \Lambda_R^- & 0\end{pmatrix}, \tag{A.14}$$

$$\mathbf{E}=\begin{pmatrix}-\mathbf{i}T_c & 0 & \mathbf{i}T_c & 0\\ 0 & \mathbf{i}T_c & 0 & -\mathbf{i}T_c\\ \mathbf{i}T_c & 0 & -\mathbf{i}T_c & 0\\ 0 & -\mathbf{i}T_c & 0 & \mathbf{i}T_c\end{pmatrix}, \tag{A.15}$$

$$\mathbf{D}\left(\langle\hat{J}^{z}\rangle\right)=\mathrm{Diag}\left(\mathbf{i}\tilde{\varepsilon}_L,-\mathbf{i}\tilde{\varepsilon}_L,\mathbf{i}\tilde{\varepsilon}_R-\frac{\Gamma_R}{2},-\mathbf{i}\tilde{\varepsilon}_R-\frac{\Gamma_R}{2}\right), \tag{A.16}$$

$$\mathbf{F}\left(\langle\hat{J}^{z}\rangle\right)=\mathrm{Diag}\left(\mathbf{i}\varepsilon'_{+}-\frac{\Gamma_{R\downarrow}}{2},-\mathbf{i}\varepsilon'_{+}-\frac{\Gamma_{R\downarrow}}{2},\mathbf{i}\varepsilon'_{-}-\frac{\Gamma_{R\uparrow}}{2},-\mathbf{i}\varepsilon'_{-}-\frac{\Gamma_{R\uparrow}}{2}\right), \tag{A.17}$$

with the parameters $(i=L,R),(\sigma=\uparrow,\downarrow)$

$$\begin{aligned}
\varepsilon &\equiv \varepsilon_L-\varepsilon_R\,,\\
\varepsilon^{\sigma} &\equiv \varepsilon+\frac{1}{2}(\delta_{\sigma\uparrow}-\delta_{\sigma\downarrow})\left(\lambda_L^z-\lambda_R^z\right)\langle\hat{J}^{z}\rangle\,,\\
\varepsilon'_{\pm} &\equiv \pm\varepsilon+B+\frac{1}{2}\left(\lambda_L^z+\lambda_R^z\right)\langle\hat{J}^{z}\rangle\,,\\
\tilde{\varepsilon}_i &\equiv B+\lambda_i^z\langle\hat{J}^{z}\rangle\,,\\
\Lambda_i^{\pm} &\equiv \frac{\mathbf{i}}{2}\left[\lambda_i^x\langle\hat{J}^{x}\rangle\pm\mathbf{i}\lambda_i^y\langle\hat{J}^{y}\rangle\right],\qquad (\Lambda_i^{\pm})^{*}=-\Lambda_i^{\mp}\,.
\end{aligned} \tag{A.18}$$

A.5. Large-spin dynamics with vanishing electronic back-action

Without the electronic spin the EOM of the large spin (6.6) or (6.19) reduce to

$$\frac{d}{dt}\langle\vec{\hat{J}}\rangle = \vec{B}\times\langle\vec{\hat{J}}\rangle - \gamma_J\langle\vec{\hat{J}}\rangle \ , \tag{A.19}$$

which are readily solved by

$$\langle\vec{\hat{J}}\rangle(t) = \mathrm{e}^{-\gamma_J t}\begin{pmatrix}\cos(Bt) & -\sin(Bt) & 0\\ \sin(Bt) & \cos(Bt) & 0\\ 0 & 0 & 1\end{pmatrix}\langle\vec{\hat{J}}\rangle_0 \ . \tag{A.20}$$

This provides the damped Larmor precession of the large spin around the external magnetic field axis with frequency B. Inserting Eqs. (A.20) into the electronic EOM leads to a set of linear first order differential equations with time-periodic coefficients. In two dimensions it corresponds to the Mathieu-Hill equation, which describes the phenomenon of parametric resonance.

Bibliography

[1] H. Haug and S. W. Koch. *Quantum theory of the optical and electronic proper- ties of semiconductors*. 4th edition. World Scientific, Singapore, 2004 (cit. on p. 1).

[2] S. Datta. *Electronic Transport in Mesoscopic Systems*. Cambridge University Press, 1997 (cit. on p. 1).

[3] D. L. Klein et al. "An approach to electrical studies of single nanocrystals". *Applied Physics Letters* 68 (1996), 2574–2576 (cit. on p. 1).

[4] L. P. Kouwenhoven, D. G. Austing, and S Tarucha. "Few-electron quantum dots". *Reports on Progress in Physics* 64 (2001), 701 (cit. on p. 1).

[5] J Güttinger et al. "Transport through graphene quantum dots". *Reports on Progress in Physics* 75 (2012), 126502 (cit. on p. 1).

[6] W. H. Lim et al. "Electrostatically defined few-electron double quantum dot in silicon". *Applied Physics Letters* 94, 173502 (2009), – (cit. on p. 1).

[7] A. Fujiwara et al. "Single electron tunneling transistor with tunable barriers using silicon nanowire metal-oxide-semiconductor field-effect transistor". *Applied Physics Letters* 88, 053121 (2006), – (cit. on p. 1).

[8] G. A. Steele, G. Gotz, and L. Kouwenhoven. "Tunable few-electron double quantum dots and Klein tunnelling in ultraclean carbon nanotubes". *Nat Nano* 4 (2009), 363–367 (cit. on p. 1).

[9] B. van Wees et al. "Quantized conductance of point contacts in a two-dimensional electron gas". *Phys. Rev. Lett.* 60 (1988), 848–850 (cit. on p. 1).

[10] M. Vanević, Y. Nazarov, and W. Belzig. "Elementary Events of Electron Transfer in a Voltage-Driven Quantum Point Contact". *Phys. Rev. Lett.* 99 (2007), 076601 (cit. on p. 1).

[11] W. G. van der Wiel et al. "Electron transport through double quantum dots". *Rev. Mod. Phys.* 75 (2002), 1–22 (cit. on pp. 1, 2).

[12] J. M. Elzerman et al. "Few-electron quantum dot circuit with integrated charge read out". *Phys. Rev. B* 67 (2003), 161308 (cit. on p. 1).

[13] T. Fujisawa, T. Hayashi, and S. Sasaki. "Time-dependent single-electron transport through quantum dots". *Reports on Progress in Physics* 69 (2006), 759 (cit. on pp. 1, 2).

[14] E. A. Chekhovich et al. "Nuclear spin effects in semiconductor quantum dots". *Nat Mater* 12 (2013). Review, 494–504 (cit. on p. 1).

[15] F. Waugh et al. "Measuring interactions between tunnel-coupled quantum dots". *Phys. Rev. B* 53 (1996), 1413–1420 (cit. on p. 1).

[16] L. Gaudreau et al. "Coherent control of three-spin states in a triple quantum dot". *Nat Phys* 8 (2012), 54–58 (cit. on p. 1).

[17] L. Kouwenhoven et al. *Electron transport in quantum dots*. Kluwer Series, E345, Proceedings of the NATO Advanced Study Institute on Mesoscopic Electron Transport, 105-214. 1997 (cit. on p. 1).

[18] H. Qin, S. Yasin, and D. A. Williams. "Fabrication and characterization of a SiGe double quantum dot structure". *Journal of Vacuum Science & Technology B* 21 (2003), 2852–2855 (cit. on p. 1).

[19] D. Darau et al. "Interference effects on the transport characteristics of a benzene single-electron transistor". *Phys. Rev. B* 79 (2009), 235404 (cit. on pp. 1, 2).

[20] Y. V. Nazarov and Y. M. Blanter. *Quantum transport: introduction to nanoscience*. Cambridge Univ. Press, 2009 (cit. on p. 1).

[21] S Andergassen et al. "Charge transport through single molecules, quantum dots and quantum wires". *Nanotechnology* 21 (2010), 272001 (cit. on p. 1).

[22] R. Hanson et al. "Spins in few-electron quantum dots". *Rev. Mod. Phys.* 79 (2007), 1217–1265 (cit. on p. 1).

[23] G. Shinkai et al. "Correlated Coherent Oscillations in Coupled Semiconductor Charge Qubits". *Phys. Rev. Lett.* 103 (2009), 056802 (cit. on p. 1).

[24] M. A. Reed et al. "Observation of discrete electronic states in a zero-dimensional semiconductor nanostructure". *Phys. Rev. Lett.* 60 (1988), 535–537 (cit. on p. 1).

[25] S. M. Reimann and M. Manninen. "Electronic structure of quantum dots". *Rev. Mod. Phys.* 74 (2002), 1283–1342 (cit. on p. 1).

[26] K. Ono et al. "Current Rectification by Pauli Exclusion in a Weakly Coupled Double Quantum Dot System". *Science* 297 (2002), 1313–1317 (cit. on p. 1).

[27] P. Roulleau et al. "Coherent electron-phonon coupling in tailored quantum systems". *Nat Commun* 2 (2011), 239 (cit. on p. 1).

[28] D. A. Bagrets and Y. V. Nazarov. "Full counting statistics of charge transfer in Coulomb blockade systems". *Phys. Rev. B* 67 (2003), 085316 (cit. on pp. 1, 23).

[29] T. Fujisawa et al. "Bidirectional Counting of Single Electrons". *Science* 312 (2006), 1634–1636 (cit. on p. 1).

[30] S. Gustavsson et al. "Counting Statistics of Single Electron Transport in a Quantum Dot". *Phys. Rev. Lett.* 96 (2006), 076605 (cit. on p. 1).

[31] T. Hayashi et al. "Coherent Manipulation of Electronic States in a Double Quantum Dot". *Phys. Rev. Lett.* 91 (2003), 226804 (cit. on p. 2).

[32] H. A. Nilsson et al. "Correlation-Induced Conductance Suppression at Level Degeneracy in a Quantum Dot". *Phys. Rev. Lett.* 104 (2010), 186804 (cit. on p. 2).

[33] P. Barthold et al. "Enhanced Shot Noise in Tunneling through a Stack of Coupled Quantum Dots". *Phys. Rev. Lett.* 96 (2006), 246804 (cit. on p. 2).

[34] G. Kießlich et al. "Noise Enhancement due to Quantum Coherence in Coupled Quantum Dots". *Phys. Rev. Lett.* 99 (2007), 206602 (cit. on pp. 2, 51, 113).

[35] D. Urban and J. König. "Tunable dynamical channel blockade in double-dot Aharonov-Bohm interferometers". *Phys. Rev. B* 79 (2009), 165319 (cit. on p. 2).

[36] M. G. Schultz. "On Master Equations and Rate Equations in Molecular Electronics: There and Back Again". PhD thesis. Fachbereich Physik der Freien Universität Berlin, 2009 (cit. on p. 2).

[37] G. Schaller, G. Kießlich, and T. Brandes. “Transport statistics of interacting double dot systems: Coherent and non-Markovian effects”. *Phys. Rev. B* 80 (2009), 245107 (cit. on p. 2).

[38] O. Karlström et al. “Canyon of current suppression in an interacting two-level quantum dot”. *Phys. Rev. B* 83 (2011), 205412 (cit. on p. 2).

[39] B. Michaelis, C. Emary, and C. W. J. Beenakker. “All-electronic coherent population trapping in quantum dots”. *EPL (Europhysics Letters)* 73 (2006), 677 (cit. on p. 2).

[40] H.-P. Breuer and F. Petruccione. *The Theory of Open Quantum Systems*. Oxford University Press, 2002 (cit. on pp. 2, 5, 15–17).

[41] M. Esposito. “Stochastic thermodynamics under coarse graining”. *Phys. Rev. E* 85 (2012), 041125 (cit. on pp. 2, 26, 28–31, 81, 95).

[42] H. Bluhm et al. “Enhancing the Coherence of a Spin Qubit by Operating it as a Feedback Loop That Controls its Nuclear Spin Bath”. *Phys. Rev. Lett.* 105 (2010), 216803 (cit. on pp. 3, 51).

[43] G. Schaller et al. “Probing the power of an electronic Maxwell’s demon: Single-electron transistor monitored by a quantum point contact”. *Phys. Rev. B* 84 (2011), 085418 (cit. on pp. 3, 52, 62, 63, 65, 81, 97).

[44] P. Strasberg et al. “Thermodynamics of a Physical Model Implementing a Maxwell Demon”. *Phys. Rev. Lett.* 110 (2013), 040601 (cit. on pp. 3, 52, 65, 81, 88, 91, 94, 96, 105, 122).

[45] G. Schaller. *Non-Equilibrium Master Equations*. Vorlesung gehalten im Rahmen des GRK 1558 , Wintersemester 2011/2012 , Technische Universität Berlin. 2014 (cit. on p. 5).

[46] C. Nietner. “Markovian transport through few-level quantum systems”. PhD thesis. Technische Universität Berlin, 2014 (cit. on p. 5).

[47] Ángel Rivas and S. F. Huelga. “Open Quantum Systems. An Introduction”. *arXiv:1104.5242* (2012) (cit. on pp. 5, 14, 15, 17).

[48] R. Alicki and K. Lendi. *Quantum Dynamical Semigroups and Applications*. Vol. Lectore Notes in Physics 286. Lectore Notes in Physics. Springer-Verlag, 1987 (cit. on pp. 5, 15, 17).

[49] C. Timm. “Tunneling through molecules and quantum dots: Master-equation approaches”. *Phys. Rev. B* 77 (2008), 195416 (cit. on pp. 9, 51).

[50] E. B. Davies. “Markovian master equations”. *Communications in Mathematical Physics* 39 (1974), 91–110 (cit. on p. 12).

[51] M. Reed and B. Simon. *Methods of Modern Mathematical Physics II*. Academic Press, San Diego, 1975 (cit. on p. 14).

[52] K. Kraus. *States, Effects, and Operations Fundamental Notions of Quantum Theory*. Lecture Notes Physics. Springer Berlin, 1983 (cit. on p. 16).

[53] A. Kossakowski. “On quantum statistical mechanics of non-Hamiltonian systems”. *Reports on Mathematical Physics* 3 (1972), 247 –274 (cit. on pp. 16, 19).

[54] G. Lindblad. “On the generators of quantum dynamical semigroups”. *Communications in Mathematical Physics* 48 (1976), 119–130 (cit. on p. 19).

[55] J. L. Skinner and D. Hsu. “Pure dephasing of a two-level system”. *The Journal of Physical Chemistry* 90 (1986), 4931–4938 (cit. on p. 21).

[56] M. Vogl, G. Schaller, and T. Brandes. “Speed of Markovian relaxation toward the ground state”. *Phys. Rev. A* 81 (2010), 012102 (cit. on p. 21).

[57] Y. Utsumi. “Full counting statistics for charge inside a quantum dot”. *Physica E: Low-dimensional Systems and Nanostructures* 40 (2007). International Symposium on Nanometer-Scale Quantum Physics, 355 –358 (cit. on p. 23).

[58] C. Flindt et al. “Universal oscillations in counting statistics”. *Proceedings of the National Academy of Sciences* 106 (2009), 10116–10119 (cit. on pp. 23, 24).

[59] C. Fricke et al. “High cumulants in the counting statistics measured for a quantumdot”. *Physica E: Low-dimensional Systems and Nanostructures* 42 (2010). 18th International Conference on Electron Properties of Two-Dimensional Systems, 848–851 (cit. on pp. 23, 24, 79).

[60] C. Flindt et al. “Counting statistics of transport through Coulomb blockade nanostructures: High-order cumulants and non-Markovian effects”. *Phys. Rev. B* 82 (2010), 155407 (cit. on p. 23).

[61] U. Seifert. “Stochastic thermodynamics, fluctuation theorems and molecular machines”. *Reports on Progress in Physics* 75 (2012), 126001 (cit. on p. 25).

[62] H. Hinrichsen, C. Gogolin, and P. Janotta. “Non-equilibrium Dynamics, Thermalization and Entropy Production”. *Journal of Physics: Conference Series* 297 (2011), 012011 (cit. on p. 25).

[63] M. Esposito and C. Van den Broeck. “Three faces of the second law. I. Master equation formulation”. *Phys. Rev. E* 82 (2010), 011143 (cit. on p. 25).

[64] C. Van den Broeck and M. Esposito. “Ensemble and Trajectory Thermodynamics: A Brief Introduction”. *arXiv:1403.1777* (2014). Course given by C. Van den Broeck at the Summer School ”Fundamental Problems in Statistical Physics XIII”, June 16-29, 2013 Leuven, Belgium (cit. on p. 25).

[65] M. Esposito and G. Schaller. “Stochastic thermodynamics for ”Maxwell demon” feedbacks”. *EPL (Europhysics Letters)* 99 (2012), 30003 (cit. on pp. 26, 52, 63, 65, 66, 81).

[66] S. Takahashi et al. “Large Anisotropy of the Spin-Orbit Interaction in a Single InAs Self-Assembled Quantum Dot”. *Phys. Rev. Lett.* 104 (2010), 246801 (cit. on p. 33).

[67] H. B. Heersche et al. “Electron Transport through Single Molecular Magnets”. *Phys. Rev. Lett.* 96 (2006), 206801 (cit. on pp. 33, 34, 51).

[68] M. Misiorny, I. Weymann, and J. Barnaś. “Spin effects in transport through single-molecule magnets in the sequential and cotunneling regimes”. *Phys. Rev. B* 79 (2009), 224420 (cit. on pp. 33, 34).

[69] J. R. Friedman and M. P. Sarachik. “Single-Molecule Nanomagnets”. *Annual Review of Condensed Matter Physics* 1 (2010), 109–128 (cit. on pp. 33, 34).

[70] A. V. Khaetskii, D. Loss, and L. Glazman. “Electron Spin Decoherence in Quantum Dots due to Interaction with Nuclei”. *Phys. Rev. Lett.* 88 (2002), 186802 (cit. on pp. 33, 37, 38, 51).

[71] I. A. Merkulov, A. L. Efros, and M. Rosen. “Electron spin relaxation by nuclei in semiconductor quantum dots”. *Phys. Rev. B* 65 (2002), 205309 (cit. on pp. 33, 38).

[72] W. A. Coish and D. Loss. “Singlet-triplet decoherence due to nuclear spins in a double quantum dot”. *Phys. Rev. B* 72 (2005), 125337 (cit. on pp. 33, 37, 38).

[73] D. J. Reilly et al. “Suppressing Spin Qubit Dephasing by Nuclear State Preparation”. *Science* 321 (2008), 817–821 (cit. on pp. 33, 51).

[74] L. Bogani and W. Wernsdorfer. “Molecular spintronics using single-molecule magnets”. *Nat Mater* 7 (2008), 179–186 (cit. on pp. 33, 51).

[75] W. Heisenberg. “Zur Theorie des Ferromagnetismus”. German. *Zeitschrift für Physik* 49 (1928), 619–636 (cit. on p. 33).

[76] O. Waldmann. “A Criterion for the Anisotropy Barrier in Single-Molecule Magnets”. *Inorganic Chemistry* 46 (2007). PMID: 17979271, 10035–10037 (cit. on p. 34).

[77] J. Fischer, B. Trauzettel, and D. Loss. “Hyperfine interaction and electron-spin decoherence in graphene and carbon nanotube quantum dots”. *Phys. Rev. B* 80 (2009), 155401 (cit. on pp. 34, 37).

[78] A. M. Stoneham. *Theory of defects in solids. Electronic structure of defects in insulators and ssemiconductor.* Clarendon Press, Oxford, 1975 (cit. on p. 34).

[79] C. P. Slichter. *Principles of Magnetic Resonance*. Springer-Verlag Berlin Heidelberg New York, 1990 (cit. on p. 34).

[80] W. A. Coish. “Spins in quantum dots: Hyperfine interaction, transport, and coherent control”. PhD thesis. Universität Basel, 2008 (cit. on p. 34).

[81] J. Hildmann. “Nuclear Spin Phenomena in Optically Active Semiconductor Quantum Dots”. PhD thesis. Universität Konstanz, 2014 (cit. on p. 34).

[82] W. A. Coish and D. Loss. “Hyperfine interaction in a quantum dot: Non-Markovian electron spin dynamics”. *Phys. Rev. B* 70 (2004), 195340 (cit. on pp. 37, 38, 51).

[83] J. R. Petta et al. “Coherent Manipulation of Coupled Electron Spins in Semiconductor Quantum Dots”. *Science* 309 (2005), 2180–2184 (cit. on pp. 37, 38).

[84] F. H. L. Koppens et al. “Control and Detection of Singlet-Triplet Mixing in a Random Nuclear Field”. *Science* 309 (2005), 1346–1350 (cit. on pp. 37, 38, 51).

[85] O. N. Jouravlev and Y. V. Nazarov. “Electron Transport in a Double Quantum Dot Governed by a Nuclear Magnetic Field”. *Phys. Rev. Lett.* 96 (2006), 176804 (cit. on p. 37).

[86] J. Fischer et al. “Spin decoherence of a heavy hole coupled to nuclear spins in a quantum dot”. *Phys. Rev. B* 78 (2008), 155329 (cit. on pp. 37, 38).

[87] A. Pályi and G. Burkard. “Hyperfine-induced valley mixing and the spin-valley blockade in carbon-based quantum dots”. *Phys. Rev. B* 80 (2009), 201404 (cit. on p. 37).

[88] Y. Yafet. “Hyperfine interaction due to orbital magnetic moment of electrons with large g factors”. *Journal of Physics and Chemistry of Solids* 21 (1961), 99 –104 (cit. on p. 38).

[89] W. A. Coish and J. Baugh. “Nuclear spins in nanostructures”. *physica status solidi (b)* 246 (2009), 2203–2215 (cit. on p. 38).

[90] W. A. Coish et al. “Quantum versus classical hyperfine-induced dynamics in a quantum dota)”. *Journal of Applied Physics* 101, 081715 (2007), – (cit. on pp. 38–40).

[91] D. Paget et al. “Low field electron-nuclear spin coupling in gallium arsenide under optical pumping conditions”. *Phys. Rev. B* 15 (1977), 5780–5796 (cit. on p. 38).

[92] S. I. Erlingsson and Y. V. Nazarov. “Evolution of localized electron spin in a nuclear spin environment”. *Phys. Rev. B* 70 (2004), 205327 (cit. on pp. 38, 51).

[93] J. Taylor et al. “Relaxation, dephasing, and quantum control of electron spins in double quantum dots”. *Phys. Rev. B* 76 (2007), 035315 (cit. on p. 38).

[94] E. A. Yuzbashyan et al. “Solution for the dynamics of the BCS and central spin problems”. *Journal of Physics A: Mathematical and General* 38 (2005), 7831 (cit. on pp. 38, 40).

[95] J. Geremia, J. K. Stockton, and H. Mabuchi. “Real-Time Quantum Feedback Control of Atomic Spin-Squeezing”. *Science* 304 (2004), 270–273 (cit. on p. 38).

[96] J. Schliemann, A. Khaetskii, and D. Loss. “Spin decay and quantum parallelism”. *Phys. Rev. B* 66 (2002), 245303 (cit. on p. 38).

[97] J. Schliemann, A. Khaetskii, and D. Loss. “Electron spin dynamics in quantum dots and related nanostructures due to hyperfine interaction with nuclei”. *Journal of Physics: Condensed Matter* 15 (2003), R1809 (cit. on p. 40).

[98] M. Feingold and A. Peres. “Regular and chaotic motion of coupled rotators”. *Physica D: Nonlinear Phenomena* 9 (1983), 433 –438 (cit. on pp. 41, 52).

[99] E. Magyari et al. “Integrable and nonintegrable classical spin clusters”. English. *Zeitschrift für Physik B Condensed Matter* 65 (1987), 363–374 (cit. on pp. 41, 42, 52).

[100] N. Srivastava and G. Müller. “Quantum and classical spin clusters: disappearance of quantum numbers and Hamiltonian chaos”. English. *Zeitschrift für Physik B Condensed Matter* 81 (1990), 137–148 (cit. on pp. 41, 45–47, 52).

[101] D. T. Robb and L. E. Reichl. “Chaos in a two-spin system with applied magnetic field”. *Phys. Rev. E* 57 (1998), 2458–2459 (cit. on pp. 41, 45, 47, 52).

[102] R. I. McLachlan and D. R. J. O’Neale. “Geometric integration for a two-spin system”. *Journal of Physics A: Mathematical and General* 39 (2006), L447 (cit. on p. 41).

[103] V. Arnold. *Mathematical Methods of Classical Mechanics*. Springer, 1989 (cit. on p. 41).

[104] J. C. Sprott. *Chaos and Time-Series Analysis*. Oxford University Press, 2003 (cit. on p. 43).

[105] A. Metelmann and T. Brandes. “Transport through single-level systems: Spin dynamics in the nonadiabatic regime”. *Phys. Rev. B* 86 (2012), 245317 (cit. on pp. 43, 52, 53, 64, 68, 69, 109, 119, 121).

[106] S. H. Strogatz. *Nonlinear dynamics and chaos*. Westview Press, 2000 (cit. on p. 43).

[107] A. Peres. “New Conserved Quantities and Test for Regular Spectra”. *Phys. Rev. Lett.* 53 (1984), 1711–1713 (cit. on pp. 45–47).

[108] N. Srivastava et al. “Integrable and nonintegrable classical spin clusters”. English. *Zeitschrift für Physik B Condensed Matter* 70 (1988), 251–268 (cit. on p. 45).

[109] E. Tannenbaum and E. J. Heller. “Semiclassical Quantization Using Invariant Tori: A Gradient-Descent Approach”. *The Journal of Physical Chemistry A* 105 (2001), 2803–2813 (cit. on p. 46).

[110] I. C. Percival. “Regular and irregular spectra”. *Journal of Physics B: Atomic and Molecular Physics* 6 (1973), L229 (cit. on p. 46).

[111] L. E. Reichl. *The transition to chaos: conservative classical systems and quantum manifestations*. Springer-Verlag New York, 2004 (cit. on p. 47).

[112] J. Emerson and L. Ballentine. “Characteristics of quantum-classical correspondence for two interacting spins”. *Phys. Rev. A* 63 (2001), 052103 (cit. on pp. 48, 49).

[113] K. Mosshammer and T. Brandes. “Semiclassical spin-spin dynamics and feedback control in transport through a quantum dot”. *Phys. Rev. B* 90 (2014), 134305 (cit. on p. 51).

[114] T. Fujisawa et al. “Spontaneous Emission Spectrum in Double Quantum Dot Devices”. *Science* 282 (1998), 932–935 (cit. on p. 51).

[115] T. Brandes and B. Kramer. “Spontaneous Emission of Phonons by Coupled Quantum Dots”. *Phys. Rev. Lett.* 83 (1999), 3021–3024 (cit. on p. 51).

[116] R. Aguado and T. Brandes. “Shot Noise Spectrum of Open Dissipative Quantum Two-Level Systems”. *Phys. Rev. Lett.* 92 (2004), 206601 (cit. on p. 51).

[117] C. Gnodtke. “Streuung beim Transport durch selbstorganisierte Quantenpunktstapel”. MA thesis. TU Berlin, 2004 (cit. on p. 51).

[118] S. I. Erlingsson, Y. V. Nazarov, and V. I. Fal’ko. “Nucleus-mediated spin-flip transitions in GaAs quantum dots”. *Phys. Rev. B* 64 (2001), 195306 (cit. on p. 51).

[119] J. Baugh et al. “Large Nuclear Overhauser Fields Detected in Vertically Coupled Double Quantum Dots”. *Phys. Rev. Lett.* 99 (2007), 096804 (cit. on p. 51).

[120] K. Ono and S. Tarucha. “Nuclear-Spin-Induced Oscillatory Current in Spin-Blockaded Quantum Dots”. *Phys. Rev. Lett.* 92 (2004), 256803 (cit. on p. 51).

[121] T. Inoshita and S. Tarucha. “Electronic-nuclear dynamics in double quantum dots in the spin-blockade regime”. *Physica E: Low-dimensional Systems and Nanostructures* 22 (2004). 15th International Conference on Electronic Propreties of Two-Dimensional Systems (EP2DS-15), 422 –425 (cit. on p. 51).

[122] S. I. Erlingsson, O. N. Jouravlev, and Y. V. Nazarov. “Coherent oscillations of current due to nuclear spins”. *Phys. Rev. B* 72 (2005), 033301 (cit. on pp. 51, 118).

[123] J. Iñarrea et al. “Hysteretic behavior in weakly coupled double-dot transport in the spin blockade regime”. *Applied Physics Letters* 91, 252112 (2007) (cit. on p. 51).

[124] J. Iñarrea, G. Platero, and A. H. MacDonald. “Electronic transport through a double quantum dot in the spin-blockade regime: Theoretical models”. *Phys. Rev. B* 76 (2007), 085329 (cit. on p. 51).

[125] M. S. Rudner and L. S. Levitov. “Self-Polarization and Dynamical Cooling of Nuclear Spins in Double Quantum Dots”. *Phys. Rev. Lett.* 99 (2007), 036602 (cit. on p. 51).

[126] M. S. Rudner and L. S. Levitov. “Phase transitions in dissipative quantum transport and mesoscopic nuclear spin pumping”. *Phys. Rev. B* 82 (2010), 155418 (cit. on p. 51).

[127] M. S. Rudner et al. “Nuclear spin dynamics in double quantum dots: Fixed points, transients, and intermittency”. *Phys. Rev. B* 84 (2011), 075339 (cit. on p. 51).

[128] C. López-Monís et al. “Limit cycles and chaos in the current through a quantum dot”. *Phys. Rev. B* 85 (2012), 045301 (cit. on pp. 51–53, 64, 68, 69, 107, 109, 110, 117, 118, 121, 123).

[129] S. Foletti et al. “Universal quantum control of two-electron spin quantum bits using dynamic nuclear polarization”. *Nat Phys* 5 (2009), 903–908 (cit. on p. 51).

[130] F. H. L. Koppens et al. “Driven coherent oscillations of a single electron spin in a quantum dot”. *Nature* 442 (2006), 766–771 (cit. on p. 51).

[131] M. Galperin et al. “Nuclear Coupling and Polarization in Molecular Transport Junctions: Beyond Tunneling to Function”. *Science* 319 (2008), 1056–1060 (cit. on p. 51).

[132] J.-X. Zhu and A. V. Balatsky. “Theory of current and shot-noise spectroscopy in single-molecular quantum dots with a phonon mode”. *Phys. Rev. B* 67 (2003), 165326 (cit. on p. 51).

[133] J. Koch and F. von Oppen. “Franck-Condon Blockade and Giant Fano Factors in Transport through Single Molecules”. *Phys. Rev. Lett.* 94 (2005), 206804 (cit. on p. 51).

[134] J. Paaske and K. Flensberg. “Vibrational Sidebands and the Kondo Effect in Molecular Transistors”. *Phys. Rev. Lett.* 94 (2005), 176801 (cit. on p. 51).

[135] H. Hübener and T. Brandes. “Vibrational Coherences in Single Electron Tunneling through Nanoscale Oscillators”. *Phys. Rev. Lett.* 99 (2007), 247206 (cit. on p. 51).

[136] R. Avriller and A. Levy Yeyati. “Electron-phonon interaction and full counting statistics in molecular junctions”. *Phys. Rev. B* 80 (2009), 041309 (cit. on p. 51).

[137] F. Haupt, T. Novotný, and W. Belzig. “Phonon-Assisted Current Noise in Molecular Junctions”. *Phys. Rev. Lett.* 103 (2009), 136601 (cit. on p. 51).

[138] T. L. Schmidt and A. Komnik. “Charge transfer statistics of a molecular quantum dot with a vibrational degree of freedom”. *Phys. Rev. B* 80 (2009), 041307 (cit. on p. 51).

[139] R. Hussein et al. “Semiclassical dynamics of nanoelectromechanical systems”. *Phys. Rev. B* 82 (2010), 165406 (cit. on p. 51).

[140] A. Metelmann and T. Brandes. “Adiabaticity in semiclassical nanoelectromechanical systems”. *Phys. Rev. B* 84 (2011), 155455 (cit. on p. 51).

[141] M. Kumar et al. “Detection of Vibration-Mode Scattering in Electronic Shot Noise”. *Phys. Rev. Lett.* 108 (2012), 146602 (cit. on p. 51).

[142] N. Traverso Ziani et al. “Electrical probe for mechanical vibrations in suspended carbon nanotubes”. *Phys. Rev. B* 84 (2011), 155423 (cit. on p. 51).

[143] M.-H. Jo et al. “Signatures of Molecular Magnetism in Single-Molecule Transport Spectroscopy”. *Nano Letters* 6 (2006), 2014–2020 (cit. on p. 51).

[144] I. Žutić, J. Fabian, and S. Das Sarma. “Spintronics: Fundamentals and applications”. *Rev. Mod. Phys.* 76 (2004), 323–410 (cit. on p. 51).

[145] A. Fert. “Nobel Lecture: Origin, development, and future of spintronics”. *Rev. Mod. Phys.* 80 (2008), 1517–1530 (cit. on p. 51).

[146] C. Timm and F. Elste. “Spin amplification, reading, and writing in transport through anisotropic magnetic molecules”. *Phys. Rev. B* 73 (2006), 235304 (cit. on p. 51).

[147] J. Fernández-Rossier and R. Aguado. “Single-Electron Transport in Electrically Tunable Nanomagnets”. *Phys. Rev. Lett.* 98 (2007), 106805 (cit. on p. 51).

[148] G. Kiesslich et al. “Single spin transport spectroscopy: Current blockade and spin decay”. *Applied Physics Letters* 95, 152104 (2009), 152104 (cit. on p. 51).

[149] L. D. Contreras-Pulido and R. Aguado. “Shot noise spectrum of artificial single-molecule magnets: Measuring spin relaxation times via the Dicke effect”. *Phys. Rev. B* 81 (2010), 161309 (cit. on p. 51).

[150] B. Sothmann and J. König. “Transport through quantum-dot spin valves containing magnetic impurities”. *Phys. Rev. B* 82 (2010), 245319 (cit. on p. 51).

[151] M. M. E. Baumgärtel et al. “Transport and Accumulation of Spin Anisotropy”. *Phys. Rev. Lett.* 107 (2011), 087202 (cit. on p. 51).

[152] N. Bode et al. “Current-induced switching in transport through anisotropic magnetic molecules”. *Phys. Rev. B* 85 (2012), 115440 (cit. on pp. 51, 52, 107, 114, 117).

[153] B. Sothmann, J. König, and Y. Gefen. “Mesoscopic Stoner Instability in Metallic Nanoparticles Revealed by Shot Noise”. *Phys. Rev. Lett.* 108 (2012), 166603 (cit. on p. 51).

[154] D. Ralph and M. Stiles. “Spin transfer torques”. *Journal of Magnetism and Magnetic Materials* 320 (2008), 1190 –1216 (cit. on pp. 52, 114).

[155] A. Brataas, A. D. Kent, and H. Ohno. “Current-induced torques in magnetic materials”. *Nat Mater* 11 (2012), 372–381 (cit. on pp. 52, 114).

[156] K. Mosshammer, G. Kiesslich, and T. Brandes. “Transport and semiclassical dynamics of coupled quantum dots interacting with a local magnetic moment”. *Phys. Rev. B* 86 (2012), 165447 (cit. on pp. 52, 53, 68, 107).

[157] M. J. A. Schuetz et al. “Superradiance-like electron transport through a quantum dot”. *Phys. Rev. B* 86 (2012), 085322 (cit. on pp. 52, 58, 120).

[158] P. A. Houle, N.-G. Zhang, and C. L. Henley. “Semiclassical mechanics of a nonintegrable spin cluster”. *Phys. Rev. B* 60 (1999), 15179–15186 (cit. on p. 52).

[159] V. Serreli et al. “A molecular information ratchet”. *Nature* 445 (2007), 523–527 (cit. on p. 52).

[160] S. Toyabe et al. “Experimental demonstration of information-to-energy conversion and validation of the generalized Jarzynski equality”. *Nat Phys* 6 (2010), 988–992 (cit. on p. 52).

[161] A. Berut et al. “Experimental verification of Landauer/’s principle linking information and thermodynamics”. *Nature* 483 (2012), 187–189 (cit. on p. 52).

[162] L. P. Kouwenhoven et al. “Quantized current in a quantum-dot turnstile using oscillating tunnel barriers”. *Phys. Rev. Lett.* 67 (1991), 1626–1629 (cit. on p. 52).

[163] M. Blaauboer and C. M. L. Fricot. “Spin pump turnstile: Parametric pumping of a spin-polarized current through a nearly closed quantum dot”. *Phys. Rev. B* 71 (2005), 041303 (cit. on p. 52).

[164] P. Jordan and E. Wigner. “Über das Paulische Äquivalenzverbot”. German. *Zeitschrift für Physik* 47 (1928), 631–651 (cit. on p. 56).

[165] C. D. Batista and G. Ortiz. “Generalized Jordan-Wigner Transformations”. *Phys. Rev. Lett.* 86 (2001), 1082–1085 (cit. on p. 56).

[166] M. G. House et al. “Detection and Measurement of Spin-Dependent Dynamics in Random Telegraph Signals”. *Phys. Rev. Lett.* 111 (2013), 126803 (cit. on p. 62).

[167] F. Bloch. “Nuclear Induction”. *Phys. Rev.* 70 (1946), 460–474 (cit. on p. 64).

[168] H. Hasegawa, M. Lakshmanan, and Y. Okazaki. “Effective g-Factor for Two Strongly Exchange-Coupled Magnetization Vectors”. *Progress of Theoretical Physics* 75 (1986), 550–555 (cit. on pp. 64, 72).

[169] M. Kobayashi. “A Solution of the Inhomogeneous Bloch Equation for a Class of Time-Varying Magnetic Fields”. *Progress of Theoretical Physics* 112 (2004), 773–783 (cit. on p. 72).

[170] P. Strasberg. Private Communication. 2014 (cit. on pp. 81, 100–102, 104, 105).

[171] H. B. Callen. *Thermodynamics and an Introduction to Thermostatistics*. John Wiley & Sons, Inc., 1985 (cit. on p. 93).

[172] B. Elattari and S. A. Gurvitz. "Influence of measurement on the lifetime and the linewidth of unstable systems". *Phys. Rev. A* 62 (2000), 032102 (cit. on p. 96).

[173] J. Rau and B. Müller. "From reversible quantum microdynamics to irreversible quantum transport". *Physics Reports* 272 (1996), 1 –59 (cit. on p. 109).

[174] M. Braun, J. König, and J. Martinek. "Theory of transport through quantum-dot spin valves in the weak-coupling regime". *Phys. Rev. B* 70 (2004), 195345 (cit. on p. 111).

[175] S. A. Gurvitz and Y. S. Prager. "Microscopic derivation of rate equations for quantum transport". *Phys. Rev. B* 53 (1996), 15932–15943 (cit. on p. 112).

[176] T. H. Stoof and Y. V. Nazarov. "Time-dependent resonant tunneling via two discrete states". *Phys. Rev. B* 53 (1996), 1050–1053 (cit. on pp. 112, 113).

List of Figures

Acknowledgements

First of all I want to thank my supervisor Prof. Dr. Tobias Brandes for giving me the opportunity to work in his group for a couple of years. Despite all the moments when I was full of doubt he encouraged and motivated me to go on and always had an open door to discuss ideas. I am thankful for the useful and productive discussions we had and also for the opportunity to take part in inspiring conferences, seminars and meetings with international scientific visitors.

Additionally, I thank Prof. Dr. Gloria Platero for agreeing to be the second referee of this thesis.

I also want to thank Dr. Gerold Kiesslich who often gave me the right hints and ideas during the first part of my studies.

I owe many thanks to Dr. Malte Vogl for being my room mate for a long time who always had an open ear and the many cups of tea, as well as the other room mates I had over the years: Wassilij Kopylov, Philipp Strasberg and Florian Lau.

Furthermore, I want to thank the many colleagues of our group for the discussions and their support. I'm grateful to Philipp Strasberg for giving me the crucial idea of how to understand generic Maxwell demon models, especially the restrictions of the coarse graining for interacting levels. I'm indebted to Dr. Anja Metelmann with whom I discussed nonlinear dynamics and Dr. Philipp Zedler who gave me courses in complex analysis. Discussions with Dr. Malte Vogl, Dr. Gernot Schaller, Dr. Christian Nietner, Dr. Victor Bastidas, Wassilij Kopylov and many other members of the group are gratefully acknowledged.

Furthermore, I want to thank Dr. Malte Vogl and Philipp Strasberg for proofreading parts of this thesis.

I should not forget to express my gratitude to my closest friends and family who comforted me and tolerated my often odd behavior.

Last but not least, I thank the SFB 910 for their financial support of this thesis.